Spring 5-19-2018

Assessment of the Viability of Microwell Plates as Sample Holders for Analytical Excitation-Emission Spectroscopy of Polyaromatic Hydrocarbons in 75% Ethanol

Lauren M. Ridley-Hoffman

Follow this and additional works at: https://scholarship.shu.edu/dissertations

 Part of the Analytical Chemistry Commons, and the Environmental Chemistry Commons

Assessment of the Viability of Microwell Plates as Sample Holders for Analytical Excitation-

Emission Spectroscopy of Polyaromatic Hydrocarbons in 75% Ethanol

by

Lauren M. Ridley-Hoffman

Submitted in partial fulfillment of the requirements for the degree of

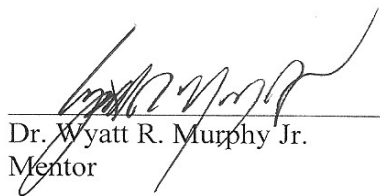Doctor of Philosophy

Seton Hall University

Department of Chemistry and Biochemistry

December 2017

We certify that we have read this thesis and that in our opinion it is adequate in scientific scope as a dissertation for the degree of Doctor of Philosophy.
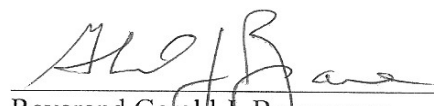
APPROVED

_____

Dr. Wyatt R. Murphy Jr.
Mentor

_____

Dr. Nicholas H. Snow
Member of Dissertation Committee

_____

Reverend Gerald J. Buonopane
Member of Dissertation Committee

_____

Dr. Cecilia H. Marzabadi
Approved for the Department of Chemistry and Biochemistry
Chairperson, Department of Chemistry and Biochemistry
Seton Hall University

iii

Dedication

This dissertation is dedicated to the memory of Dr. Carolyn Summerill Bentivegna, whose guidance and mentorship meant more to me than most will know. Thank you for all the opportunities and experiences you gave me and shared with me. My trip with NOAA was the best experience and it would not have happened without you. I wish you could see this finished product of all our hard work.

I need to thank my dear friend Emi Hanawa-Romero. If there is one thing you need to have while finishing a Ph.D. it is a best friend who knows exactly what you are going through. She has been my rock, my confidant, my coffee and lunch buddy, my ride home after seminar, and my best friend.

I would not be where I am today without two very special people in my life, my parents Joyce and Mike. They have always allowed me to follow my dreams no matter where the road has taken me. I know that it could not have been easy to support me both emotionally and financially all these years. I could not done this without them. I love them deeply and I hope that I have made them proud.

Last and certainly not least I must thank my husband Michael. He has not had it easy the last years, weeks, or months. My constant stress and mood swings while trying to accomplish this dissertation have been rough. His has always pushed me to be great and I hope that he knows his love and support are why I finally finished.

Table of Contents

List of Figures

List of Tables

Equations

$$A = \varepsilon \times c \times l$$
$$A = absorbance \quad \varepsilon = molar\ absorptivity$$
$$c = concentration \quad l = pathlength$$

$$\phi_{f(c)} = \phi_{f(s)} \left(\frac{A_{(s)}}{A_{(c)}}\right) \left(\frac{\eta_{(c)}}{\eta_{(s)}}\right)^2 \left(\frac{P_{(c)}}{P_{(s)}}\right)$$
$$\Phi_f = quantum\ yield \quad\quad A = absorbance$$
$$\eta = refractive\ index\ of\ solvent \quad s = reference\ standard$$
$$P = area\ under\ emission\ spectra \quad c = compound\ of\ study$$

$$\Delta \bar{v} = \overline{v_a} - \overline{v_f}$$
$$\Delta \bar{v} = energy\ difference$$
$$\overline{v_a} = maximum\ first\ absorption\ band$$
$$\overline{v_f} = maximum\ emission\ band$$

$$r = \frac{\sum_i[(x_i - \bar{x})(y_i - \bar{y})]}{\{[\sum_i(x_i - \bar{x})^2]\,[\sum_i(y_i - \bar{y})^2]\}^{1/2}}$$

$$LOD = y_B + 3\frac{\sqrt{\frac{\sum_i(y_i - \hat{y}_i)^2}{n - 2}}}{\sqrt{\sum_i(x_i - \bar{x})^2}}$$

$$LOQ = y_B + 10\frac{\sqrt{\frac{\sum_i(y_i - \hat{y}_i)^2}{n - 2}}}{\sqrt{\sum_i(x_i - \bar{x})^2}}$$

Chemical Structures
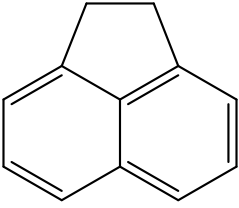
acenaphthene
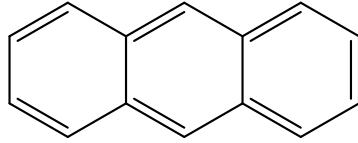
anthracene
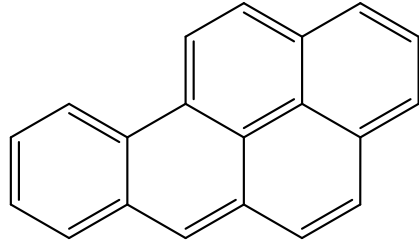
benzo [a] pyrene
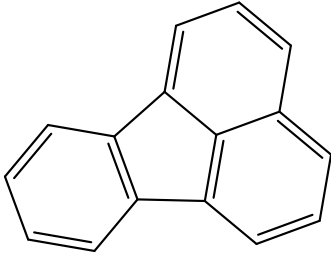
fluoranthene
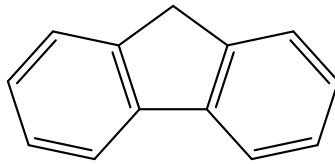
fluorene

naphthalene

OH

1 - naphthol

OH
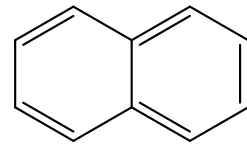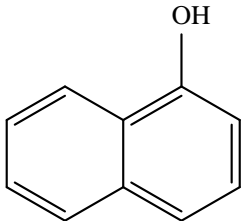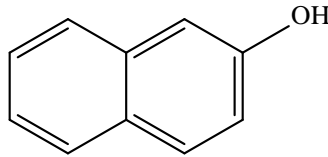
2 - naphthol

phenanthrene

OH
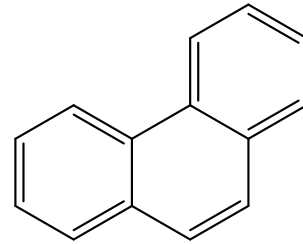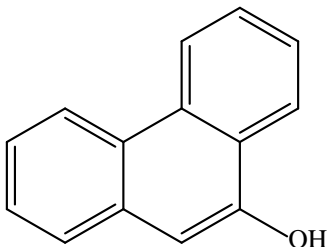
9 - phenanthrol

pyrene

OH
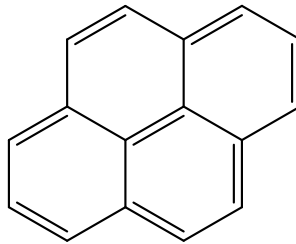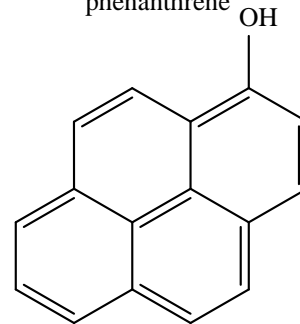
1 - pyrenol

Abstract

Polyaromatic hydrocarbons (PAHs) in the environment are a significant concern as many compounds in this class are potential carcinogens. PAHs resulting from petroleum spills can contaminate natural waters and the products obtain from them (fish and fish products in particular). Previous studies by Pena, et. al. on ethanolic extracts of organs from menhaden captured in the vicinity of the Deepwater Horizon (Macondo oil well) spill have shown that fluorescence excitation spectroscopy is a useful technique for detecting the presence of PAH metabolites and fluorescent vitamins. The study has also concluded that previous methods for analyzing PAHs using fluorescence spectroscopy used less than desirable fluorescence wavelengths. Continuous biomonitoring of this spill is essential. Due to the high volume of samples needed to assess accurate biomonitored data, a new technique using microwell sample holders was developed (purchased through Horiba Scientific). In order to address optimal fluorescence wavelength monitoring, the study used EEMS (excitation emission spectroscopy) as a tool for accurate and reliable data of all PAHs determined.

Currently, there is no evidence in the literature that high quality fluorescence spectral measurements (e.g. EEMS) have been attempted in microwells. Several concerns arise in these measurements. First, fluorescence measurements are normally made on samples in 1 cm quartz or fused silica cuvettes. Two optical configurations, right angle and front face, are used. Front face detection (small angle detection) is normally used for highly absorbing, scattering or turbid samples. Microwells present an optically similar arrangement to front face detection. Second, the quantum yields for fluorescence (photons emitted/photons absorbed) vary strongly among the PAHs of interest.

Comparison of standard fluorescence cuvettes to the Horiba MicroMax microwell Plate reader was conducted using twelve PAHs or their metabolites.

xx

Chapter 1

Historical

Following the explosion and continued release of British Petroleum's Deepwater Horizon (DWH) Oil Rig concerns arose for the Gulf of Mexico's wildlife and fisheries. The Mississippi Canyon 252 pipeline burst on April 20th, 2010 and persisted for 87 days until the well was officially plugged on August 3rd, 2010. The incident contributed to an estimated total of 700,000 metric tons of crude oil spilling into the Gulf of Mexico and is the largest spill in United States history.[1] Crude oil and its toxicity is associated with polycyclic aromatic hydrocarbons (PAHs) and contribute to both acute and chronic illness.[2] Sources of PAHs include petro genic (oil spillages) and pyrogenic (combustion).[3] The concerns for the marine fisheries were especially important because of contamination of the catch, quantity and quality of the fish, and finally the potential of bio – amplification to high level food sources.

PAH contamination can be monitored in the aquatic environment using fish tissues and bile.[3, 4, 5, 6] Menhaden are of particular interest since they are considered "the most important fish in the sea".[7] Known by many names (bunker, pogies, etc.) they are a common prey species in the marine ecosystem and are consumed by predators such as tuna, salmon, bluefish, marine mammals and aquatic birds.[8] Critical to the commercial fisheries of the Gulf and Atlantic coasts; menhaden are considered one of the most economically important species in North America.[7] It is heavily fished by the bait and reduction industries where menhaden are used for pet food, fertilizer and oil-based products such as cosmetics and fish oil supplements.[9] While ecologically and economically important, little research has been done on menhaden with regard to the accumulation and/or impact of environmental contaminants. Organisms take up PAHs and store them in adipose tissue until metabolism and/or excretion occurs. Through metabolism, PAHs can be transformed into carcinogenic metabolites that have the ability to interact with DNA and cause mutations that can lead to cancer.[10] Accepted techniques for biomonitoring focus on PAHs and not their metabolites.[11]

PAHs have been routinely used for biomonitoring crude oil spills and oil combustion related contamination using fluorescent technologies.[3, 12, 13, 14, 15, 16] PAHs are easily detected by fluorescence and ultraviolet absorption spectroscopy due to their distinguishing absorption spectra, large extinction coefficients, and high emission quantum yields. Spectra are related to the number and positioning of rings and are used to identify classes of PAHs that may be present. Excitation Emission Matrix Spectroscopy (EEMs) use spectroscopic signatures in a three dimensional spectrum of each fluorescent species. EEMs are used to detect PAHs and pesticides in polluted water samples, water collected post DWH oil spill, and raw fish oils and hearts of Atlantic and Gulf menhaden.[17, 18, 19]

Many organic molecules detected via fluorescence are called fluorescent aromatic compounds (FACs) in the literature. Methods for detection include fixed wavelength fluorescence, synchronous fluorescence scanning, high performance liquid chromatography (HPLC) with fluorescence detection, and EEMs.[4, 5, 17, 20, 21, 22, 23] Optimal wavelengths for excitation and emission in most FACs are overlapping making it problematic to separate the presence of one PAH from another and are referred to as "PAH-like" when detected. Even with this distinguishing issue, FAC methods have an advantage over typical methods such as gas chromatography – mass spectrometry (GCMS) in that they are better able to detect substituted and unsubstituted PAH compounds and metabolites typically found in natural samples.[24] Adding a chromatographic step to detection methods (fluorescence or mass spectrometry) can increase sensitivity and selection for a variety of environmentally toxic compounds and these methods are generally accepted by government regulators like the FDA or EPA.[21, 22, 25, 26] Conversely, the described chromatographic methods are labor intensive and subject to diminished recovery due to sample handling.[26] Direct analysis methods like fluorescence have advantages in sample preparation and high sample throughput. Although specific detection in a mixture is low, fluorescence offers the detection of a broad variety of parent compounds as well as their metabolites.

The goals of this research project were to produce spectroscopic signatures of PAHs and their metabolites in 75% ethanol, evaluate EEMs as a method in the menhaden studies, and assess the viability of microwell plates as sample holders versus standard quartz fluorescence cuvettes.

References

1. McNutt, M. K.; Chu, S.; Lubchenco, J.; Hunter, T.; Dreyfus, G.; Murawski, S. A.; Kennedy, D. M. Applications of Science and Engineering to Quantify and Control the Deepwater Horizon Oil Spill. *PNAS* **2012**, *109* (50), 20222–20228.

2. Harvey, J. S.; Lyons, B. P.; Page, T. S.; Stewart, C.; Parry, J. M. An Assessment of the Genotoxic Impact of the Sea Empress Oil Spill by the Measurement of DNA Adduct Levels in Selected Invertebrate and Vertebrate Species. *Mutation Research/Genetic Toxicology and Environmental Mutagenesis* **1999**, *441* (1), 103–114.

3. Murawski, S. A.; Hogarth, W. T.; Peebles, E. B.; Barbeiri, L. Prevalence of External Skin Lesions and Polycyclic Aromatic Hydrocarbon Concentrations in Gulf of Mexico Fishes, Post-Deepwater Horizon. *Transactions of the American Fisheries Society* **2014**, *143* (4), 1084–1097.

4. Kreitsberg, R.; Zemit, I.; Freiberg, R.; Tambets, M.; Tuvikene, A. Responses of Metabolic Pathways to Polycyclic Aromatic Compounds in Flounder Following Oil Spill in the Baltic Sea near the Estonian Coast. *Aquatic Toxicology* **2010**, *99* (4), 473–478.

5. Lin, E. L. C.; Cormier, S. M.; Racine, R. N. Synchronous Fluorometric Measurement of Metabolites of Polycyclic Aromatic Hydrocarbons in the Bile of Brown Bullhead. *Environmental Toxicology and Chemistry* **1994**, *13* (5), 707–715.

6. Fuentes-Rios, D.; Orrego, R.; Rudolph, A.; Mendoza, G.; Gavilán, J. F.; Barra, R. EROD Activity and Biliary Fluorescence in Schroederichthys Chilensis (Guichenot 1848): Biomarkers of PAH Exposure in Coastal Environments of the South Pacific Ocean. *Chemosphere* **2005**, *61* (2), 192–199.

7. Franklin, H. B. *The Most Important Fish In The Sea*, 2nd ed.; Shearwater, 2008.

8. Del Rio, R.; Bargu, S.; Baltz, D.; Fire, S.; Peterson, G.; Wang, Z. Gulf Menhaden (Brevoortia Patronus): A Potential Vector of Domoic Acid in Coastal Louisiana Food Webs. *Harmful Algae* **2010**, *10* (1), 19–29.

9. McMillin, J. B.; Bick, R. J.; Benedict, C. R. Influence of Dietary Fish Oil on Mitochondrial Function and Response to Ischemia. *Am. J. Physiol.* **1992**, *263* (5 Pt 2), H1479-1485.

10. Neff, J. M. *Polycyclic Aromatic Hydrocarbons in the Aquatic Environment: Sources, Fates, and Biological Effects*; Applied Science Publishers, 1979.

11. Chopra, S. *Extending the Limits of Solid Phase Microextraction*, 1st ed.; Seton Hall University Dissertations and Theses: Seton Hall University, 2014.

12. Krahn, M. M.; Ylitalo, G. M.; Buzitis, J.; Bolton, J. L.; Wigren, C. A.; Chan, S.-L.; Varanasi, U. Analyses for Petroleum-Related Contaminants in Marine Fish and Sediments Following the Gulf Oil Spill. *Marine Pollution Bulletin* **1993**, *27*, 285–292.

13. Jewett, S. C.; Dean, T. A.; Woodin, B. R.; Hoberg, M. K.; Stegeman, J. J. Exposure to Hydrocarbons 10 Years after the Exxon Valdez Oil Spill: Evidence from Cytochrome P4501A Expression and Biliary FACs in Nearshore Demersal Fishes. *Marine Environmental Research* **2002**, *54* (1), 21–48.

14. Jung, J.-H.; Kim, M.; Yim, U. H.; Ha, S. Y.; An, J. G.; Won, J. H.; Han, G. M.; Kim, N. S.; Addison, R. F.; Shim, W. J. Biomarker Responses in Pelagic and Benthic Fish over 1 Year Following the Hebei Spirit Oil Spill (Taean, Korea). *Marine Pollution Bulletin* **2011**, *62* (8), 1859–1866.

15. Trisciani, A.; Corsi, I.; Torre, C. D.; Perra, G.; Focardi, S. Hepatic Biotransformation Genes and Enzymes and PAH Metabolites in Bile of Common Sole (Solea Solea, Linnaeus, 1758) from an Oil-Contaminated Site in the Mediterranean Sea: A Field Study. *Mar. Pollut. Bull.* **2011**, *62* (4), 806–814.

16. Kim, M.; Yim, U. H.; Hong, S. H.; Jung, J.-H.; Choi, H.-W.; An, J.; Won, J.; Shim, W. J. Hebei Spirit Oil Spill Monitored on Site by Fluorometric Detection of Residual Oil in Coastal Waters off Taean, Korea. *Marine Pollution Bulletin* **2010**, *60* (3), 383–389.

17. Ferretto, N.; Tedetti, M.; Guigue, C.; Mounier, S.; Redon, R.; Goutx, M. Identification and Quantification of Known Polycyclic Aromatic Hydrocarbons and Pesticides in

Complex Mixtures Using Fluorescence Excitation–emission Matrices and Parallel Factor Analysis. *Chemosphere* **2014**, *107*, 344–353.

18. Zhou, Z.; Guo, L.; Shiller, A. M.; Lohrenz, S. E.; Asper, V. L.; Osburn, C. L. Characterization of Oil Components from the Deepwater Horizon Oil Spill in the Gulf of Mexico Using Fluorescence EEM and PARAFAC Techniques. *Marine Chemistry* **2013**, *148*, 10–21.

19. Pena, E. A.; Ridley, L. M.; Murphy, W. R.; Sowa, J. R.; Bentivegna, C. S. Detection of Polycyclic Aromatic Hydrocarbons (PAHs) in Raw Menhaden Fish Oil Using Fluorescence Spectroscopy: Method Development. *Environmental Toxicology and Chemistry* **2015**, *34* (9), 1946–1958.

20. Aas, E.; Beyer, J.; Goksoyr, A. Fixed Wavelength Fluorescence (FF) of Bile as a Monitoring Tool for Polyaromatic Hydrocarbon Exposure in Fish: An Evaluation of Compound Specificity, Inner Filter Effect and Signal Interpretation. *Biomarkers* **2000**, *5* (1), 9–23.

21. Rey-Salgueiro, L.; Martínez-Carballo, E.; García-Falcón, M. S.; González-Barreiro, C.; Simal-Gándara, J. Occurrence of Polycyclic Aromatic Hydrocarbons and Their Hydroxylated Metabolites in Infant Foods. *Food Chemistry* **2009**, *115* (3), 814–819.

22. Rey-Salgueiro, L.; García-Falcón, M. S.; Martínez-Carballo, E.; Simal-Gándara, J. Effects of Toasting Procedures on the Levels of Polycyclic Aromatic Hydrocarbons in Toasted Bread. *Food Chemistry* **2008**, *108* (2), 607–615.

23. Elcoroaristizabal, S.; de Juan, A.; García, J. A.; Durana, N.; Alonso, L. Comparison of Second-Order Multivariate Methods for Screening and Determination of PAHs by Total Fluorescence Spectroscopy. *Chemometrics and Intelligent Laboratory Systems* **2014**, *132*, 63–74.

24. Ariese, F.; Kok, S. J.; Verkaik, M.; Gooijer, C.; Velthorst, N. H.; Hofstraat, J. W. Synchronous Fluorescence Spectrometry of Fish Bile: A Rapid Screening Method for the Biomonitoring of PAH Exposure. *Aquatic Toxicology* **1993**, *26* (3), 273–286.

25. García-Falcón, M. S.; Soto-González, B.; Simal-Gándara, J. Evolution of the Concentrations of Polycyclic Aromatic Hydrocarbons in Burnt Woodland Soils. *Environmental Science & Technology* **2006**, *40* (3), 759–763.

26. Pérez-Gregorio, M. R.; García-Falcón, M. S.; Martínez-Carballo, E.; Simal-Gándara, J. Removal of Polycyclic Aromatic Hydrocarbons from Organic Solvents by Ashes Wastes. *Journal of Hazardous Materials* **2010**, *178* (1–3), 273–281.

Introduction

Fluorescence is the emission of photons from electronically excited states that have the same spin state as the ground state. Electronic transitions occur in the ultra-violet (UV), visible, and near-infrared (NIR) spectra regions.[1] The Perrin-Jablonski diagram (often called the Jablonski diagram) is a simplified picture showing these electronic transitions and their associated vibrational levels (Figure 1).[2] The Jablonski diagram however neglects rotational levels related to vibrational levels which are impossible to resolve in solution. Most compounds have a broad absorption spectrum except for those whose structures are restricted, like aromatic compounds. The rigidity and symmetry of many polyaromatic hydrocarbons often yields a structured fluorescence spectrum.
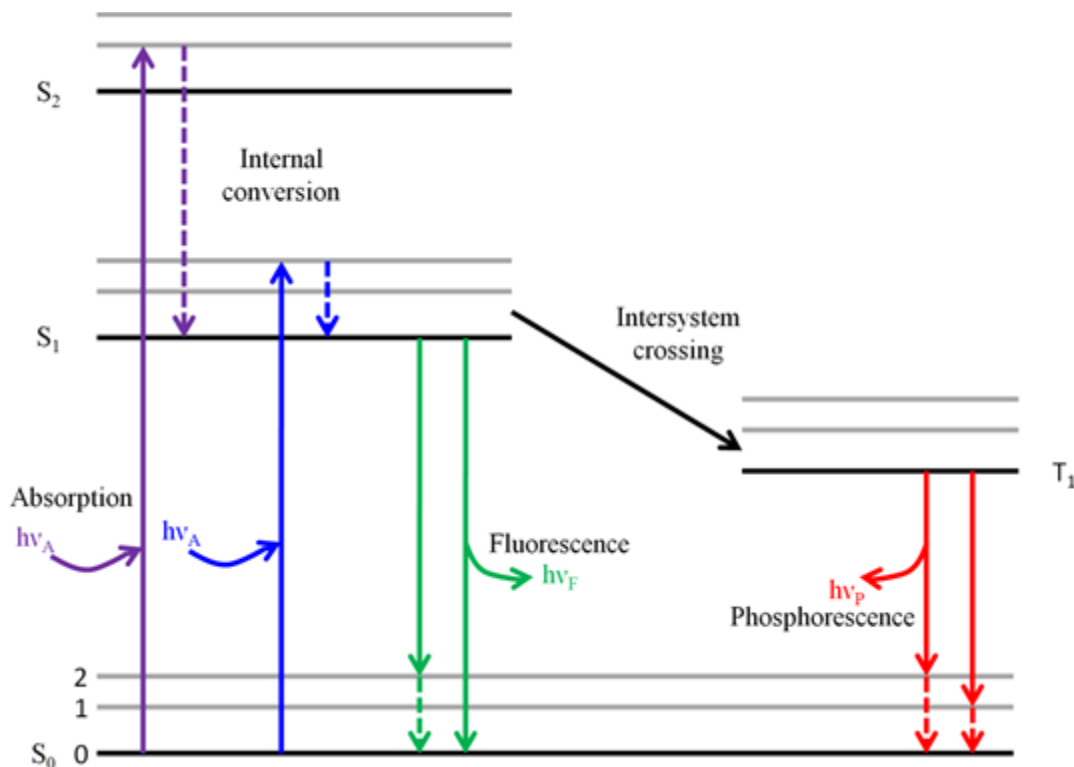
Figure1: Perrin-Jablonski diagram.[2]

Absorption of light by a molecule results in the promotion of an electron in the singlet ground state, S^0, to higher energy excited singlet states (S^1, S^2, ect.).[3] Once a molecule has absorbed

8

energy and has reached a higher electronic level, the molecule can quickly lose this excess energy via several mechanisms. The excited electron can fall back to the ground state via emission of a photon. If this process takes place for all the molecules that absorbed light, then the quantum efficiency of the solution will be a maximum, unity. If, however, any other route is followed, the quantum efficiency will be less than one and may even be almost zero.[3] Most organic compounds follow Kasha's Rule. Kasha's Rule states that absorption can occur to several excited singlet states, S^1, S^2, S^3, etc. However, any photoinduced processes occur from the lowest singlet state, S^1 back to the ground state S^0.[4]

The photophysics of a molecule are best described as a series of reactions and associated rates. The first step is absorption

$$M + h\nu \rightarrow M^* \qquad\qquad I_a$$

This rate is expressed as the intensity of light absorbed, I_a. The absorption occurs between the ground state, which in organic compounds is virtually always a singlet state, to one of several excited singlet electronic states. Normally this absorption terminates in an excited vibrational state of the electronic excited states. The system quickly relaxes to the lowest energy electronic and vibrational excited state through the process of internal conversion, with the emission of heat. The lowest energy electronic excited state can then relax through one of several paths.

$$M^* \rightarrow M + h\nu' \qquad\qquad k_r \text{ (fluorescence)}$$

$$M^* \rightarrow M + \text{heat} \qquad\qquad k_{nr} \text{ (non-radiative decay)}$$

$$M^* + Q \rightarrow \text{products} \qquad\qquad k_q \text{ (excited state quenching)}$$
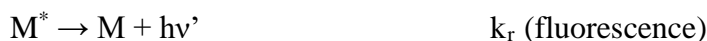
Other possible pathways exist (intersystem crossing, etc.) but they are not significant for this study. The radiative quantum yield, Φ_r, can be expressed as a ratio of the radiative rate to the sum of all the other rates

$$\Phi_r = \frac{k_r}{\sum k}$$

Fluorophores or fluorochromes are compounds that decay mainly by the radiative pathway. Most organic fluorophores are aromatic with the exception of a few highly unsaturated aliphatic compounds. Increasing the degree of conjugation leads to a shift of the absorbance

9

spectra to longer wavelengths.[5] Examples of this conjugation rule can be seen in the first four members of the oligoacene series (naphthalene, anthracene, tetracene, and pentacene (Figure 2)). Absorption bands can be seen at approximately 310, 375, 470, and 585 nm respectively while each compound then emits fluorescence in the ultraviolet, violet, green, and red respectively.[1]

naphthalene

anthracene

tetracene

pentacene
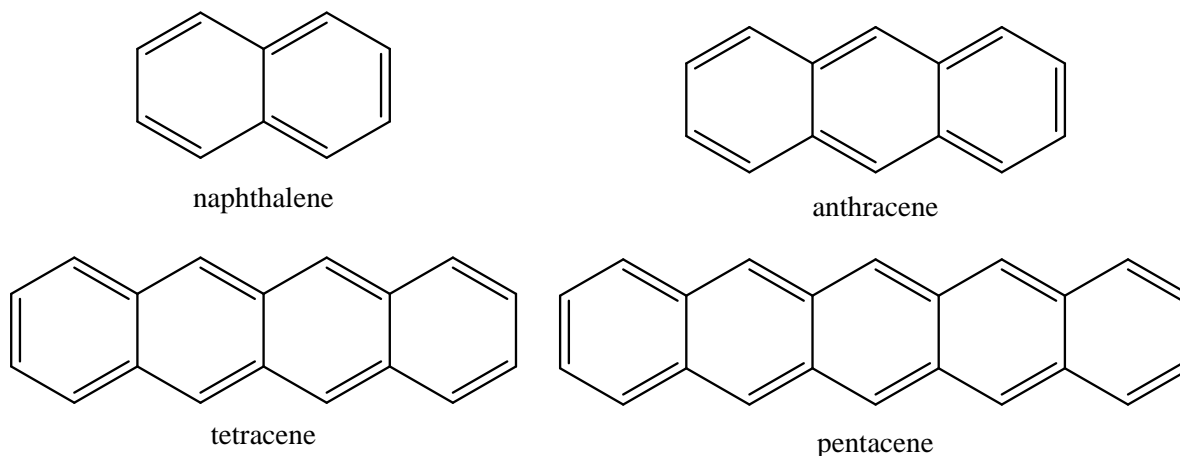
Figure 2: First four compounds of the oligoacene series of aromatic compounds.

Substitution on a fluorophore by chemical groups like –OH (electron donating group), changes the molar absorption coefficient and shifts the energy of the absorption and fluorescence spectra, an effect known as auxochromic effect. Furthermore, compared to parent PAH spectra, substituted compound spectra appear broad and unstructured. This can be seen when comparing 1– and 2 – naphthol with naphthalene.[1]

Solvents are well known to influence reaction rates and chemical equilibria, but they can also influence the spectral bands observed during fluorescence spectroscopy. Shifts in absorption and emission bands called solvatochromatic shifts, are caused by changes in solvent nature or composition mainly polarity. A bathochromatic (red) shift or hyspochromatic (blue) shift relates to positive and negative solvatochromism correspondingly with increasing solvent polarity.[6] Shifts result from interactions of the dipole moment of the fluorophore with the reactive fields induced in the solvent. The excited states of aromatic compounds posses dipole moments (μ^*) which are greater than in the ground state (μ).[5] Photons absorbed by the fluorophore results in

the creation of a dipole which disturbs the solvent environment causing it to reorganize the cage surrounding the fluorophore, a process called solvent relaxation.[7]

Fluorophores possess several factors that help to distinguish them including adherence to the Beer-Lambert Law in absorption, linearity of the fluorescence intensity with concentration and fluorescence quantum yields. The Beer-Lambert Law predicts that optical intensity (absorbance) is directly proportional to the concentration of the absorbing compound and is calculated using Equation 1. Deviations from the Beer-Lambert Law can be caused by both instrumental and fundamental factors. As long as the concentration is such that the absorbance is in the range of 0.01 to 1.0, instrument factors are largely minimized. The most common fundamental factor in deviation from the Beer-Lambert Law is aggregation of the analyte at higher concentrations. The terms in the equation are as follows: A stands for absorbance, measured directly from the instrumentation, ε stands for the molar absorptivity of the molecule (and is distinct for different compounds), c stands for the concentration of the compound, and l stands for the path length of the cell used in the study and is usually a 1 cm cuvette.

$$A = \varepsilon \times c \times l$$

Equation 1: Beer-Lambert Law

In fluorescence if the absorbance of the compound is high, the emitted light that reaches a detector is attenuated by the inner filter effect. Minimization of this effect occurs when low concentrations of compounds are analyzed.[5] It can be more fully mitigated through mathematically adjusting for sample absorbance.

Fluorescence quantum yields (Φ_f) can also be thought of as the ratio of the number of emitted photons over the number of absorbed photons and can be affected by both temperature and solvent. Quantum yields can be determined by using a comparative method that involves testing the sample and a known standard like fluorescein or quinine at identical absorbance and excitation wavelengths and is shown in detail in Equation 2.[8,9]

11

$$\phi_{f(c)} = \phi_{f(s)} \left(\frac{A_{(s)}}{A_{(c)}}\right) \left(\frac{\eta_{(c)}}{\eta_{(s)}}\right)^2 \left(\frac{P_{(c)}}{P_{(s)}}\right)$$

Equation 2: Equation used for determining the fluorescence quantum yield of a compound where Φ_f = quantum yield, A = absorbance, η = refractive index of solvent, P = area under emission spectra, s = reference standard. c = compound of study

Fluorophores can create three related spectra: absorbance, emission and excitation. Absorbance spectra measure particular wavelengths where a molecule can absorb light between the ultraviolet and visible region (190 – 380 nm and 380 – 750 nm respectively).[10] Excitation spectroscopy, in contrast, measures the wavelengths of light necessary to produce fluorescence from the molecule. Remembering how absorbance is calculated using Beer-Lambert Law ($\log_{10}(I_t/I_0$, where I_t is the intensity of the light transmitted and I_0 is the incident intensity)) and that excitation spectrum intensity is proportional to the number of photons absorbed, peaks in absorbance and excitation spectra will not have the same peak intensities. However, they will appear at the same wavelengths.[4] Emission spectroscopy measures the intensity of emission of the photons as the excited electron relaxes from the excited state to the ground state as a function of a particular excitation wavelength. The vibrational levels are similar in the ground and excited states, so that emission spectrum is the approximate "mirror" image of the absorption spectrum in highly rigid molecules.[1] More flexible molecules will have a variety of structural processes that broaden the emission bands. The shape of the emission spectrum will remain the same regardless of the excitation wavelengths, however, the intensity of the emission spectrum will change with different excitation wavelengths.[11]

There are several rules and tendencies that emission spectra follow. One of these rules comes from physicist and mathematician Sir George Gabriel Stokes. His theory coined Stokes' rule states that the wavelength of emission should always be higher than that of absorbance.[1] Stokes shift ($\Delta\bar{v}$) is the energy difference (gap) between the maximum of the first absorption band ($\overline{v_a}$) and the maximum emission band ($\overline{v_f}$) and is measured in wavenumbers (cm^{-1}).[5] The

12

Stokes shift can be calculated using Equation 3 and an example can be seen in Figure 3.[12] The detection of a fluorescent compound is easiest when the Stokes shift is larger as the emission spectra are more separated from the incident light.

$$\Delta \bar{\nu} = \overline{\nu_a} - \overline{\nu_f}$$

Equation 3: Equation used to determine Stokes Shift.[1]
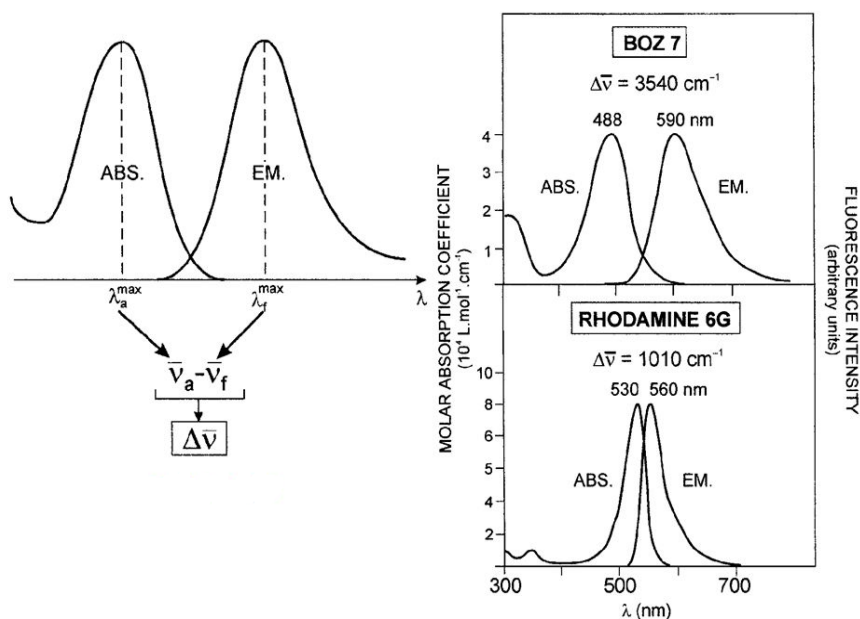
Figure 3: Definition and example of the Stokes Shift. [1, 11]

One complication that emission spectrum have is light scattering effects. When a beam of light interacts with a molecule, part of it is transmitted, part of it is reflected and part of it is scattered. Light scattering effects can be elastic or inelastic and are called Rayleigh and Raman scattering, respectively. Rayleigh scattering is most common and can occur on first and second order degrees. First order Rayleigh scatter is due to the sample elastically scattering the incident light, and is an issue when the emission monochromator is tuned close to the excitation monochromator. Second order Rayleigh scatters occurs for the same reason at a wavelength twice that of the excitation wavelength (Figure 4).[13] It is due to the use of diffraction gratings to

monochromatize the excitation light. Raman scattering in fluorescence is due to inelastic solvent scatter and occurs at a constant wavenumber difference from the excitation wavelength (Figure 4). Raman bands appear to the long wavelength side of the Rayleigh bands at wavelengths due to the solvent principle vibrations. Water appears at 3600 cm^{-1} lower wavenumber than the exciting light. Highly fluorescent samples generally overpower this peak and Raman scattering band can be proven by changing excitation wavelengths.[5]
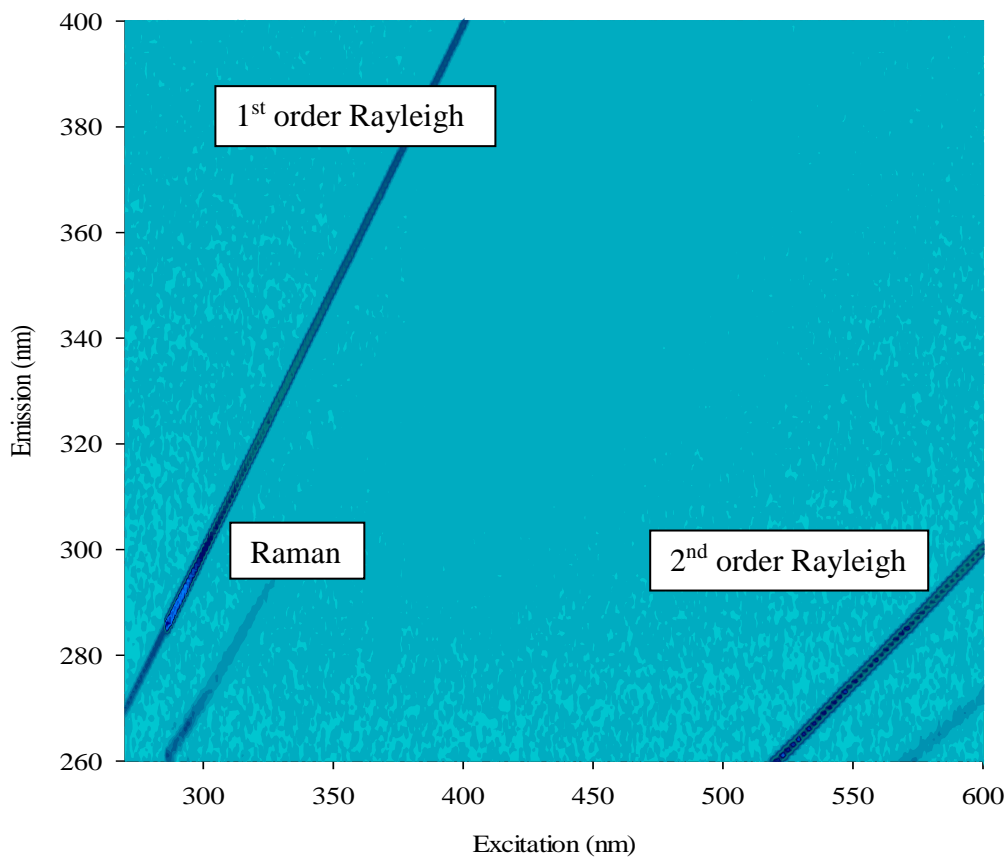
Figure 4: Example of first and second order Rayleigh and Raman scattering in excitation-emission spectroscopy (vide infra).

Traditionally fluorescence spectroscopy is performed two – dimensionally as either an emission spectrum at a fixed excitation wavelength and scanning the emission wavelength, or synchronous scanning at a constant offset wavelength both the excitation and emission

wavelengths. Fluorescence data is a moderately straightforward technique but the use of two –

dimensional spectrum is limited as many researchers will only tabulate one, two, or three data

points from the emission spectrum. More recently, researchers are using the three – dimensional

excitation – emission matrix (EEM) spectroscopy analysis of their samples, emission spectrum

as a function of a range of excitation wavelengths.[14] Fluorescence EEMs are now a method used

for the characterization of organic matter from aqueous environments.[15] The EEMs technique is

a rapid, non-invasive, and accurate investigative tool for a wide variety of media.[16, 17]

Fluorescence is a highly sensitive method, particularly due to the absence of a

background signal. One simply detects the photons emitted by the sample per second. Basically,

if there is no sample emission, there is no signal (apart from electronic noise). Contrast this with

absorption spectroscopy, where one is determining the difference between transmitted and

incident light. Figure 5 is a general schematic of a fluorescence spectrofluorometer. Fluorescence

begins with an exciting light source, usually a xenon arc lamp, chosen because it produces high

intensity light from the ultraviolet to the near infrared spectral region.[18] Single – grating

monochromators are used for choosing both excitation and emission wavelengths and are

motorized for automatic scanning of wavelengths.[19] A monochromator works by selecting

specific wavelengths from the broadband xenon arc lamp radiation. Most monochromators use

diffraction gratings. White light shining onto a diffraction grating is reflected while being split

into individual wavelengths, much like a prism. Rotation of the diffraction grating relative to a

set of narrow slits allows for the passage of near monochromatic wavelengths of light.[20] Slits are

used to control the bandwidth of light exiting the monochromator. Some instruments are

equipped with dual or triple monochromators to yield more monochromatic light and reject

Rayleigh scattering more efficiently.

A sample compartment is placed between the excitation and emission monochromator,

and used to perform several functions. First, it holds the sample in such a way so that excitation

energy can be directed onto the sample, and allows for the collection of emission signal either at

right angles or at small angles to the exciting light source. A thin quartz plate beam splitter

reflects ca 4 % of the exciting light towards a photodiode.[5] The signal from this photodiode is used to compensate for time or wavelength fluctuations in lamp intensity. By calculating a ratio of output signals of the sample to the reference detector, the spectrum can be corrected for time or wavelength fluctuations of the excitation energy.[1] The emission monochromator has the same structure as the excitation monochromator, and wavelength selects the emission light.

Once a signal has passed through the emission monochromator, it is sent to a photomultiplier tube (PMT). A PMT is a signal amplifier and is a current source. A terminating resistor of 50 ohms is typically used to convert the photocurrent to voltage. Photomultiplier tubes are able to amplify very weak signals by as much as 10^9, and can have background signals (with proper cooling) as low as 1-5 counts per second.[5] Signals are sent to a detection system that counts the photons passing through the emission monochromator.
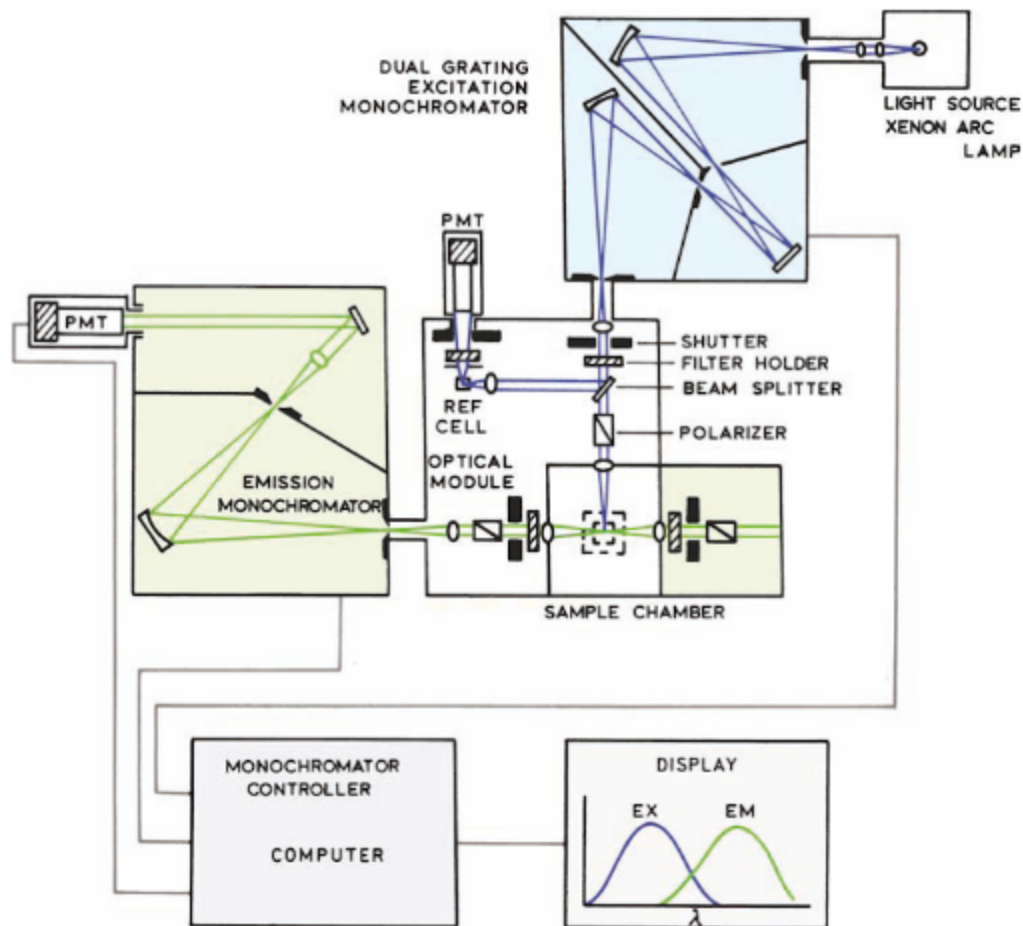
Figure 5: Schematic of a typical fluorescence spectrofluorometer.[5]

Fluorescence spectroscopy utilizes cuvettes or microwell plates as sample holders. Typical cuvettes for fluorescence are made of fused silica (quartz) with four polished windows and in a variety of shapes and sizes. Special treatments or quartz materials are used to change the measurable range of fluorescence from as low as 170 nm up to 2700 nm. Typical fluorescence cuvettes have a path length of 10 mm and hold approximately 3.5 mL, however path lengths can range from 1mm – 40 mm and can hold volumes of 1.7 mL – 14 mL.[23] Cuvettes can be a problem if sample volume is small. Microwell plates can work with much smaller volumes as well as more than once sample. Typical microwell plates are made of polystyrene. Plates come in a variety of colors and hold 96 – 1536 samples at a single time. The bottom of the plate can be

17

made of polystyrene or glass. Well shapes can vary as well from circular to square and volume of sampled used in in the micro-liter (μL) range.[24] Selection of plates depends on the experiment of choice.

Depending on the type of spectrofluorometer in use, one can add additional components for more complex fluorescence experiments. One of these additions is a microwell plate reader (Figure 6).[21] Current fluorescence experiments are moving from single samples to multiple samples for high-throughput screening.[22] The optics used in microwell plate readers is slightly different from that used for a standard cuvette. Figure 7 shows a cartoon of the fiber optic cable assembly and instrument arrangement used.[21] Microwell plates must remain horizontal, and it is not possible to use right-angle observation as can be used with a cuvette. The exciting light is directed by a mirror into a fiber-optic bundle going to the sample. Typically, the microplate is moved to position each well in the observation path by an x–y scanning stage. Returning signal from the sample is focused on a second mirror before entering the emission monochromator.[21] Programming of the instrument can allow the user to choose certain methods to be performed on certain wells.
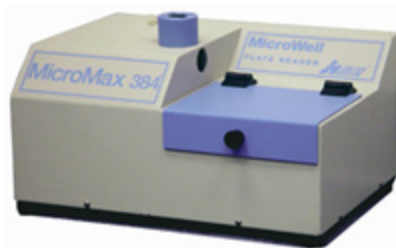
Figure 6: Example of a microwell plate reader.[21]
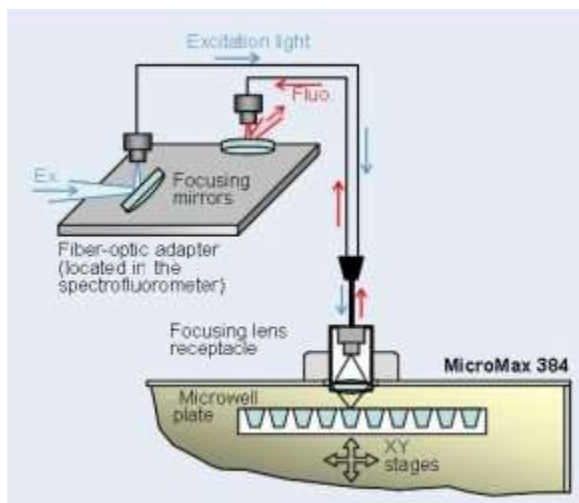
Figure 7: Optics used in a microwell plate reader.[21]

Several statistical methods are used to provide information on the precision and accuracy of the measurements and technical advantages of one instrumental method over another. Some of these statistical methods include linear regression, limits of detection, and limits of quantitation. Linear regression of a calibration curve (signal vs concentration) provides the correlation coefficient, slope and intercept of the data. The correlation coefficient (r^2) of a sample is based on a -1 to 1 scale. Zero indicates that the data has no correlation while one or negative one means "perfect" positive or negative correlation respectively and is determined by Equation 4 via computer. The slope represents the response factor for the measurement. The intercept in most instrumental methods should be $y = 0$ for $x = 0$, since x is typically concentration, however due to constraints of instrumentation and preparation of samples, the intercept can drift from this ideal value.[25] Using the data from a linear regression, one can determine the limit of detection (LOD) and the limit of quantitation (LOQ). The LOD is the lowest concentration of a compound that can be detected for a given sample, instrument and method, while LOQ is the lowest concentration of a compound that can be reliably detected with confidence (quantitated). Both LOD and LOQ are a measure of the ratio of signal – to – noise and generally the LOD is lower than the LOQ, but in some cases they may be equal.[26] Equations 5 and 6 are used to determine the LOD and LOQ from linear regression and are based on the blank signal and standard

19

deviations of the slope.[25] These equations are complex, therefore a computer program can be used to solve for all variables. LOD and LOQ determined from these equations are signal intensities that can then be converted to concentrations using slope and intercept.

$$r = \frac{\sum_i[(x_i - \bar{x})(y_i - \bar{y})]}{\{[\sum_i(x_i - \bar{x})^2]\,[\sum_i(y_i - \bar{y})^2]\}^{1/2}}$$

Equation 4: Correlation coefficient.[25]

$$LOD = y_B + 3\,\frac{\sqrt{\dfrac{\sum_i(y_i - \hat{y}_i)^2}{n - 2}}}{\sqrt{\sum_i(x_i - \bar{x})^2}}$$

Equation 5: Limit of detection.[25]

$$LOQ = y_B + 10\,\frac{\sqrt{\dfrac{\sum_i(y_i - \hat{y}_i)^2}{n - 2}}}{\sqrt{\sum_i(x_i - \bar{x})^2}}$$

Equation 6: Limit of quantitation.[25]

References

1. Valeur, B.; Berberan-Santos, M. *Molecular Fluorescence: Principles and Applications*, 1st ed.; Wiley-VCH, 2013.

2. http://nptel.ac.in/courses/102103044/module2/lec6/1.html (accessed Apr 9, 2018).

3. UV-Vis Luminescence Spectroscopy - Theory https://teaching.shu.ac.uk/hwb/chemistry/tutorials/molspec/lumin1.htm (accessed Mar 12, 2018).

4. Williams, A. T. R.; Winfield, S. A.; Miller, J. N. Relative Fluorescence Quantum Yields Using a Computer-Controlled Luminescence Spectrometer. *Analyst* **1983**, *108* (1290), 1067–1071.

5. Lakowicz, J. *Principles of Fluorescnece Spectroscopy*, 1st ed.; Plenum Press: New York, 1983.

6. Suppan, P. Invited Review Solvatochromic Shifts: The Influence of the Medium on the Energy of Electronic States. *Journal of Photochemistry and Photobiology A: Chemistry* **1990**, *50* (3), 293–330.

7. Mataga, N.; Kaifu, Y.; Koizumi, M. Solvent Effects upon Fluorescence Spectra and the Dipolemoments of Excited Molecules. *BCSJ* **1956**, *29* (4), 465–470.

8. Horiba Scientific. A Guide to Recording Fluorescence Quantum Yields.

9. Carmona, N. A.; Cohen, B.; Organero, J. A.; Douhal, A. Excited State Intermolecular Proton and Energy Transfer of 1-Hydroxypyrene Interacting with the Human Serum Albumin Protein. *Journal of Photochemistry and Photobiology A: Chemistry* **2012**, *234*, 3–11.

10. UV-Visible Spectroscopy https://www2.chemistry.msu.edu/faculty/reusch/virttxtjml/spectrpy/uv-vis/spectrum.htm (accessed May 15, 2017).

11. Geddes, C. D. *Reviews in Fluorescence 2016*; Springer, 2017.

12. Fery-Forgues, S.; Le Bris, M. T.; Mialocq, J. C.; Pouget, J.; Rettig, W.; Valeur, B. Photophysical Properties of Styryl Derivatives of Aminobenzoxazinones. *The Journal of Physical Chemistry* **1992**, *96* (2), 701–710.

13. Rinnan, Å.; Booksh, K. S.; Bro, R. First Order Rayleigh Scatter as a Separate Component in the Decomposition of Fluorescence Landscapes. *Analytica Chimica Acta* **2005**, *537* (1–2), 349–358.

14. Chen, W.; Westerhoff, P.; Leenheer, J. A.; Booksh, K. Fluorescence Excitation−Emission Matrix Regional Integration to Quantify Spectra for Dissolved Organic Matter. *Environmental Science & Technology* **2003**, *37* (24), 5701–5710.

15. Bieroza, M.; Baker, A.; Bridgeman, J. Exploratory Analysis of Excitation–emission Matrix Fluorescence Spectra with Self-Organizing Maps—A Tutorial. *Education for Chemical Engineers* **2012**, *7* (1), e22–e31.

16. Senesi, N.; Miano, T. M.; Provenzano, M. R.; Brunetti, G. CHARACTERIZATION, DIFFERENTIATION, AND CLASSIFICATION OF HUMIC SUBSTANCES BY FLUORESCENCE SPECTROSCOPY. *Soil Science* **1991**, *152* (4), 259.

17. Coble, P. G. Characterization of Marine and Terrestrial DOM in Seawater Using Excitation-Emission Matrix Spectroscopy. *Marine Chemistry* **1996**, *51* (4), 325–346.

18. Xenon (Xe) Arc Lamps https://www.newport.com/f/xenon-arc-lamps (accessed Mar 18, 2018).

19. Fluorolog, T. "The Modular Fluorolog Can Grow with Your Needs, Adding Capabilities as Your Changing Research Calls for It.". 20.

20. Monochromators : SHIMADZU (Shimadzu Corporation) https://www.shimadzu.com/an/uv/support/fundamentals/monochromators.html (accessed Mar 19, 2018).

21. Fluorescence Microwell Plate Reader | MicroMax 384 from HORIBA scientific - HORIBA http://www.horiba.com/scientific/products/fluorescence-

spectroscopy/accessories/details/micromax-384-microwell-plate-reader-542/ (accessed Mar 20, 2018).

22. Collins, L. A.; Torrero, M. N.; Franzblau, S. G. Green Fluorescent Protein Reporter Microplate Assay for High-Throughput Screening of Compounds Against Mycobacterium Tuberculosis. *Antimicrob. Agents Chemother.* **1998**, *42* (2), 344–347.

23. Fluorometer Cells, Standard Rectangular, Stopper Top, Starna http://www.starnacells.com/d_cells_f/T023.html (accessed Mar 20, 2018).

24. Nunc Plate Selection Guide https://www.thermofisher.com/us/en/home/life-science/cell-culture/cell-culture-plastics/nunc-plate-selection-guide.html (accessed Mar 20, 2018).

25. Miller, J. N.; Miller, J. C. *Statistics and Chemometrics for Analytical Chemistry*, 4th ed.; Pearson Education, 2000.

26. Meier, P. C.; Zund, R. E. *Statistical Methods in Analytical Chemistry*, Second.; John Wiley & Sons Inc.: Canada, 200AD.

Chapter 3

Experimental and Instrumental Design

I.   Materials

Standard solutions were prepared in 75 % ethanol (Koptec, 200 Proof Pure, CAS # 64 – 17 – 5, Lot # 07515, Health: 1, Flammability: 3, Reactivity: 0) and made from acenaphthene (Matheson, Coleman & Bell, CAS # 83 – 32 – 9, Lot # 12526, Health: 2, Flammability: 1, Reactivity: 0), anthracene (Aldrich, CAS # 120 – 12 – 7, Lot # 13704KG, Health: 0, Flammability: 1, Reactivity: 0), benzo[a]pyrene (TCI America, CAS # 50 – 32 – 8, Batch NPEZF – RA, Health: 3, Flammability: 0, Reactivity: 0), fluoranthene (TCI America, CAS # 206 – 44 – 0, Lot # FREGF – LN, Health: 1, Flammability: 1, Reactivity: 0), fluorene (TCI America, CAS # 86 – 73 – 7, Lot # YNV2D – SB, Health: 1, Flammability: 1, Reactivity: 0), naphthalene (Sigma Aldrich, CAS # 91 – 20 – 3, Lot # 14205KB, Health: 2, Flammability: 2, Reactivity: 0), 1 – naphthol (Alfa Aesar, CAS # 90 – 15 – 3, Lot # 10159725, Health: 2, Flammability: 1, Reactivity: 1), 2 – naphthol (TCI America, CAS # 135 – 19 – 3, Lot # TDJEF – HM, Health: 2, Flammability: 1, Reactivity: 0), phenanthrene (Sigma-Aldrich, CAS # 85 – 01 – 8, Lot # MKBG8322V, 36H2506, Health: 2, Flammability: 0, Reactivity: 0), 9 – phenanthrol (Acros Organics, CAS # 484 – 17 – 3, Lot # 19895001, Health: 0, Flammability: 0, Reactivity: 0), pyrene (Alfa Aesar, CAS # 129 – 00 – 0, Lot # 10172628, Health: 2, Flammability: 1, Reactivity: 1), and 1 – pyrenol (Sigma Aldrich, CAS # 15315 – 79 – 7, Lot # 06906MF, Health: 0, Flammability: 0, Reactivity: 0). See Appendix A for a list of all chemical structures.

Reference solutions were made from fluorescein (Alfa Aesar, CAS # 2321 – 07 – 5, Lot # 10172004, Health: 1, Flammability: 1, Reactivity: 1), quinine bisulfate (TCI America, CAS # 6119 – 70 – 6, Lot # 2CI0354, Health: 1, Flammability: 0, Reactivity: 0), sodium hydroxide (Spectrum, CAS # 1310 – 73 – 2, Lot # SV0303, Health: 3, Flammability: 0, Reactivity: 2), and sulfuric acid (Macron Fine Chemicals, CAS # 7664 – 93 – 9, Lot # 0000086316, Health: 3, Flammability: 0, Reactivity: 1).

Solutions for cuvette cleaning are made from sulfuric acid (Macron Fine Chemicals, CAS # 7664 – 93 – 9, Lot # 0000086316, Health: 3, Flammability: 0, Reactivity: 1), NOCHROMIX (Aldrich, Product # 328693, Lot # 04431CC, Health: 2, Flammability: 0, Reactivity: 1), and nitric acid (Macron Fine Chemicals, CAS # 7697 – 37 – 2, Health: 3, Flammability: 0, Reactivity: 1, oxidizer). A cuvette washer was used for all solution rinsing (Vakuwash® Cuvette Washer, Catalog # 58020 – 014).

All standard fluorescence spectroscopy was performed using standard quartz cuvettes (Starna Cell, Std Rect Fluorometer w/Stopper, Q, 10 mm, Catalog # 23 – Q – 10). Plated samples were performed in 96 microwell plates ((Corning Incorporated, Catalog # 3615, Corning 96 Well Black Special Optic), (Corning Incorporated, Catalog # 4580, 96 Well Half Area, Black with 0.2um Glass Bottom, Lot # 10614020, Lot # 30914007), and (ThermoScientific, Catalog #237105, Nunc F96 MicroWell Black Polystyrene Plate, Lot # 130803)). Plates were covered with Optical Adhesive Covers ((Life Technologies Corporation, Catalog # 4360954, Lot # 201501 347) and (VWR, Catalog # 60941 – 078, Lot # TSRT2VWR100)). Cuvettes, plates and adhesive covers were dried using Kimwipes (VWR, Catalog # 82003 – 820)

Solutions were prepared in 100 mL amber glass volumetric flasks (VWR, Catalog # 89090 – 530, low actinic, Lot # 55640 – 100). Dilutions of samples were prepared in either 12 mL amber vials (VWR Wheaton, Catalog # 97047 – 750, phenolic top, PTFE liner, Lot # 082113, Lot # 0000037695, Lot # 000024751), or 4 mL amber vials (Wheaton, Catalog # 224982, sample vial with rubber lined cap , Lot # 1566583) using automated pipettes (Gilson Pipetman (P 20, Catalog #F123600), Gilson Pipetman (P 100, Catalog # F123615), Labnet Labpette (P 200, Catalog # P3940 – 200), Gilson Pipetman (P 1000, Catalog # F123602), Eppendorf Research (P 1000, Catalog # 3120000062), and Gilson Pipetman (P 5000, Catalog # F123603)) and disposable sterile pipette tips (1000 µL (VWR, Catalog #83007 – 386, Lot # 5056 – 521C6 – 521B), 10 – 200 µL (VWR, Catalog # 53509 – 222, Lot # 4050 – 418C4 – 418AL), and 0.5 – 5.0 mL (VWR, Catalog # 89087 – 530, Lot # 527C6 – 527)). Samples were transferred to cuvettes from vials

using disposable pipettes (VWR, 7.5 mL non – sterile polyethylene graduated transfer pipettes, Catalog # 16001 – 188, Lot # 141025).

II. Sample Preparation

i. 75 % Ethanol

A 2.5 L solution was prepared at 75 % ethanol and 25 % de – ionized water using 200 proof ethanol purchased from Koptec. Using a 1000 mL (1 L) graduated cylinder (T.D. (to deliver)), 1,875 mL of 200 proof ethanol was poured into a 2.5 L glass container previously washed (using tap water, de – ionized water, and air dried). Added to the container was an additional 625 mL of de – ionized water using one of the same 1000 mL graduated cylinders used previously. This solution was used to prepare both stock solutions of compounds as well as dilutions. The solution used stood for a maximum of one month before being prepared again in the same condition.

ii. Stock Solutions

Stock solutions of PAHs were prepared at 0.1 mg/mL concentrations. For each 100 mL volumetric flask, 10 mg of compound was weighed on an analytical balance (calibrated February 28, 2011). The compound was added to the volumetric flask and approximately 100 mL of 75 % ethanol was added to the volumetric mark.

III. Instrumentation

i. UV – Vis

A Hewlett-Packard 8452A Diode Array UV – Vis spectrophotometer with 2 nm spectral resolution, with a deuterium lamp (range 200 nm - 800 nm) and a Cary 500 Scan UV – Vis – NIR spectrophotometer with 0.1 nm spectral resolution, with a deuterium lamp (200 – 350nm) or a tungsten lamp (350 – 1100nm) were used to measure and record absorption spectra. A quartz fluorescence cuvette was used to hold samples and referenced against an appropriate solvent blank. The HP spectrophotometer was controlled by a DELL PC with Olis Spectraworks (version 4.8.46) and the Cary 500 was controlled by a DELL PC using Cary WinUV Scan software (version 3.00(182)) supplied by the manufacturers.

ii. Fluorescence

A Horiba Scientific Fluorolog – 3 Research Spectrofluorometer (Part # FL3C – 11, 450W ozone free Xenon arc lamp, 1200 g/mm grating) was used for all emission, excitation, EEMs, quantum yields and LoD/LoQ experiments. The instrument includes a second optical channel to measure and correct for variations in lamp intensity. Attachments include a microwell plate reader (Part # Micromax – 384) and a Fiber Optic Platform Light (Part # FL – 3000). Data was recorded and displayed on Dell PC using FluorEssecnce (version 3.5), software supplied by the manufacturer. Software was also used to store data, control the instrument, and analyze raw data.

IV.   Instrumental Methods

i.   UV – Vis

UV – Vis spectra obtained on the HP 8452A were run at 2 nm intervals from 260 nm - 500 nm. Blank subtraction was provided in the software by first obtaining a spectra of 75 % ethanol. These spectra were used to obtain optimum excitation wavelengths of each PAH tested.

UV – Vis spectra obtained on the Cary 500 were run at 0.5 nm intervals, a scan rate of 0.5 seconds, and a range of 260 nm - 500 nm. Blank subtraction was also provided in the software by obtaining a spectra of 75 % ethanol. These spectra were used for calculation of quantum yields.

Ranges for UV – Vis spectra were determined based on the lamp profile of the Horiba Fluorolog – 3.

ii.   Emission

Optimum emission spectra were generated based on excitation wavelengths previously seen in UV – Vis spectra. Each peak was tested for maximum signal. Samples were collected every 1 nm with a peak integration time of 1 sec. Correction of spectra was completed using instrumentation factors provided in the software as well as a subtraction of blank spectra using the same parameters. Spectra was also normalized to a 0 - 1 scale based on highest and lowest peak height.

iii. Excitation

Optimum excitation spectra were generated based on emission wavelengths previously seen. Each peak was tested for maximum signal. Samples were collected every 1 nm with a peak integration time of 1 sec. Correction of spectra was completed using instrumentation factors provided in the software and subtraction of blank spectra using the same parameters. Lamp variations were also corrected for by dividing out the reference (lamp spectra) from the signal spectra. Spectra was also normalized to a 0 – 1 scale based on highest and lowest peak height.

iv. Excitation – Emission Matrices (EEMs)

Three – dimensional spectra were obtained using optimum emission and excitations scan parameters. Samples were collected every 1 nm in both emission and excitation ranges with a peak integration time of 0.1 sec for optimum resolution. Correction of spectra was completed using instrumentation factors provided in the software and subtraction of blank spectra using the same parameters. Lamp variations were also corrected for by dividing out the reference (lamp spectra) from the signal spectra.

v. MicroMax

The MicroMax microwell plate reader and its fiber optic attachment for delivery of excitation and emission signals was optimized. Optimization was determined by the position of the fiber optic cable relevant to well depth (similar to cuvette path length) and fill volume (sample volume placed in well) for a maximum emission signal. Optimization was determined using fluorescein.

vi. Limits of Detection and Quantitation

Limits of detection and quantitation were determined by calculating a standard curve of each compound. Concentration ranges depended on the overall quantum yield of the sample (i.e. a higher quantum yield sample used lower concentrations). Standard curves were produced based on highest emission peak intensity and each curve consisted of seven points. Microsoft Excel was employed for linear regression analysis. From the data observed here, Equation 5 and 6 on page 20 were used to determine the emission intensity associated with the limit of detection and

quantitation.[1] These intensities were converted to concentrations by subtracting the y – intercept from the limit of detection or quantification and dividing by the slope of the standard curve. After determining both concentrations, samples were prepared and tested to ensure proper calculation.

vii.   Quantum Yields

Quantum yields (Φ_f) were calculated relative to quinine bisulfate ($C_{20}H_{26}N_2O_6S$) in 0.5 M H_2SO_4, anthracene ($C_{14}H_{10}$) in 100 % ethanol, naphthalene ($C_{10}H_8$) in 100 % ethanol, phenanthrene ($C_{14}H_{10}$) in 100 % ethanol, pyrene ($C_{16}H_{10}$) in 100 % ethanol, and fluorene ($C_{13}H_{10}$) in 100 % ethanol based on Equation 3.[2,3]

V.   Cuvette Cleansing

Standard quartz fluorescence cuvettes were cleaned between sampling using one of three methods designed for optimization. Microwell plates were used once and did not requiring cleaning prior to disposal.

i.   Rinsing

Samples of same species but different dilutions were run using the same cuvette starting with lowest concentration. Between samples, cuvettes were cleaned by rinsing with solvent (75 % ethanol) two to three times and a final rise with de – ionized water.

ii.   NOCHROMIX

Between samples of different chemical species, cuvettes were cleaned by soaking in NOCHROMIX for a minimum of 8 hours. Cuvettes were then removed and soaked in de – ionized water for 1 hour, then removed and set to dry. Before use, cuvettes were rinsed with de – ionized water and 75 % ethanol.

iii.   Nitric Acid

Between samples of different chemical species, cuvettes were cleaned by soaking in a 50 % aqueous nitric acid for a minimum of 8 hours and a maximum of 24 hours. Cuvettes were removed and rinsed with de – ionized water using a cuvette cleaner. Again, cuvettes were soaked

in concentrated nitric acid for 1 hour. Cuvettes were removed and rinsed with de – ionized water, then set to dry. Before use, cuvettes were rinsed with de – ionized water and 75 % ethanol.

VI. Graphical Analyses

i. Excel

Raw data was transferred from Horiba software FluorEssence (version 3.5) to Microsoft Excel (Excel 2003-Excel 2013) for blank subtraction and emission/excitation clean-up (EEMs spectra only). Clean – up consisted of removal of first and second order Rayleigh scattering that may have occurred due to overlapping excitation and emission ranges during EEM collection.

ii. Sigma Plot

Clean data was transferred from Microsoft Excel to Sigma Plot (version 13.0) for graphical representation.

References

1. Miller, J. N.; Miller, J. C. *Statistics and Chemometrics for Analytical Chemistry*, 4th ed.; Pearson Education, 2000.

2. Dawson, W. R.; Windsor, M. W. Fluorescence Yields of Aromatic Compounds. *J. Phys. Chem.* **1968**, *72* (9), 3251–3260.

3. Valeur, B.; Berberan-Santos, M. *Molecular Fluorescence: Principles and Applications*; Wiley-VCH, 2013.

Chapter 4

Experimental Results and Discussion

I.   UV – Visible Spectra

The UV – Visible spectrum of the twelve compounds of study can be found in Figures 8 – 19 on pages 32 – 43. Absorbance values were not recorded below 260 nm since the xenon arc lamp used in the spectrofluorometer for the collection of emission spectra was ozone-free and began excitation at 250 nm. An absorption spectrum of each compound of study was necessary for determining the parameters for fluorescence studies. After measuring the absorption of each compound, a list of peak wavelengths was generated. Each peak wavelength shown in the absorption spectra was used as an excitation wavelength to generate emission spectra. The range of absorption for each compound was used to set the excitation wavelengths used to collect the EEMs. The emission spectra collected were used to set the emission wavelengths scanned to yield the EEMs. The UV – Vis spectra collected were compared to known UV – Vis data found in the literature.[1] This data allows assessment of any solvent effects, since current samples were dissolved in 75 % ethanol, which is an atypical solvent media. Absorption and emission spectra can show a wide variety of solvent effects, including no changes. Note that high resolution absorption spectra were not critical to this work and were only done to confirm excitation regions.
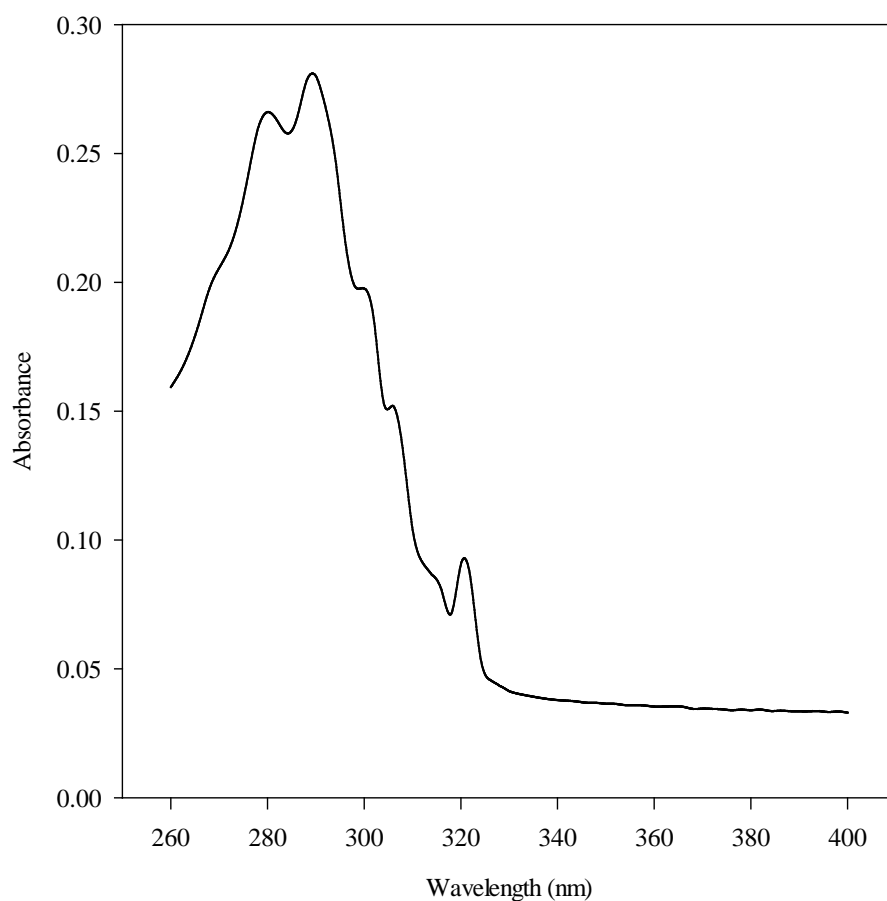
Figure 8: UV – Vis absorbance spectra of acenaphthene in 75 % ethanol.

When compared to the literature spectra using cyclohexane as a solvent, acenaphthene in 75 % ethanol (Figure 8) showed no differences in λ_{max} values. The spectrum was observed between 260 nm and 330 nm at a concentration of 0.005 mg/mL. Peaks can be seen at 280, 290, and 320 nm and shoulders are seen at 300 and 308 nm. The extinction coefficient for the maximum peak at 290 nm and an absorbance of 0.2800 is 9 x 10^3 M^{-1} cm^{-1}.
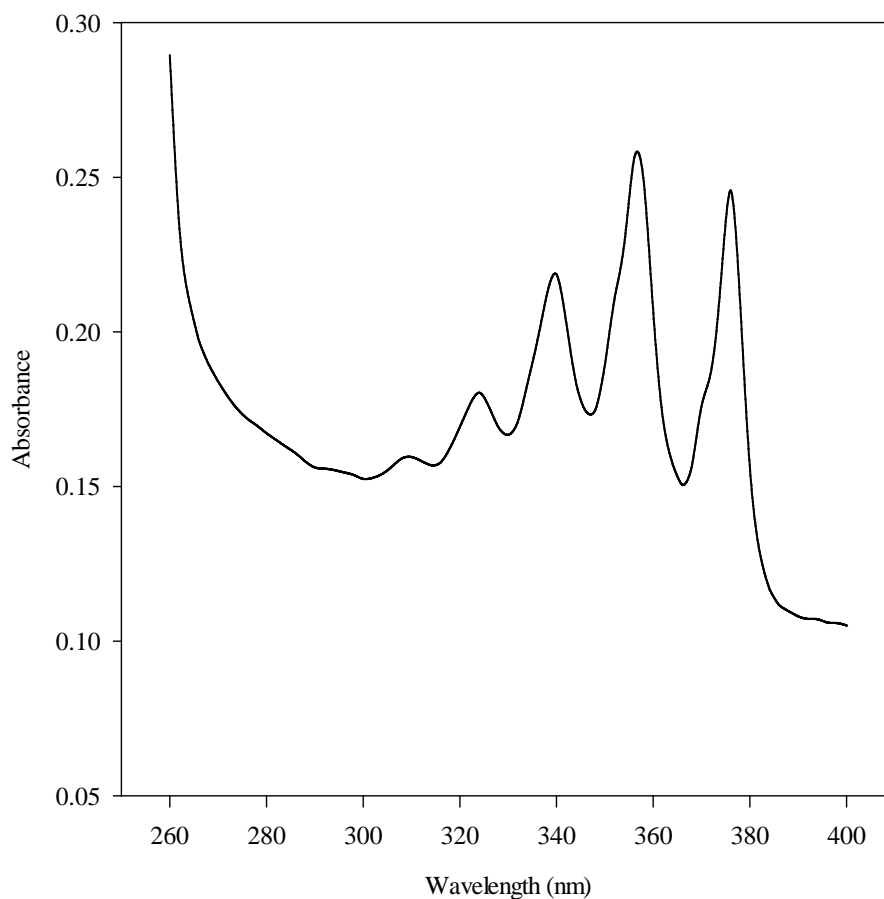
Figure 9: UV – Vis absorbance spectra of anthracene in 75 % ethanol.

When compared to the literature spectra using cyclohexane as a solvent, anthrancene in 75 % ethanol (Figure 9) showed no difference in λ_{max} values. The spectrum was observed between 300 nm and 400 nm at a concentration of 0.005 mg/mL. Peaks can be seen at 308, 324, 340, 356, and 374 nm. The extinction coefficient for the maximum peak at 356 nm and an absorbance of 0.2559 is 9 x 10^3 M^{-1} cm^{-1}.
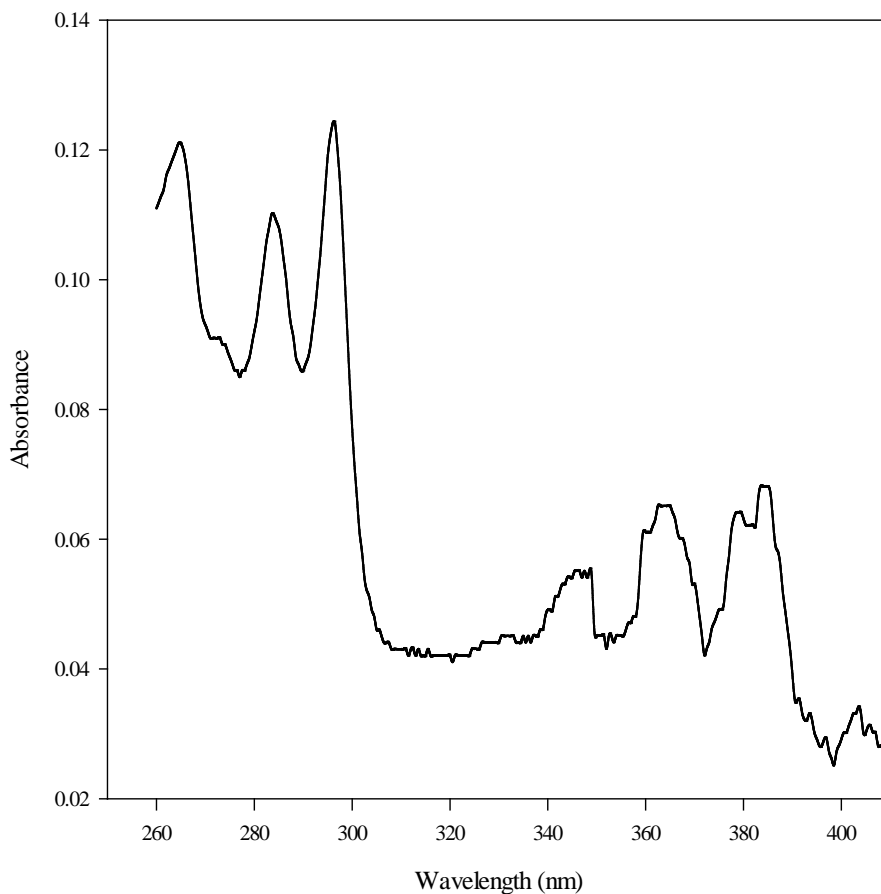
Figure 10: UV – Vis absorbance spectra of benzo [a] pyrene in 75 % ethanol.

When compared to the literature spectra using ethanol (100 %) as a solvent, benzo [a] pyrene in 75 % ethanol (Figure 10) showed no difference in λ_{max} values. The spectrum was observed between 260 nm and 310 nm at a concentration of 0.00002 mg/mL. Peaks can be seen at 264, 284, 296, 332, 348, 364, 378, and 384 nm and a shoulder at 278 nm. The extinction coefficient for the maximum peak at 296 nm and an absorbance of 0.1240 is 6 x 10^3 M^{-1} cm^{-1}.
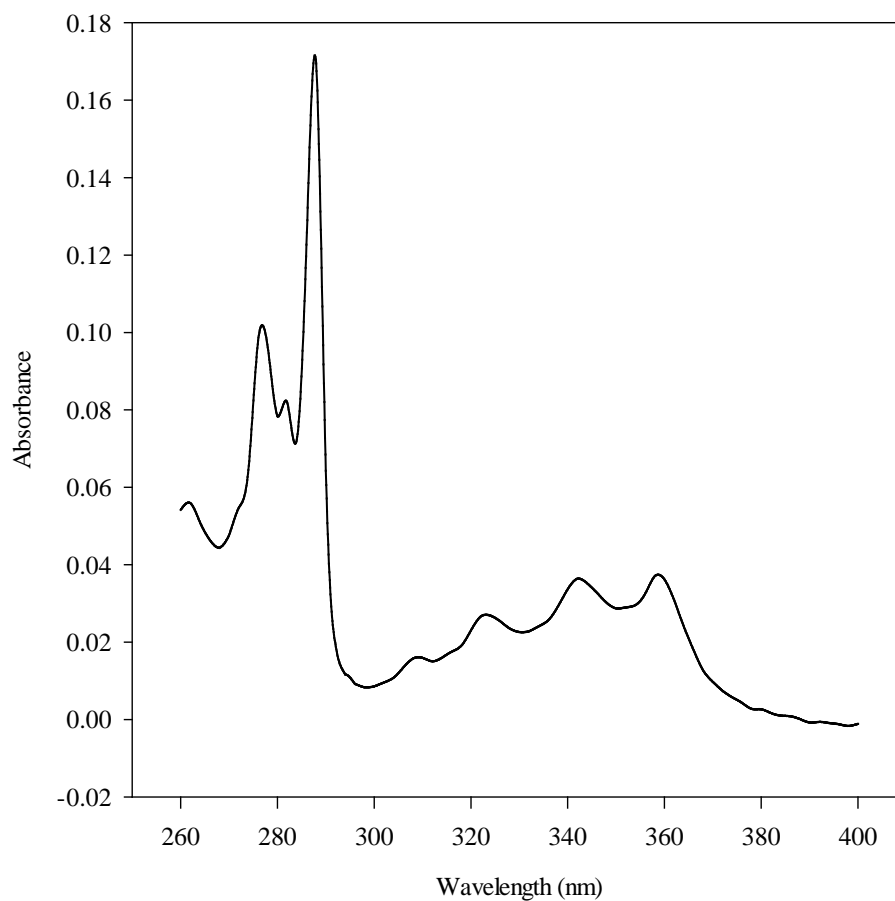
Figure 11: UV – Vis absorbance spectra of fluoranthene in 75 % ethanol.

When compared to the literature spectra using cyclohexane as a solvent, fluoranthene in 75 % ethanol (Figure 11) showed no difference in λ_{max} values. The spectrum was observed between 260 nm and 400 nm at a concentration of 0.001 mg/mL. Sharp distinct peaks can be seen at 276, 280, and 288 nm, while broader peaks can be seen at 262, 308, 324, 340, and 360 nm. The extinction coefficient for the maximum peak at 288 nm and an absorbance of 0.1695 is 3 x 10^4 M^{-1} cm^{-1}.
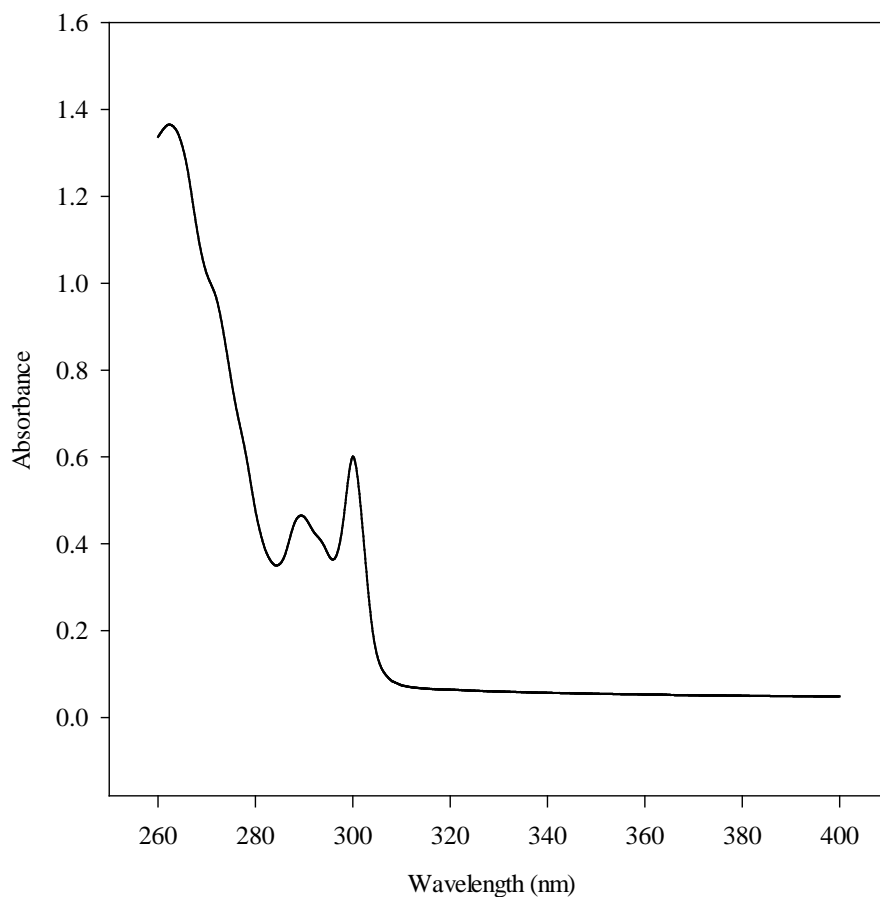
Figure 12: UV – Vis absorbance spectra of fluorene in 75 % ethanol.

When compared to the literature spectra using cyclohexane as a solvent, fluorene in 75 %
ethanol (Figure 12) showed one difference at approximately 280 nm, where a small peak
(shoulder) is not seen. This variation may be due to instrumental errors, as well as the collection
parameters. The HP 8452A has a collection mode set at 2 nm intervals, so the resolution may be
insufficient to fully resolve the spectral features. The spectrum was observed between 260 and
310 nm at a concentration of 0.01 mg/mL. Peaks can be seen at 262, 288, and 300 nm and
shoulders at 272 and 292 nm. The extinction coefficient for the maximum peak at 262 nm and an
absorbance of 1.3646 is $2 \times 10^4 \, M^{-1} \, cm^{-1}$.
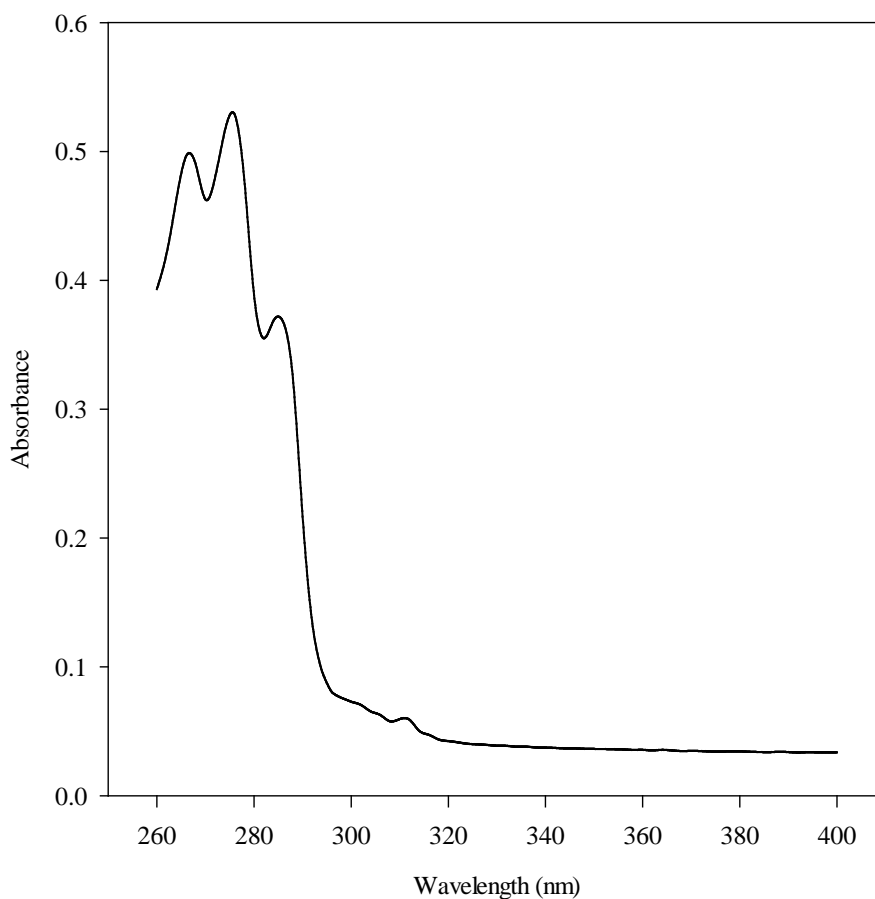
Figure 13: UV – Vis absorbance spectra of naphthalene in 75 % ethanol.

When compared to the literature spectra using cyclohexane as a solvent, naphthalene in 75 % ethanol (Figure 13) showed two differences, one between 260 nm and 280 nm, the second at approximately 288 nm. The first difference is an increase in peak definition, two peaks shown instead of one, which may be due to the decreased hydrophobicity of 75 % ethanol, while the second is the loss of a peak that may be due to the aforementioned resolution limitations.[3] The spectrum was observed between 260 nm and 300 nm at a concentration of 0.01 mg/mL. Peaks can be seen at 266, 276, and 284 nm. The extinction coefficient for the maximum peak at 276 nm and an absorbance of 0.5289 is 9×10^3 M^{-1} cm^{-1}.
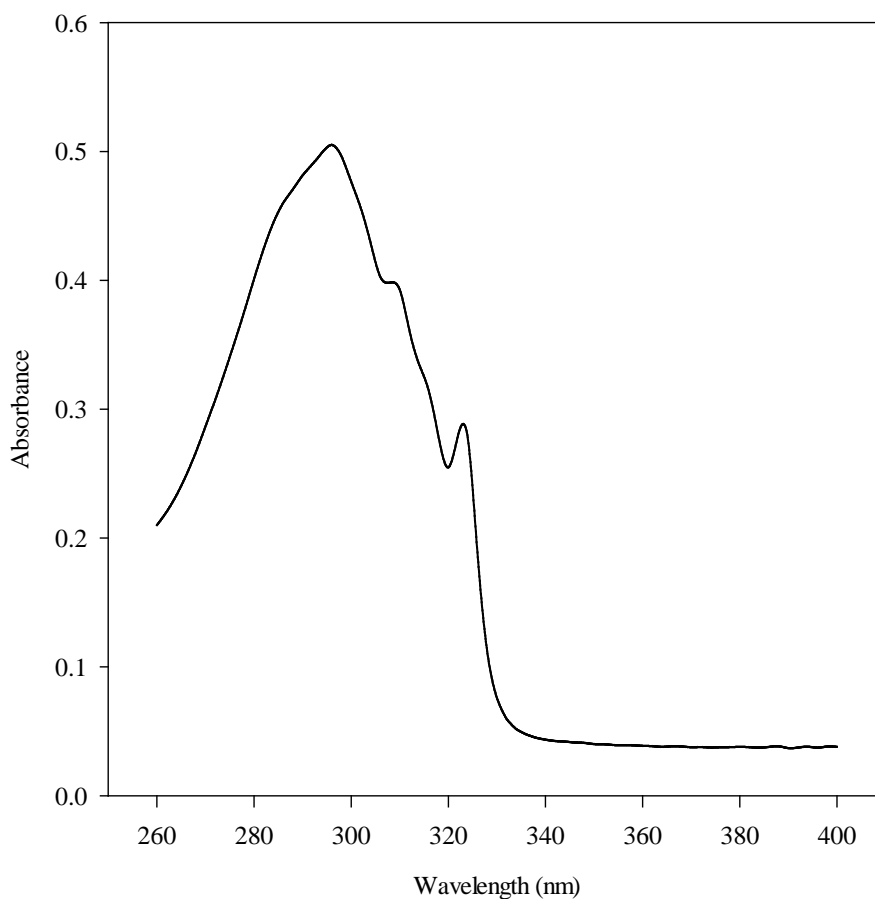
Figure 14: UV – Vis absorbance spectra of 1 – naphthol in 75 % ethanol.

When compared to the literature spectra using ethanol (100 %) as a solvent, 1 – naphthol in 75 % ethanol (Figure 14) showed no difference in λ_{max} values. The spectrum was observed between 260 nm and 340 nm at a concentration of 0.01 mg/mL. Peaks can be seen at 296 and 324 nm and a shoulder at 310 nm. The extinction coefficient for the maximum peak at 296 nm and an absorbance of 0.5052 is 7×10^3 M^{-1} cm^{-1}.
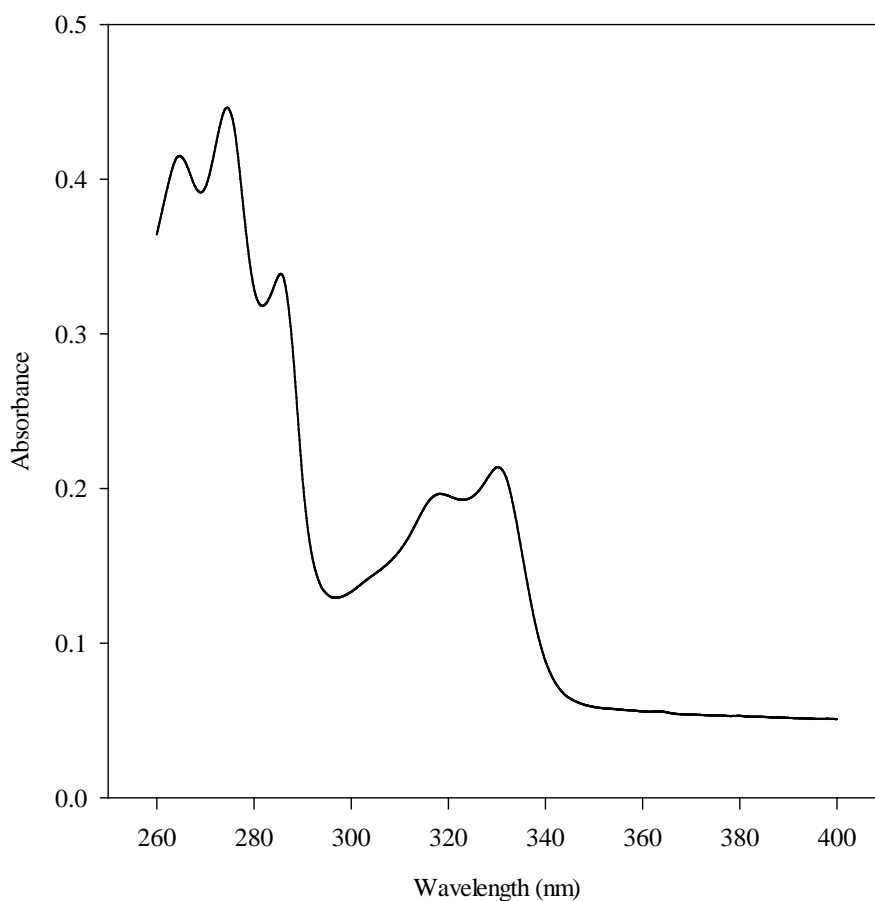
Figure 15: UV – Vis absorbance spectra of 2 – naphthol in 75 % ethanol.

When compared to the literature spectra using ethanol (100 %) as a solvent, 2 – naphthol in 75 % ethanol (Figure 15,) showed no differences in λ_{max} values. The spectrum was observed between 260 nm and 350 nm at a concentration of 0.01 mg/ML. Peaks can be seen at 264, 274, 284, 318, and 330 nm. The extinction coefficient for the maximum peak at 274 nm and an absorbance of 0.4452 is 6 x 10^3 M^{-1} cm^{-1}.
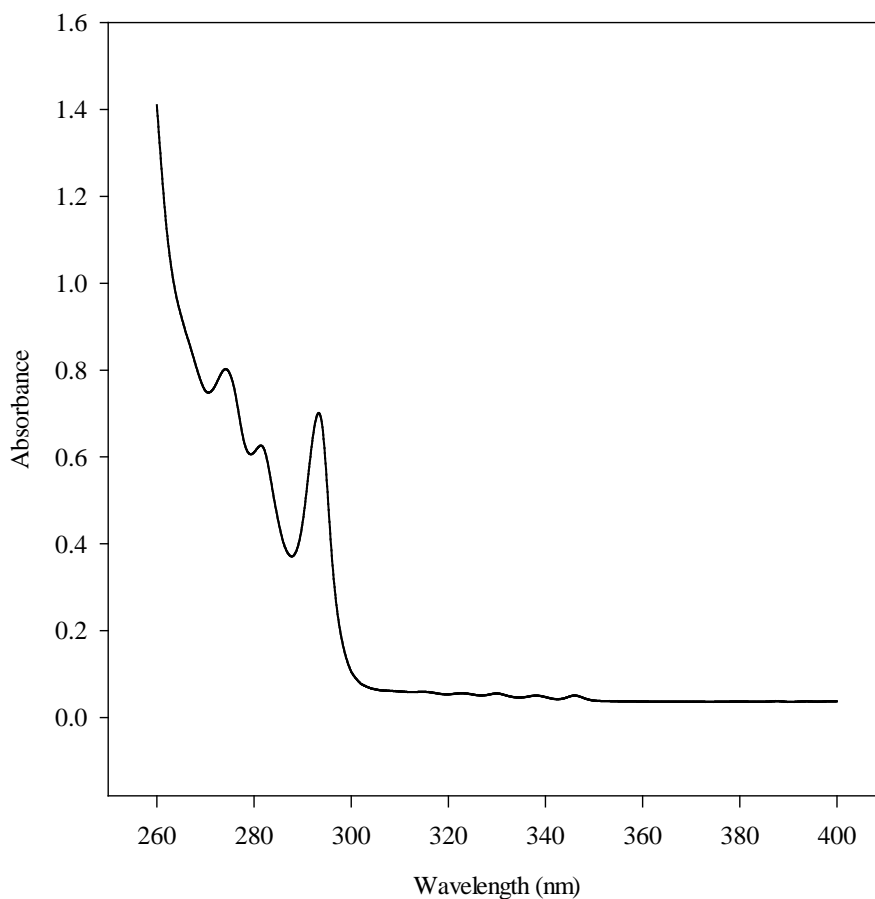
Figure 16: UV – Vis absorbance spectra of phenanthrene in 75 % ethanol.

When compared to the literature spectra using cyclohexane as a solvent, phenanthrene in 75 % ethanol (Figure 16) showed no difference in λ_{max} values. The spectrum was observed between 260 nm and 300 nm at a concentration of 0.01 mg/mL. Peaks can be seen at 274, 282, and 292 nm. The extinction coefficient for the maximum peak at 274 nm and an absorbance of 0.8021 is $1 \times 10^4 \, M^{-1} \, cm^{-1}$.
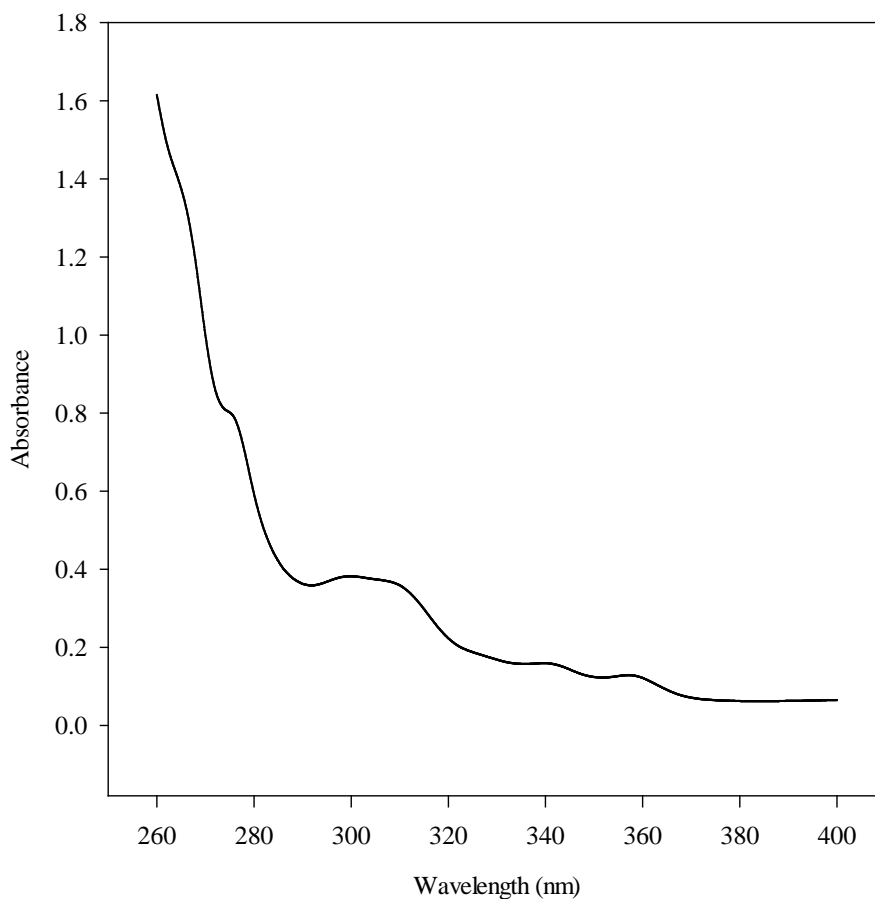
Figure 17: UV – Vis absorbance spectra of 9 – phenanthrol in 75 % ethanol.

A comparison of the spectrum of 9 – phenanthrol (Figure 17) in 75 % ethanol to literature data could not be done. Extensive literature searches where performed and only the maximum absorbance was reported. This absorbance was at a lower wavelength than could be recorded within the instrumentational limitations of the spectrofluorometer. The spectrum was observed between 260 and 380 nm at a concentration of 0.01 mg/mL. A small broad peak can be seen at 302 nm while shoulders can be seen at 274, 340, and 360 nm. The extinction coefficient for the maximum peak at 302 nm and an absorbance of 0.3800 is 7×10^3 M^{-1} cm^{-1}.
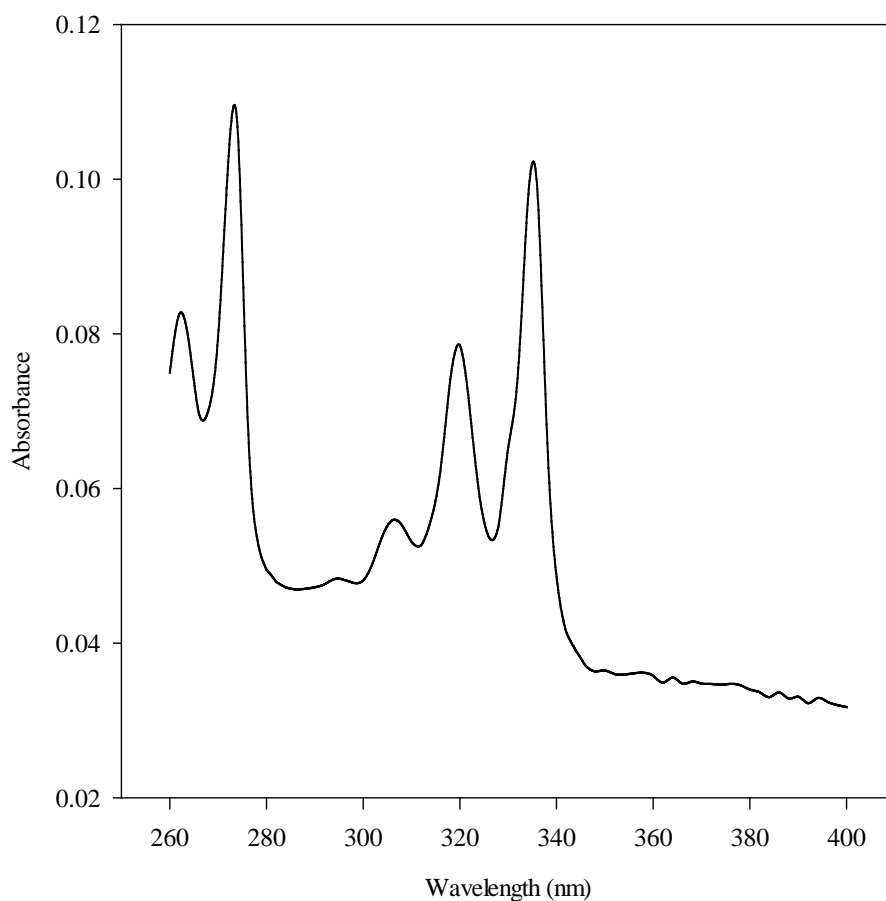
Figure 18: UV – Vis absorbance spectra of pyrene in 75 % ethanol.

When compared to the literature spectra using cyclohexane as a solvent, pyrene in 75 % ethanol (Figure 18) showed no difference in λ_{max} values. The spectrum was observed between 260 nm and 350 nm at a concentration of 0.0003 mg/mL. Sharp distinct peaks can be seen at 262, 272, 318, and 336 nm, while two smaller broader peaks can be seen at 292 and 306 nm. The extinction coefficient for the maximum peak at 272 nm and an absorbance of 0.1014 is 7 x 10^4 M^{-1} cm^{-1}.
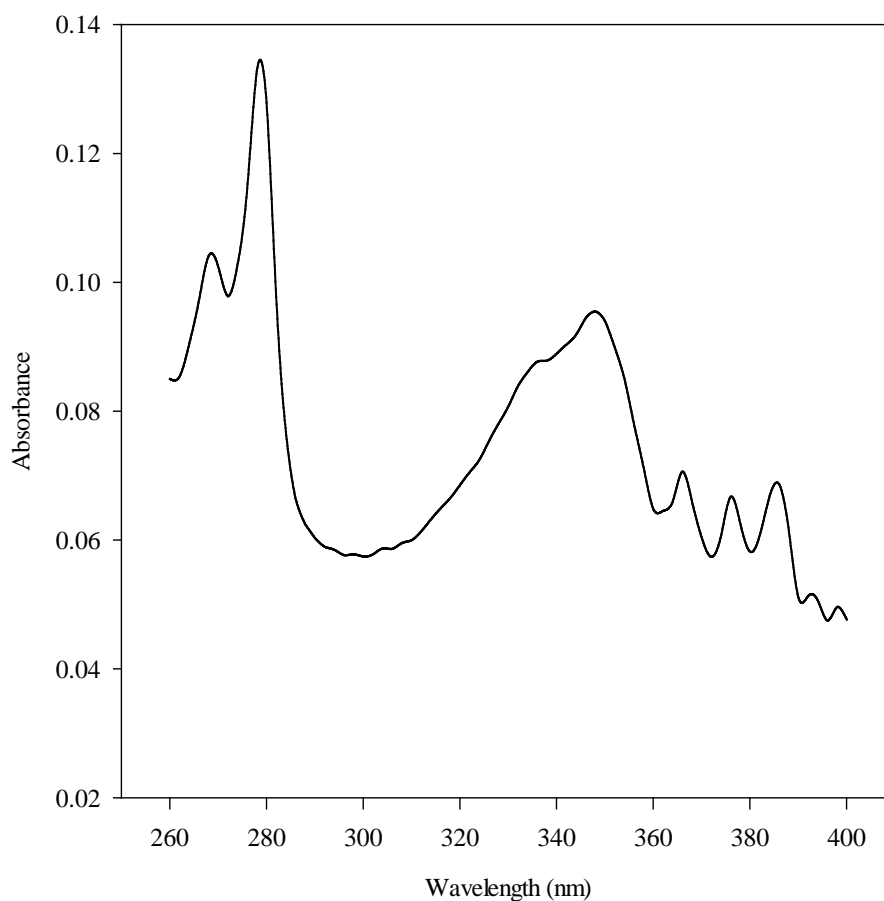
Figure 19: UV – Vis absorbance spectra of 1 – pyrenol in 75 % ethanol.

When compared to the literature spectra using THF or water as a solvent, 1 – pyrenol in 75 % ethanol (Figure 19) showed one difference in spectra at approximately 370-380 nm. This difference may be due to the change in solvent polarity, as two peaks are visible in this region instead of one.[2] The spectrum was observed between 260 nm and 400 nm at a concentration of 0.0005 mg/mL. Sharp distinct peaks can be seen at 268, 278, 366, 376, and 386 nm, while smaller broad peaks can be seen at 348 nm and a shoulder can been seen at 336 nm. The extinction coefficient for the maximum peak at 278 nm and an absorbance of 0.1328 is 6 x 10^4 M^{-1} cm^{-1}.

II.   Excitation and Emission Spectrum

Optimum conditions for fluorescence spectroscopy for all compounds were in 75 % ethanol. The excitation wavelength for the emission spectra was the most intense peak observed in the absorption spectra. The emission wavelength used to measure excitation spectra was that of the most intense emission. Full excitation and emission spectrum were conducted using concentrations of samples producing signals less than 1×10^6 counts per second (CPS) (Figures 20 – 31). Emission and excitation spectrum were normalized on a 0 – 1 photon intensity scale by dividing each signal intensity by the maximum signal intensity recorded. Signals for both were corrected for lamp profile and dark counts. The range of emission signals were between 290 nm and 600 nm with individual parameters for each compound found in Table 1 on page 45. Excitation data can be found between 260 nm and 400 nm with individual parameters for each compound found in Table 2 on page 45. Excitation spectra are closely related to the UV – Vis absorption spectra with only minor peak shifts due to the experimental parameters of both the UV – Vis spectrophotometer and the spectrofluorometer (UV – Vis sample collection was every 2.0 nm while spectrofluorometer sample collection was every 1.0 nm).

Baselines on all spectra will not show a minimum of zero due to the configuration of the photomultiplier tube (PMT) used. The PMT will add additional shot noise and thermionic noise to the baseline unless it is cooled.[6] Furthermore, each spectrum was divided by the reference signal (R1) generated by the photodiode monitoring the intensity of the lamp at each excitation wavelength. This signal is in mV and generally less than one. The spectra are also normalized to the maximum. Normalization will accentuate the signal to noise ratio in weaker fluorophores, while stronger fluorophores will show little to no change.

Compound	λ_{ex} (nm)	λ_{em} (nm) (range)
Acenaphthene	290	300 – 380
Anthracene	340	350 – 475
Benzo [a] pyrene	296	375 – 480
Fluoranthene	308	375 – 600
Fluorene	262	290 – 350
Naphthalene	286	300 – 400
1 – Naphthol	296	300 – 600
2 – Naphthol	264	325 – 440
Phenanthrene	294	330 – 430
9 – Phenanthrol	304	350 – 480
Pyrene	294	350 – 460
1 – Pyrenol	268	375 – 460

Table 1: Optimum emission wavelength parameters for a standard quartz cuvette.

Compound Name	λ_{em} (nm)	λ_{ex} (nm) (range)
Acenaphthene	338	260 – 330
Anthracene	425	260 – 390
Benzo [a] pyrene	403	260 – 400
Fluoranthene	462	260 – 380
Fluorene	317	250 – 310
Naphthalene	337	260 – 320
1 – Naphthol	370	260 – 340
2 – Naphthol	358	260 – 350
Phenanthrene	366	260 – 300
9 – Phenanthrol	389	260 – 380
Pyrene	416	260 – 360
1 – Pyrenol	438	260 – 390

Table 2: Optimum excitation wavelength parameters for a standard quartz cuvette.
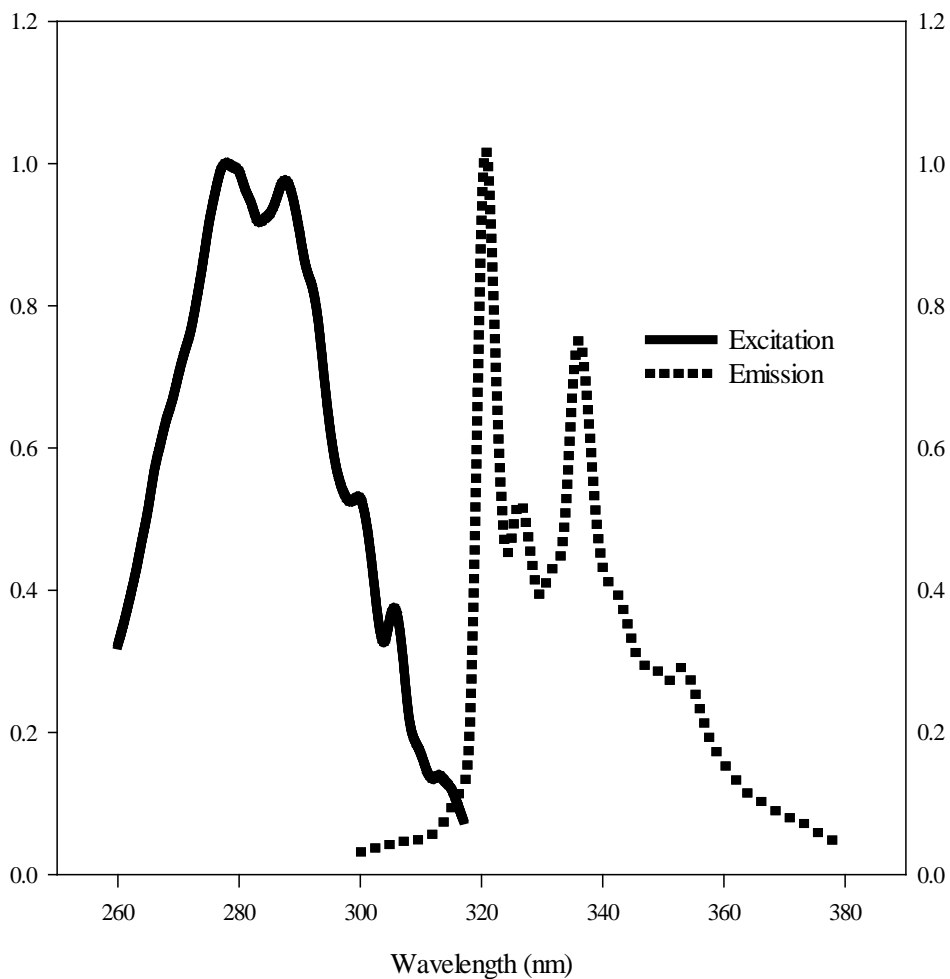
Figure 20: Emission and excitation spectra of acenaphthene in 75 % ethanol in a standard quartz fluorescence cuvette.

The excitation and emission spectrum of acenaphthene in 75 % ethanol can be seen in Figure 20 at a concentration of 0.002 mg/mL. The excitation spectrum is observed between 260 and 320 nm. Peaks can be seen at 280, 290, and 320 nm with a shoulder at 308 nm. The emission spectrum is observed between 300 and 380 nm. Peaks can be seen at 281, 286, 336, and 353 nm and a shoulder at 341 nm.
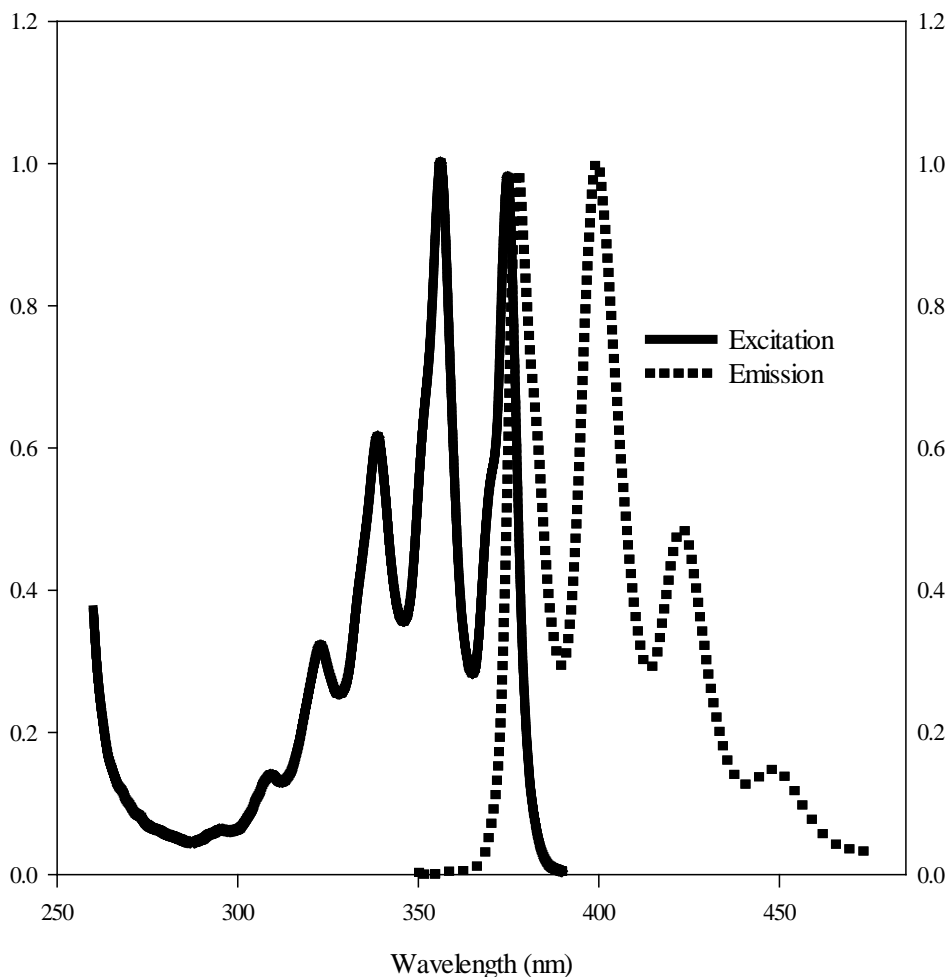
Figure 21: Emission and excitation spectra of anthracene in 75 % ethanol in a standard quartz fluorescence cuvette.

The excitation and emission spectrum of anthracene in 75 % ethanol can be seen in Figure 21 at a concentration of 0.002 mg/mL. The excitation spectrum is observed between 260 and 380 nm. Peaks can be seen at 308, 324, 340, 356, and 374 nm. The emission spectrum is observed between 350 and 460 nm. Peaks can be seen at 377, 399, and 423 nm with a small broad peak at 447 nm. Due to the rigid structure of anthracene, the 0–0 band overlap is distinct.
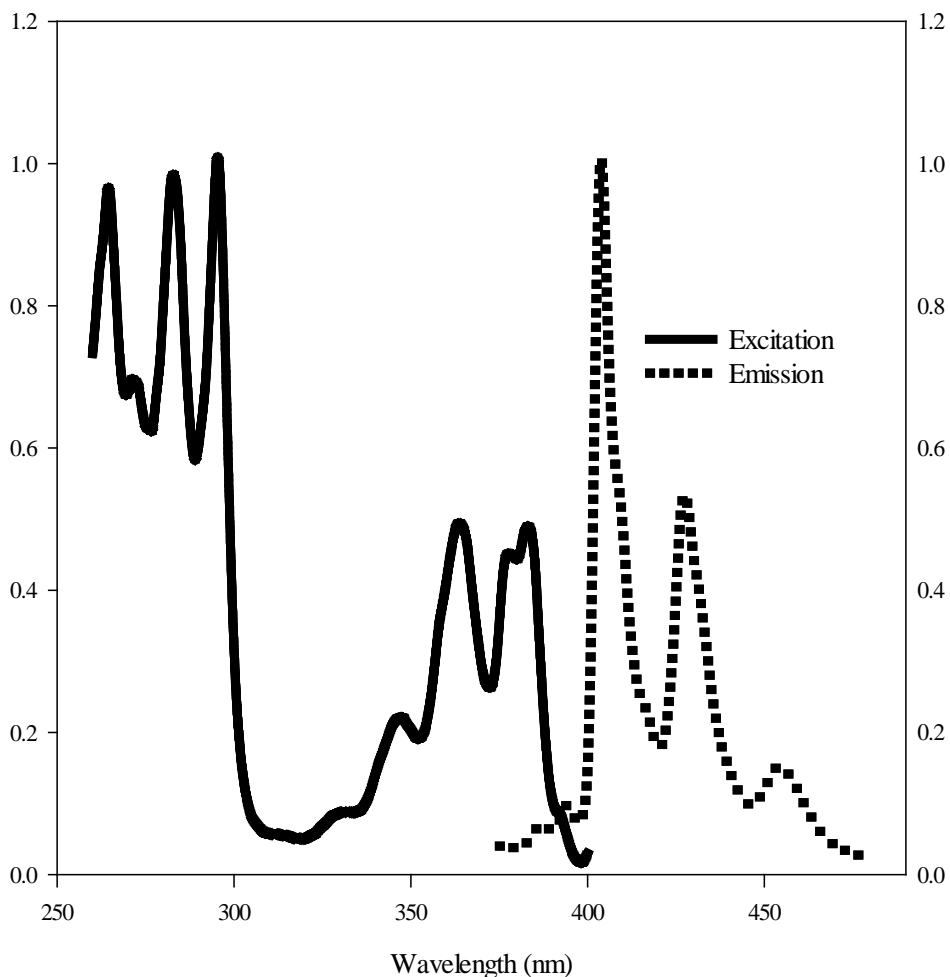
Figure 22: Emission and excitation spectra of benzo [a] pyrene in 75 % ethanol in a standard quartz fluorescence cuvette.

The excitation and emission spectrum of benzo [a] pyrene in 75 % ethanol can be seen in Figure 22 at a concentration of 0.00006 mg/mL. The excitation spectrum is observed between 260 and 400 nm. Peaks can be seen at 264, 284, 296, 332, 348, 364, 378, and 384 nm and a shoulder at 271 nm. The emission spectrum is observed between 375 and 480 nm. Sharp peaks can be seen at 404 and 427 nm, a small broad peak can be seen at 452 nm and small shoulders can be seen at 379 and 387 nm.
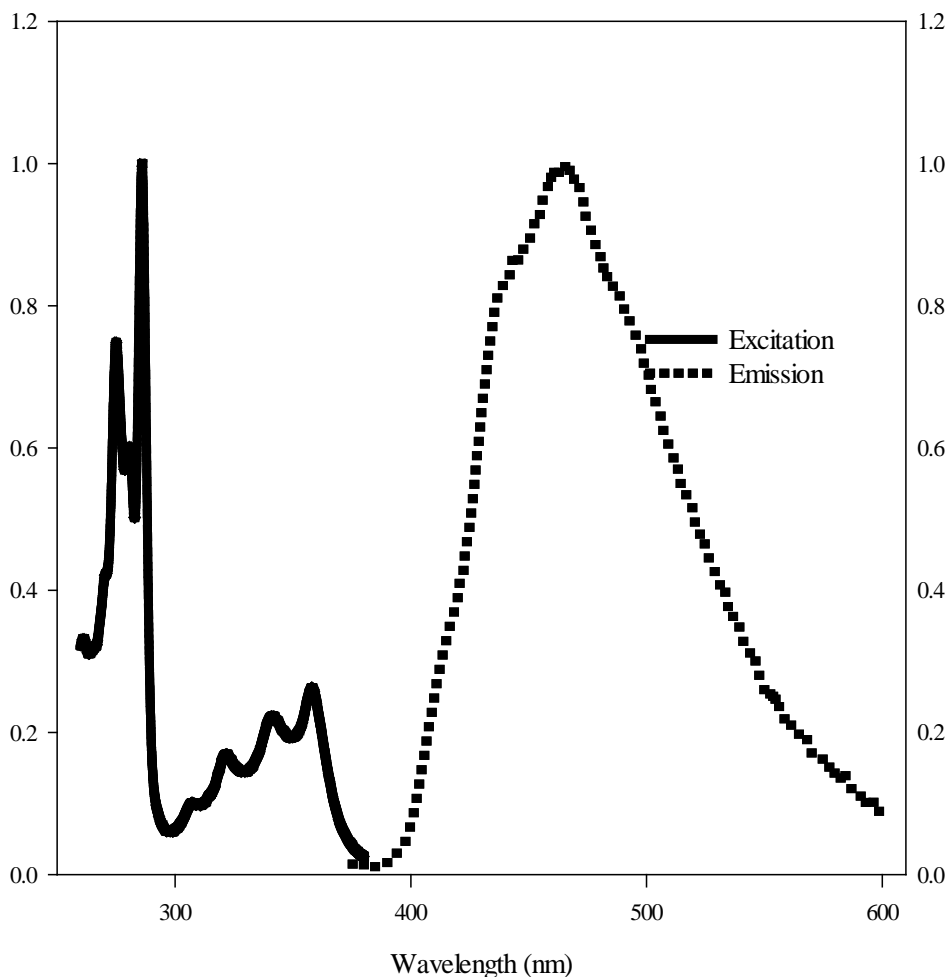
Figure 23: Emission and excitation spectra of fluoranthene in 75 % ethanol in a standard quartz fluorescence cuvette.

The excitation and emission spectrum of fluoranthene in 75 % ethanol can be seen in Figure 23 at a concentration of 0.002 mg/mL. The excitation spectrum is observed between 260 and 380 nm. Sharp peaks can be seen at 276, 280, and 288 nm, while broader peaks can be seen at 262, 308, 324, 340, and 360 nm. The emission spectrum is observed between 375 and 600 nm. A broad peak can be seen at 465 nm, while two small shoulders are seen at 443 and 484 nm.
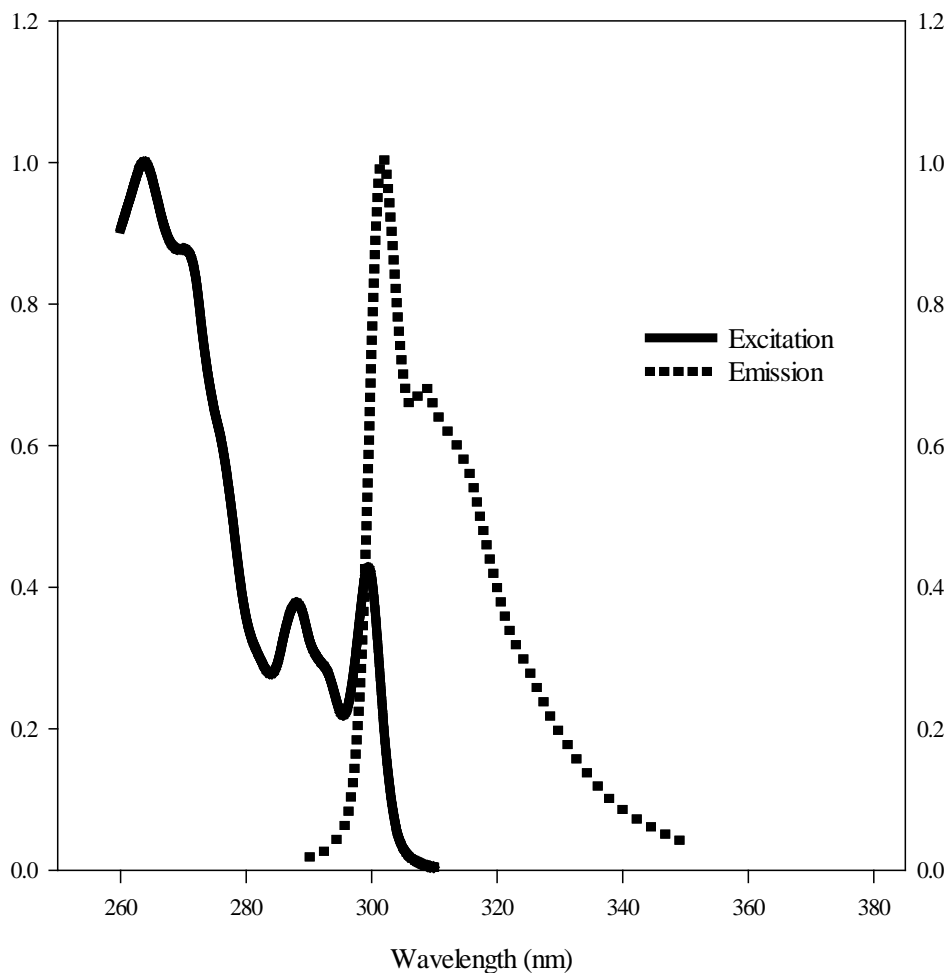
Figure 24: Emission and excitation spectra of fluorene in 75 % ethanol in a standard quartz fluorescence cuvette.

The excitation and emission spectrum of fluorene in 75 % ethanol can be seen in Figure 24 at a concentration of 0.00055 mg/mL. The excitation spectrum is observed between 250 and 310 nm. The excitation spectrum begins at a lower wavelength then other compounds studied do the maximum excitation peak occurring at 262 nm. Peaks can be seen at 262, 288, and 300 nm and shoulders at 272 and 292 nm. The emission spectrum is observed between 290 and 350 nm. A sharp peak can be seen at 302 nm, a broad peak can be seen at 308 nm, and a shoulder can be seen at 315 nm. Due to the rigid structure of fluorene, the 0-0 band overlap is distinct.
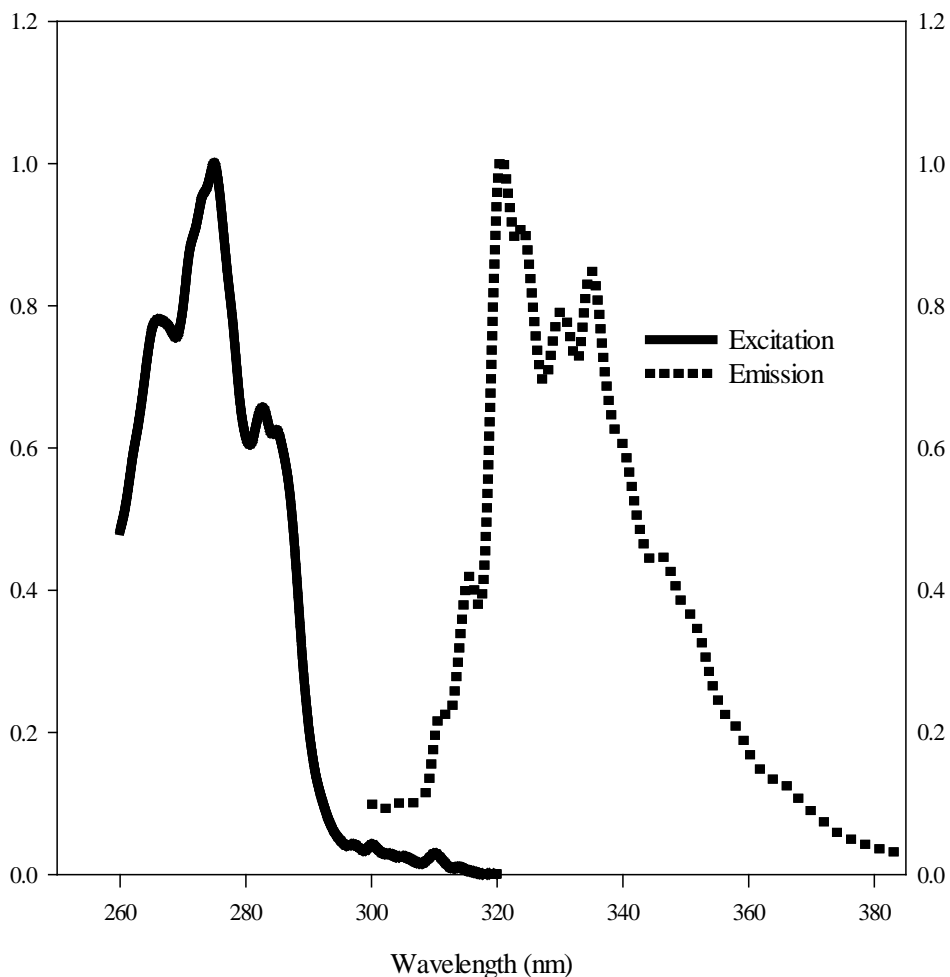
Figure 25: Emission and excitation spectra of naphthalene in 75 % ethanol in a standard quartz fluorescence cuvette.

The excitation and emission spectrum of naphthalene in 75 % ethanol can be seen in Figure 25 at a concentration of 0.001 mg/mL. The excitation spectrum is observed between 260 and 320 nm. Peaks can be seen at 266, 276, and 283 nm and a shoulder at 285 nm. Smaller signals are seen between 295 and 320 nm but were not used in the construction of the emission spectrum. The emission spectrum is observed between 300 and 400 nm. Sharp peaks can be seen at 315, 321, 330, and 335 nm and shoulders can be seen at 311, 324, 339, 350, and 365 nm.
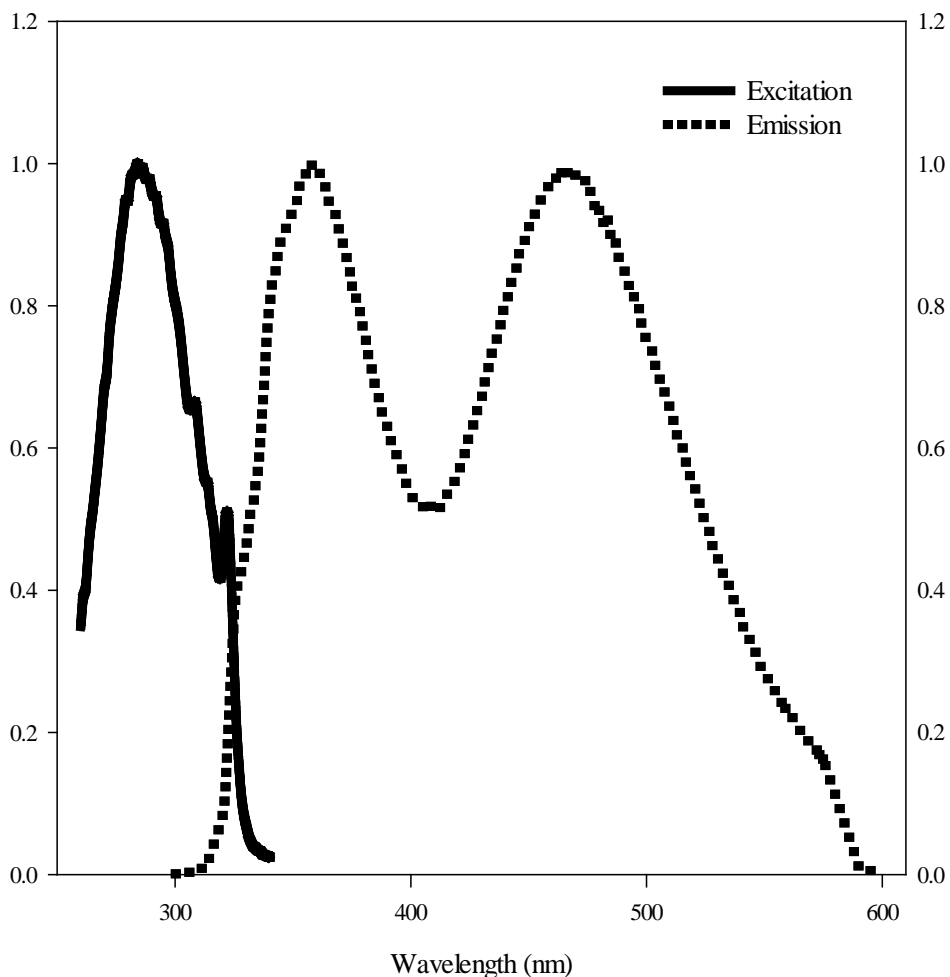
Figure 26: Emission and excitation spectra of 1 – naphthol in 75 % ethanol in a standard quartz fluorescence cuvette.

The excitation and emission spectrum of 1 – naphthol in 75 % ethanol can be seen in Figure 26 at a concentration of 0.005 mg/mL. The excitation spectrum is observed between 260 and 340 nm. Peaks can be seen at 282 and 322 nm and a shoulder at 306 nm. The emission spectrum is observed between 300 and 600 nm. Two broad peaks can be seen at 356 and 461 nm and a shoulder can be seen at 570 nm.
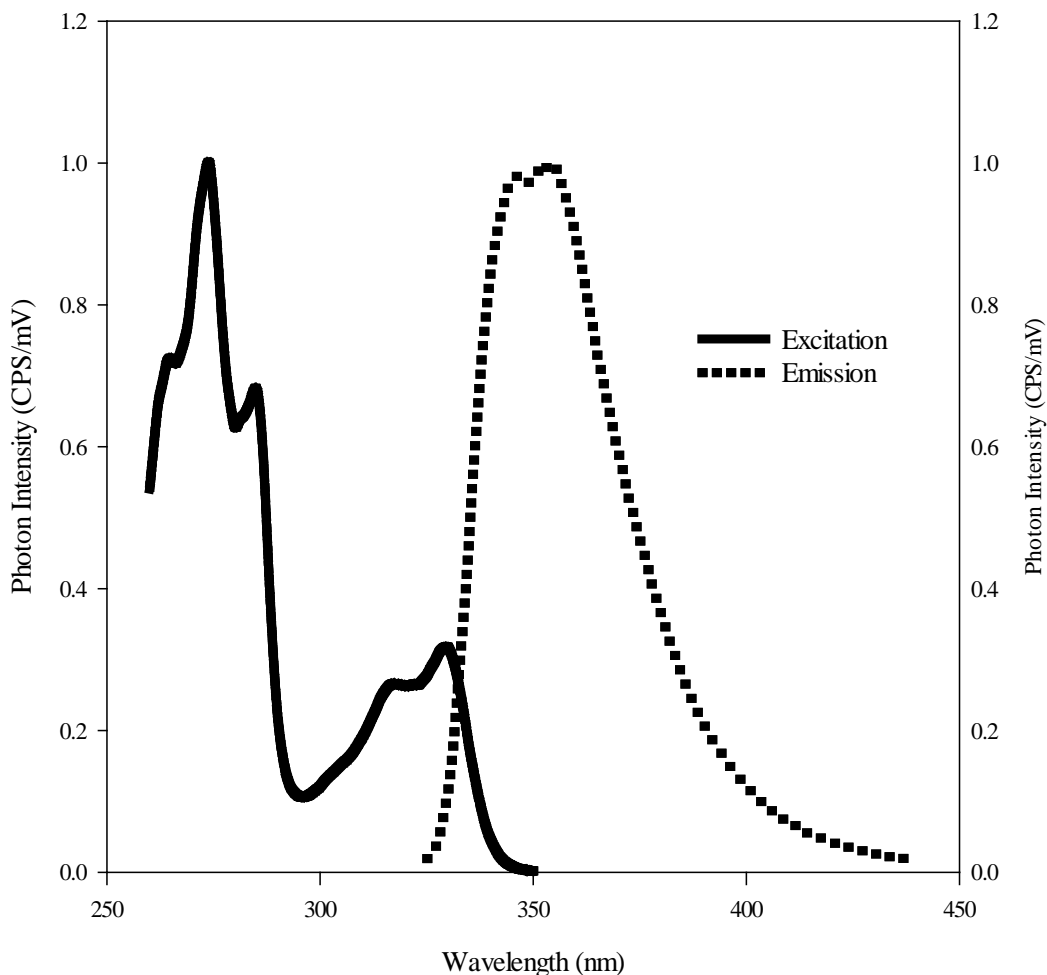
Figure 27: Emission and excitation spectra of 2 – naphthol in 75 % ethanol in a standard quartz fluorescence cuvette.

The excitation and emission spectrum of 2 – naphthol in 75 % ethanol can be seen in Figure 27 at a concentration of 0.002 mg/mL. The excitation spectrum is observed between 260 and 350 nm. Sharp peaks can be seen at 274 and 285 nm, broad peaks can be seen at 315 and 327 nm, and shoulders can be seen at 264 and 307 nm. The emission spectrum is observed between 325 and 440 nm. A peak can be seen at 352 nm and a shoulder can be seen at 345 nm. Due to the rigid structure of 2 – naphthol, the 0-0 band overlap is distinct.
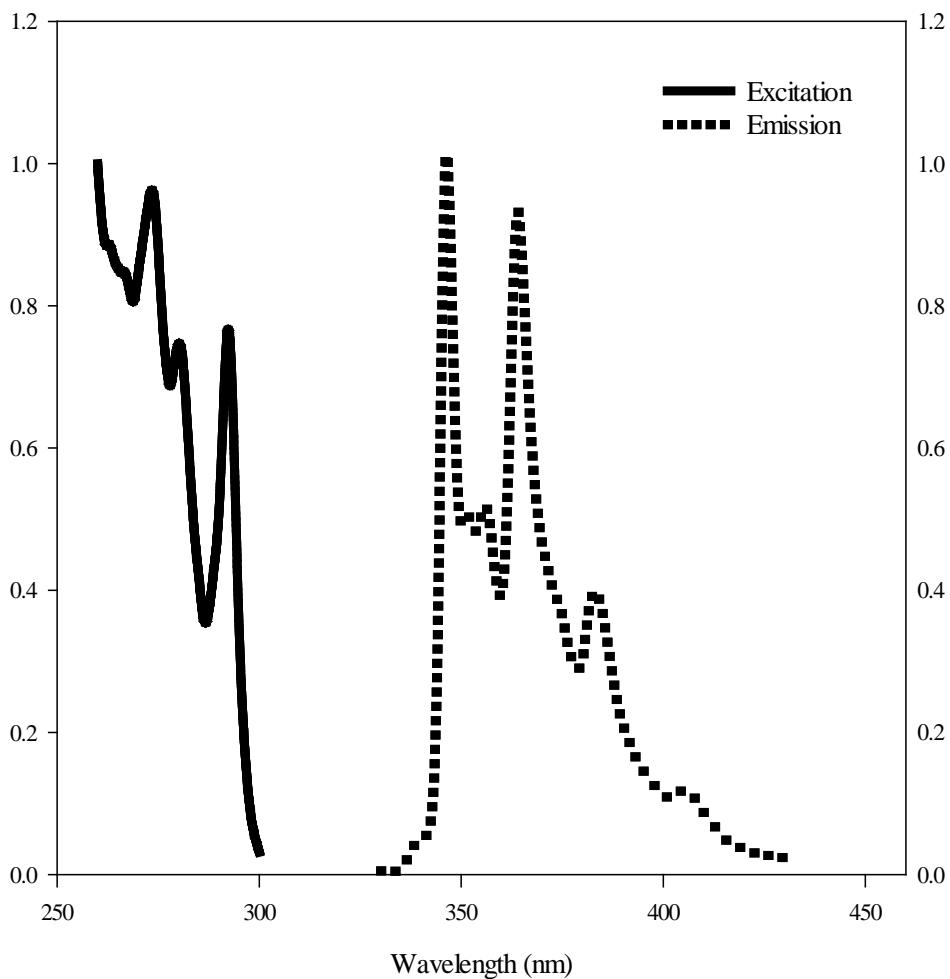
Figure 28: Emission and excitation spectra of phenanthrene in 75 % ethanol in a standard quartz fluorescence cuvette.

The excitation and emission spectrum of phenanthrene in 75 % ethanol can be seen in Figure 28 at a concentration of 0.001 mg/mL. The excitation spectrum is observed between 260 and 300 nm. Peaks can be seen at 273, 280, and 292 nm and a shoulder can be seen at 263 nm. The emission spectrum is observed between 330 and 430 nm. Sharp peaks can be seen at 346, 355, 364, and 382 nm and a broad peak can be seen at 403 nm.
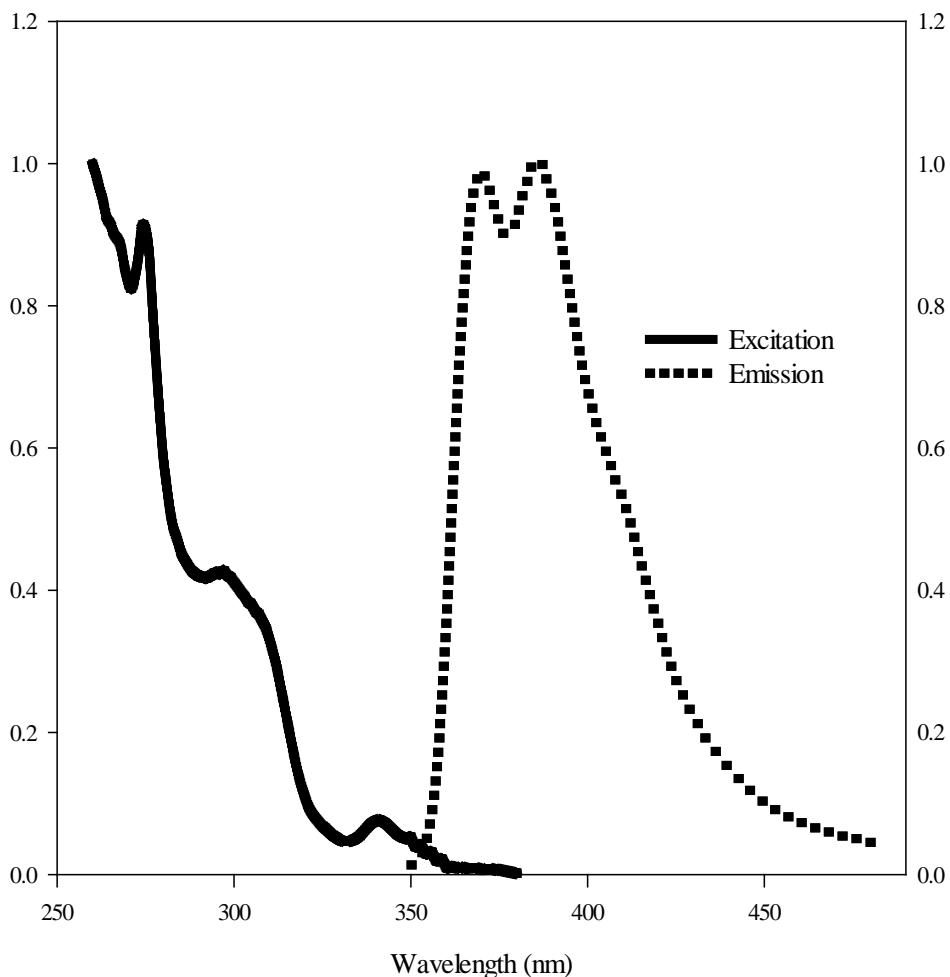
Figure 29: Emission and excitation spectra of 9 – phenanthrol in 75 % ethanol in a standard quartz fluorescence cuvette.

     The excitation and emission spectrum of 9 – phenanthrol in 75 % ethanol can be seen in Figure 29 at a concentration of 0.003 mg/mL. The excitation spectrum is observed between 260 and 380 nm. A sharp peak can be seen at 274 nm, two broad peaks can be seen at 296 and 338 nm, and a shoulder can be seen at 266 nm. The emission spectrum is observed between 350 and 480 nm. Two peaks can be seen at 369 and 385 nm and a small shoulder can be seen at 410 nm.
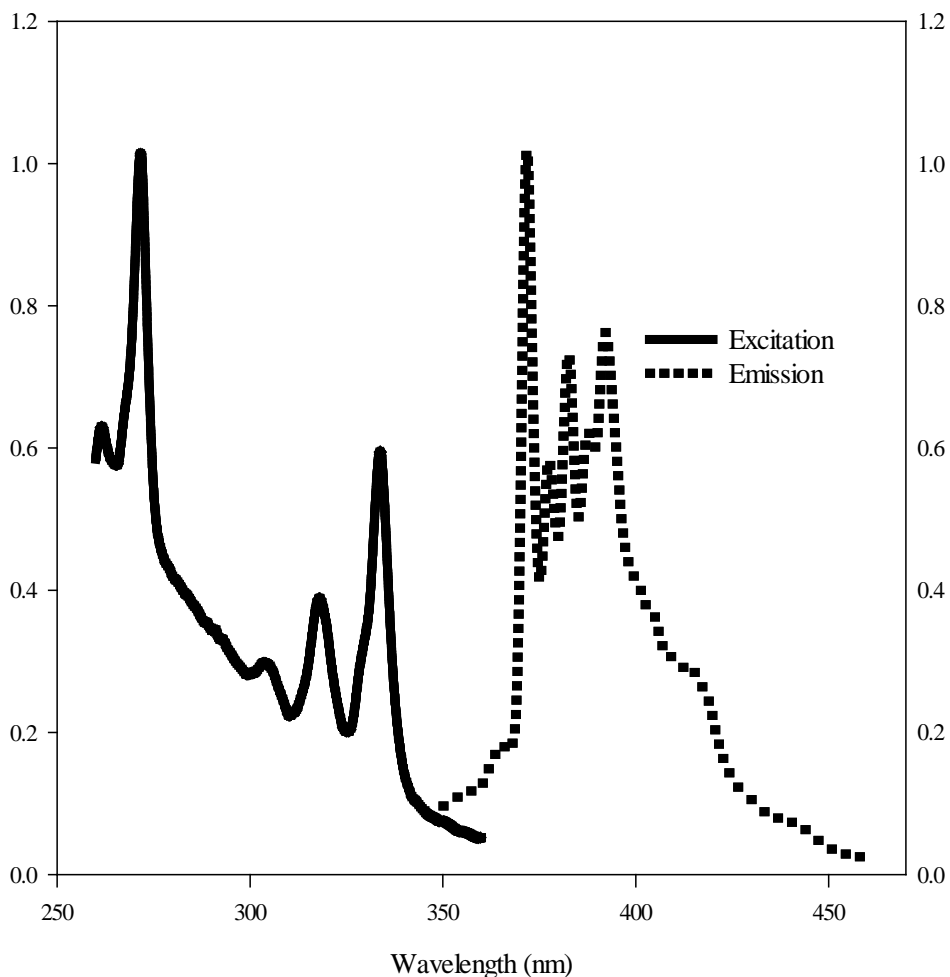
Figure 30: Emission and excitation spectra of pyrene in 75 % ethanol in a standard quartz fluorescence cuvette.

The excitation and emission spectrum of pyrene in 75 % ethanol can be seen in Figure 30 at a concentration of 0.0003 mg/mL. The excitation spectrum is observed between 260 and 360 nm. Sharp peaks can be seen at 261, 272, 318, and 334 nm, a broad peak can be seen at 303 nm, and a shoulder can be seen at 285 nm. The emission spectrum is observed between 350 and 40 nm. Sharp peaks can be seen at 372, 377, 382, and 392 nm and shoulders can be seen at 363, 402, 413, and 442 nm.
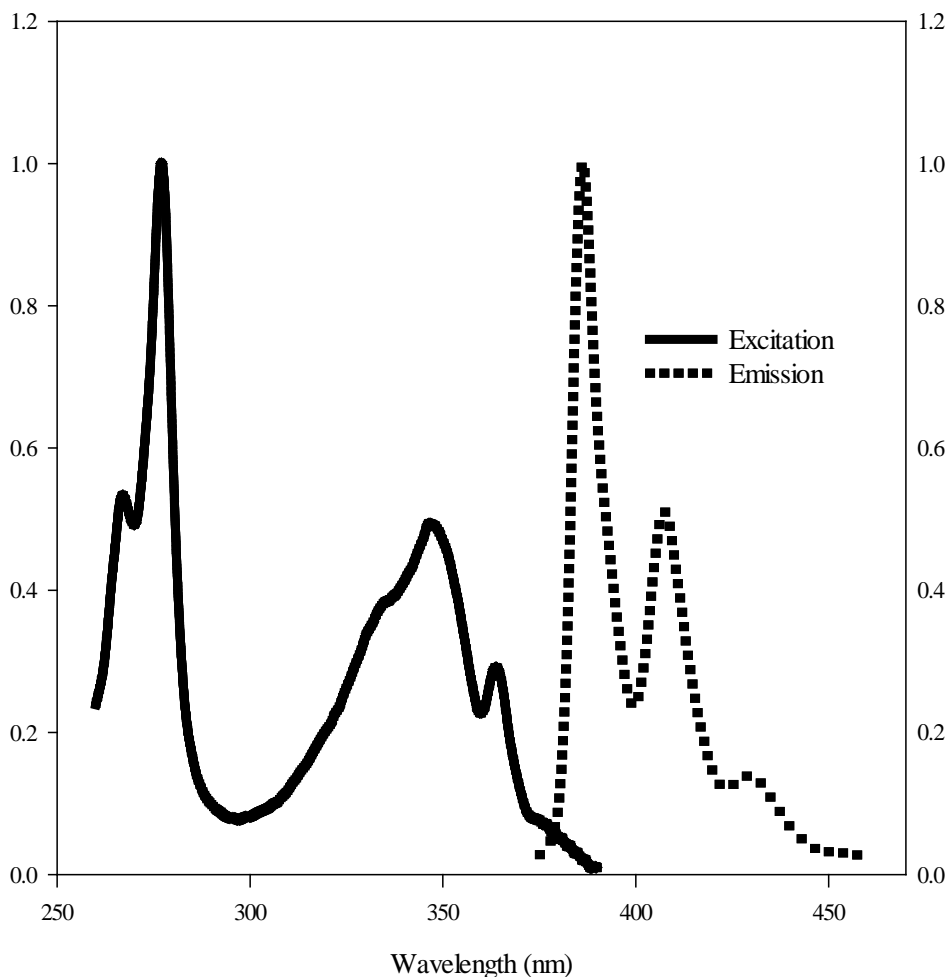
Figure 31: Emission and excitation spectra of 1 – pyrenol in 75 % ethanol in a standard quartz fluorescence cuvette.

The excitation and emission spectrum of 1 – pyrenol in 75 % ethanol can be seen in Figure 31 at a concentration of 0.0005 mg/mL. The excitation spectrum is observed between 260 and 390 nm. Sharp peaks can be seen at 267, 277, and 363 nm, a broad peak can be seen at 345 nm, and a shoulder can be seen at 334 nm. The emission spectrum is observed between 375 and 460 nm. Peaks can be seen at 386 and 407 nm and a broad peak can be seen at 428 nm.

Additional differences can be seen in the emission spectra between parent PAHs and their metabolites. In naphthalene (Figure 25, page 52), there are seven distinctive peaks seen in the emission spectra, while 1 – naphthol (Figure 26, page 53) shows two peaks and 2 – naphthol

(Figure 27, page 54) shows 1 peak. In phenanthrene (Figure 28, page 55), there are six distinctive peaks seen in the emission spectra, while 9 – phenanthrol (Figure 30, page 56) shows two distinctive peaks. In pyrene (Figure 30, page 57), there are five distinctive peaks in the emission spectra, while 1 – pyrenol (Figure 31, page 58) shows three distinctive peaks. It can be seen in these compounds that the addition of the hydroxy group diminishes the vibrational pattern of the compound upon relaxation of the electron.[3] Loss of peak structure between parent and metabolites are typical of the loss of symmetry of the compounds upon substitution. Addition of a single hydroxyl group will eliminate several symmetry features.[4] Decreases in the number of peaks based on the position of the hydroxy group are apparent, as seen between 1 – naphthol (Figure 26, page 53) and 2 – naphthol (Figure 27, page 54) (two peaks versus one peak respectively). The loss of the additional peak in 2 – naphthol is due to the solvent conditions. Distinct peaks can be seen in acidic conditions at lower wavelengths while in basic conditions one peak is found at longer wavelengths.[2] This is due to the ability of some of these hydroxylated derivatives to act as photoacids.[5] There is also a notable difference in the number of peaks seen in the emission spectra of the compounds based on the size and the intricacy of the compound.[3] The small and symmetric compound napthalene (Figure 25, page 52) shows seven distinct emission peaks while the large bulky benzo[a]pyrene (Figure 22, page 49) only shows three distinct peaks. Again, this is due to the high degree of symmetry for naphthalene (D_{2h}) vs. benzo[a]pyrene (C_s).

III.   Excitation – Emission Matrices (EEMs)

High resolution excitation – emission matrices (EEMs) of all compounds were obtained
using the range of excitations and emissions previously optimized and can be found in Table 3.
Both a contour (heat map) and three – dimensional (mesh) plot of each EEM is displayed
(Figures 32 – 55). Intensity units are listed as counts per second (CPS) relative to the R1 detector
that measures lamp intensity variations as a function of wavelength in millivolts (mV). Three –
dimensional scans show optimal excitation and emission in one spectra. Further, the additional
data offers better information for identification and analysis.[7] This provides more separation and
therefore better detection and characterization of different types of fluorescent compounds.
Comparison of two – dimensional excitation and emission spectra with the three – dimensional
EEMs show no variations in compound fluorescence.[8] As mentioned in the introduction first
order Rayleigh scattering can be seen in some compounds due to the overlapping of wavelengths
scanned in the excitation and emission monochromators.[2,3]

Compound Name	λ_{ex} (nm) (range)	λ_{em} (nm) (range)
Acenaphthene	260-330	300-380
Anthracene	260-390	350-475
Benzo [a] pyrene	260-400	375-480
Fluoranthene	260-380	375-600
Fluorene	250-310	290-350
Naphthalene	260-320	300-400
1 – Naphthol	260-340	300-600
2 – Naphthol	260-350	325-440
Phenanthrene	260-300	330-430
9 – Phenanthrol	260-380	350-480
Pyrene	260-360	350-460
1 – Pyrenol	260-390	375-460

Table 3: Optimum EEM wavelength parameters for a standard quartz cuvette.

Figure 32: Contour plot of acenaphthene in 75 % ethanol in a standard quartz fluorescence cuvette.

Figure 33: Three – dimensional mesh plot of acenaphthene in 75 % ethanol in a standard quartz fluorescence cuvette.

The EEM spectrum of acenaphthene in 75 % ethanol is shown in Figure 32 and 33. In the contour plot, the intensity of the fluorescence signal (CPS/mV) corresponds to the color shown in the legend. The most intense signal of acenaphthene (2.14×10^7 CPS/mV) can be seen at an excitation of 288 nm and an emission of 321 nm. First order Rayleigh lines are apparent in acenaphthene beginning at excitation wavelengths of approximately 310 – 320 nm and emission wavelengths of approximately 310 – 320 nm. The mesh plot shows substantial structure in the excitation and emission spectra of acenaphthene, rigidity of the naphthalene portion of the molecule and its vibration patterns between the ground (S_0) and excited states (S_1).

Figure 34: Contour plot of anthracene in 75 % ethanol in a standard quartz fluorescence cuvette.

Figure 35: Three – dimensional mesh plot of anthracene in 75 % ethanol in a standard quartz fluorescence cuvette.

The EEM spectrum of anthracene in 75 % ethanol is shown in Figure 34 and 35. In the contour plot, the intensity of the fluorescence signal (CPS/mV) corresponds to the color shown in the legend. The most intense signal of anthracene (7.65×10^6 CPS/mV) can be seen at an excitation of 356 nm and an emission of 399 nm. First order Rayleigh lines are apparent in anthracene beginning at an excitation wavelength of approximately 375 and an emission wavelength of approximately 370 nm. The mesh plot shows finely structured excitation and emission spectra of anthracene, which is characteristic of the rigidity of the molecule.
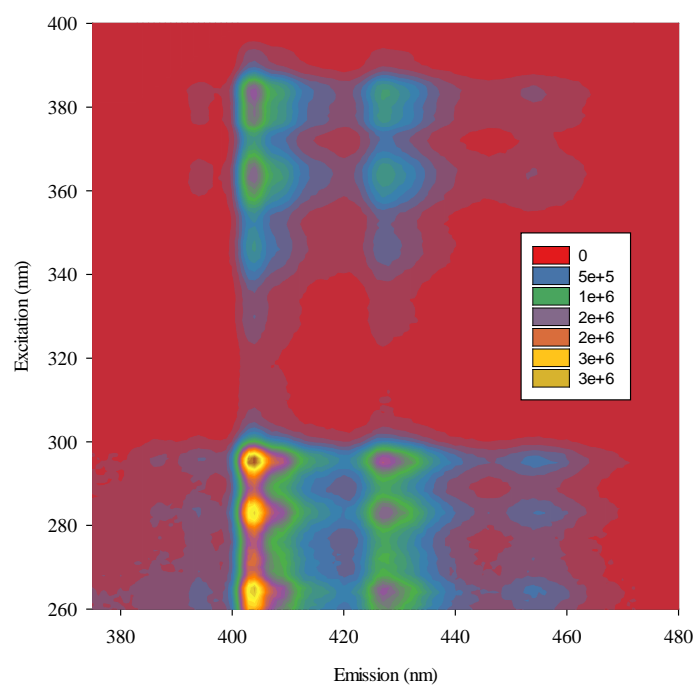
Figure 36: Contour plot of benzo [a] pyrene in 75 % ethanol in a standard quartz fluorescence cuvette.
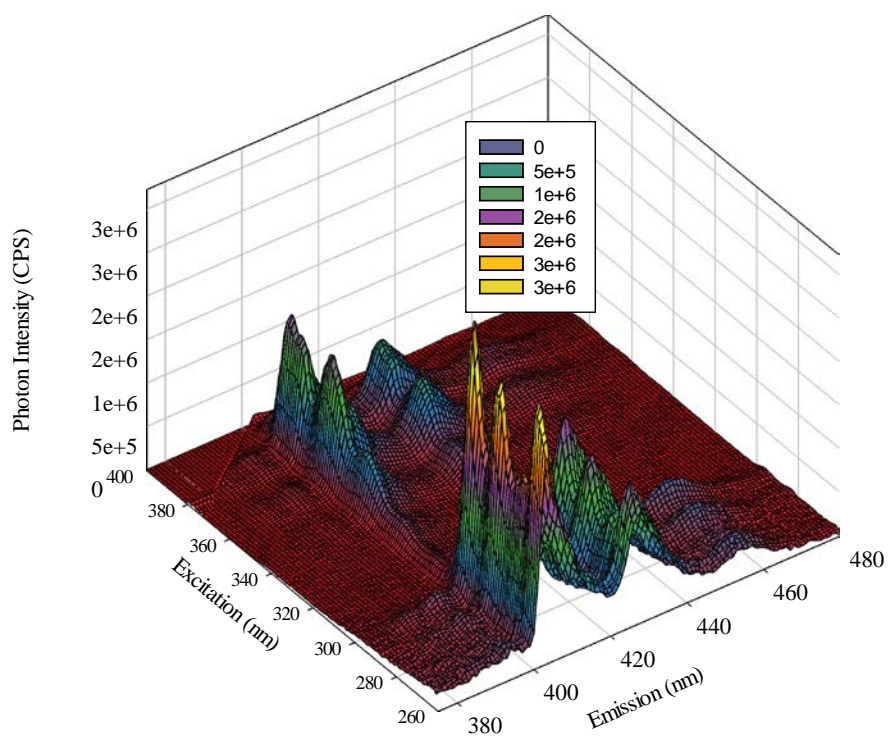
Figure 37: Three – dimensional mesh plot of benzo [a] pyrene in 75 % ethanol in a standard quartz fluorescence cuvette.

The EEM spectrum of benzo [a] pyrene in 75 % ethanol is shown in Figure 36 and 37. In the contour plot, the intensity of the fluorescence signal (CPS/mV) corresponds to the color shown in the legend. The most intense signal of benzo [a] pyrene (3.23 x 10^6 CPS/mV) can be seen at an excitation of 296 nm and an emission of 404 nm. Any optical scattering is not present for this compound. The mesh plot shows finely structured excitation and emission spectra of benzo [a] pyrene, which is characteristic of the rigidity of the molecule.
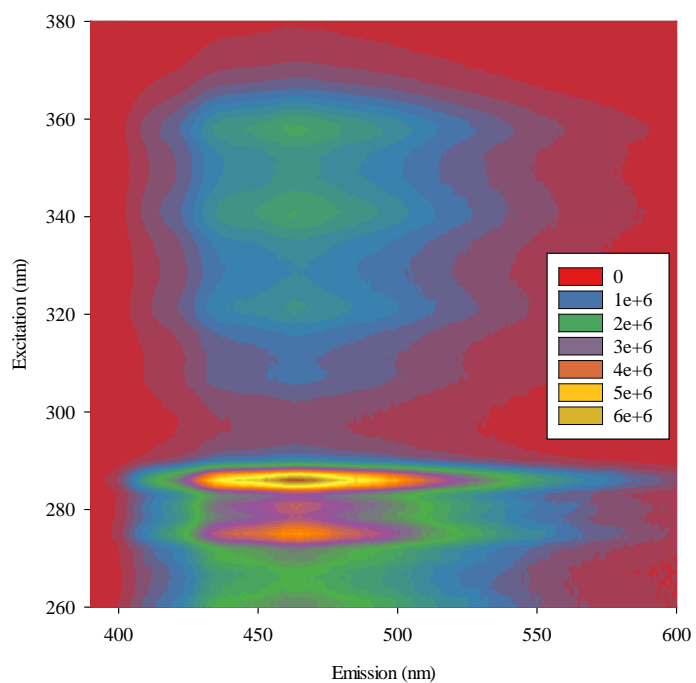
Figure 38: Contour plot of fluoranthene in 75 % ethanol in a standard quartz fluorescence cuvette.
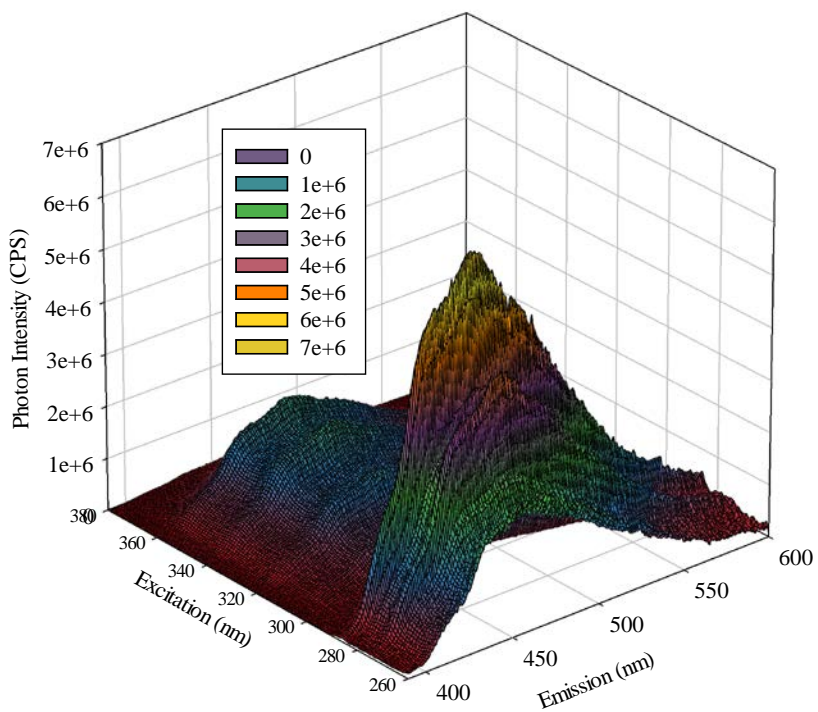
Figure 39: Three – dimensional mesh plot of fluoranthene in 75 % ethanol in a standard quartz fluorescence cuvette.

The EEM spectrum of fluoranthene in 75 % ethanol is shown in Figure 38 and 39. In the contour plot, the intensity of the fluorescence signal (CPS/mV) corresponds to the color shown in the legend. The most intense signal of fluoranthene (6.45 x 10^6 CPS/mV) can be seen at an excitation of 286 nm and an emission of 464 nm. Any optical scattering is not present for this compound. The mesh plot shows structure in the excitation and emission spectra of fluoranthene, which is characteristic of the flexibility of the molecule and its vibration patterns between the ground (S_0) and excited states (S_1).
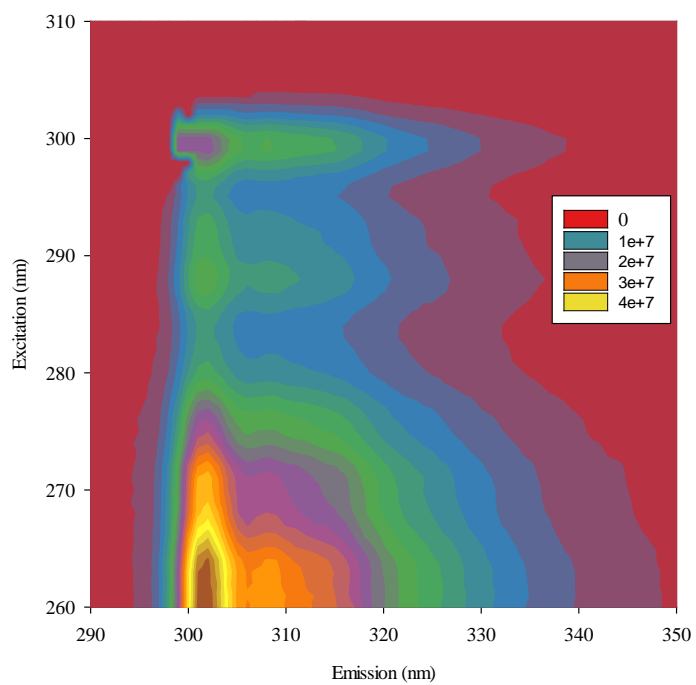
Figure 40: Contour plot of fluorene in 75 % ethanol in a standard quartz fluorescence cuvette.
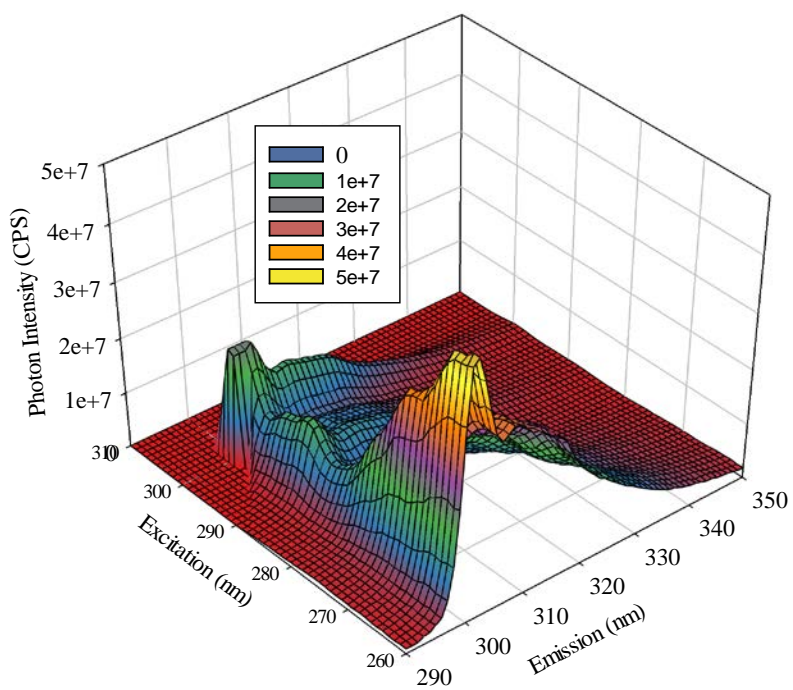
Figure 41: Three – dimensional mesh plot of fluorene in 75 % ethanol in a standard quartz fluorescence cuvette.

The EEM spectrum of fluorene in 75 % ethanol is shown in Figure 40 and 41. In the contour plot, the intensity of the fluorescence signal (CPS/mV) corresponds to the color shown in the legend. The most intense signal of fluorene (4.61 x 10^7 CPS/mV) can be seen at an excitation of 261 nm and an emission of 302 nm. First order Rayleigh lines are apparent in acenaphthene beginning at an excitation wavelength of approximately 300 nm and an emission wavelength of approximately 300 nm. The mesh plot shows less structure in the excitation and emission spectra of fluorene, which is characteristic of the flexibility of the molecule and an essentially one principle vibrational mode causing relaxation between the ground (S_0) and excited states (S_1).
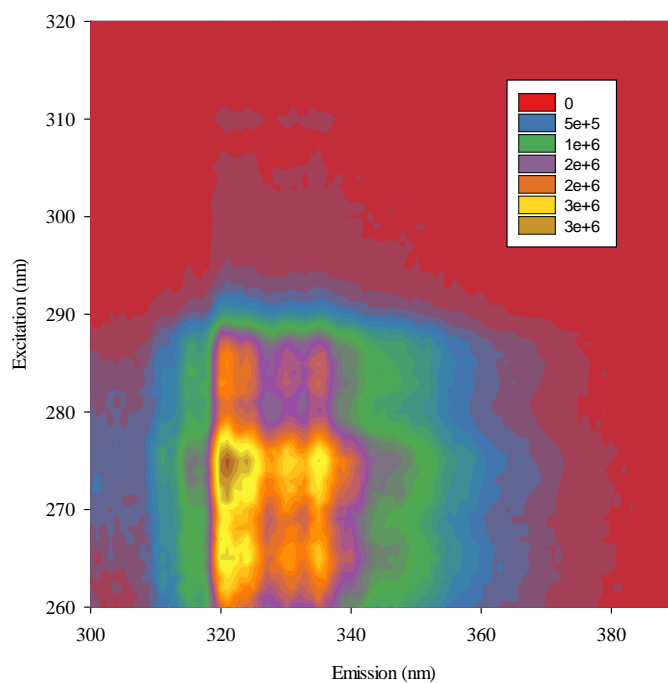
Figure 42: Contour plot of naphthalene in 75 % ethanol in a standard quartz fluorescence cuvette.
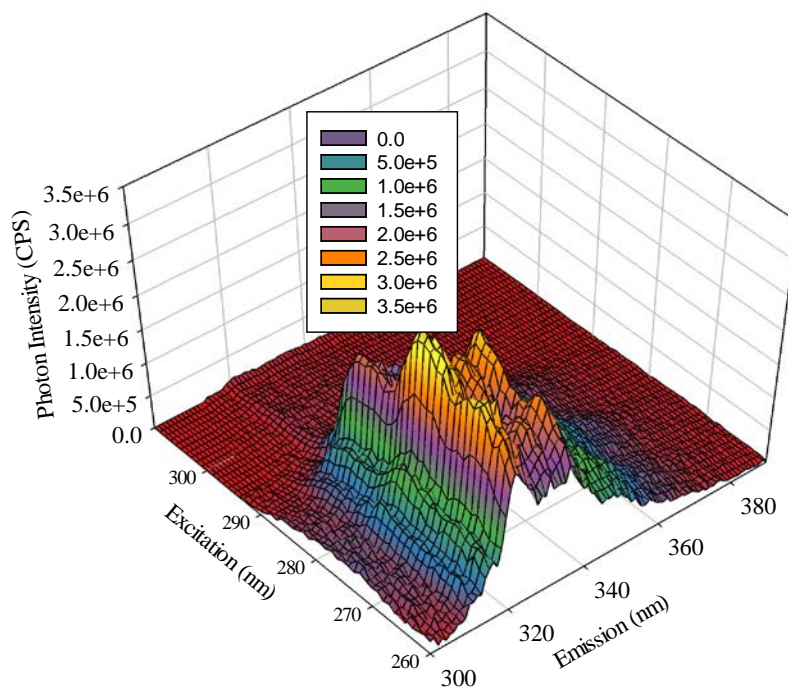
Figure 43: Three – dimensional mesh plot of naphthalene in 75 % ethanol in a standard quartz fluorescence cuvette.

The EEM spectrum of naphthalene in 75 % ethanol is shown in Figure 42 and 43. In the contour plot, the intensity of the fluorescence signal (CPS/mV) corresponds to the color shown in the legend. The most intense signal of naphthalene (3.29 x 10^6 CPS/mV) can be seen at an excitation of 275 nm and an emission of 321 nm. Any optical scattering is not present for this compound. The mesh plot shows highly structured excitation and emission spectra of naphthalene, which is characteristic of the rigidity of the molecule.
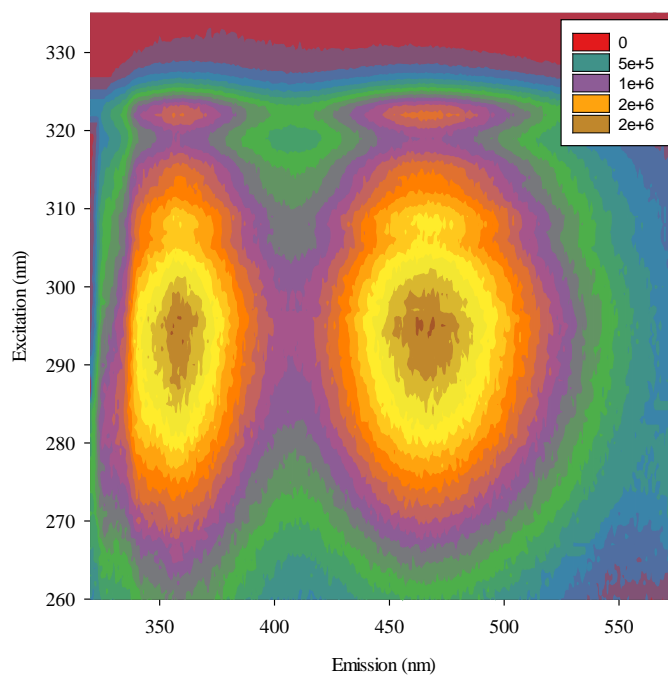
Figure 44: Contour plot of 1 – naphthol in 75 % ethanol in a standard quartz fluorescence cuvette.
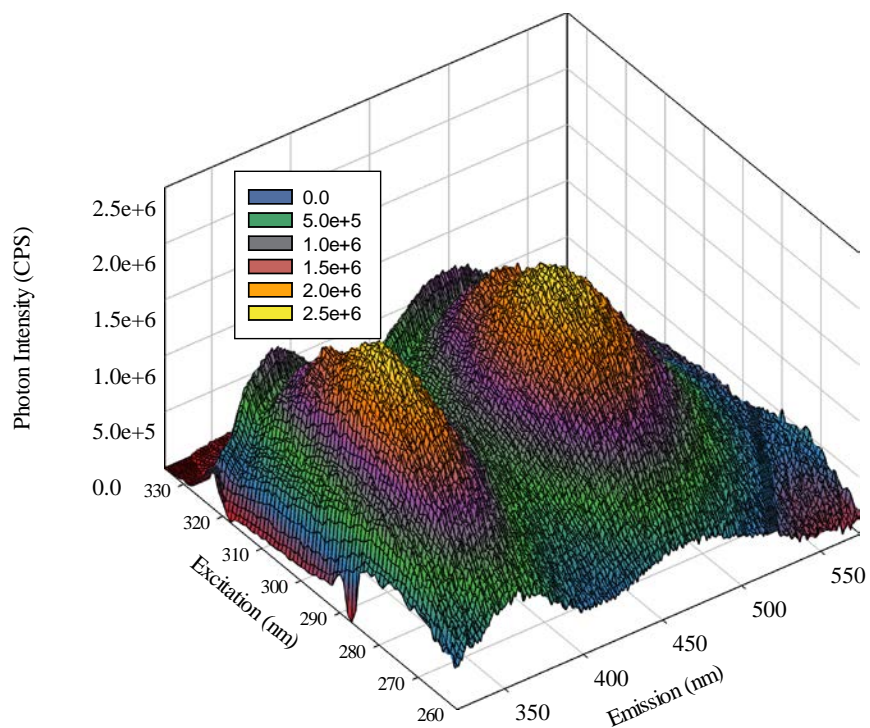
Figure 45: Three – dimensional mesh plot of 1 – naphthol in 75 % ethanol in a standard quartz fluorescence cuvette.

The EEM spectrum of 1 – naphthol in 75 % ethanol is shown in Figure 40 and 41. In the contour plot, the intensity of the fluorescence signal (CPS/mV) corresponds to the color shown in the legend. The most intense signal of 1 – naphthol (2.07 x 10^6 CPS/mV) can be seen at an excitation of 295 nm and an emission of 464 nm. Any optical scattering is not present for this compound. The mesh plot shows a lack of fine structure in the excitation and emission spectra of 1 – naphthol, which is characteristic of the flexibility of the molecule and its vibration patterns between the ground (S_0) and excited states (S_1).
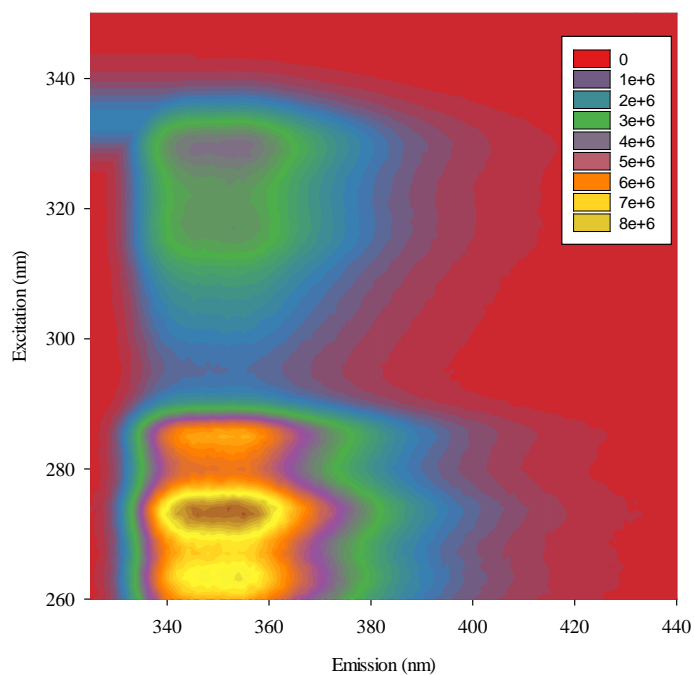
Figure 46: Contour plot of 2 – naphthol in 75 % ethanol in a standard quartz fluorescence cuvette.
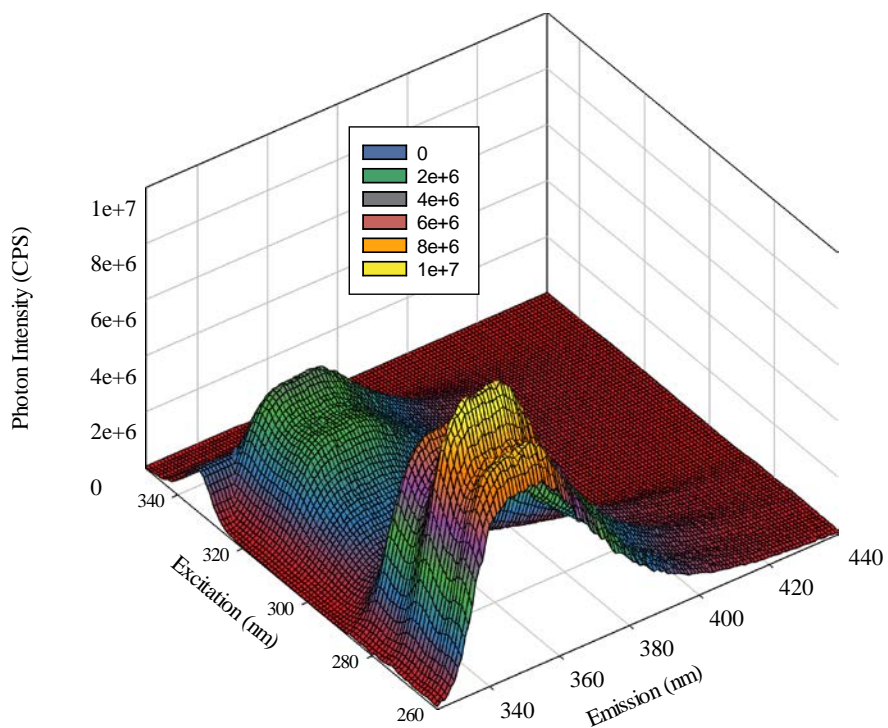
Figure 47: Three – dimensional mesh plot of 2 – naphthol in 75 % ethanol in a standard quartz fluorescence cuvette.

The EEM spectrum of 2 – naphthol in 75 % ethanol is shown in Figure 46 and 47. In the contour plot, the intensity of the fluorescence signal (CPS/mV) corresponds to the color shown in the legend. The most intense signal of 2 – naphthol (8.93×10^6 CPS/mV) can be seen at an excitation of 273 nm and an emission of 355 nm. First order Rayleigh lines are apparent in 2 – naphthol beginning at an excitation wavelength of approximately 330 nm and an emission wavelength of approximately 330 nm. The mesh plot shows a lack of fine structure in the excitation and emission spectra of 2 – naphthol, which is characteristic of the flexibility of the molecule and its vibration patterns between the ground (S_0) and excited states (S_1).
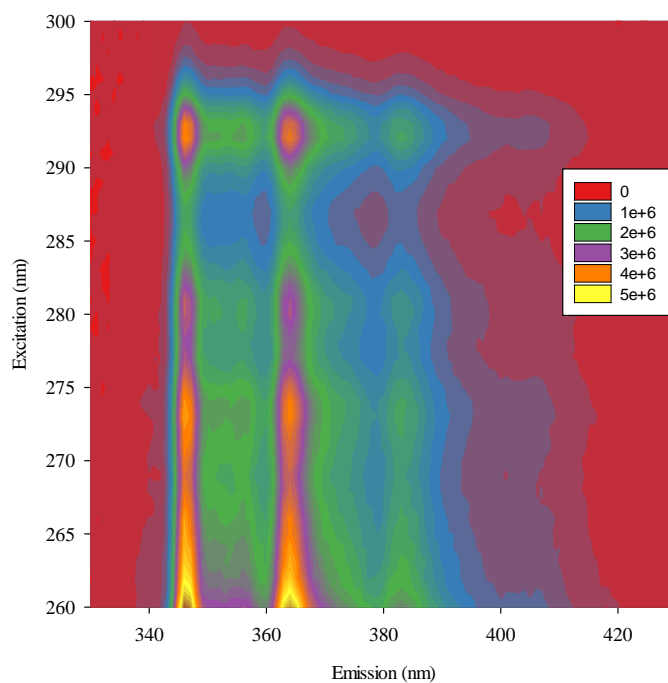
Figure 48: Contour plot of phenathrene in 75 % ethanol in a standard quartz fluorescence cuvette.
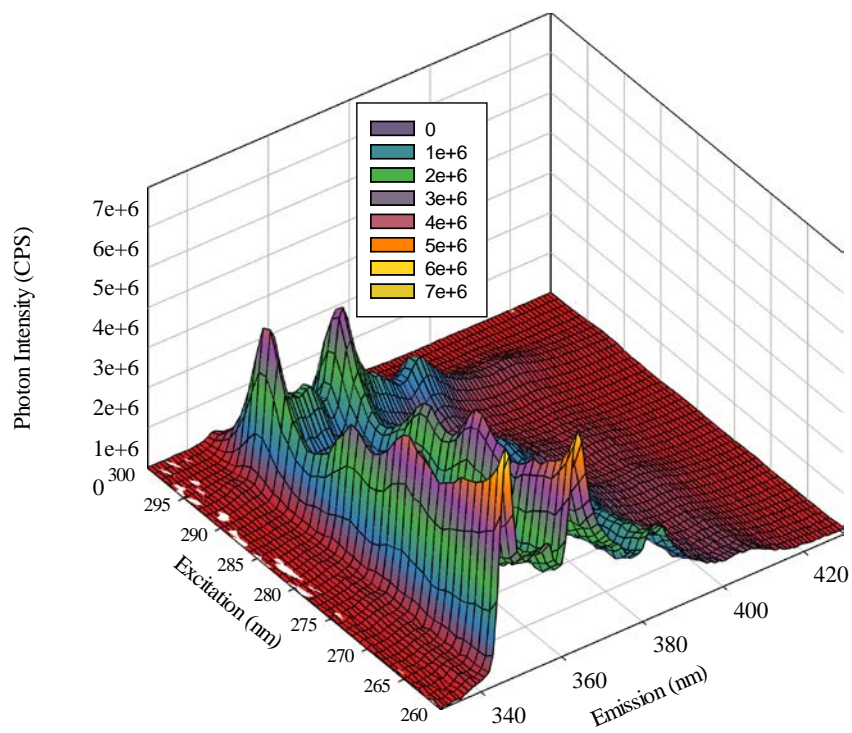
Figure 49: Three – dimensional mesh plot of phenanthrene in 75 % ethanol in a standard quartz fluorescence cuvette.

The EEM spectrum of phenanthrene in 75 % ethanol is shown in Figure 48 and 49. In the contour plot, the intensity of the fluorescence signal (CPS/mV) corresponds to the color shown in the legend. The most intense signal of phenanthrene (5.96×10^6 CPS/mV) can be seen at an excitation of 260 nm and an emission of 346 nm. Any optical scattering is not present for this compound. The mesh plot shows finely structured excitation and emission spectra of phenanthrene, which is characteristic of the rigidity of the molecule.
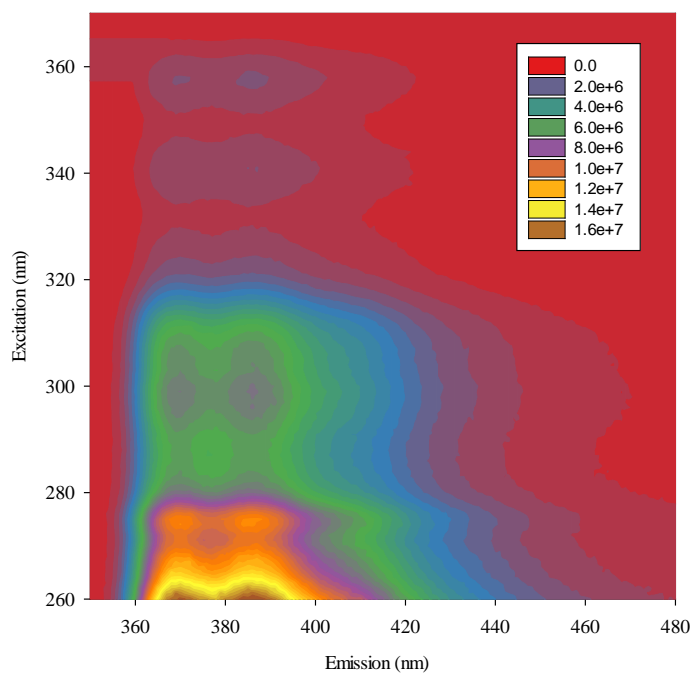
Figure 50: Contour plot of 9 – phenanthrol in 75 % ethanol in a standard quartz fluorescence cuvette.
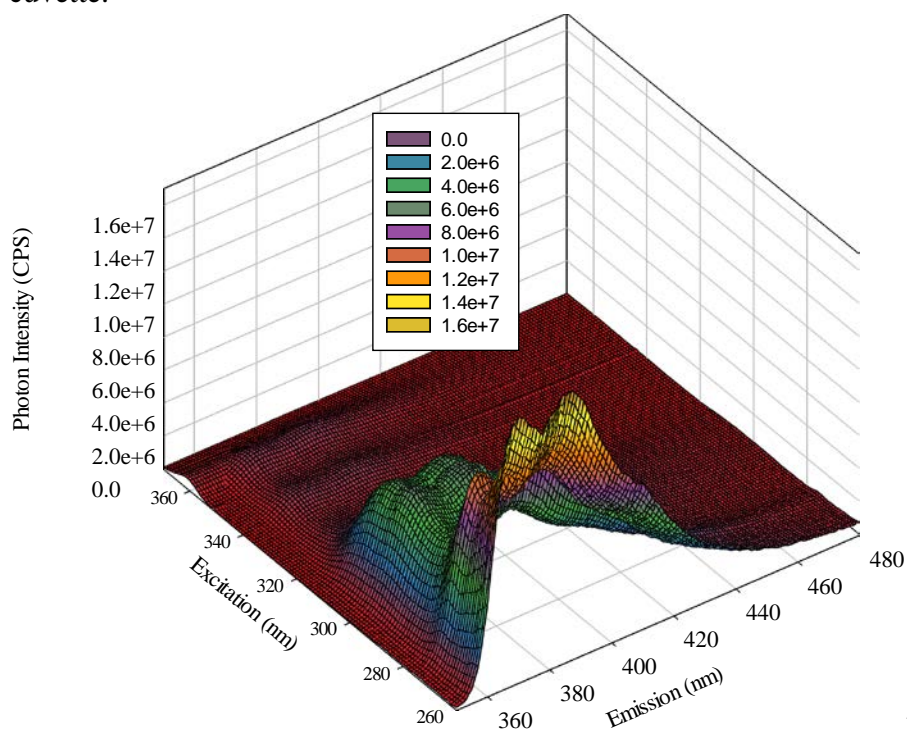
Figure 51: Three – dimensional mesh plot of 9 – phenanthrol in 75 % ethanol in a standard quartz fluorescence cuvette.

The EEM spectrum of 9 – phenanthrol in 75 % ethanol is shown in Figure 50 and 51. In the contour plot, the intensity of the fluorescence signal (CPS/mV) corresponds to the color shown in the legend. The most intense signal of 9 – phenanthrol (1.64 x 10^7 CPS/mV) can be seen at an excitation of 260 nm and an emission of 387 nm. Any optical scattering is not present for this compound. The mesh plot shows a lack of fine structure in the excitation and emission spectra of 9 – phenanthrol, which is characteristic of the flexibility of the molecule and its vibration patterns between the ground (S_0) and excited states (S_1).
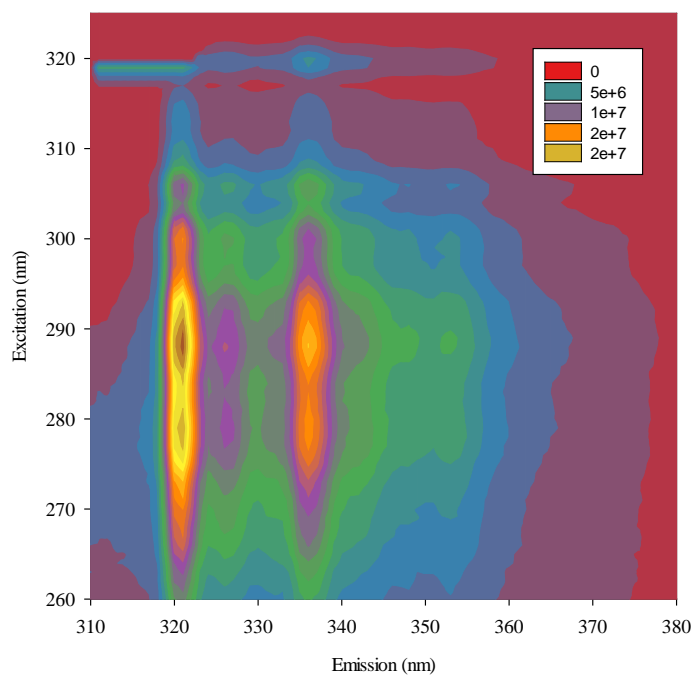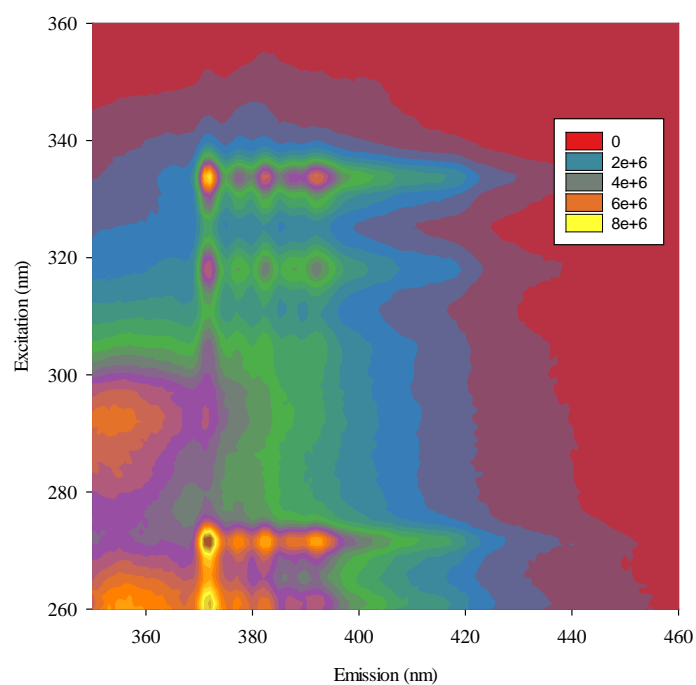
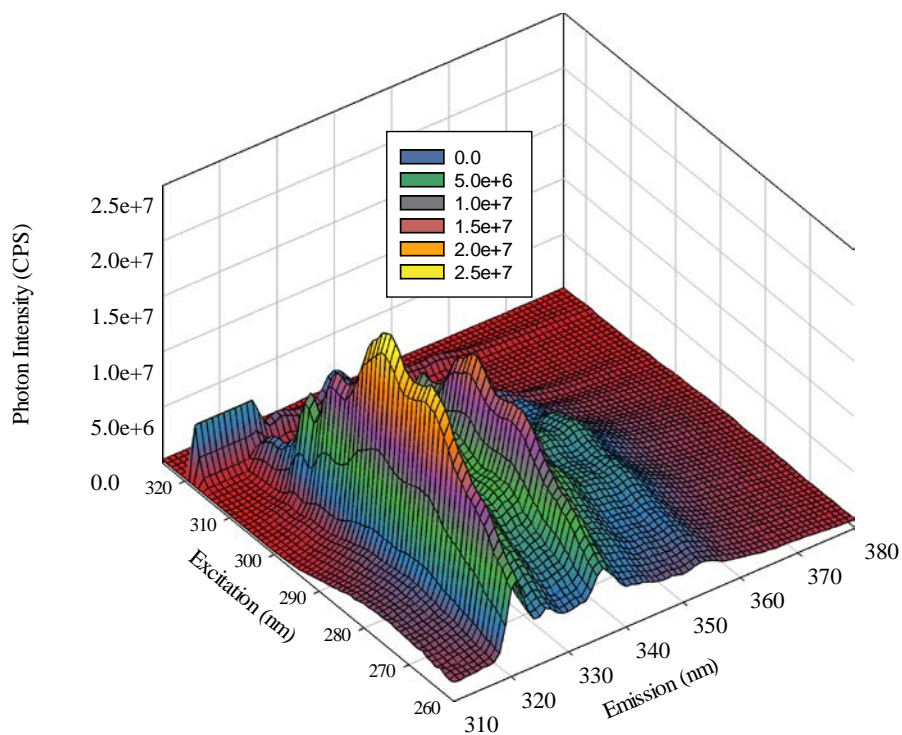Figure 52: Contour plot of pyrene in 75 % ethanol in a standard quartz fluorescence cuvette.
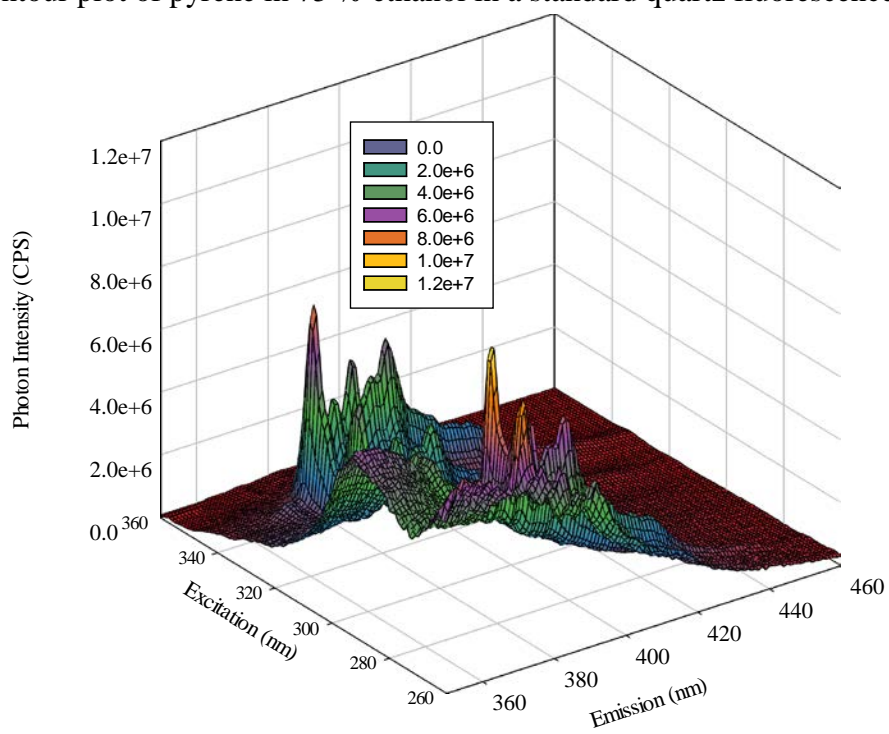
Figure 53: Three – dimensional mesh plot of pyrene in 75 % ethanol in a standard quartz

fluorescence cuvette.

The EEM spectrum of pyrene in 75 % ethanol is shown in Figure 52 and 83. In the contour plot, the intensity of the fluorescence signal (CPS/mV) corresponds to the color shown in the legend. The most intense signal of pyrene (9.64×10^6 CPS/mV) can be seen at an excitation of 272 nm and an emission of 372 nm. Any optical scattering is not present for this compound. The mesh plot shows finely structured excitation and emission spectra of pyrene, which is characteristic of the rigidity of the molecule.
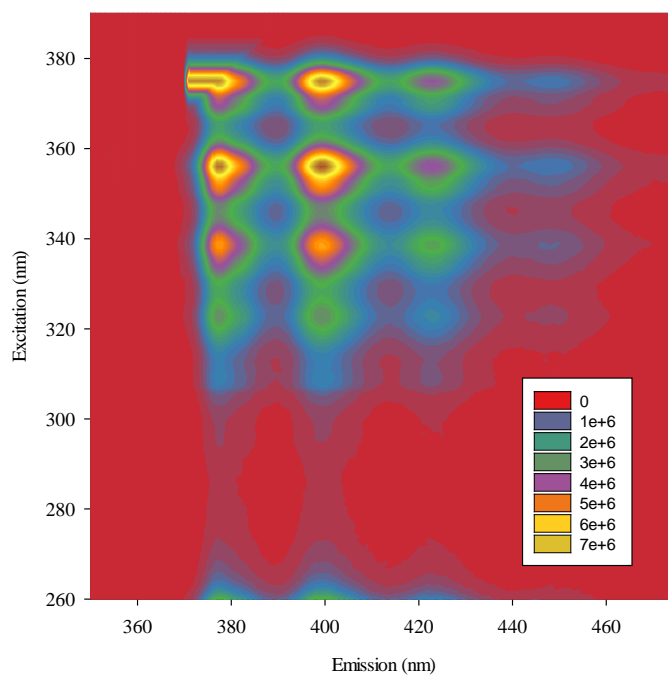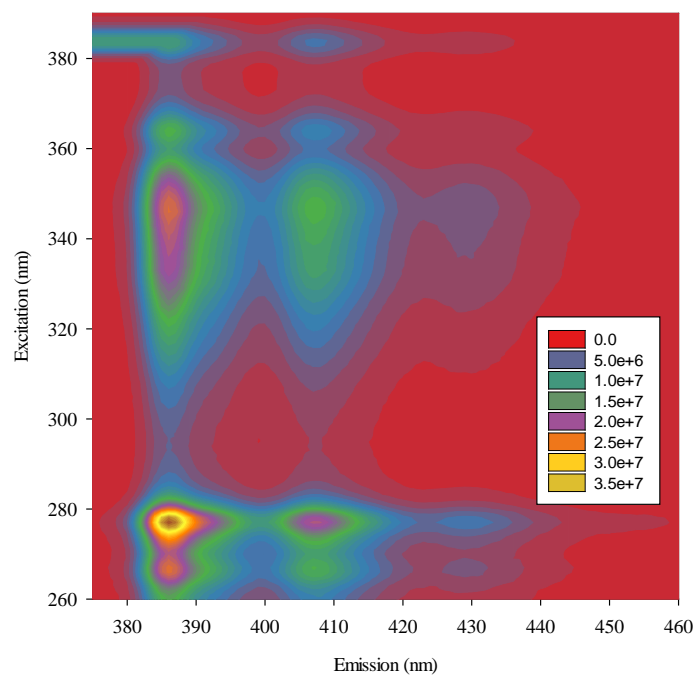
Figure 54: Contour plot of 1 – pyrenol in 75 % ethanol in a standard quartz fluorescence cuvette.
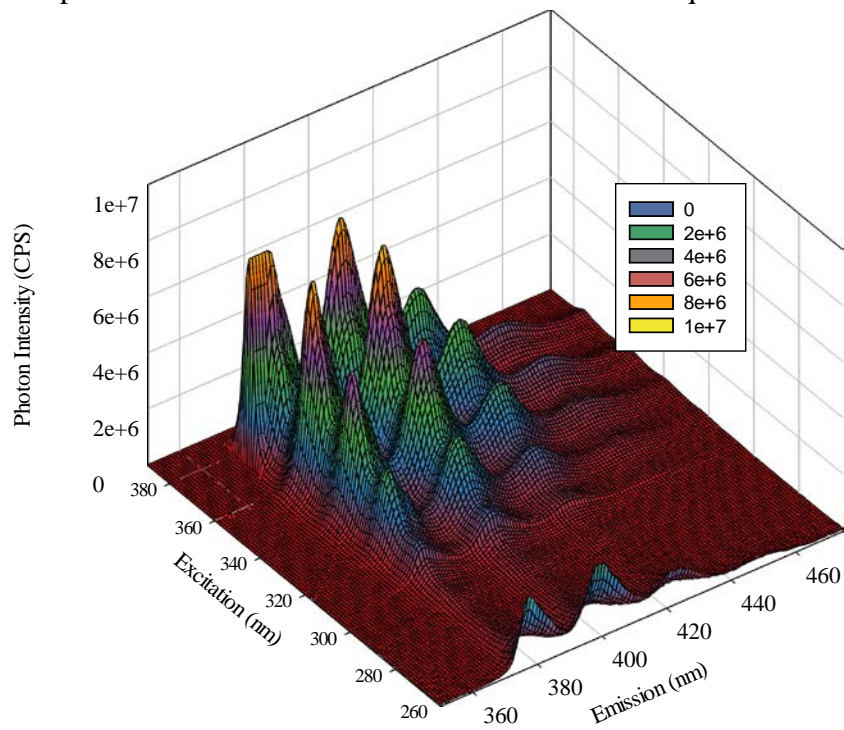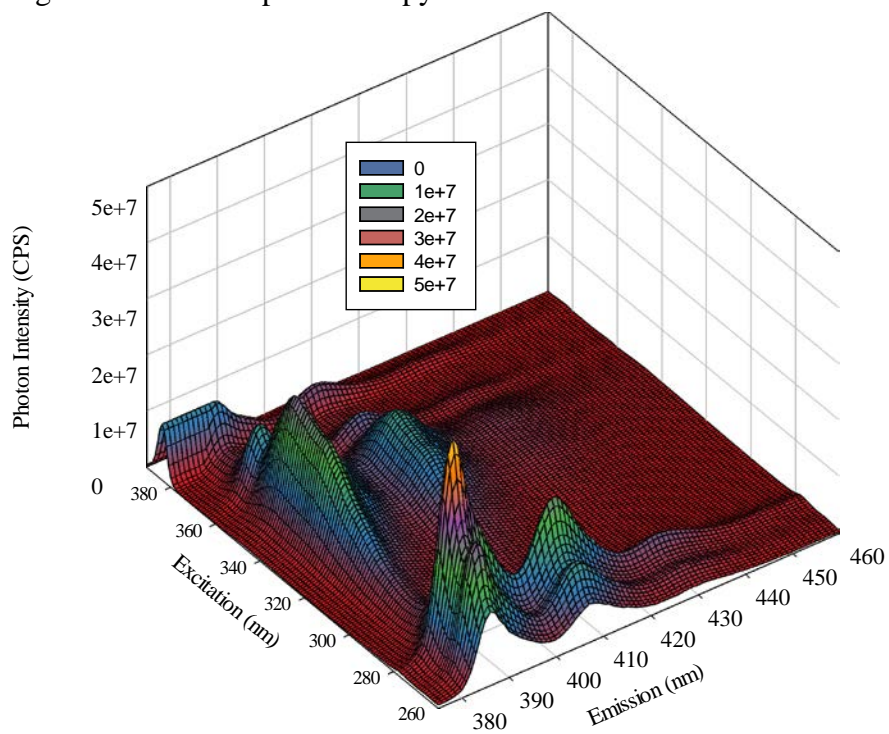

Figure 55: Three – dimensional mesh plot of 1 – pyrenol in 75 % ethanol in a standard quartz fluorescence cuvette.

The EEM spectrum of 1 – pyrenol in 75 % ethanol is shown in Figure 54 and 55. In the contour plot, the intensity of the fluorescence signal (CPS/mV) corresponds to the color shown in the legend. The most intense signal of 1 – pyrenol (3.86 x 10^7 CPS/mV) can be seen at an excitation of 277 nm and an emission of 386 nm. First order Rayleigh lines are apparent in 1 – pyrenol beginning at an excitation wavelength of approximately 380 nm and an emission wavelength of approximately 380 nm. The mesh plot shows a lack of fine structure in the excitation and emission spectra of 1 – pyrenol, which is characteristic of the flexibility of the molecule and its vibration patterns between the ground (S_0) and excited states (S_1).

IV.   Quantum Yields

The quantum efficiencies, or yields, (Φ_f) were calculated using Equation 2. Quantum yields can change depending on temperature and solvent. Substitutions on parent fluorophores will also change the nature of the quantum yield. The quantum yields of the PAHs and their metabolites were measured using a reference standard appropriate to the particular fluorophore.[3] Reference standards were chosen based on similar excitation (absorption) wavelength (nm) and intensity of absorption peaks were kept similar using concentration of sample and reference. Tables 4 – 9 on pages 85 – 90 show the quantum yield data for all PAHs studied using various reference standards (known quantum yields) optimizing for excitation (absorption) wavelength (nm) and intensity of absorption peak.

Compound Name	1 – Naphthol	Fluoranthene	Benzo [a] pyrene
area under emission curve (sample)	1.01×10^8	3.2×10^8	2.86×10^7
area under emission curve (standard)	7.93×10^8	9.76×10^8	4.67×10^7
absorbance of sample at excitation wavelength	0.12	0.15	0.09
absorbance of standard at excitation wavelength	0.13	0.15	0.1
refractive index of sample solvent (squared)	1.86	1.86	1.86
refractive index of standard solvent (squared)	1.81	1.81	1.81
Φ_r (standard)	0.546	0.546	0.546
Φ_r (sample)	**0.065**	**0.19**	**0.31**

Table 4: Quantum Yields of polycyclic aromatic hydrocarbons and metabolites using quinine bisulfate in 0.5 M H_2SO_4.

Table 4 shows quantum yield data when quinine bisulfate in 0.5 M H_2SO_4 was used as a reference standard for 1 – naphthol, fluoranthene, and benzo [a] pyrene at excitation wavelengths

of 324 nm, 342 nm, and 302 nm respectively. 1 – naphthol in cyclohexane has a quantum yield of 0.21 while in a non-polar solvent (solvent not specified in reference) it has a quantum yield of 0.17.[9] When placed in 75 % ethanol, the quantum yield of 1 – naphthol drops significantly to 0.065. The higher polarity of the solvent as well as hydrogen bonding with the addition of the hydroxyl group decreases the quantum efficiency of the molecule. Fluoranthene has a quantum yield of 0.21 in a polar solvent.[10] In 75 % ethanol, the quantum yield of fluoranthene is 0.19. The change in solvent only slightly decreases the quantum efficiency of the molecule. Benzo [a] pyrene has a quantum yield of 0.42 in a polar solvent.[10] The change of solvent to 75 % ethanol decreases the quantum efficiency to 0.31.

Compound Name	Anthracene	1 – Pyrenol	9 – Phenanthrol	2 – Naphthol
area under emission curve (sample)	1.93×10^8	4.73×10^8	6.34×10^7	2.07×10^8
area under emission curve (standard)	1.75×10^8	1.67×10^8	4.74×10^7	1.46×10^8
absorbance of sample at excitation wavelength	0.094	0.089	0.063	0.084
absorbance of standard at excitation wavelength	0.099	0.099	0.071	0.084
refractive index of sample solvent (squared)	1.86	1.86	1.86	1.86
refractive index of standard solvent (squared)	1.85	1.85	1.85	1.85
Φ_r (standard)	0.27	0.27	0.27	0.27
Φ_r (sample)	**0.29**	**0.69**	**0.32**	**0.39**

Table 5: Quantum Yields of polycyclic aromatic hydrocarbons and metabolites using anthracene in 100 % ethanol.

Table 5 shows quantum yield data when anthracene in 100 % ethanol is used as a reference standard for anthracene, 1 – pyrenol, 9 – phenanthrol, and 2 – naphthol at excitation wavelengths of 310 nm, 340 nm, 310 nm, and 330 nm respectively. Anthracene in 100 % ethanol has a

quantum efficiency of 0.27 while in 75 % ethanol its quantum yield is 0.29, only a slight increase with the addition of water.[11] 1 – Pyrenol has a quantum yield of 0.66 in a 5 mM phosphate buffer at pH 8, while in 75 % ethanol it showed a quantum efficiency of 0.69, a slight increase with a decrease in pH.[12] 9 – Phenanthrol does not have a known quantum yield for comparison. It is shown to have a quantum efficiency of 0.32 in 75 % ethanol. 2 – Naphthol has a quantum yield of 0.27 in a non-polar solvent and 0.32 in cyclohexane.[9] In 75 % ethanol the quantum yield of 2 – naphthol increases to 0.39.

Compound Name	Naphthalene
area under emission curve (sample)	5.96×10^7
area under emission curve (standard)	2.55×10^7
absorbance of sample at excitation wavelength	0.091
absorbance of standard at excitation wavelength	0.090
refractive index of sample solvent (squared)	1.86
refractive index of standard solvent (squared)	1.85
Φ_r (standard)	0.205
Φ_r (sample)	**0.49**

Table 6: Quantum Yields of polycyclic aromatic hydrocarbons and metabolites using naphthalene in 100 % ethanol.

Table 6 shows quantum yield studies of compounds when naphthalene in 100 % ethanol is used a reference standard for naphthalene in 75 % ethanol at an excitation wavelength of 266 nm. Naphthalene has a quantum yield of 0.205 in 100 % ethanol, but with the addition of water, making the solvent more polar, the quantum yield increases to 0.49.[11]

Compound Name	Phenanthrene	Acenaphthene
area under emission curve (sample)	5.18×10^7	3.68×10^7
area under emission curve (standard)	1.21×10^7	1.05×10^7
absorbance of sample at excitation wavelength	0.087	0.063
absorbance of standard at excitation wavelength	0.081	0.074
refractive index of sample solvent (squared)	1.86	1.86
refractive index of standard solvent (squared)	1.85	1.85
Φ_r (standard)	0.125	0.125
Φ_r (sample)	**0.58**	**0.38**

Table 7: Quantum Yields of polycyclic aromatic hydrocarbons and metabolites using phenanthrene in 100 % ethanol.

Table 7 shows the quantum yields when phenanthrene in 100 % ethanol is used as a reference standard for phenanthrene in 75 % ethanol, and acenaphthene at excitation wavelengths of 294 nm and 282 nm respectively. Phenanthrene has a quantum yield of 0.125 in 100 % ethanol, but with the addition of water, making the solvent more polar, the quantum yield increases to 0.58.[11] Acenaphthene has a quantum yield of 0.39 in a polar solvent and 0.60 in cyclohexane, while in 75 % ethanol it shows a quantum efficiency of 0.38.[13]

Compound Name	Pyrene
area under emission curve (sample)	3.44×10^7
area under emission curve (standard)	1.83×10^7
absorbance of sample at excitation wavelength	0.077
absorbance of standard at excitation wavelength	0.096
refractive index of sample solvent (squared)	1.86
refractive index of standard solvent (squared)	1.85
Φ_r (standard)	0.53
Φ_r (sample)	**0.81**

Table 8: Quantum Yields of polycyclic aromatic hydrocarbons and metabolites using pyrene in 100 % ethanol.

Table 8 shows the quantum yields when pyrene in 100 % ethanol is used as a reference standard for pyrene in 75 % ethanol at an excitation wavelength of 274 nm. Pyrene has a quantum yield of 0.53 in 100 % ethanol, while in 75 % ethanol it has a much higher quantum efficiency of 0.81.[11] The addition of water to the ethanol increases the polarity of the solvent and therefore increased the quantum yield.

Compound Name	Fluorene
area under emission curve (sample)	7.63×10^7
area under emission curve (standard)	1.37×10^8
absorbance of sample at excitation wavelength	0.057
absorbance of standard at excitation wavelength	0.073
refractive index of sample solvent (squared)	1.86
refractive index of standard solvent (squared)	1.85
Φ_r (standard)	0.68
Φ_r (sample)	0.30

Table 9: Quantum Yields of polycyclic aromatic hydrocarbons and metabolites using fluorene in 100 % ethanol.

Table 9 shows quantum yield when fluorene in 100 % ethanol is used as a reference standard for fluorene in 75 % ethanol at an excitation wavelength of 272 nm. Fluorene in 100 % ethanol has a quantum yield of 0.68, while in 75 % ethanol the quantum efficiency of fluorene decreases to 0.30.[11] The increased polarity of the solvent decreases the quantum yield.

Determination of these quantum yields using 75 % ethanol as a solvent was performed initially to decide how well the compounds could potentially be affected by the use of the microwell plate and fiber optic cable. A lower initial fluorescence intensity while using a cuvette could be significantly diminished or eliminated (lost) during use of the fiber optic cable.

V.   Limits of Detection and Quantitation

Calibration plots for each compound were made with the concentrations adjusted because of the variation in quantum yields. Low quantum yield fluorophores produced higher concentrations for calibration than high quantum yield fluorophores. It is useful to think of the quantum yield as the equivalent of the extinction coefficient in absorption spectroscopy. The signal intensity of the highest peak from the emission spectra was used in the plot. Calibration plots for each compound were used to determine both the limit of detection (LoD) and the limit of quantitation (LoQ).[14] Calibration plots can be seen in even numbered Figures 56 – 78. LoD and LoQ were determined by Equation 5 and 6. Limits of detection range from 6.4×10^{-6} and 9.4×10^{-4} mg/mL while limits of quantitation range from 2.1×10^{-5} and 5×10^{-3} mg/mL. The accuracy of the limits of detection and quantitation were also tested and can be seen in odd numbered Figures 57 – 79. It can be seen from these accuracy tests that the spectra of all of the compounds were well above the base line of a cuvette only filled with the solvent. It can also be seen that all the original peaks from the emission spectra were intact and clearly visible. The method for calculating the LoD and LoQ for each compound is on the conservative side, underestimating a true concentration for detection and quantitation. This will be further elaborated upon in the discussion and conclusions.

Compound	Slope	Intercept	R^2
Acenaphthene	1.13×10^8	3.35×10^4	0.998
Anthracene	5.43×10^7	1.13×10^4	0.999
Benzo [a] pyrene	1.45×10^9	2.63×10^3	0.994
Fluoranthene	1.91×10^7	1.71×10^3	0.998
Fluorene	2.78×10^8	1.18×10^4	0.998
Naphthalene	2.23×10^7	2.58×10^2	0.998
1 – Naphthol	6.47×10^6	6.24×10^3	0.985
2 – Naphthol	2.96×10^7	5.80×10^3	0.999
Phenanthrene	5.38×10^7	4.22×10^3	0.999
9 – Phenanthrol	6.63×10^7	2.59×10^4	0.999
Pyrene	8.34×10^8	4.88×10^4	0.991
1 – Pyrenol	2.78×10^8	5.85×10^2	0.997

Table 10: Calibration plot analysis of PAHs and metabolites in 75 % ethanol in a standard quartz fluorescence cuvette.

Table 10 shows the analysis of the calibration plots including the slope, intercept, and r^2 value.[15] Correlation of the slope (r^2 value) for most of the compounds were 0.99. 1 – Naphthol was the only compound that showed a lower correlation of 0.985. This lower correlation can be explained by the quantum yield of 1 – naphthol. It has the lowest quantum yield of the compounds tested therefore it was the hardest to regulate the intensity of signal at low concentrations.

Compound	LoD (mg/mL)	LoQ (mg/mL)
Acenaphthene	1.7×10^{-4}	5.8×10^{-4}
Anthracene	1.3×10^{-4}	4.2×10^{-4}
Benzo [a] pyrene	6.4×10^{-6}	2.1×10^{-5}
Fluoranthene	1.8×10^{-4}	5.9×10^{-4}
Fluorene	3.8×10^{-5}	1.3×10^{-4}
Naphthalene	1.3×10^{-4}	4.3×10^{-4}
1 – Naphthol	9.4×10^{-4}	3.1×10^{-3}
2 – Naphthol	1.4×10^{-4}	4.8×10^{-4}
Phenanthrene	5.0×10^{-5}	1.7×10^{-4}
9 – Phenanthrol	1.4×10^{-4}	4.8×10^{-4}
Pyrene	6.1×10^{-5}	2.0×10^{-4}
1 – Pyrenol	3.7×10^{-5}	1.2×10^{-4}

Table 11: Limits of detection and quantitation values of PAHs and metabolites in 75 % ethanol in a standard quartz fluorescence cuvette.

Table 11 shows the values of limit of detection and quantitation for all the compounds. Compounds with higher quantum yields had lower limits of detection, such as pyrene, while compounds with lower quantum yield had higher limits of detection, such as 1 – naphthol. Benzo [a] pyrene had lower limits of detection despite showing a lower quantum yield.

Figure 56: Calibration plot of acenaphthene in 75 % ethanol in a standard quartz fluorescence cuvette.

The calibration plot of acenaphthene in 75 % ethanol can be seen in Figure 56. Seven points were used to construct the plot using an excitation wavelength of 290 nm and an emission wavelength of 338 nm. The concentration of 0.0003 mg/mL yielded a fluorescence intensity of 5.3 x 10^4 CPS/mv while a concentration of 0.006 mg/mL yielded a fluorescence intensity of 7.0 x 10^5 CPS/mV. The R^2 value for this calibration plot was 0.998.

Figure 57: Accuracy of calculations for limit of detection and quantitation of acenaphthene in 75 % ethanol in a standard quartz fluorescence cuvette.

An emission spectrum was generated to test the accuracy of the calculations performed using the calibration plots to determine the LoD and LoQ of acenaphthene in 75 % ethanol and can be seen in Figure 57. The LoD calculated is 1.74×10^{-4} mg/mL and produces a fluorescence intensity of 5.1×10^4 CPS/mV. The LoQ calculated is 5.80×10^{-4} mg/mL and produces a fluorescence intensity of 9.2×10^4 CPS/mV.

Figure 58: Calibration plot of anthracene in 75 % ethanol in a standard quartz fluorescence cuvette.

The calibration plot of anthracene in 75 % ethanol can be seen in Figure 58. Seven points were used to construct the plot using an excitation wavelength of 340 nm and an emission wavelength of 425 nm. The concentration of 0.0003 mg/mL yielded a fluorescence intensity of 2.2×10^4 CPS/mV and a concentration of 0.007 mg/mL yielded a fluorescence intensity of 3.9×10^5 CPS/mV. The R^2 value for this calibration plot was 0.999.

Figure 59: Accuracy of calculations for limit of detection and quantitation of anthracene in 75 % ethanol in a standard quartz fluorescence cuvette.

An emission spectrum was generated to test the accuracy of the calculations performed using the calibration plots to determine the LoD and LoQ of anthracene in 75 % ethanol and can be seen in Figure 59. The LoD calculated is 1.26×10^{-4} mg/mL and produces a fluorescence intensity of 4.1×10^4 CPS/mV. The LoQ calculated is 4.18×10^{-4} mg/mL and produces a fluorescence intensity of 5.6×10^4 CPS/mV.

Figure 60: Calibration plot of benzo [a] pyrene in 75 % ethanol in a standard quartz fluorescence cuvette.

The calibration plot of benzo [a] pyrene in 75 % ethanol can be seen in Figure 60. Seven points were used to construct the plot using an excitation wavelength of 296 nm and an emission wavelength of 404 nm. The concentration of 0.00003 mg/mL yielded a fluorescence intensity of 4.6×10^4 CPS/mv while a concentration of 0.00009 mg/mL yielded a fluorescence intensity of 1.4×10^5 CPS/mV. The R^2 value for this calibration plot was 0.994.

Figure 61: Accuracy of calculations for limit of detection and quantitation of benzo [a] pyrene in 75 % ethanol in a standard quartz fluorescence cuvette.

An emission spectrum was generated to test the accuracy of the calculations performed using the calibration plots to determine the LoD and LoQ of benzo [a] pyrene in 75 % ethanol and can be seen in Figure 61. The LoD calculated is 6.39×10^{-6} mg/mL and produces a fluorescence intensity of 1.2×10^4 CPS/mV. The LoQ calculated is 2.13×10^{-5} mg/mL and produces a fluorescence intensity of 3.4×10^4 CPS/mV.
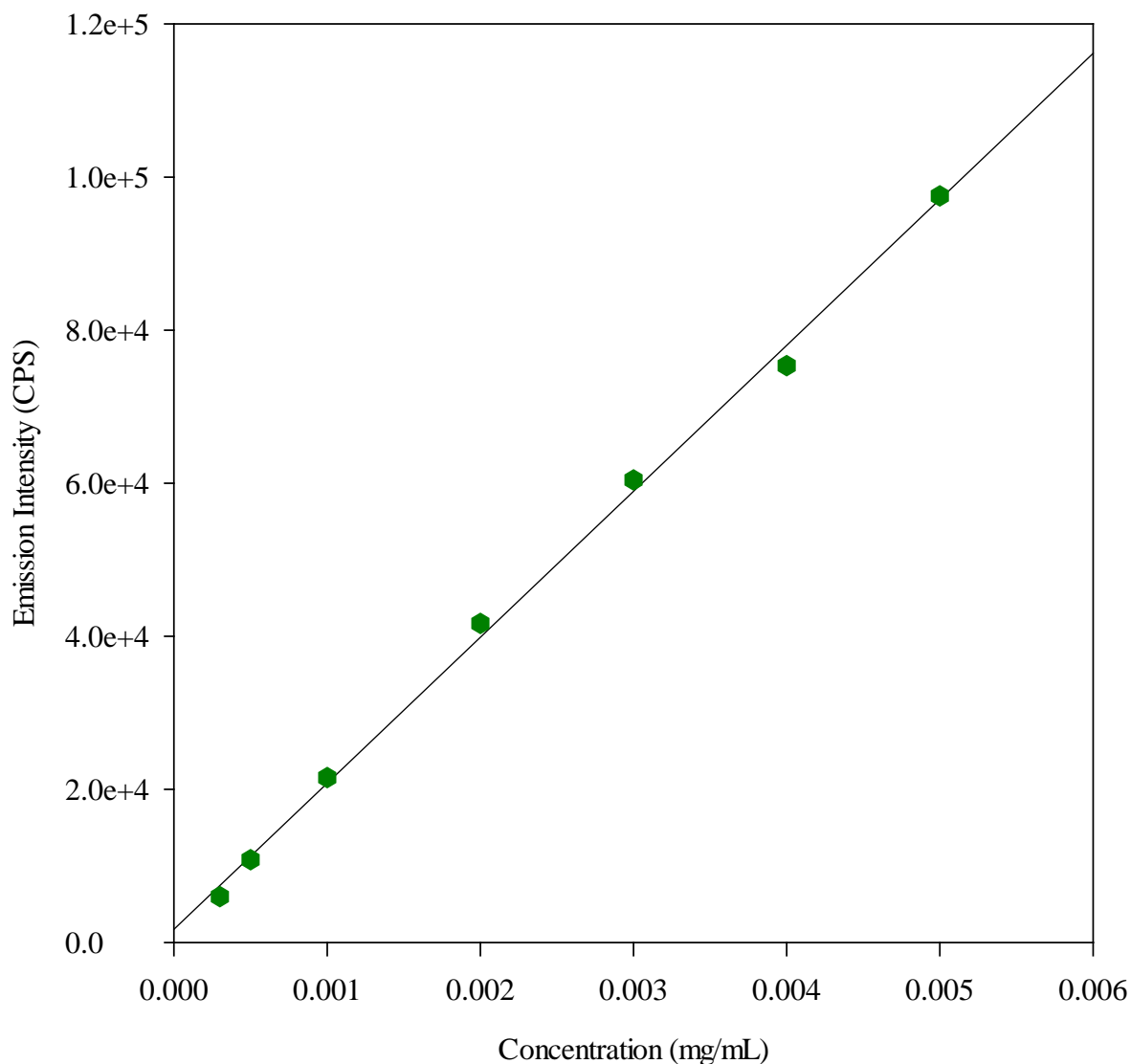
Figure 62: Calibration plot of fluoranthene in 75 % ethanol in a standard quartz fluorescence cuvette.

The calibration plot of fluoranthene in 75 % ethanol can be seen in Figure 62. Seven points were used to construct the plot using an excitation wavelength of 308 nm and an emission wavelength of 462 nm. The concentration of 0.0003 mg/mL yielded a fluorescence intensity of 6.0×10^3 CPS/mv while a concentration of 0.005 mg/mL yielded a fluorescence intensity of 9.8×10^4 CPS/mV. The R^2 value for this calibration plot was 0.998.

Figure 63: Accuracy of calculations for limit of detection and quantitation of fluoranthene in 75 % ethanol in a standard quartz fluorescence cuvette.

An emission spectrum was generated to test the accuracy of the calculations performed using the calibration plots to determine the LoD and LoQ of fluoranthene in 75 % ethanol and can be seen in Figure 63. The LoD calculated is 1.77×10^{-4} mg/mL and produces a fluorescence intensity of 5.1×10^3 CPS/mV. The LoQ calculated is 5.89×10^{-4} mg/mL and produces a fluorescence intensity of 1.3×10^4 CPS/mV.

Figure 64: Calibration plot of fluorene in 75 % ethanol in a standard quartz fluorescence cuvette.

The calibration plot of fluorene in 75 % ethanol can be seen in Figure 64. Seven points were used to construct the plot using an excitation wavelength of 262 nm and an emission wavelength of 303 nm. The concentration of 0.0001 mg/mL yielded a fluorescence intensity of 3.9×10^4 CPS/mv while a concentration of 0.00085 mg/mL yielded a fluorescence intensity of 2.4×10^5 CPS/mV. The R^2 value for this calibration plot was 0.998.

Figure 65: Accuracy of calculations for limit of detection and quantitation of fluorene in 75 % ethanol in a standard quartz fluorescence cuvette.

An emission spectrum was generated to test the accuracy of the calculations performed using the calibration plots to determine the LoD and LoQ of fluorene in 75 % ethanol and can be seen in Figure 65. The LoD calculated is 3.76×10^{-5} mg/mL and produces a fluorescence intensity of 2.2×10^4 CPS/mV. The LoQ calculated is 1.25×10^{-4} mg/mL and produces a fluorescence intensity of 4.6×10^4 CPS/mV.

Figure 66: Calibration plot of naphthalene in 75 % ethanol in a standard quartz fluorescence cuvette.

The calibration plot of naphthalene in 75 % ethanol can be seen in Figure 66. Seven points were used to construct the plot using an excitation wavelength of 286 nm and an emission wavelength of 337 nm. The concentration of 0.0005 mg/mL yielded a fluorescence intensity of 1.1×10^4 CPS/mv while a concentration of 0.004 mg/mL yielded a fluorescence intensity of 8.8 $\times 10^5$ CPS/mV. The R^2 value for this calibration plot was 0.998.

Figure 67: Accuracy of calculations for limit of detection and quantitation of naphthalene in 75 % ethanol in a standard quartz fluorescence cuvette.

An emission spectrum was generated to test the accuracy of the calculations performed using the calibration plots to determine the LoD and LoQ of naphthalene in 75 % ethanol and can be seen in Figure 67. The LoD calculated is 1.30×10^{-4} mg/mL and produces a fluorescence intensity of 3.2×10^3 CPS/mV. The LoQ calculated is 4.34×10^{-4} mg/mL and produces a fluorescence intensity of 9.9×10^3 CPS/mV.
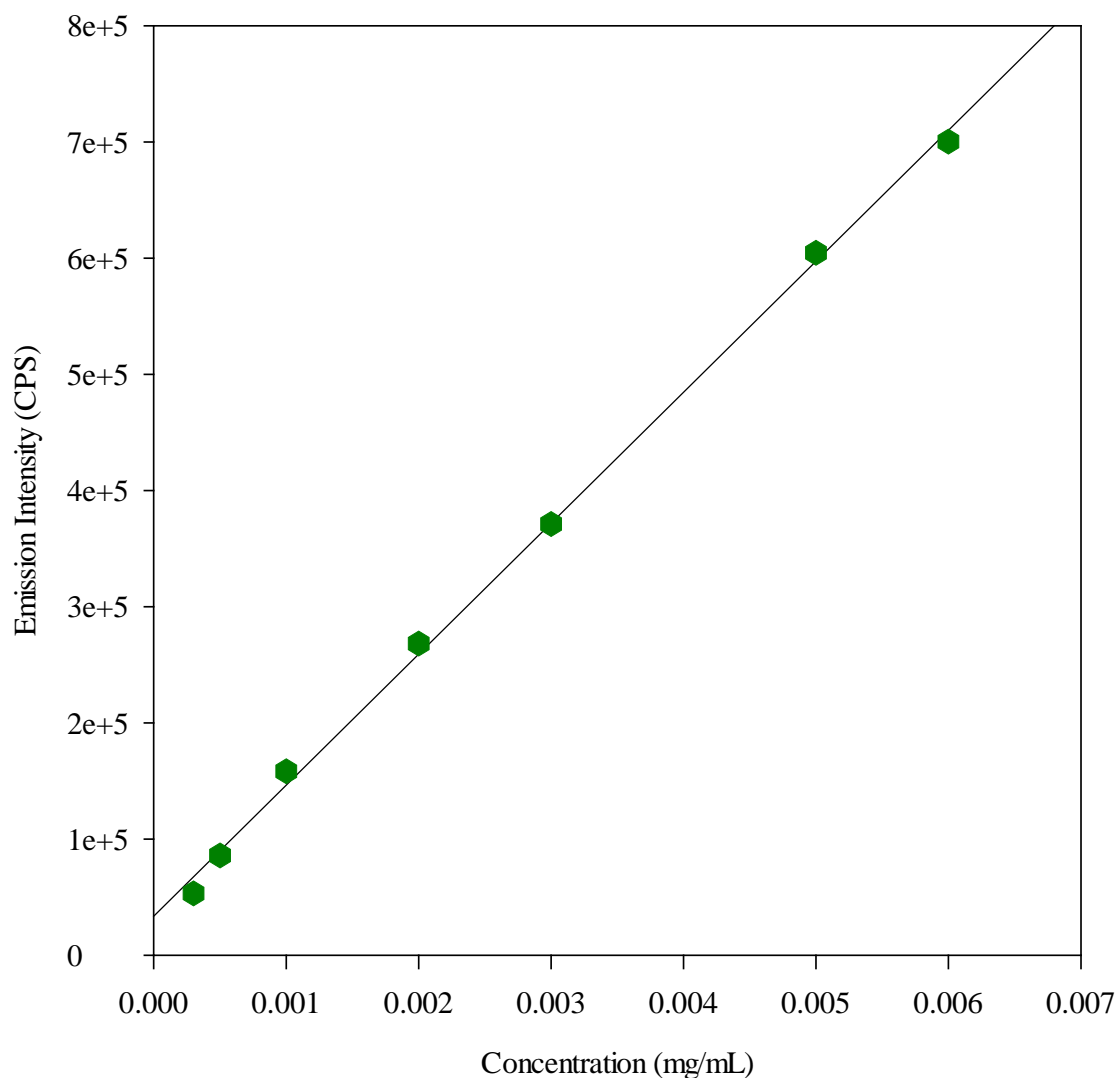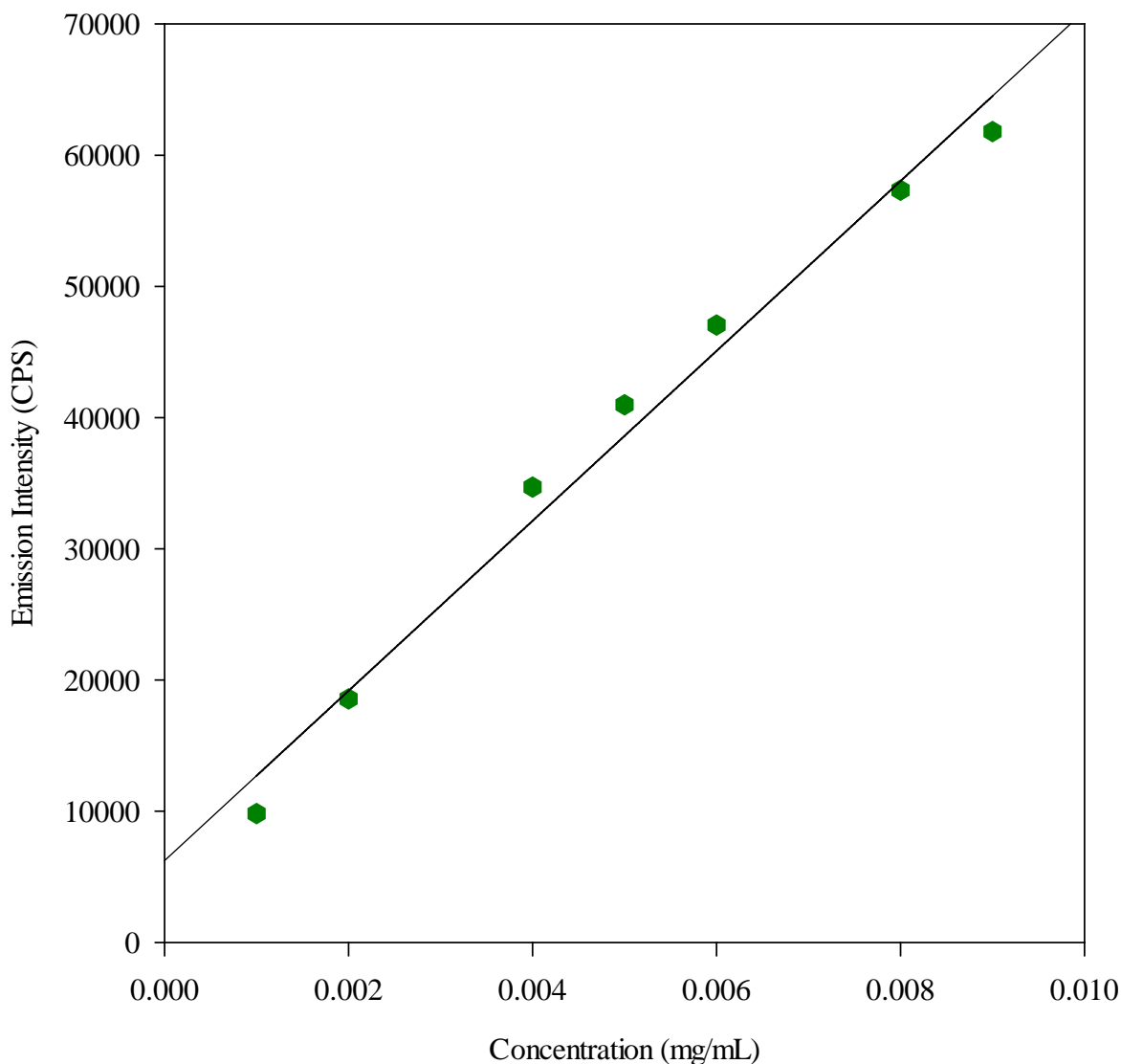
Figure 68: Calibration plot of 1 – naphthol in 75 % ethanol in a standard quartz fluorescence cuvette.

The calibration plot of 1 – naphthol in 75 % ethanol can be seen in Figure 68. Seven points were used to construct the plot using an excitation wavelength of 296 nm and an emission wavelength of 368 nm. The concentration of 0.001 mg/mL yielded a fluorescence intensity of 9.8 x 10^3 CPS/mv while 0.009 mg/mL yielded a fluorescence intensity of 6.2 x 10^4 CPS/mV. The R^2 value for this calibration plot was 0.985.
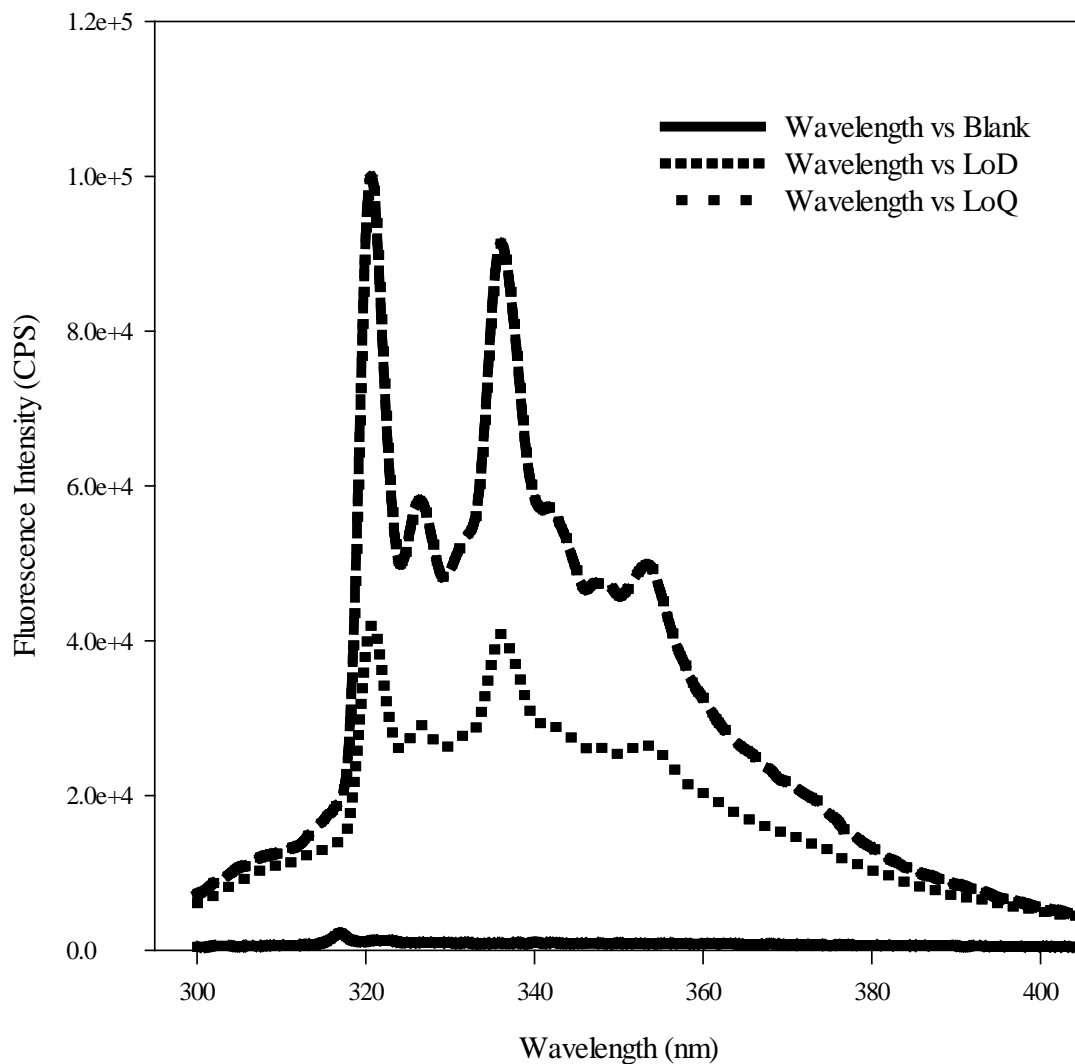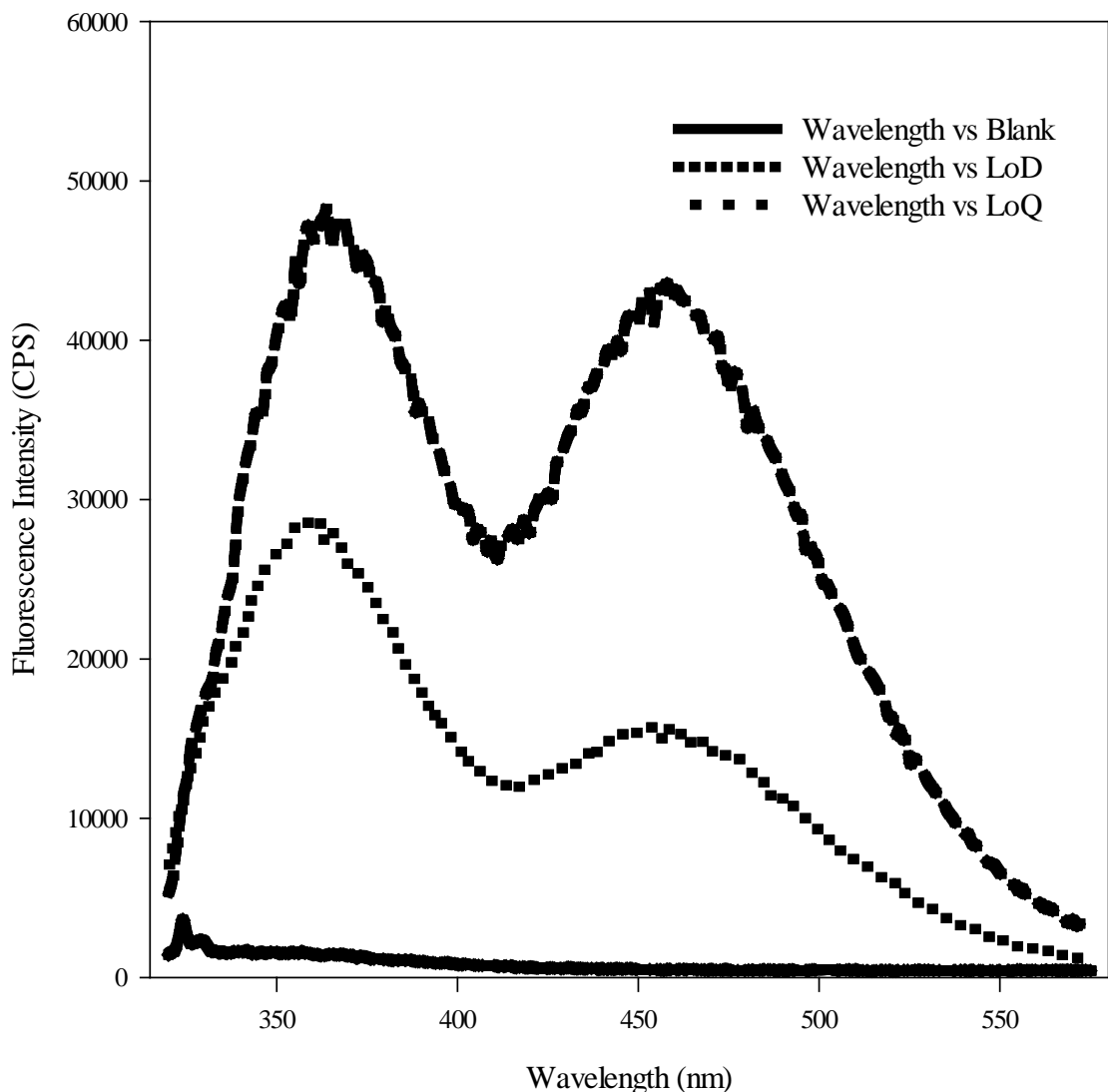
Figure 69: Accuracy of calculations for limit of detection and quantitation of 1 – naphthol in 75 % ethanol in a standard quartz fluorescence cuvette.

An emission spectrum was generated to test the accuracy of the calculations performed using the calibration plots to determine the LoD and LoQ of 1 – naphthol in 75 % ethanol and can be seen in Figure 69. The LoD calculated is 9.36×10^{-4} mg/mL and produces a fluorescence intensity of 1.2×10^4 CPS/mV. The LoQ calculated is 3.12×10^{-3} mg/mL and produces a fluorescence intensity of 2.6×10^4 CPS/mV.
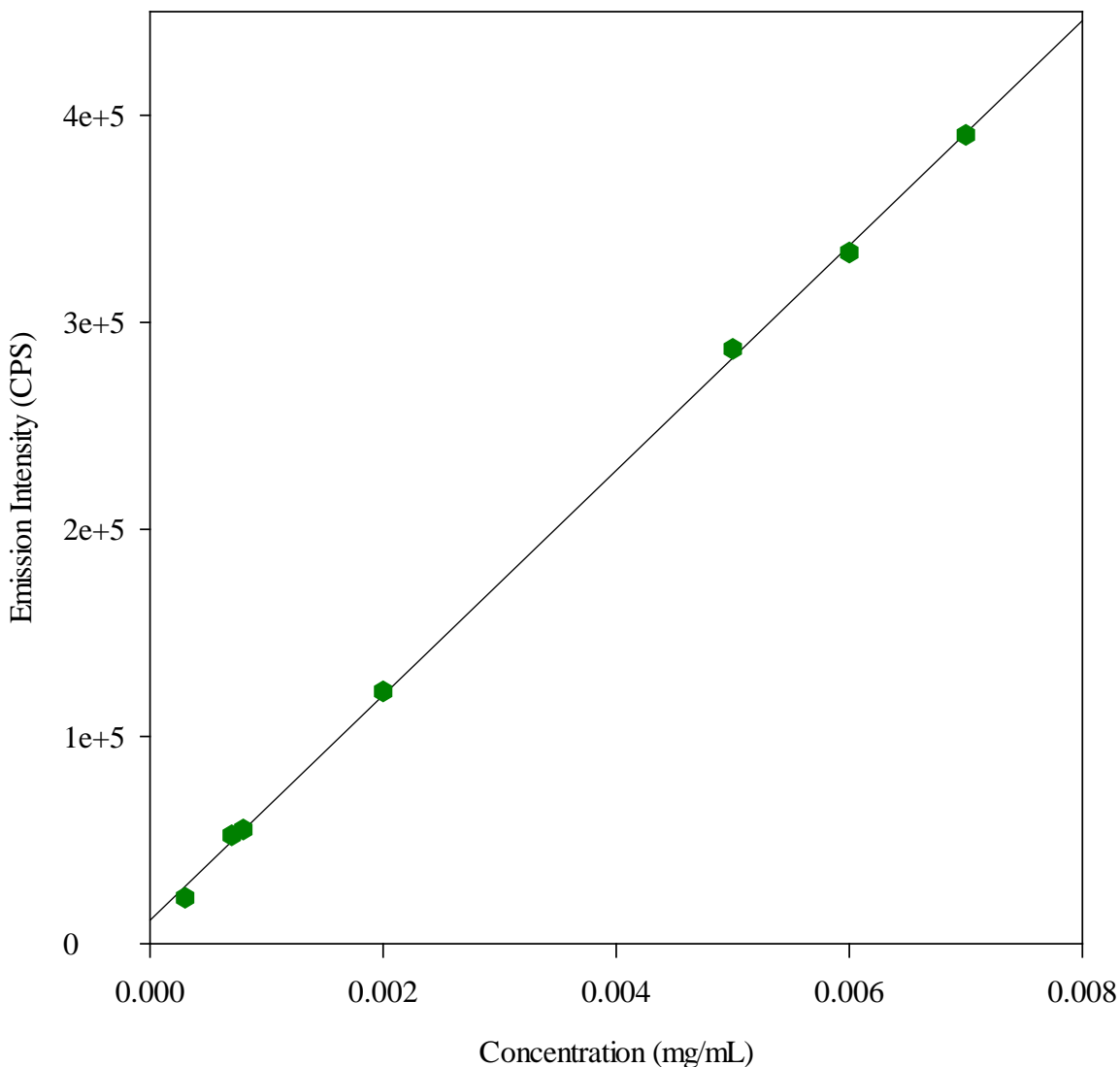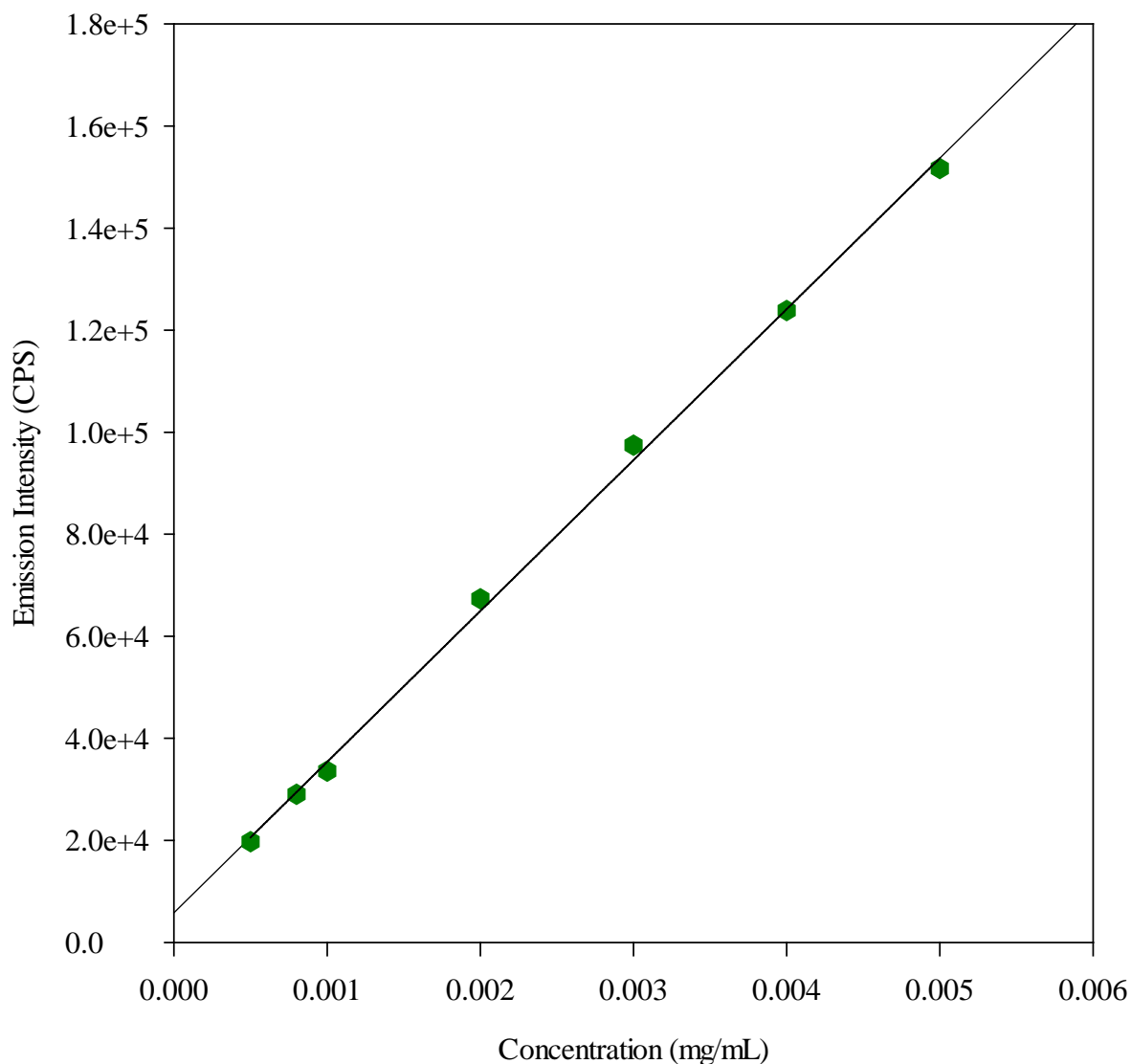
Figure 70: Calibration plot of 2 – naphthol in 75 % ethanol in a standard quartz fluorescence cuvette.

The calibration plot of 2 – naphthol in 75 % ethanol can be seen in Figure 70. Seven points were used to construct the plot using an excitation wavelength of 264 nm and an emission wavelength of 358 nm. The concentration of 0.0005 mg/mL yielded a fluorescence intensity of 2.0×10^4 CPS/mv while a 0.005 mg/mL yielded a fluorescence intensity of 1.5×10^5 CPS/mV. The R^2 value for this calibration plot was 0.999.
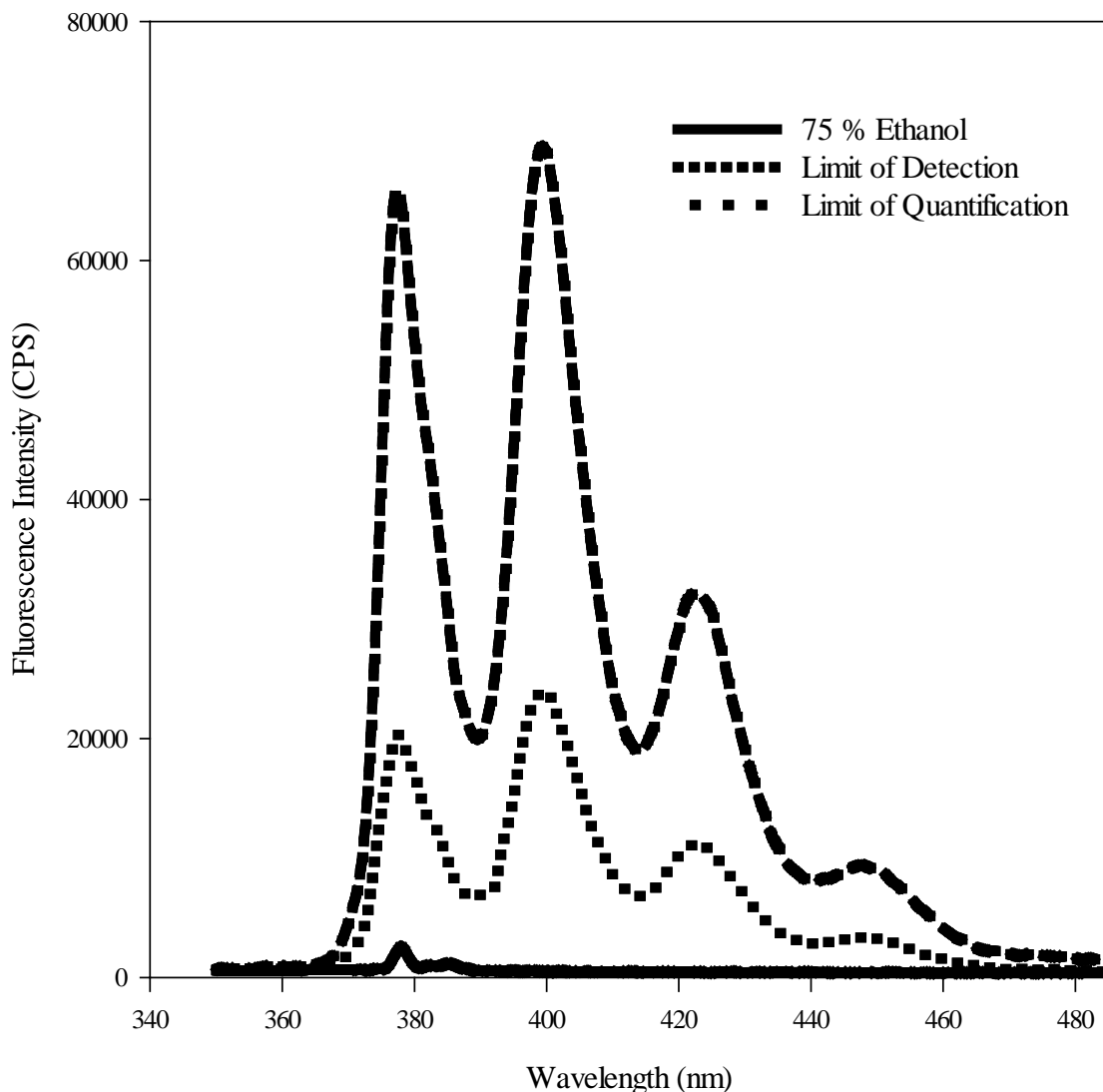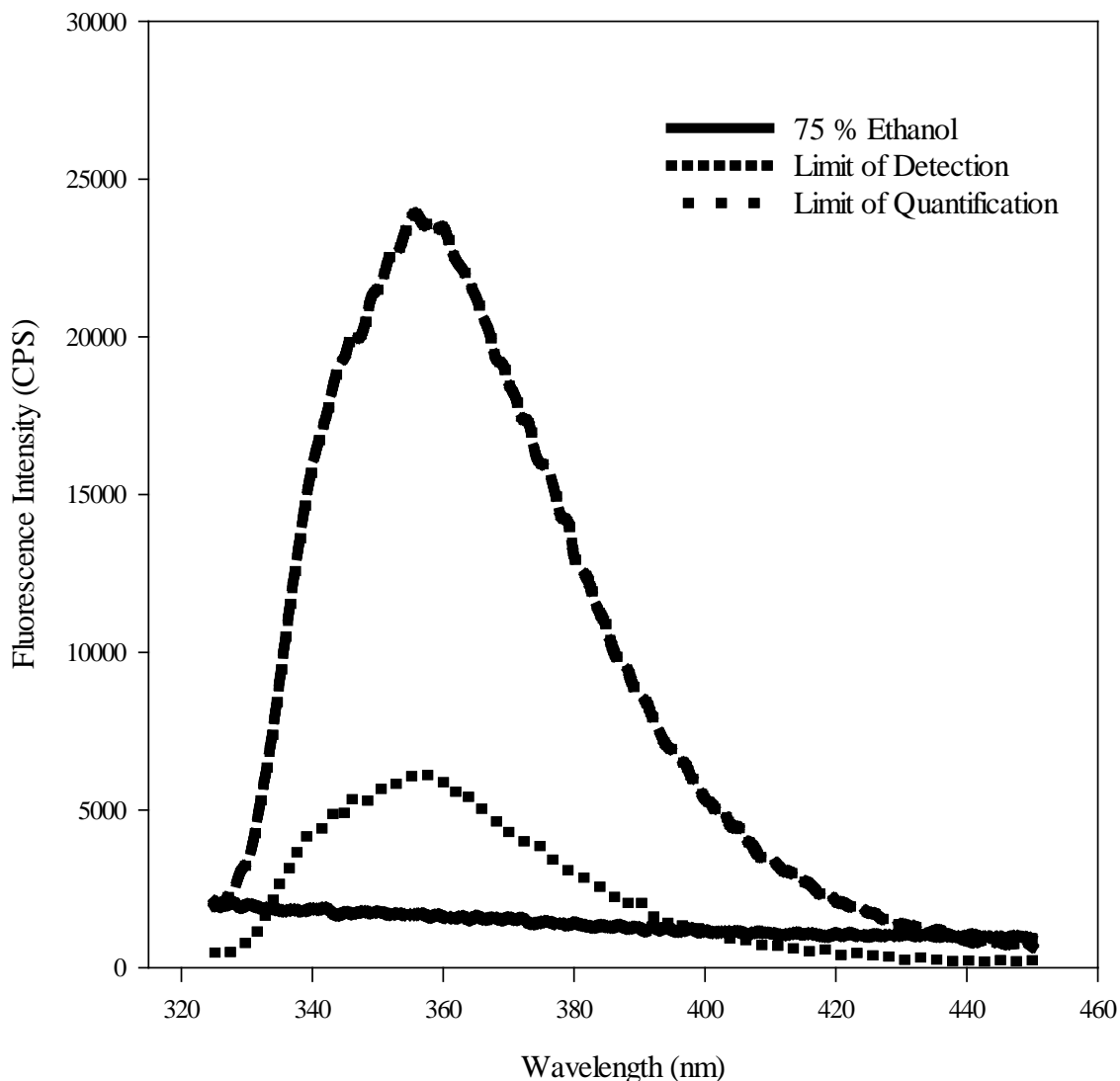
Figure 71: Accuracy of calculations for limit of detection and quantitation of 2 – naphthol in 75 % ethanol in a standard quartz fluorescence cuvette.

An emission spectrum was generated to test the accuracy of the calculations performed using the calibration plots to determine the LoD and LoQ of 2 – naphthol in 75 % ethanol and can be seen in Figure 71. The LoD calculated is 1.44×10^{-4} mg/mL and produces a fluorescence intensity of 1.0×10^{4} CPS/mV. The LoQ calculated is 4.79×10^{-4} mg/mL and produces a fluorescence intensity of 2.0×10^{4} CPS/mV.
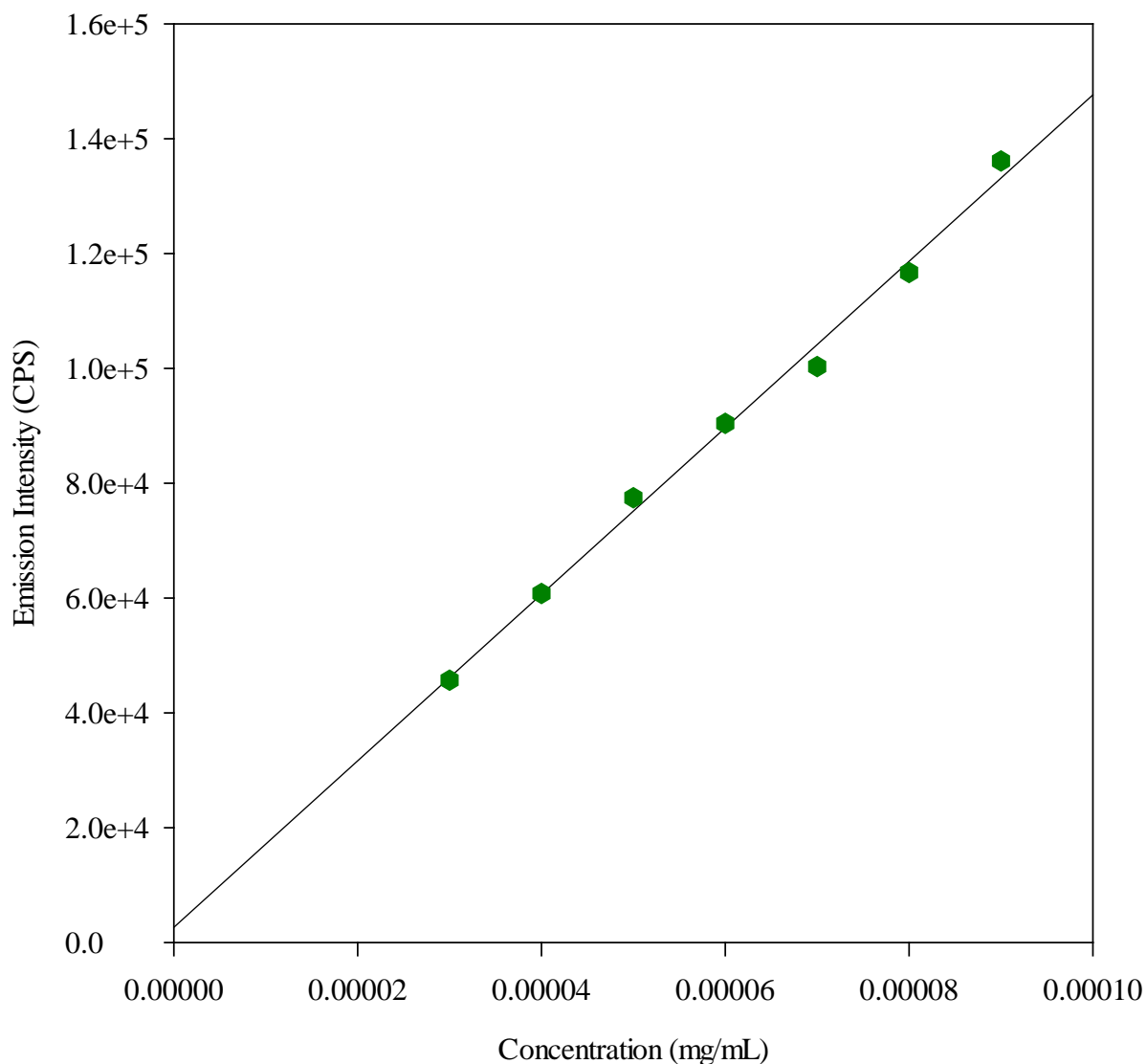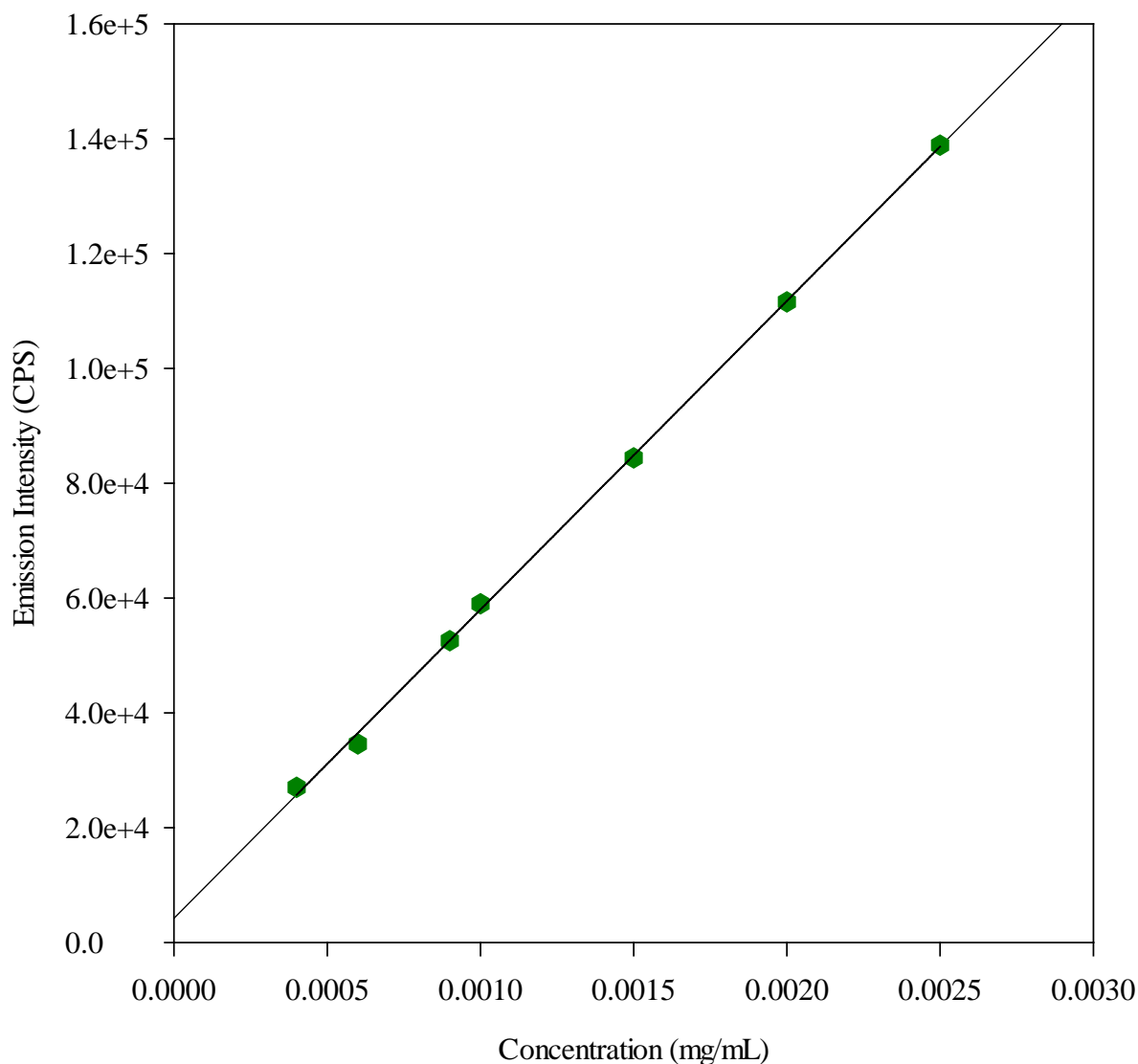
Figure 72: Calibration plot of phenanthrene in 75 % ethanol in a standard quartz fluorescence cuvette.

 The calibration plot of phenanthrene in 75 % ethanol can be seen in Figure 72. Seven points were used to construct the plot using an excitation wavelength of 294 nm and an emission wavelength of 366 nm. The concentration of 0.0004 mg/mL yielded a fluorescence intensity of 2.7×10^4 CPS/mv while a concentration of 0.0025 mg/mL yielded a fluorescence intensity of 1.4×10^5 CPS/mV. The R^2 value for this calibration plot was 0.999.
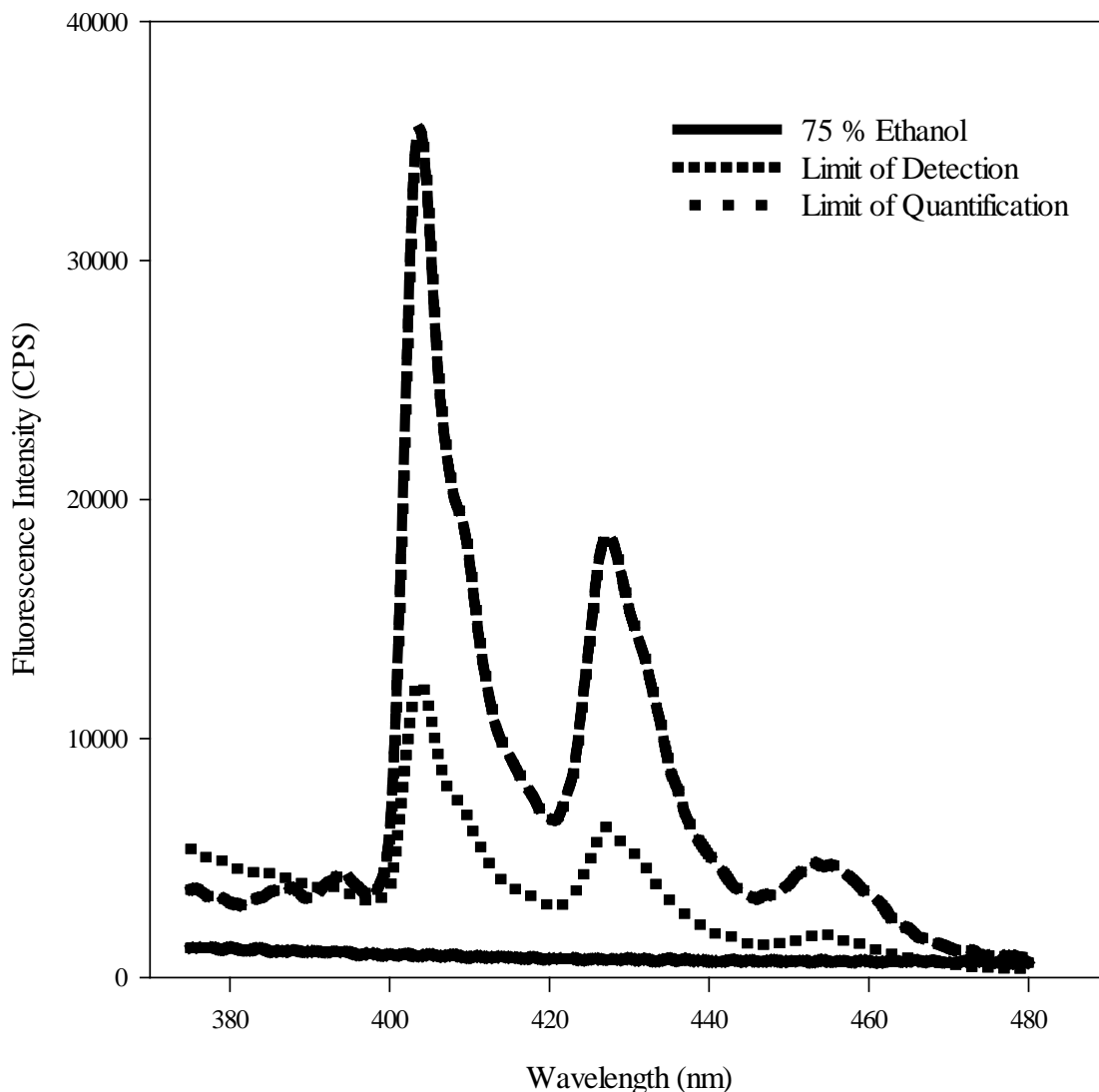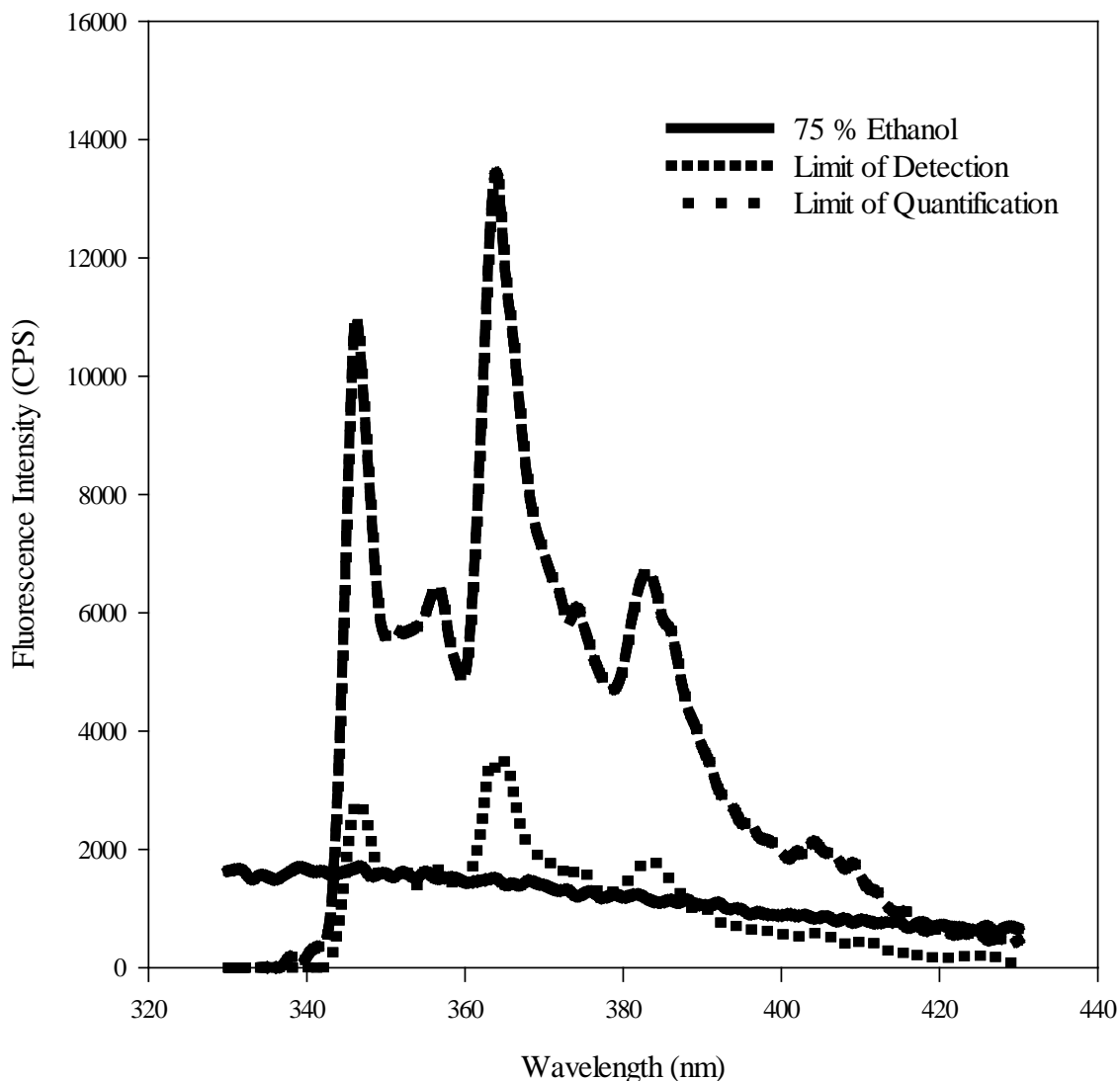
Figure 73: Accuracy of calculations for limit of detection and quantitation of phenanthrene in 75 % ethanol in a standard quartz fluorescence cuvette.

An emission spectrum was generated to test the accuracy of the calculations performed using the calibration plots to determine the LoD and LoQ of phenanthrene in 75 % ethanol and can be seen in Figure 73. The LoD calculated is 4.97×10^{-5} mg/mL and produces a fluorescence intensity of 6.9×10^3 CPS/mV. The LoQ calculated is 1.66×10^{-4} mg/mL and produces a fluorescence intensity of 1.3×10^4 CPS/mV.
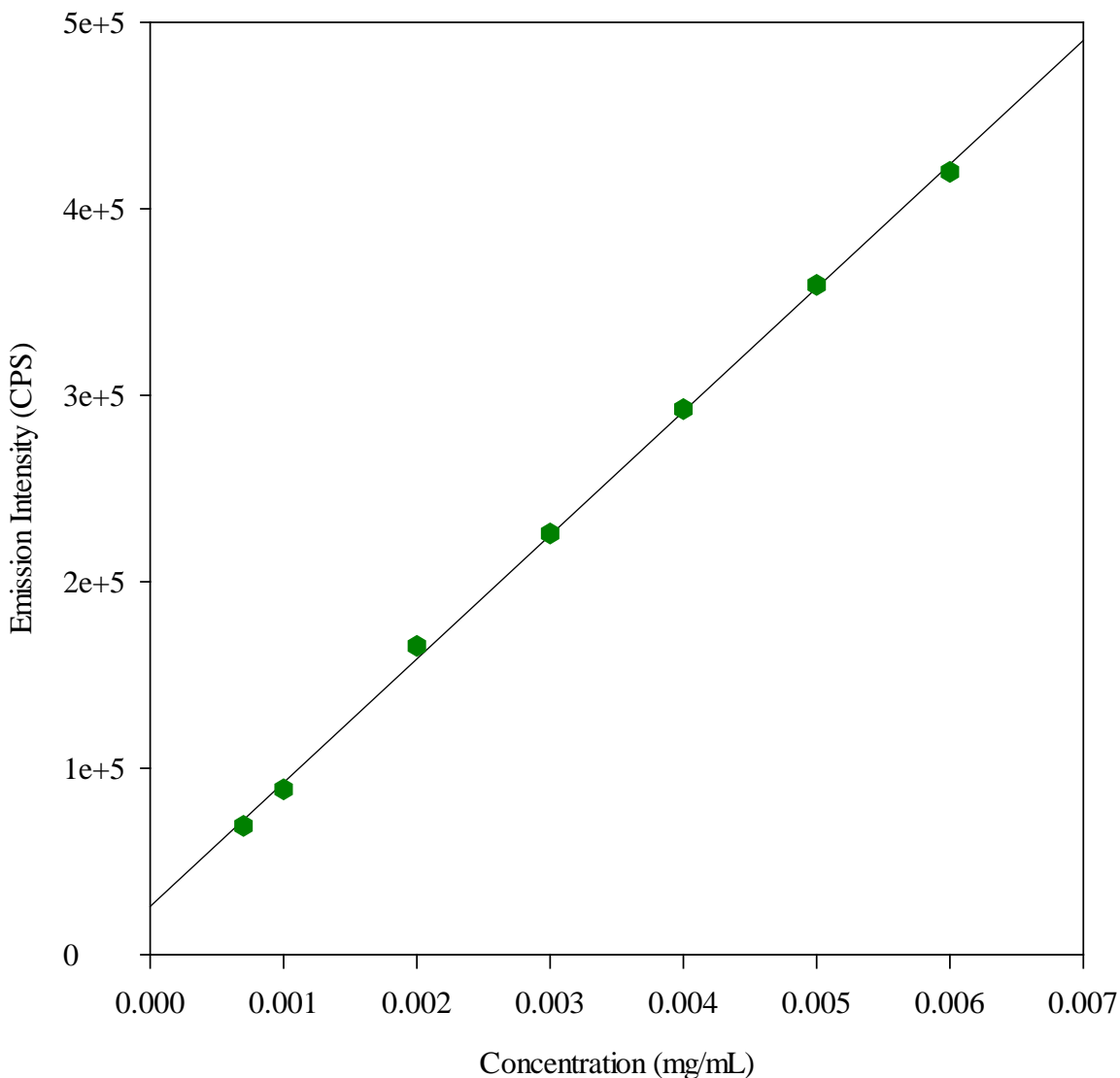
Figure 74: Calibration plot of 9 – phenanthrol in 75 % ethanol in a standard quartz fluorescence cuvette.

The calibration plot of 9 – phenanthrol in 75 % ethanol can be seen in Figure 74. Seven points were used to construct the plot using an excitation wavelength of 304 nm and an emission wavelength of 389 nm. The concentration of 0.0007 mg/mL yielded a fluorescence intensity of 6.9×10^4 CPS/mv while a concentration 0.006 mg/mL yielded a fluorescence intensity of 4.2×10^5 CPS/mV. The R^2 value for this calibration plot was 0.999.
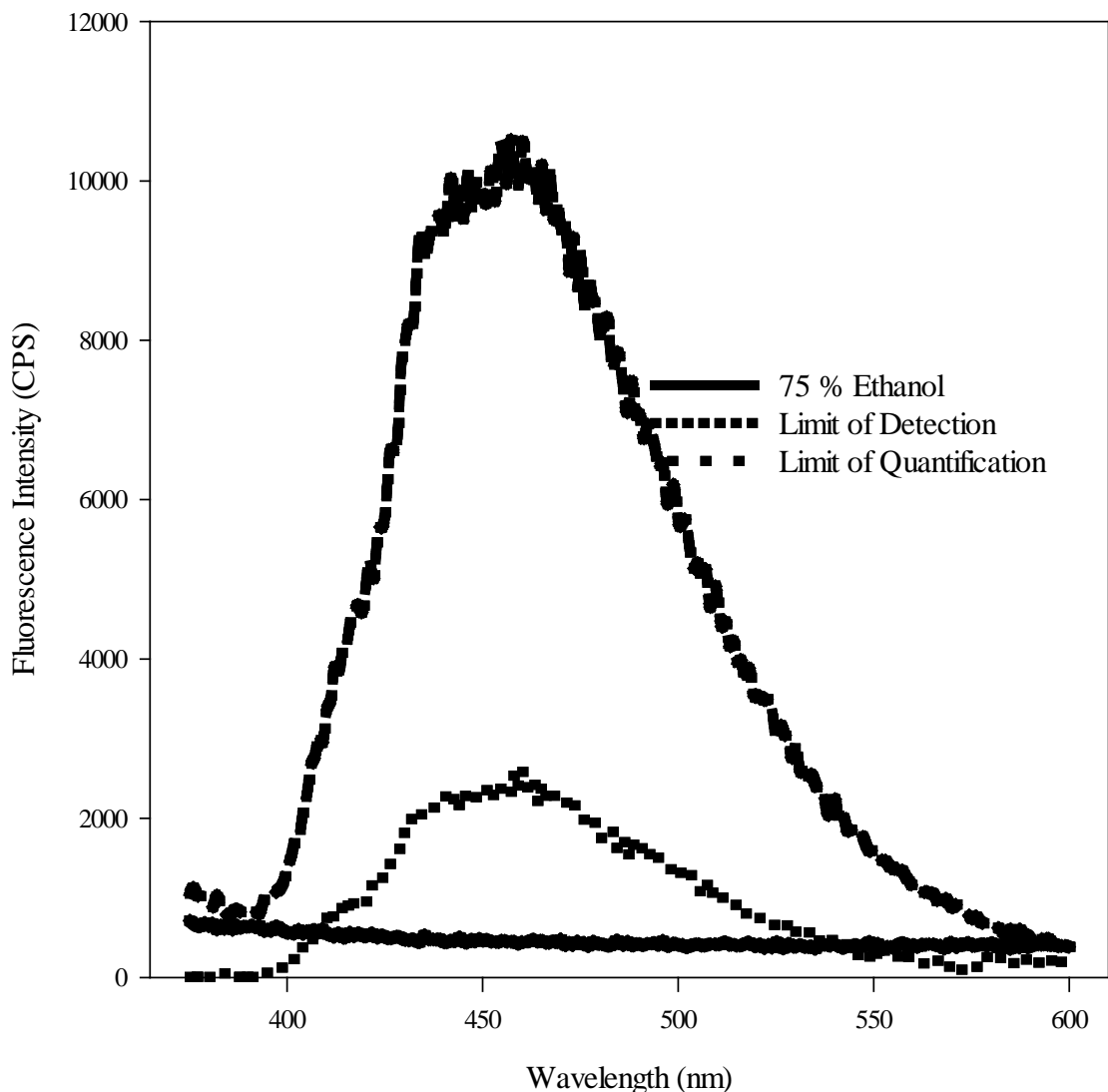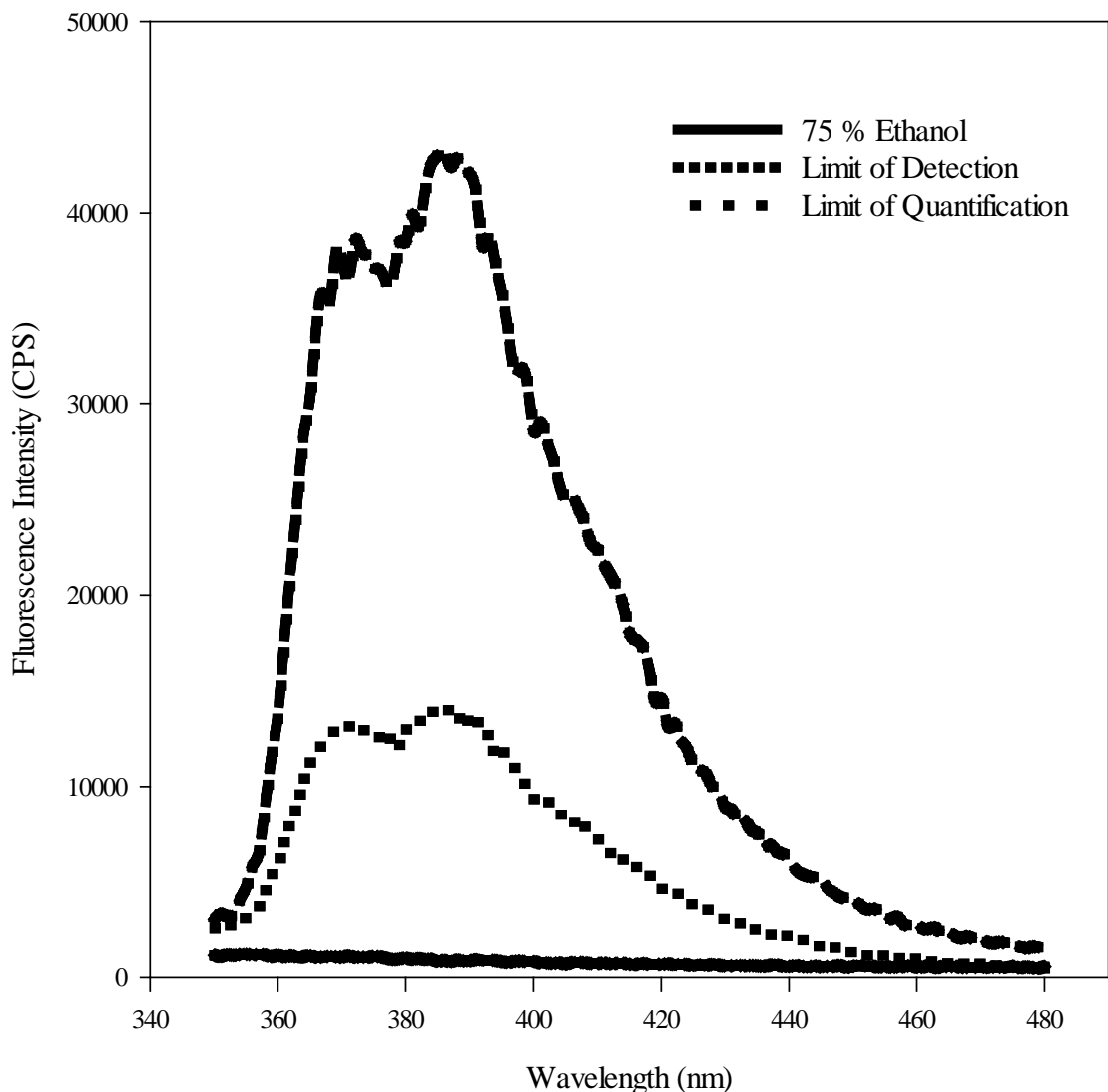
Figure 75: Accuracy of calculations for limit of detection and quantitation of 9 – phenanthrol in 75 % ethanol in a standard quartz fluorescence cuvette.

An emission spectrum was generated to test the accuracy of the calculations performed using the calibration plots to determine the LoD and LoQ of 9 – phenanthrol in 75 % ethanol and can be seen in Figure 75. The LoD calculated is 1.44×10^{-4} mg/mL and produces a fluorescence intensity of 3.5×10^4 CPS/mV. The LoQ calculated is 4.81×10^{-4} mg/mL and produces a fluorescence intensity of 5.8×10^4 CPS/mV.
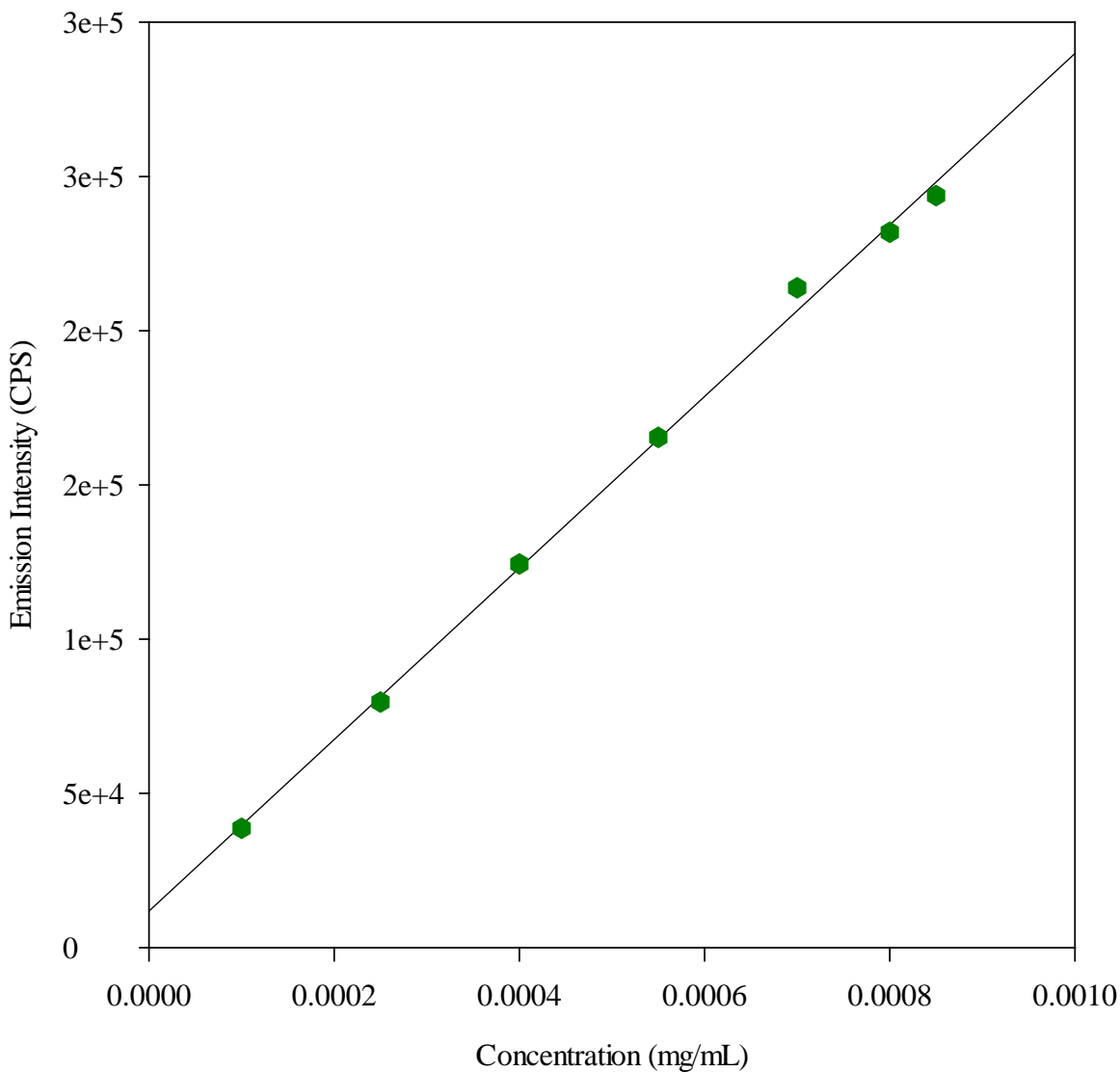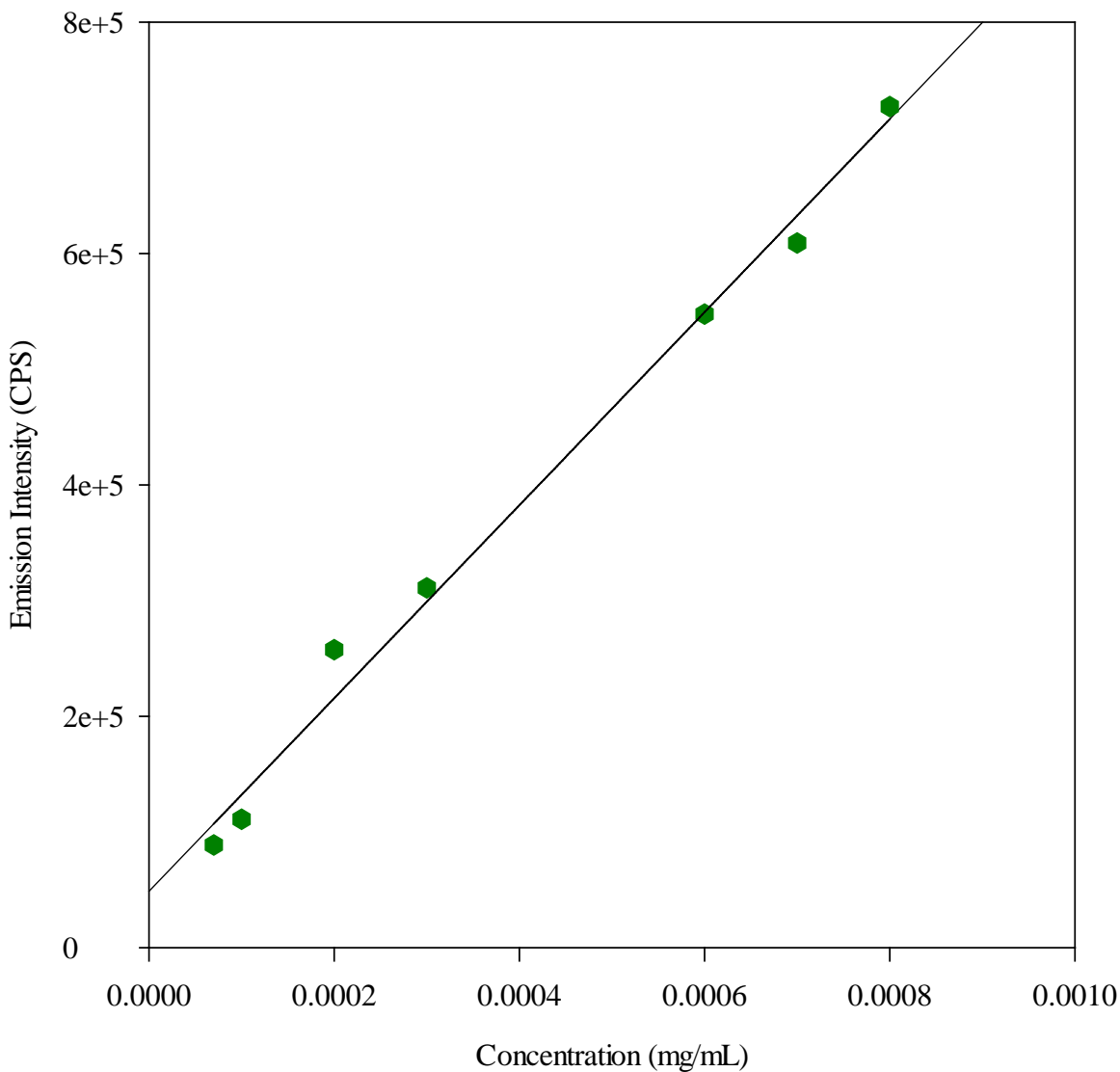
Figure 76: Calibration plot of pyrene in 75 % ethanol in a standard quartz fluorescence cuvette.

      The calibration plot of pyrene in 75 % ethanol can be seen in Figure 76. Seven points were used to construct the plot using an excitation wavelength of 334 nm and an emission wavelength of 372 nm. The concentration of 0.00007 mg/mL yielded a fluorescence intensity of 8.9 x 10^4 CPS/mv while a concentration of 0.0008 mg/mL yielded a fluorescence intensity of 7.3 x 10^5 CPS/mV. The R^2 value for this calibration plot was 0.991.
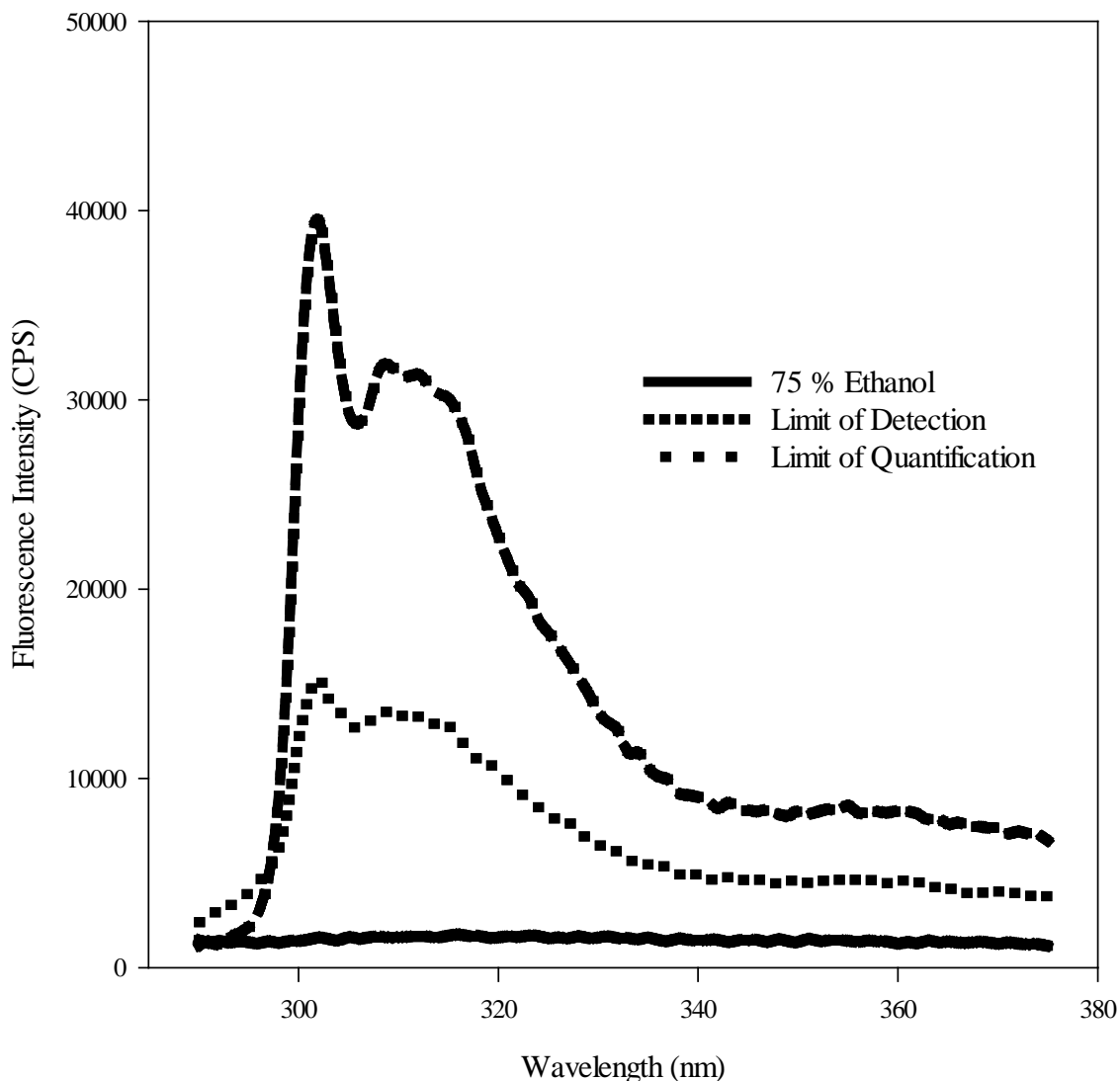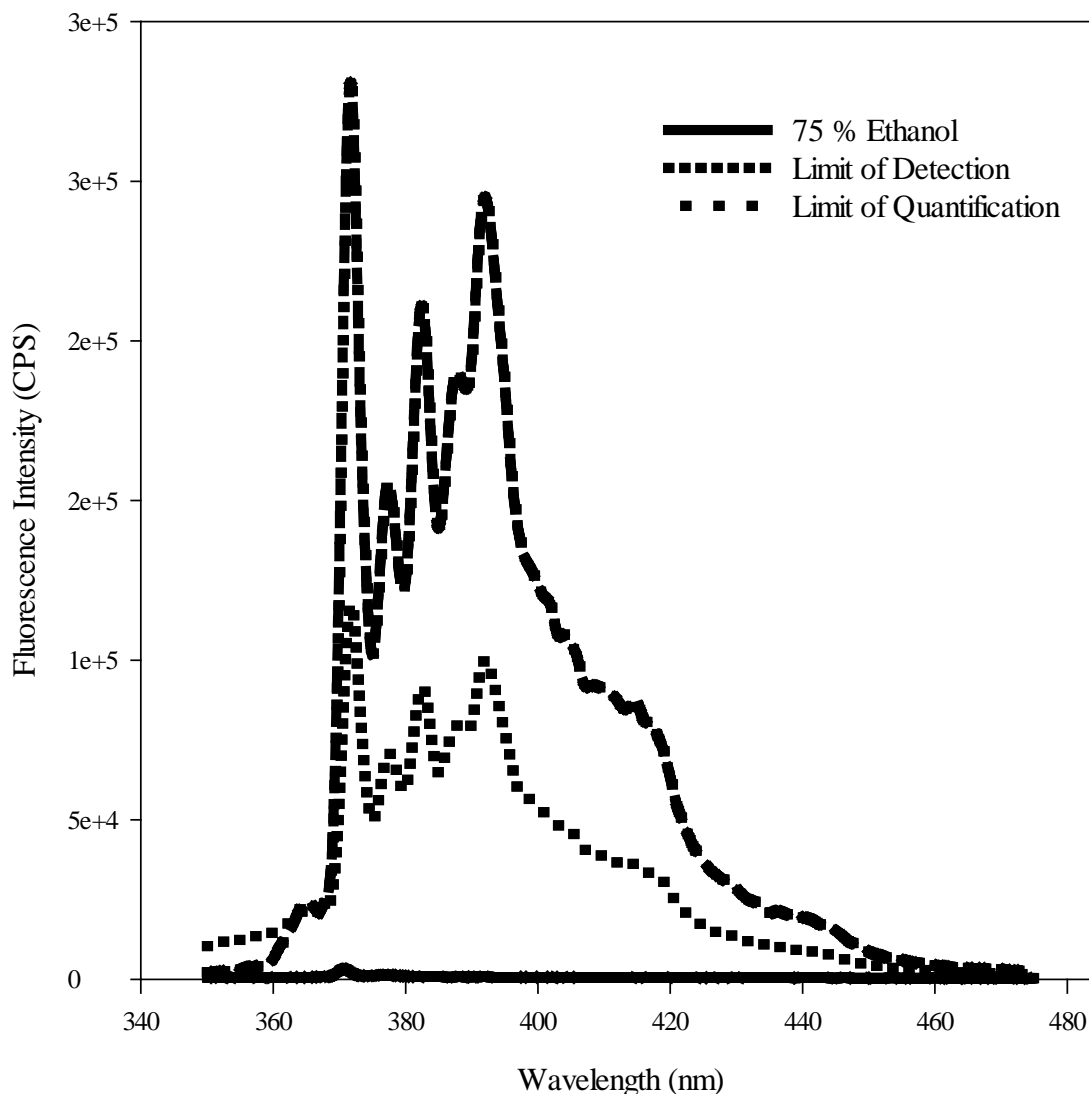
Figure 77: Accuracy of calculations for limit of detection and quantitation of pyrene in 75 % ethanol in a standard quartz fluorescence cuvette.

An emission spectrum was generated to test the accuracy of the calculations performed using the calibration plots to determine the LoD and LoQ of pyrene in 75 % ethanol and can be seen in Figure 77. The LoD calculated is 6.14 x 10^{-5} mg/mL and produces a fluorescence intensity of 5.6 x 10^5 CPS/mV. The LoQ calculated is 2.05 x 10^{-4} mg/mL and produces a fluorescence intensity of 2.2 x 10^5 CPS/mV.
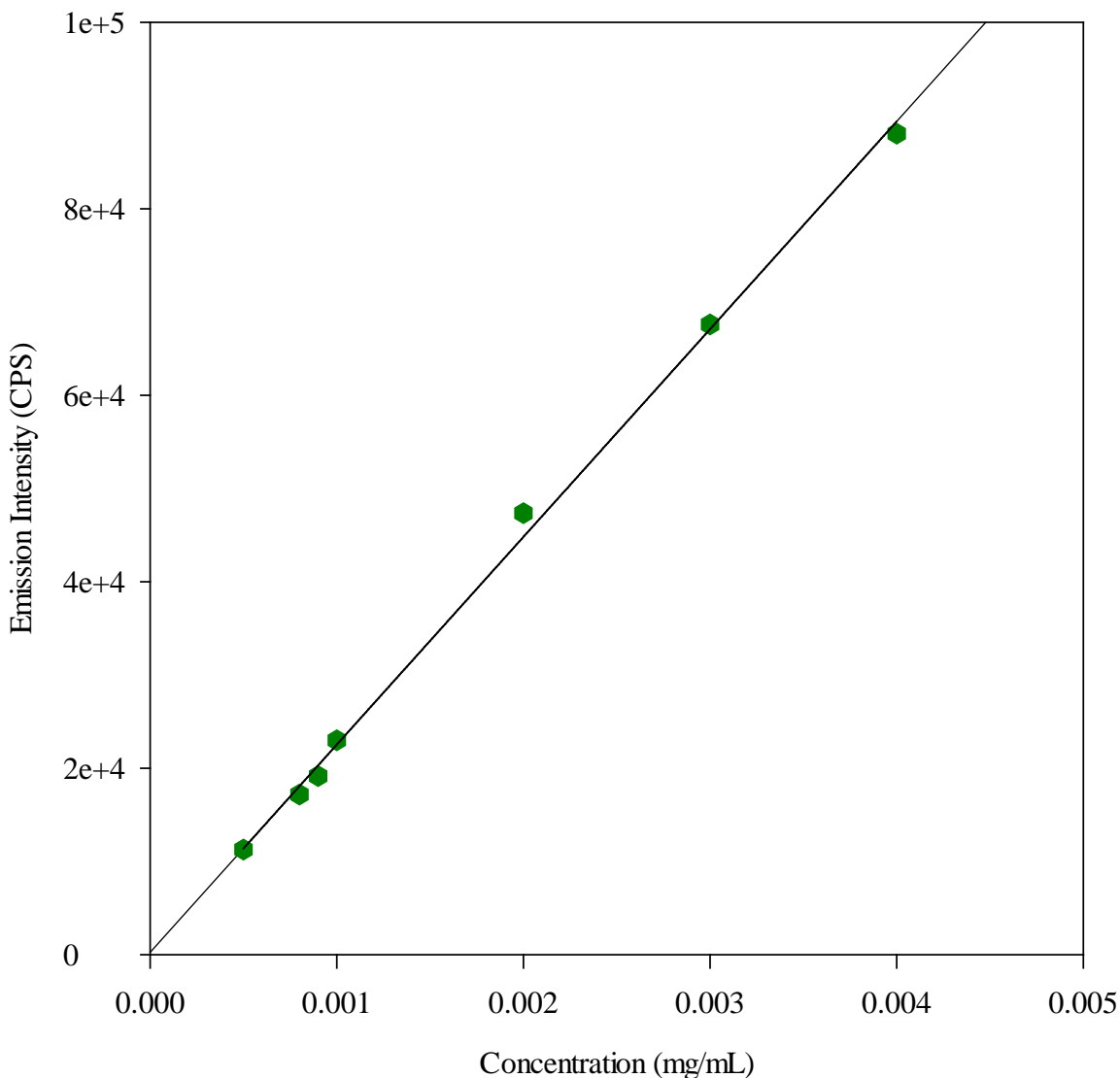
115
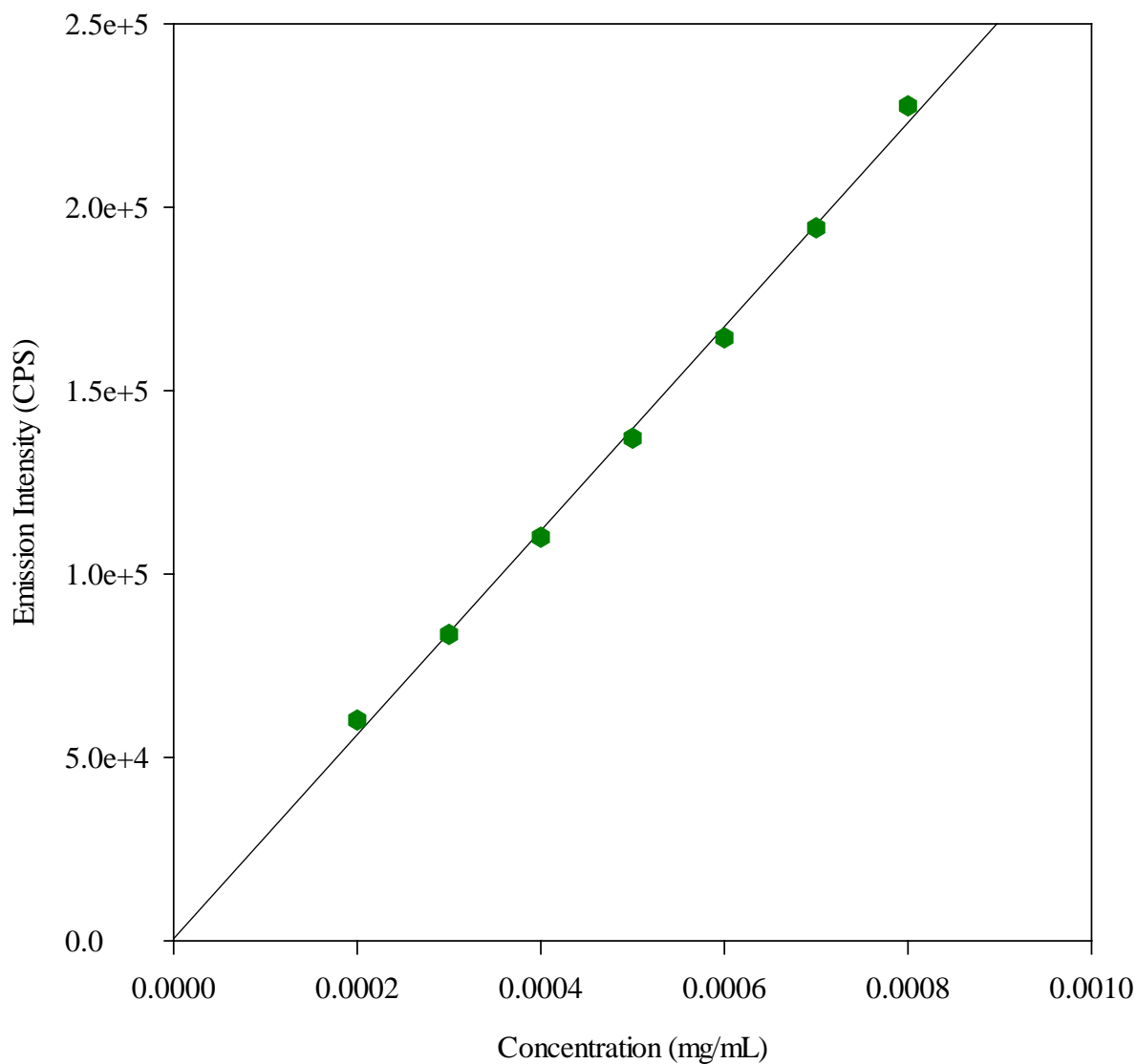
Figure 78: Calibration plot of 1 – pyrenol in 75 % ethanol in a standard quartz fluorescence cuvette.

The calibration plot of 1 – pyrenol in 75 % ethanol can be seen in Figure 78. Seven points were used to construct the plot using an excitation wavelength of 268 nm and an emission wavelength of 409 nm. The concentration of 0.0002 mg/mL yielded a fluorescence intensity of 6.0×10^4 CPS/mv while a concentration of 0.0008 mg/mL yielded a fluorescence intensity of 2.3 $\times 10^5$ CPS/mV. The R^2 value for this calibration plot was 0.997.
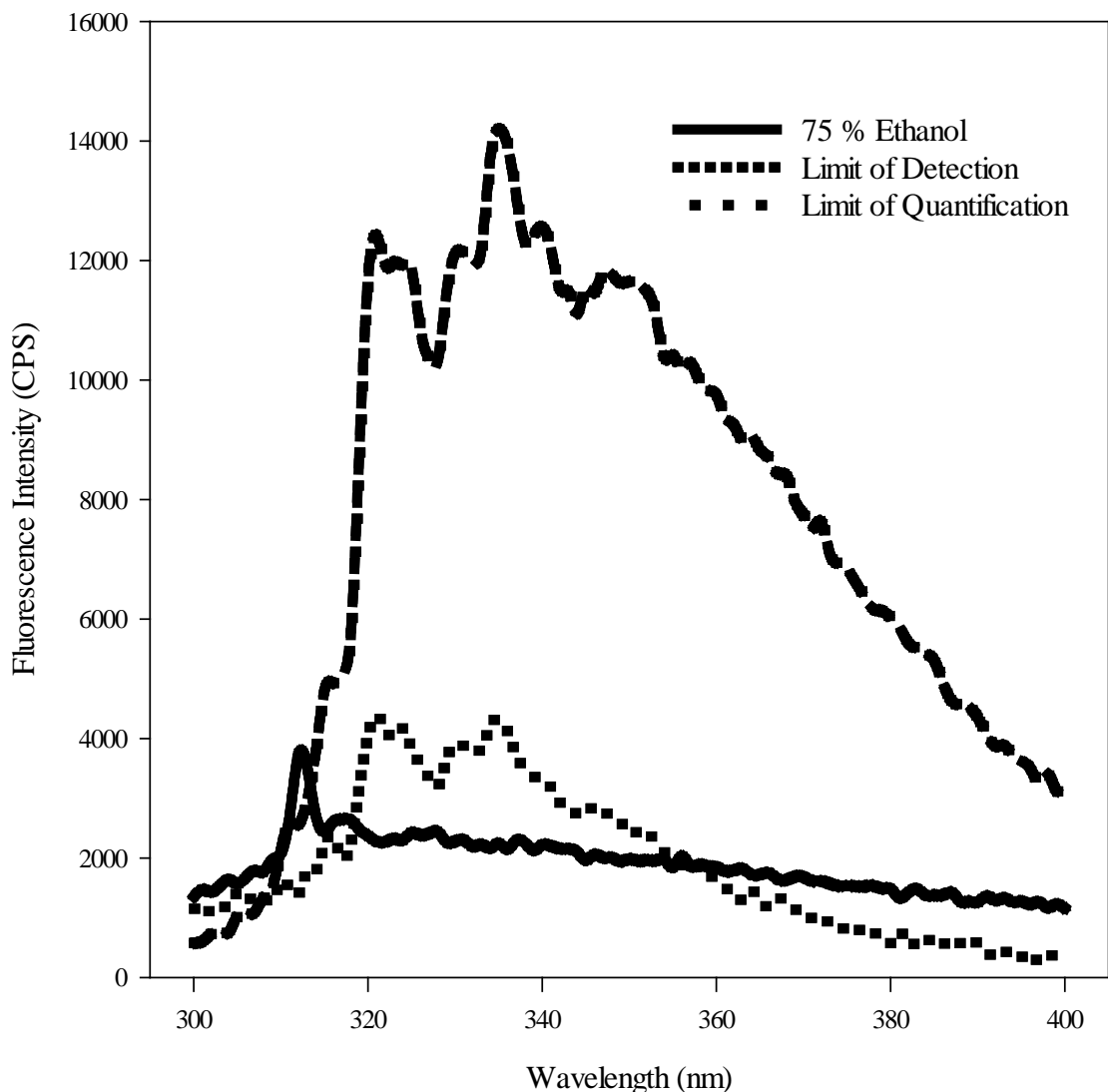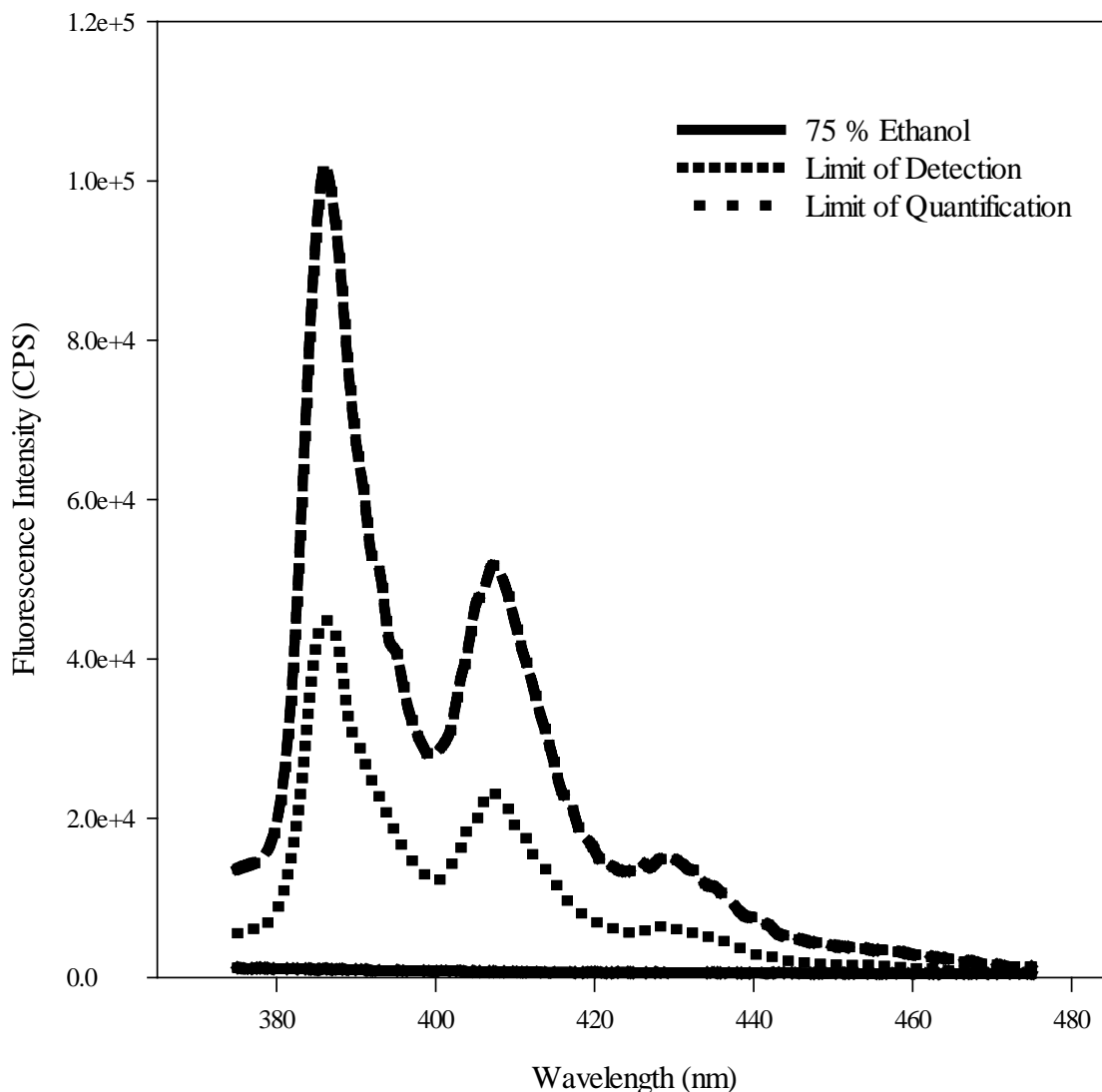
Figure 79: Accuracy of calculations for limit of detection and quantitation of 1 – pyrenol in 75 % ethanol in a standard quartz fluorescence cuvette.

An emission spectrum was generated to test the accuracy of the calculations performed using the calibration plots to determine the LoD and LoQ of 1 – pyrenol in 75 % ethanol and can be seen in Figure 79. The LoD calculated is 3.69×10^{-5} mg/mL and produces a fluorescence intensity of 1.1×10^4 CPS/mV. The LoQ calculated is 1.23×10^{-4} mg/mL and produces a fluorescence intensity of 3.5×10^4 CPS/mV.

VI.   Cuvette Cleaning

For accurate and precise measurements, it was necessary to clean the standard quartz fluorescence cuvettes scrupulously. When measurements of samples first began, cleaning was minimal, and was done by rinsing with de-ionized water and 75 % ethanol. After several UV – Vis scans of several different sample types, it was apparent that cross contamination between samples was occurring. To eliminate this contamination NoChroMix was used. NoChroMix is a white crystalline, inorganic oxidizer (likely potassium persulfate) packaged in pre-measured, hermetically sealed pouches. When mixed with sulfuric acid, it forms a strong cleaning solution which chemically cleans glassware without leaving residue on the glass surface, removing stains and deposits, and rinses freely.[16] Cuvettes were soaked in solution overnight, removed and soaked in de-ionized water for 30 minutes. They were then rinsed with 75 % ethanol before use. To ensure that this cleaning technique was sufficient measurements of 75 % ethanol alone were taken. Residual amounts of sample were still present in absorption scans. A more powerful cleaning method was needed.

The Horiba Fluorolog-3 Spectrophotometer operation manual has a chapter describing how to optimize data. The first page of the chapter describes cuvette preparation which included cleaning sample cells systematically before use to diminish background influences.[17] This process includes soaking cuvettes in a 50 % aqueous solution of nitric acid for 24 hours, rinsing with deionized water, cleaning with Alconox and a test tube brush, re-rinsing with de-ionized water, soaking in concentrated nitric acid, and rinsing a final time. This method was performed, and absorbance spectra of 75 % ethanol were measured. There was no apparent residual contamination of samples. However, this method is very time consuming and tedious.

To save time while still removing all contamination a new method for cuvette cleaning was developed. This method is similar to the Horiba operations manual, however some steps have been eliminated or condensed.[17] Cuvettes were soaked in a 50 % aqueous nitric acid solution for 8 – 12 hours. They were removed from solution and rinsed with de-ionized water using a cuvette washer. The all-plastic washer replaces old-fashioned devices that are often more fragile than the

cuvettes themselves.[18] The mouth of the inverted cuvette is pressed against the rubber cushion to induce suction. De – ionized water is poured into the funnel and is forcibly sprayed into the cuvette and drained into the flask. Continued pressure on the cuvette creates an airflow which dries it. The cuvettes are then soaked in concentrated nitric acid for an additional hour and re – rinsed using the cuvette washer. Before the sample is introduced, the cuvette is gently rinsed with 75 % ethanol. It is important to note that only one sample type can be used per cleaned cuvette, i.e. only naphthalene at varying concentration can be placed in one cuvette while another cuvette must be used to hold pyrene. This method works very well to eliminate all contamination. Variations of this procedure were tested however some amounts of residual contamination can be found. This method was developed to optimize both cleaning and time.

VII.   MicroMax Plate Reader

There were several obstacles to address before any data could be collected with the plate reader. Many of the issues faced were due to the fiber optic assembly. When using the plate reader, both the excitation and emission signals must travel through the fiber optic cable all while making sure that the signal accurately focused on the sample and not the top or the bottom of the microwell plate itself.[17] In addition, the types of plates used were also a factor that needed to be addressed. Minimization of background scattering signals was a priority to minimize spectral distortion. Due to the volatility of the solvent used for preparation of all the samples, an adhesive plastic film cover was employed to minimize evaporation of the solvent. These issues were addressed below.

i.   Fiber Optic Positioning

Horiba Scientific's MicroMax 384 Microwell-Plate Reader Operation Manual describes the calibration and alignment of the MicroMax 384. The manual is vague on the exact placement of the fiber optic assembly as seen in Figure 80.[17] Determination of an optimal position for the assembly was done by preparing a 100 nM sample of fluorescein in 0.1 N NaOH according the manual directions. The microwell plate was filled to a maximum volume of 200 µL and placed in the MicroMax. Within the FluorEssence program the monochromators were set to 485 nm and 513 nm for excitation and emission of fluorescein respectively. The signal was recorded continuously, and the fiber optic cable was moved up and down to obtain the maximum signal intensity. Once this signal was found, the fiber optic cable was held in position with a screw on the assembly. The assembly and screw were taped in place to minimize movement of the fiber optic cable. Additional studies were performed to guarantee that the placement of the assembly was correct. The results of these studies can be found in the following sections.

Figure 80: Positioning variance of fiber optic cable in MicroMax microwell plate reader. Photo courtesy of Lauren M. Ridley-Hoffman.

ii.   Microwell Plates

In addition to being vague on the placement of the fiber optic assembly, there was an uncertainty regarding the type of microwell plates that should be used. In order to produce accurate results as compared to a standard quartz fluorescence cuvette, several plates were tested. An optimal microwell plate would produce a background (blank with no solvent) signal similar (as low as) to the same conditions in a cuvette. The first plates suggested by Horiba were made of black polystyrene, including the bottom of the well. Horiba states that background, auto – fluorescence and inter-well crosstalk are improved with Nunc Black or White microplates. Black microplates were recommended for florescence measurements.[19] The recommended plates had large background scattering with solvent (75 % ethanol), compared to a standard quartz fluorescence cuvette. Intensity of signal for the black plate was approximately 45,000 CPS, while the average intensity of signal in a standard quartz fluorescence cuvette is approximately 660

CPS. To attempt to minimize this background scatter, glass bottom plates were explored. Glass bottom plates have well walls made of black polystyrene, while the bottom of the well is made with glass and are flat bottomed versus round like an all-black polystyrene plate. Several of these plates were tested and the results can be seen in Figure 81. Types of glass bottom plates included a shallow well plate where the well was square but not deep and could hold 300 µL, while the deep well plate had a circular well that was deeper in height, but could only hold 200 µL of solution.[20, 21] When compared to the average background scatter signal of a standard quartz fluorescence cuvette of 660 CPS, the shallow well plate showed an average signal of 25,000 CPS while the deep well plate had an average signal of 4,000 CPS. Although not an exact match for signal in the cuvette due to the assembly and inner workings of the fiber optic cable, the deep well glass bottom plate was chosen as the best for use.

Several additional studies were performed to ensure that the best plate was chosen. Figures 82 and 83 show several reproducibility studies of the microwell plate. Figure 82 shows the background scatter of the same plate using three different wells of solvent (75 % ethanol) only. It can be seen here that even a change in well will have a change in background scatter. Additional study was done using the standard 100 nM fluorescein to ascertain the source of this error. The results can be seen in Figure 83. It was determined that at the max peak of intensity of fluorescein (which was measured to be 517 nm, not the 513 nm which the Horiba manual had stated) the average signal intensity over all 96 wells was 174,200 CPS and had a ± 10,500 CPS standard deviation and a 6% RSD. This % RSD was within the error of an Eppendorf pipette[22] (the % RSD for a typical Eppendorf pipette is 5 – 10 %). The variability between wells is within this deviation. It appears that the key source of error is due to the pipette used for sample transfer and not the plate or wells themselves. As Eppendorf-type pipets are the ones most commonly used by environmental and biological scientists, improving on this error via other types of pipets or syringes is not useful to the goals at hand.
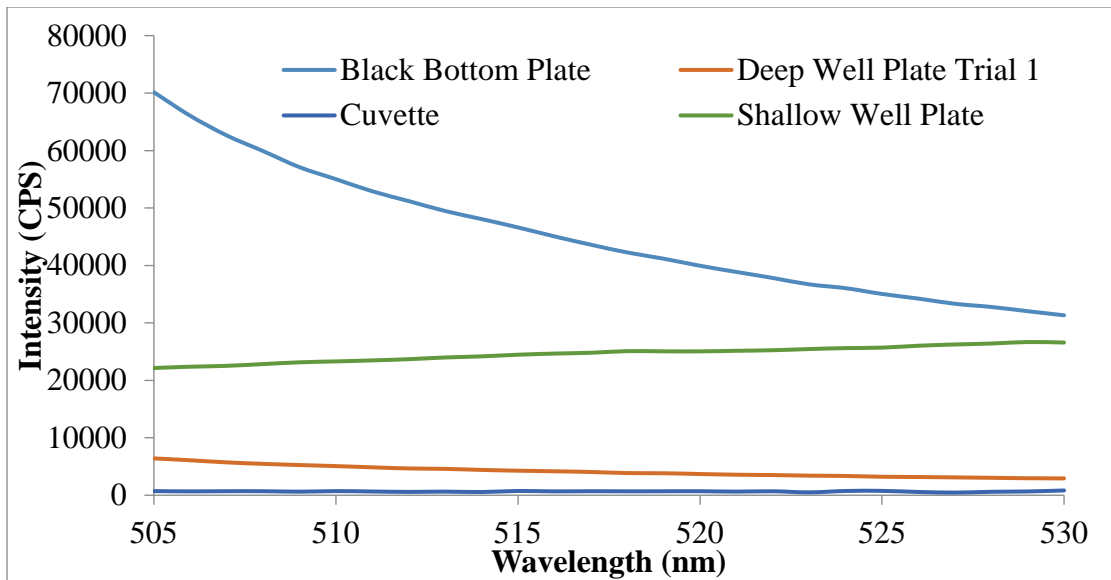
Figure 81: Background scatter intensity of several types and brands of microwell plates.
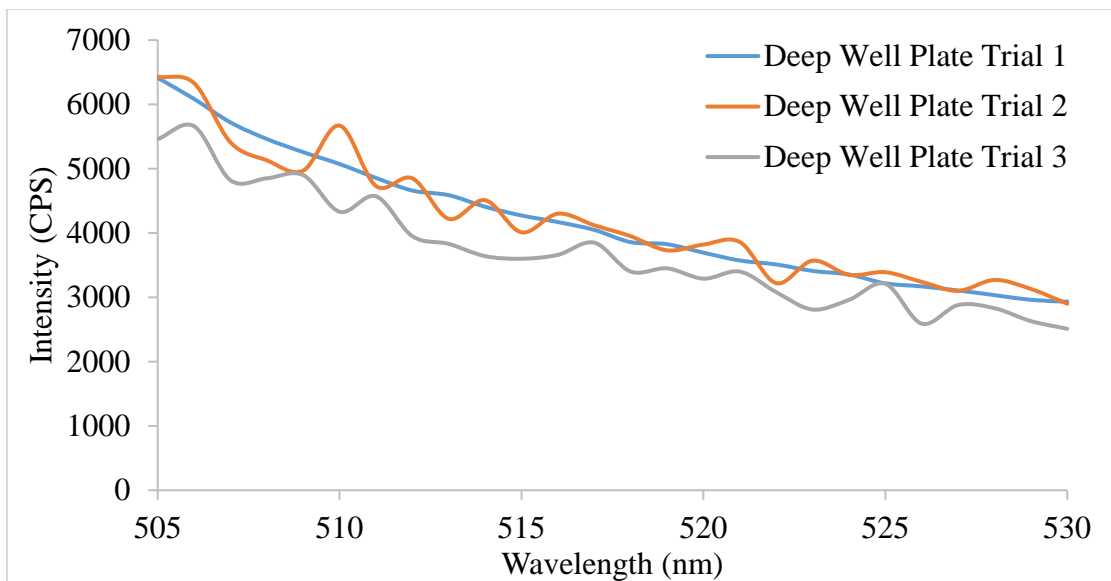
Figure 82: Variations in background scatter of the deep well glass bottom plate (same plate, different wells).
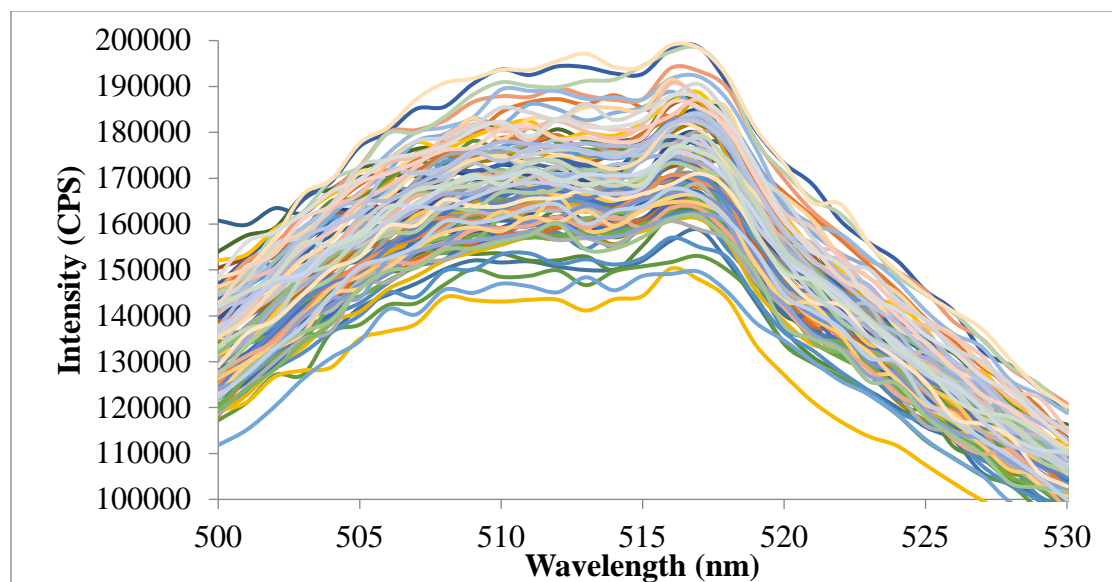
Figure 83: Reproducibility between wells of the same deep well glass bottom microwell plate using a standard solution of fluorescein (100 nM in 0.1 N NaOH) filled using an Eppendorf pipette.

iii.   Well Fill Depths

Once the correct plates were chosen and the Eppendorf pipette error was determined, the effects of fill volume were investigated. Each well can hold a maximum of 200 µL, however, the optimal fill volume for maximum signal was unknown. Several tests were performed to determine the optimal fill volume. Figures 84 and 85 show studies using 1 – naphthol. Fill volumes from 85 µL to 200 µL with a 5 µL interval were tested. The slit was varied as well to maximize signal intensity. The effect of adhesive plastic film covers relative to open top plates was also investigated. Film covers were used to prevent evaporation of solvent when running lengthy experiments (see the next section for the discussion of the film covers). Figure 84 shows the intensity of signal for a covered plate and an uncovered plate. It can be seen in this graph between 120 µL and 125 µL the uncovered plate reaches a maximum signal and plateaus at higher fill volumes. For the same fill volume, the covered plate showed a decrease in signal intensity and plateaus at low intensity for fill volumes above 125 µL. It can be determined from this graph that at approximately 125 µL one can expect to see the greatest signal of 1 – naphthol in a covered or uncovered plate. Figure 85 is a three – dimensional graph showing intensity of

signal as a function of fill volume and slit width on both covered and uncovered plates. It becomes very apparent on this graph that at approximately 125 µL fill volume there is a strong signal intensity at all slit widths. This confirms that the previously determined fill volume of 125 µL yields the most intense signal.

To further confirm a fill volume of 125 µL, the same studies were performed using 1 – pyrenol. The main difference between 1 – naphthol and 1 – pyrenol is their quantum yields. 1 – Naphthol has a very low quantum yield of 0.065 while the quantum yield of 1 – pyrenol is 0.69, a ten times higher quantum efficiency. Figure 86 shows the intensity of signal between a covered plate and an uncovered plate. It can be concluded that between 125 µL and 130 µL the uncovered plate reaches a maximum signal and plateaus at higher fill volumes. In the same fill volume region, the covered plate shows a decrease in signal intensity and plateaus at low intensity for higher fill volumes. Figure 87 is a three – dimensional graph showing intensity of signal as a function of fill volume and slit width on both covered and uncovered plates. It can be determined from this graph that due to the higher quantum yield of 1 – pyrenol there are several more fill volumes and slit widths that would produce high intensity emission signals, including 125 µL. However, to accommodate the full range of quantum yields and all compounds of study, 125 µL was chosen as the fill volume for all remaining data collections.
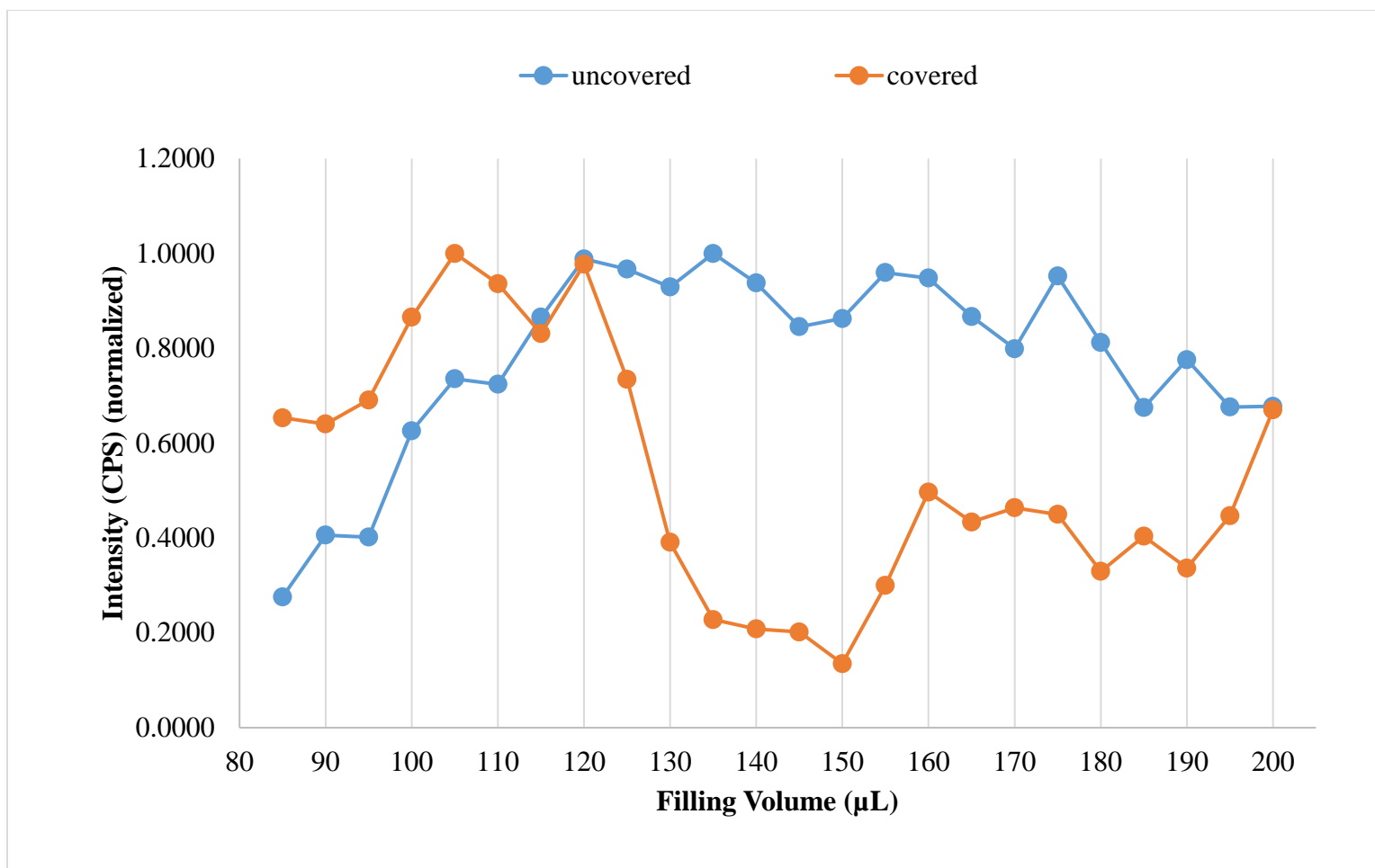
Figure 84: Filling depth study using 1 – naphthol.
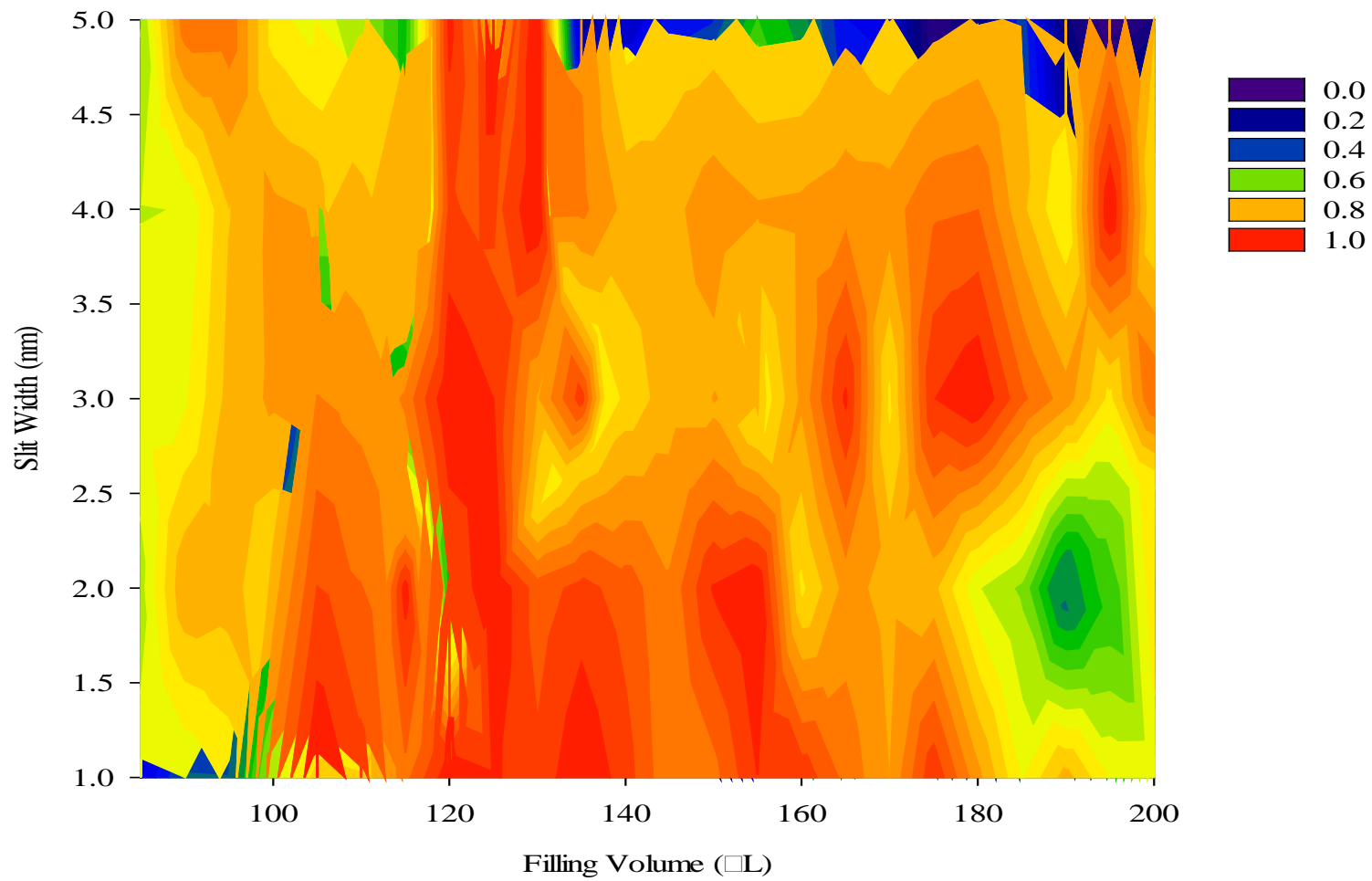
Figure 85: Contour plot of filling volume versus slit width for 1 – naphthol.
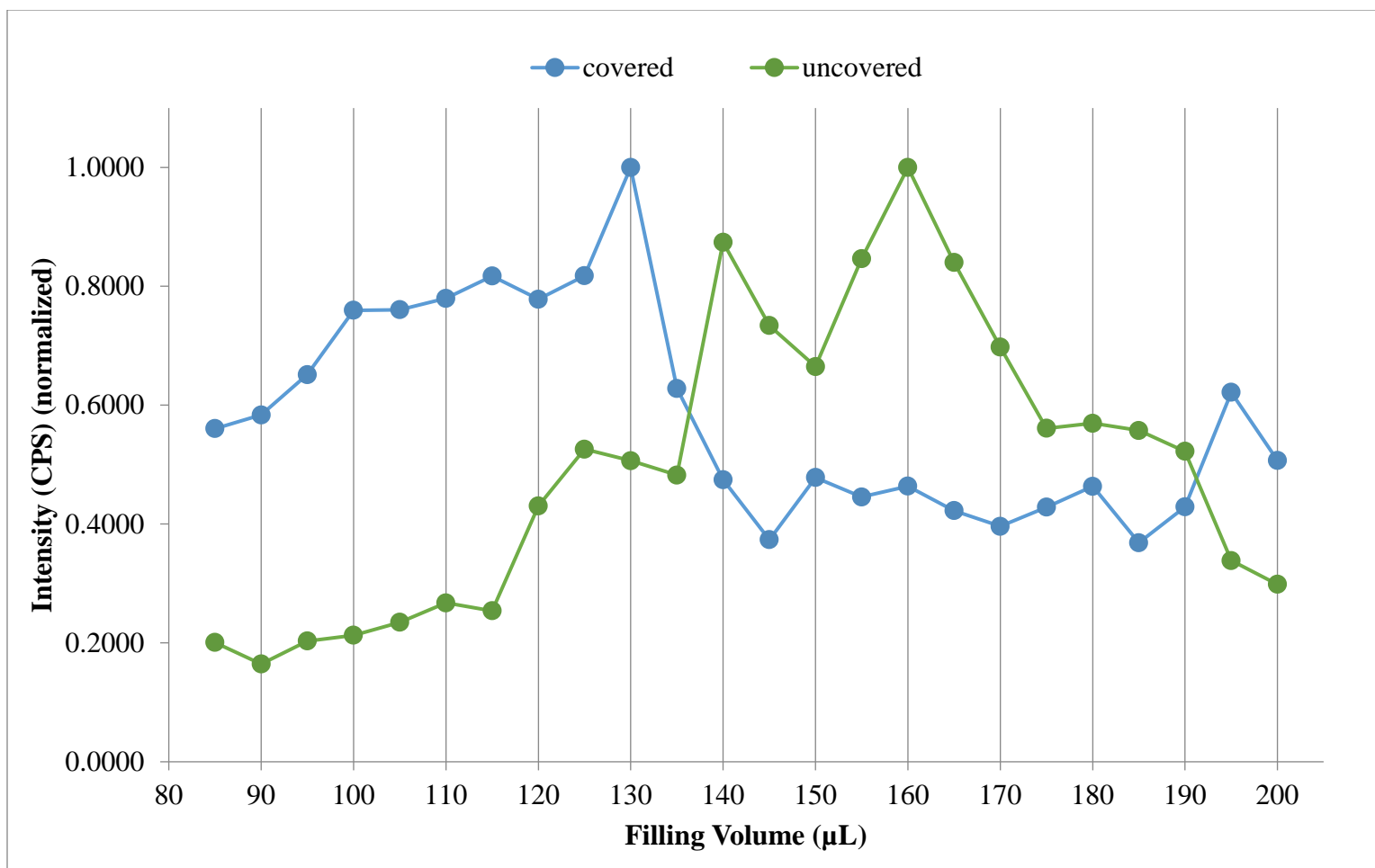
Figure 86: Filling depth study using 1 – pyrenol.
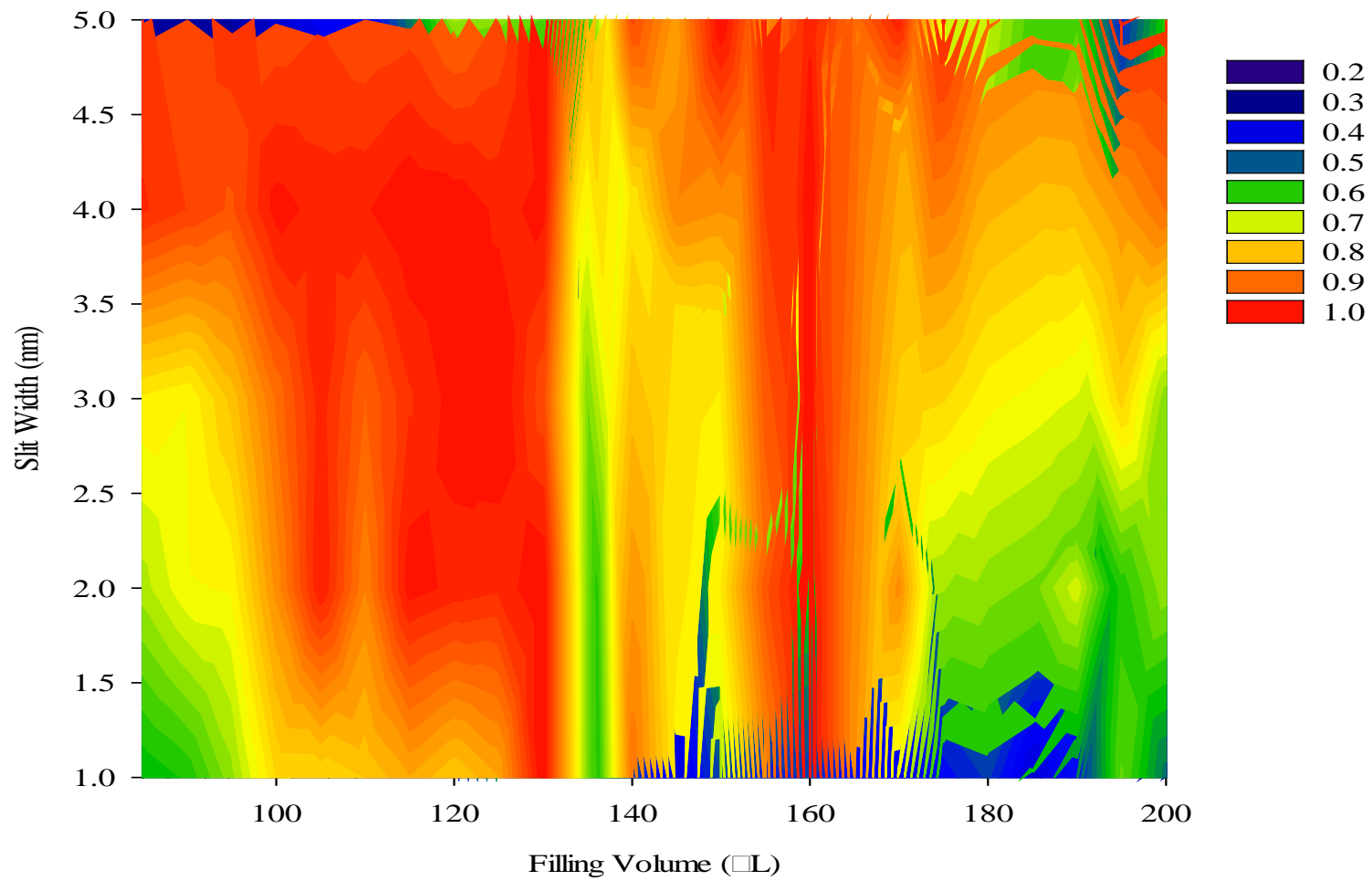
Figure 87: Contour Plot of filling volume versus slit width for 1 – pyrenol.

iv.   Optical Film Plate Covers

The optical film covers play a very significant role in the collection of data. Using a solvent with a low boiling point means that evaporation will happen rapidly at room temperatures. Once it was decided that film covers needed to be used, a small sample was acquired from Applied Biosystems. Once these were consumed, a new larger batch was purchased from VWR. Upon use, it was noticed that the same concentrations of compounds that had previously shown data were no longer showing any signal. Since the only difference was the type of film covered purchased, the absorbance of each film was tested. Both film manufacturers state that their films are made for Real Time PCR, with a high optical clarity, and are optimized for fluorescent DNA detection.[23, 24] In order to test the optical clarity and fluorescence optimization, a small rectangular piece of film was cut and applied to a standard quartz fluorescence cuvette and a UV – Vis spectrum was generated for both types of film and compared to the absorbance of a blank cuvette. Figure 88 shows the results. Since the compounds of study mainly absorb photons between 260 nm and 400 nm, the VWR brand of film purchased absorbs light in this same region. Therefore, any light coming through the fiber optic cable was being absorbed before reaching the sample in the plate. The Applied Biosystems film absorbs less light than even the cuvette in the region of concern and was used for all remaining data collections.
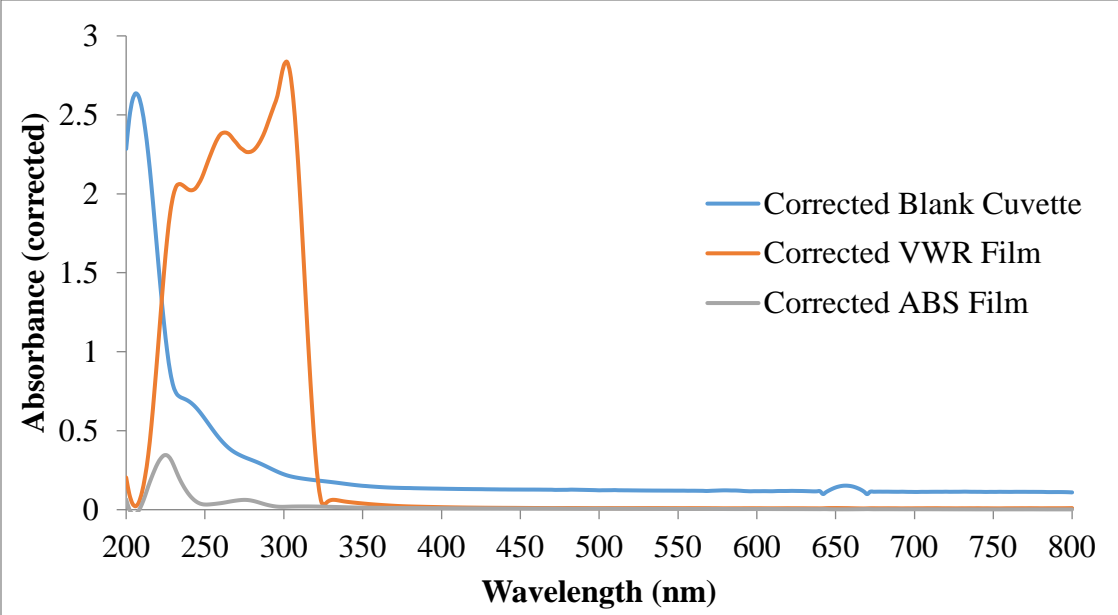
Figure 88: UV – Vis spectra of two brands of optical films for microwell plates.

v. Excitation and Emission Spectrum

The emission and excitation spectra of all compounds were measured using the microwell plate as the sample holder (Figures 89 – 100). Full excitation and emission spectra were measured using concentrations of samples producing signals less than 1×10^6 counts per second (CPS) and have been normalized using the maximum signal intensity for both the excitation and emission. Monochromator positions for both excitation and emission remained consistent from standard quartz fluorescence cuvette to microwell plate. However, the range of wavelengths scanned was decreased (Tables 12 and 13). The microwell plate showed a large background scatter signal at the beginning of all scans. To eliminate the presence of this large band, scans were run according to cuvette parameters, but graphs were generated without using some of the recorded data to show peaks caused only by fluorescence of the compounds. This discrepancy between excitation and emission wavelength ranges in the cuvette and the plate are caused by compounding factors. The fiber optic cable will always cause some distortion of the transmitted through it in both directions. These factors contribute to the difference in ranges between the cuvette and the plate. Any other differences in emission and excitation spectra between a standard quartz fluorescence cuvette and a glass bottom microwell plate are due to the loss of light intensity greater optical light path. Signal intensities for the same concentration of sample will always be lower in the microwell plate since any excitation and emission signal must travel through the fiber optic cable and an extra focusing lens twice before reaching the sample and detector.

Compound	λ_{ex} (nm)	λ_{em} (nm) (range)
Acenaphthene	290	319-360
Anthracene	340	365-455
Benzo [a] pyrene	296	390-460
Fluoranthene	308	375-550
Fluorene	262	280-400
Naphthalene	286	300-380
1 – Naphthol	296	306-580
2 – Naphthol	264	330-430
Phenanthrene	294	330-450
9 – Phenanthrol	304	350-470
Pyrene	294	350-475
1 – Pyrenol	268	375-475

Table 12: Optimum Emission Parameters in a microwell plate.

Compound	λ_{em} (nm)	λ_{ex} (nm) (range)
Acenaphthene	338	260-315
Anthracene	425	260-365
Benzo [a] pyrene	403	260-388
Fluoranthene	462	260-380
Fluorene	317	260-314
Naphthalene	337	260-300
1 – Naphthol	370	260-330
2 – Naphthol	358	260-350
Phenanthrene	366	260-300
9 – Phenanthrol	389	260-375
Pyrene	416	260-350
1 – Pyrenol	438	260-375

Table 13: Optimum Excitation Parameters in a microwell plate

Figure 89: Emission and excitation spectra of acenaphthene in 75 % ethanol in a microwell plate.

The excitation and emission spectrum of acenaphthene in 75 % ethanol can be seen in Figure 89 at a concentration of 0.005 mg/mL. The excitation spectrum is observed between 260 and 315 nm. The emission spectrum is observed between 319 and 360 nm. There are no shifts in maximum peak wavelength in the spectrum observed in the plate when compared to the spectrum observed in the cuvette. However, differences in the resolution of the spectrum are apparent due to the lower signal produced when using the fiber optic assembly. The peak at an excitation wavelength of 290 nm in the cuvette is barely visible in the plate. Since this peak was used as the excitation of choice to generate the emission spectrum, it is apparent that the lower signal intensity has no apparent effects on the emission spectrum itself.

Figure 90: Emission and excitation spectra of anthracene in 75 % ethanol in a microwell plate.

The excitation and emission spectrum of anthracene in 75 % ethanol can be seen in Figure 90 at a concentration of 0.004 mg/mL. The excitation spectrum is observed between 260 and 365 nm. The emission spectrum is observed between 365 and 455 nm. While using the plate, an excitation peak at 374 nm has been eliminated due to signal noise with use of the fiber optic assembly. The removal of this peak has no effect on the emission spectrum as it is not the peak of maximum intensity.

Figure 91: Emission and excitation spectra of benzo [a] pyrene in 75 % ethanol in a microwell plate.

The excitation and emission spectrum of benzo [a] pyrene in 75 % ethanol can be seen in Figure 91 at a concentration of 0.00006 mg/mL. The excitation spectrum is observed between 260 and 388 nm. The emission spectrum is observed between 390 and 460 nm. There are no shifts in peak placement in the spectrum observed in the plate when compared to the spectrum observed in the cuvette. However, differences in the resolution of the spectrum are apparent. The small broad peak at an emission wavelength of 452 nm in the cuvette is now complicated by noise and is undistinguishable as a peak in the plate.

Figure 92: Emission and excitation spectra of fluoranthene in 75 % ethanol in a microwell plate.

The excitation and emission spectrum of fluoranthene in 75 % ethanol can be seen in Figure 92 at a concentration of 0.005 mg/mL. The excitation spectrum is observed between 260 and 380 nm. The emission spectrum is observed between 375 and 550 nm. There are no shifts in peak placement in the spectrum observed in the plate when compared to the spectrum observed in the cuvette. However, differences in the resolution of the spectrum are apparent. The emission spectrum of fluoranthene in the cuvette is smooth with on peak and two small shoulders flanking. The major peak is still seen at 465 nm, but the second shoulder at 484 nm has disappeared with the addition of noise from the lower signal intensity.

Figure 93: Emission and excitation spectra of fluorene in 75 % ethanol in a microwell plate.

The excitation and emission spectrum of fluorene in 75 % ethanol can be seen in Figure 93 at a concentration of 0.007 mg/mL. The excitation spectrum is observed between 260 and 314 nm. The emission spectrum is observed between 280 and 400 nm. There are no shifts in peak placement or resolution in the spectrum observed in the plate when compared to the spectrum observed in the cuvette.
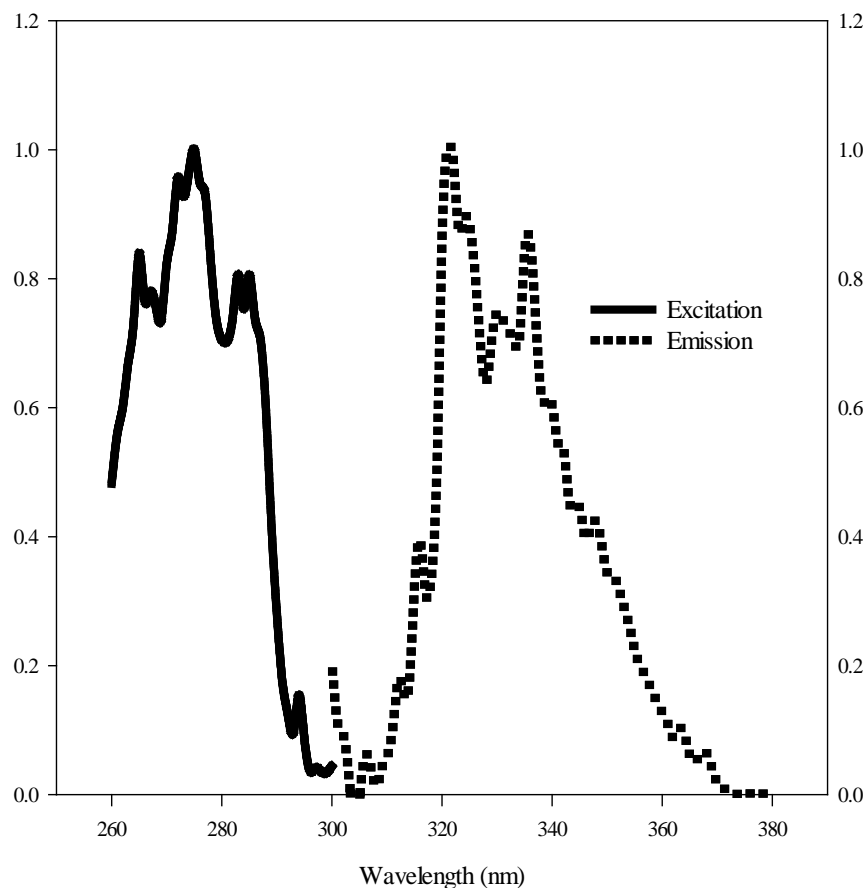
Figure 94: Emission and excitation spectra of naphthalene in 75 % ethanol in a microwell plate.

The excitation and emission spectrum of naphthalene in 75 % ethanol can be seen in Figure 94 at a concentration of 0.005 mg/mL. The excitation spectrum is observed between 260 and 300 nm. The emission spectrum is observed between 300 and 380 nm. There are no shifts in peak placement in the spectrum observed in the plate when compared to the spectrum observed in the cuvette. However, differences in the resolution of the spectrum are apparent. The shoulder at an excitation wavelength of 285 nm now is a sharp peak. In addition, a small peak has formed at an excitation wavelength of approximately 268 nm. Changes are due to the noise produced by the fiber optic assembly.

139
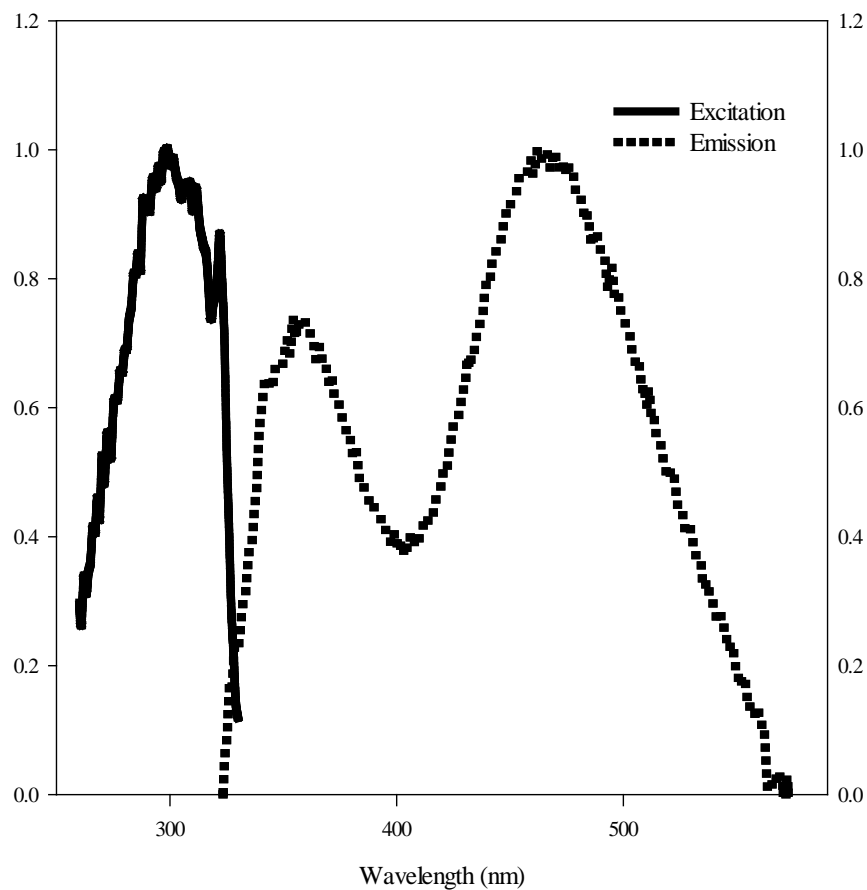
Figure 95: Emission and excitation spectra of 1 – naphthol in 75 % ethanol in a microwell plate.

The excitation and emission spectrum of 1 – naphthol in 75 % ethanol can be seen in Figure 95 at a concentration of 0.04 mg/mL. The excitation spectrum is observed between 260 and 330 nm. The emission spectrum is observed between 306 and 580 nm. There are no shifts in peak placement in the spectrum observed in the plate when compared to the spectrum observed in the cuvette. However, differences in the resolution of the spectrum are apparent. The shoulder found at an excitation wavelength of 306 nm has been lost.
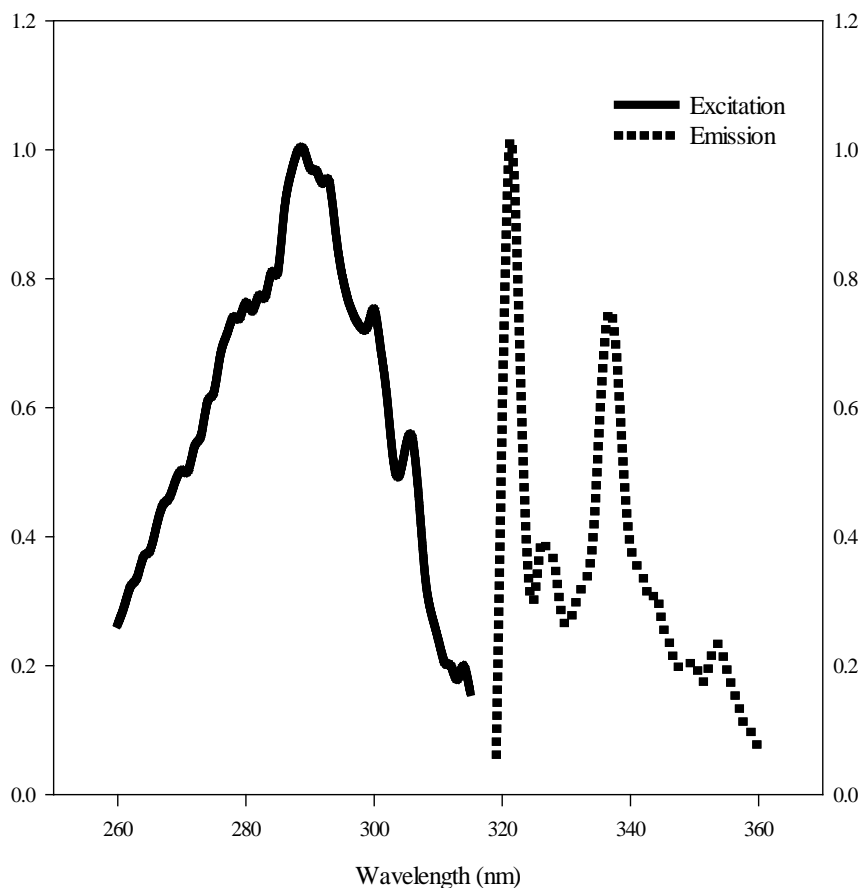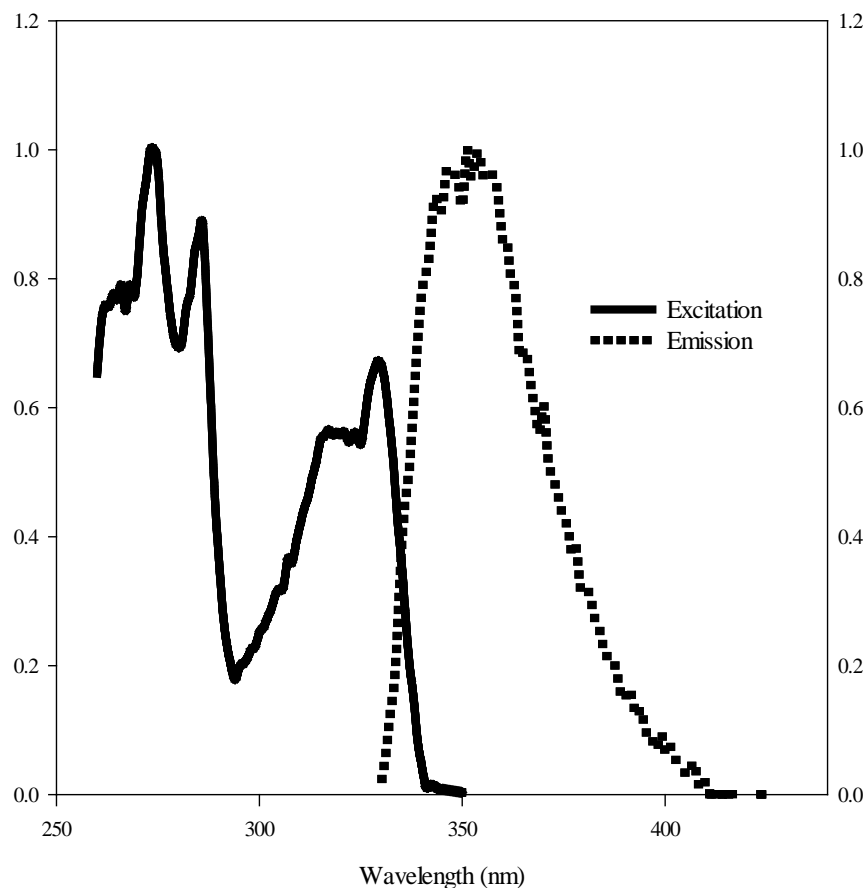
Figure 96: Emission and excitation spectra of 2 – naphthol in 75 % ethanol in a microwell plate.

The excitation and emission spectrum of 2 – naphthol in 75 % ethanol can be seen in Figure 96 at a concentration of 0.006 mg/mL. The excitation spectrum is observed between 260 and 350 nm. The emission spectrum is observed between 330 and 430 nm. There are no shifts in peak placement in the spectrum observed in the plate when compared to the spectrum observed in the cuvette. However, differences in the resolution of the spectrum are apparent. The peak and shoulder seen in the emission spectrum at 352 nm and 345 nm respectively are difficult to observe with the additional noise. The structure of the emission spectrum has no effect on the overall appearance of the EEM spectrum.
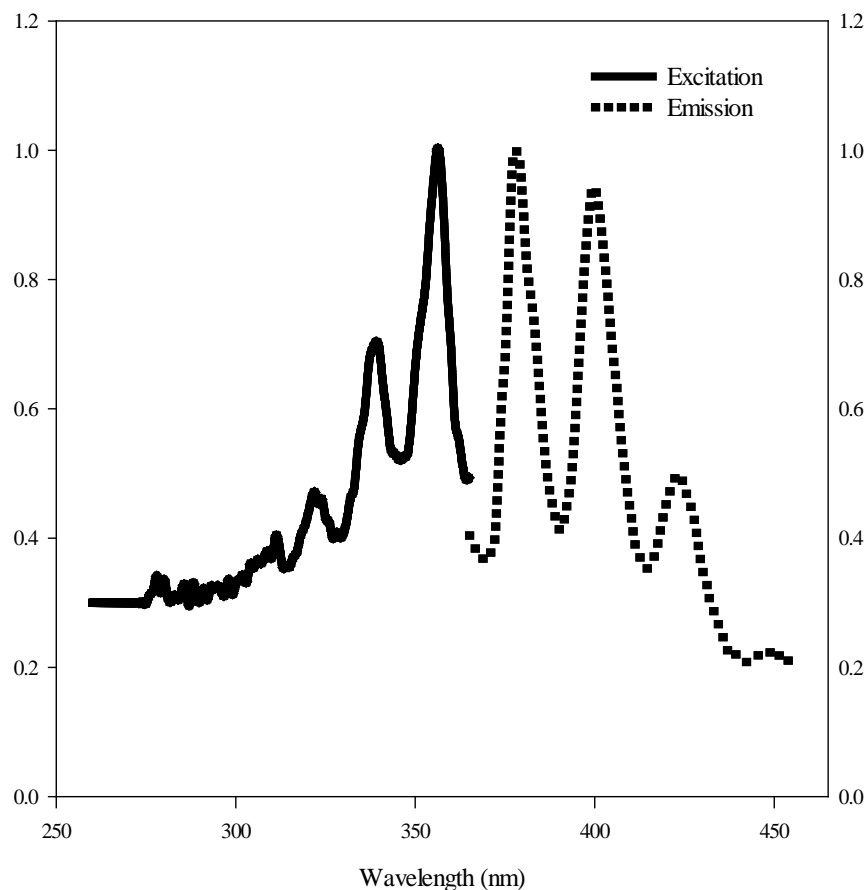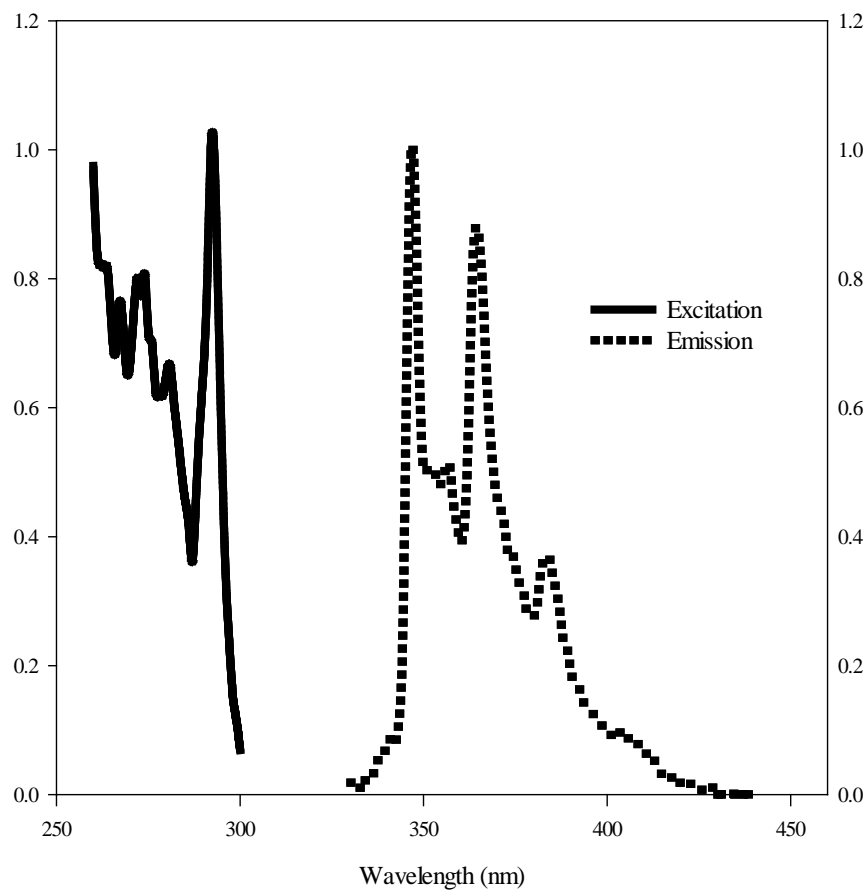
Figure 97: Emission and excitation spectra of phenanthrene in 75 % ethanol in a microwell plate.

The excitation and emission spectrum of phenanthrene in 75 % ethanol can be seen in Figure 97 at a concentration of 0.0025 mg/mL. The excitation spectrum is observed between 260 and 300 nm. The emission spectrum is observed between 330 and 450 nm. There are no shifts in peak placement or resolution in the spectrum observed in the plate when compared to the spectrum observed in the cuvette.
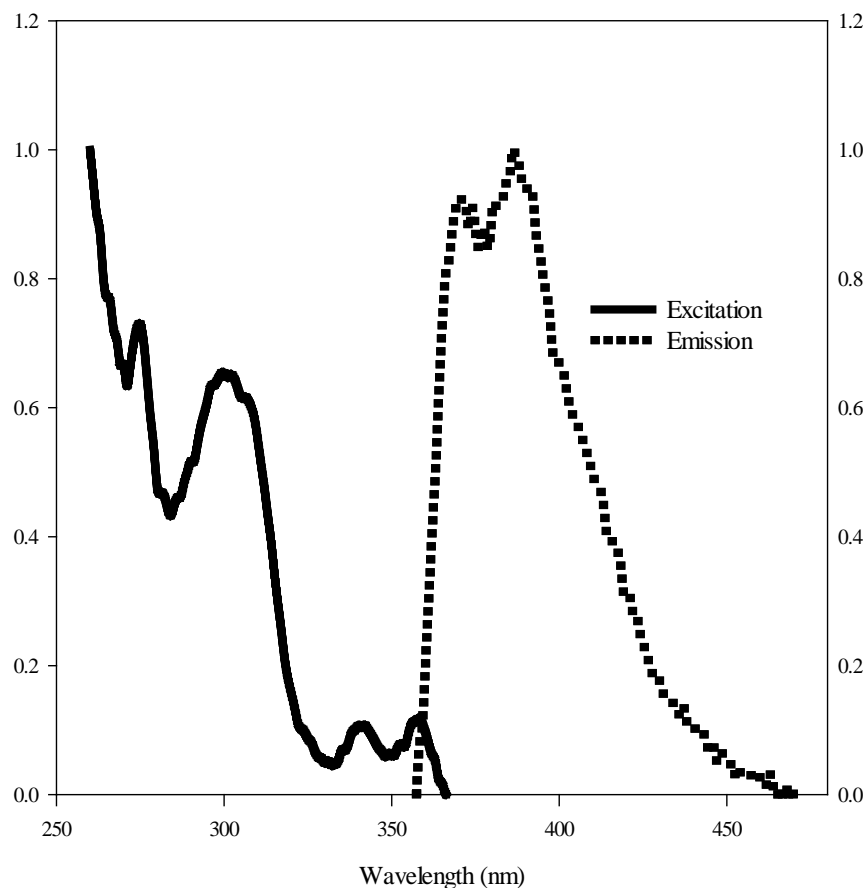
Figure 98: Emission and excitation spectra of 9 – phenanthrol in 75 % ethanol in a microwell plate.

The excitation and emission spectrum of 9 – phenanthrol in 75 % ethanol can be seen in Figure 98 at a concentration of 0.004 mg/mL. The excitation spectrum is observed between 260 and 375 nm. The emission spectrum is observed between 350 and 470 nm. There are no shifts in peak placement or resolution in the spectrum observed in the plate when compared to the spectrum observed in the cuvette. There is an additional peak apparent in the excitation spectrum at 358 nm that has no effect on the emission spectrum.
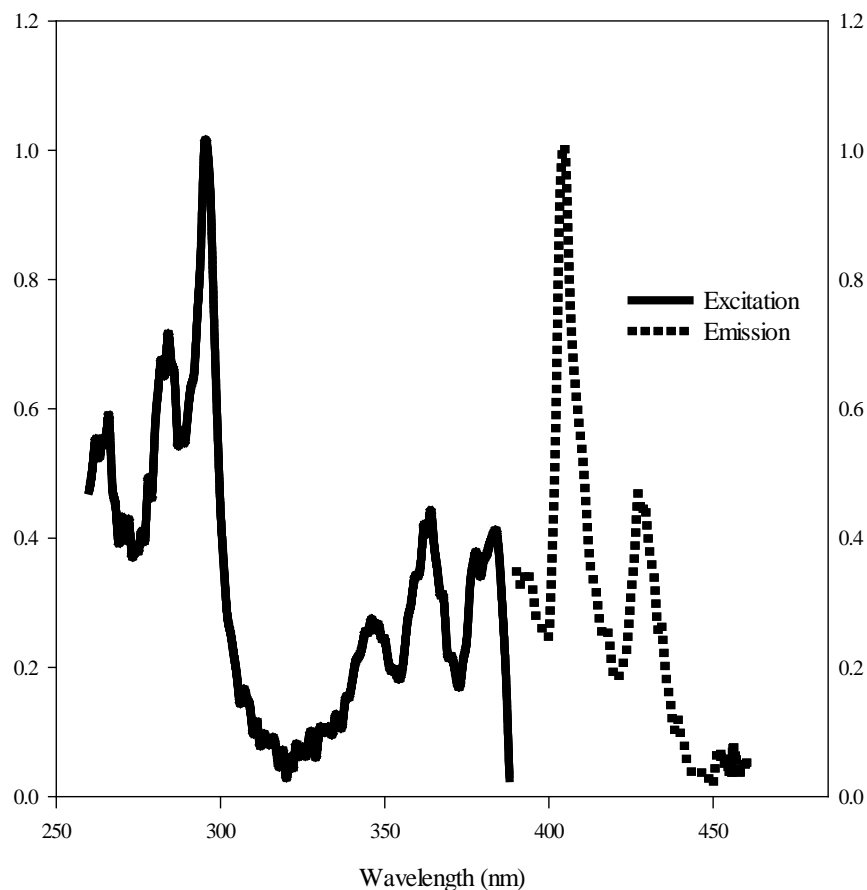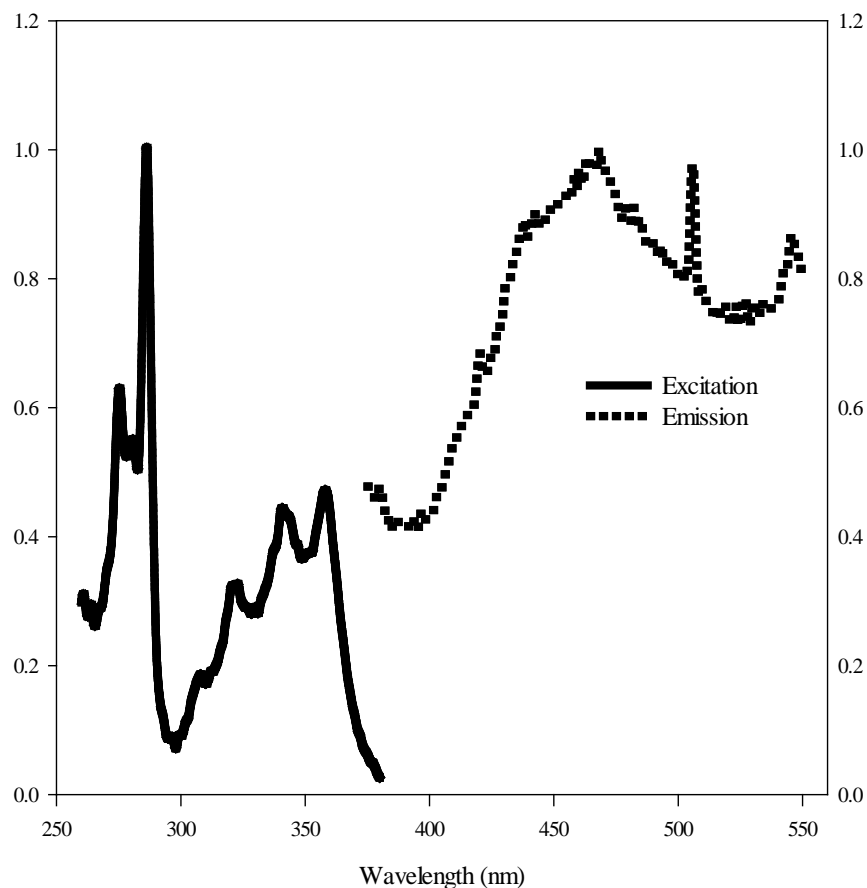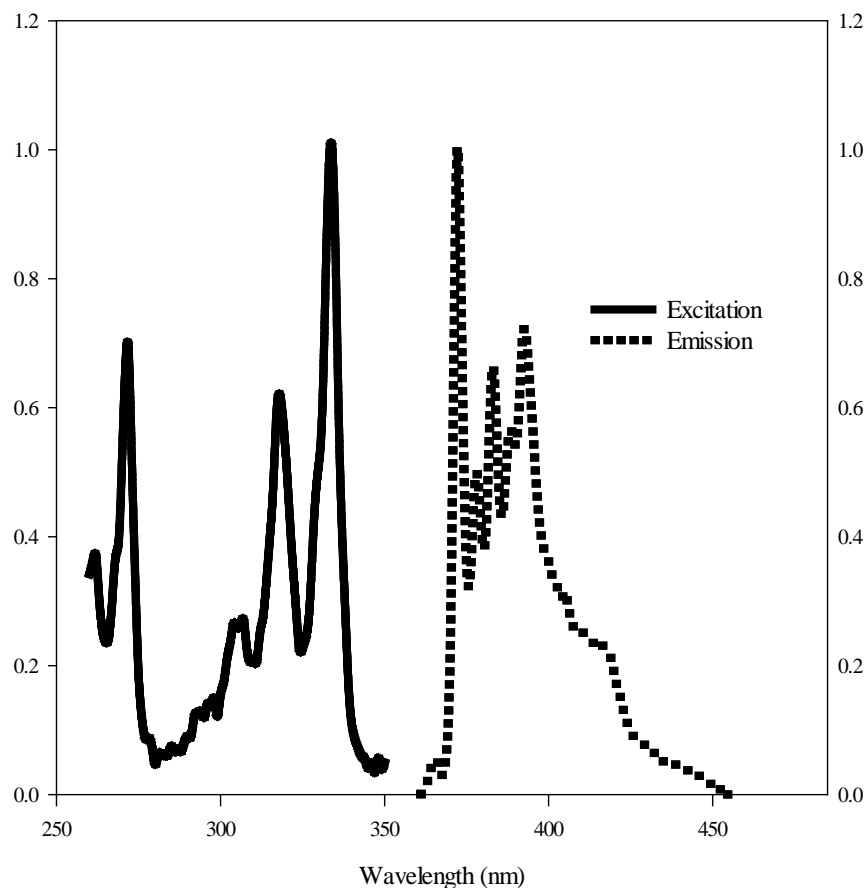
Figure 99: Emission and excitation spectra of pyrene in 75 % ethanol in a microwell plate.

The excitation and emission spectrum of pyrene in 75 % ethanol can be seen in Figure 99 at a concentration of 0.0008 mg/mL. The excitation spectrum is observed between 260 and 350 nm. The emission spectrum is observed between 350 and 475 nm. There are no shifts in peak placement or resolution in the spectrum observed in the plate when compared to the spectrum observed in the cuvette. The excitation spectrum however shows a change in the maximum peak. When looking at the spectrum observed in a cuvette the maximum peak observed is at an excitation wavelength of 272 nm, while the second intense peak appears at and excitation wavelength of 334 nm. When looking at the spectrum observed in a plate, the maximum peak observed is at an excitation wavelength of 334 nm and the second intense peak appears at an excitation wavelength of 272 nm. This "flip" of intensities could be due to the fluorescence of

precipitate formation on the walls and bottom of the well. Pyrene does not readily dissolve in 75 % ethanol, therefore the potential for precipitation is greater.
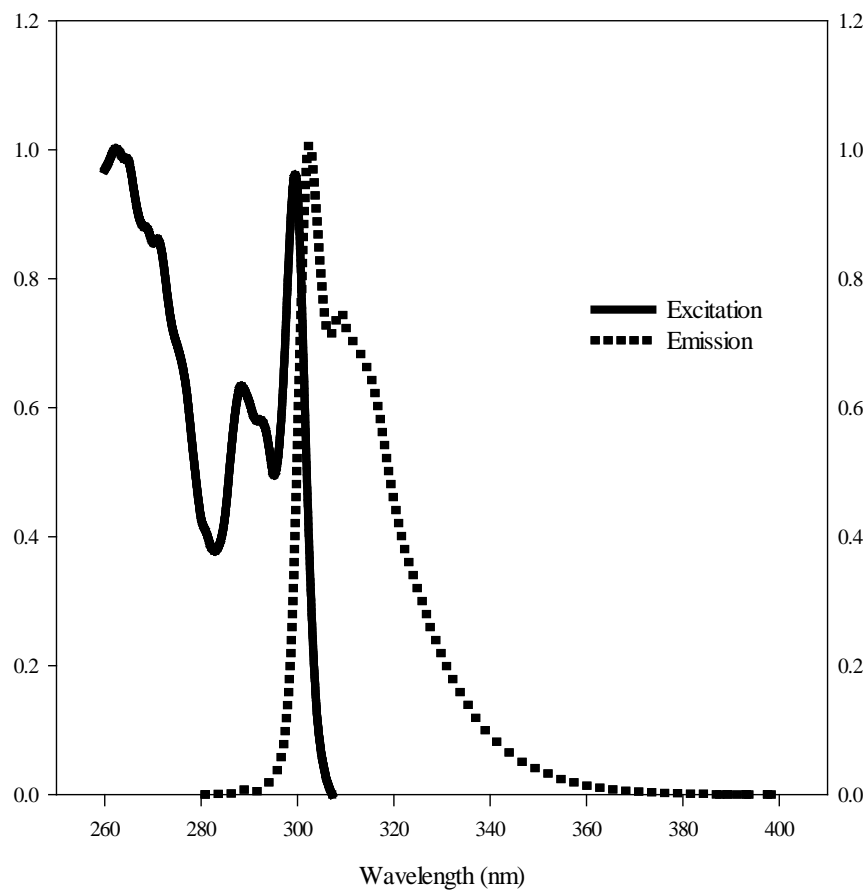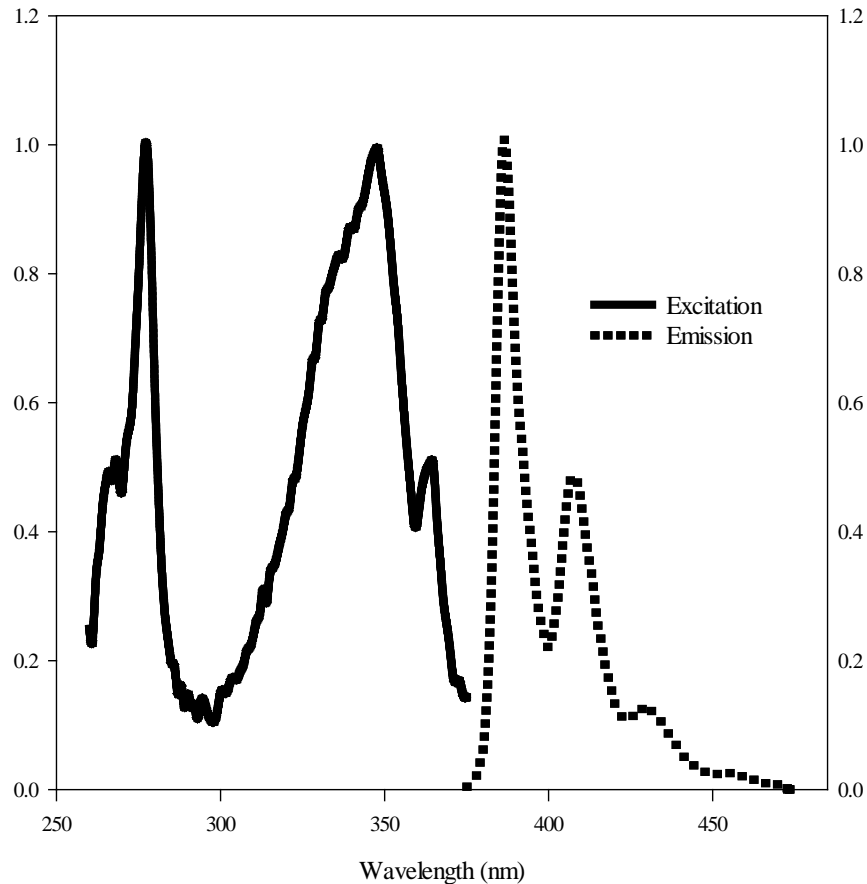

Figure 100: Emission and excitation spectra of 1 – pyrenol in 75 % ethanol in a microwell plate.

The excitation and emission spectrum of 1 – pyrenol in 75 % ethanol can be seen in Figure 100 at a concentration of 0.0008 mg/mL. The excitation spectrum is observed between 260 and 375 nm. The emission spectrum is observed between 375 and 475 nm. There are no shifts in peak placement or resolution in the spectrum observed in the plate when compared to the spectrum observed in the cuvette. The excitation spectrum however shows a change in peak intensity. When looking at the spectrum observed in a cuvette the peak observed is at an excitation wavelength of 345 nm has an intensity of 0.4744 arbitrary units while the same peak when observed in the spectrum produced in a plate shows and intensity of 0.9525 arbitrary units. This increase of intensity could be due to the fluorescence of precipitate formation on the walls

145

and bottom of the well. 1 – pyrenol does not readily dissolve in 75 % ethanol, therefore the potential for precipitation is greater.

vi. Emission-Excitation Matrices (EEMs)

High resolution excitation – emission matrices (EEMs) of all compounds were measured using the range of excitations and emission previously optimized and can be found in Table 14. Differences from a standard quartz fluorescence cuvette varied in the range of wavelengths recorded to minimize background scatter signal, decrease the presence of first and second order Rayleigh bands, and decrease Raman bands.[2, 3] Both a contour and three – dimensional mesh plots of each EEM have been reported below (Figures 101 – 124). Intensity units are listed as counts per second (CPS) relative to the R1 detector that measures lamp intensity variations as a function of wavelength in millivolts (mV). Three – dimensional scans show optimal excitation and emission in one spectra. Further, the additional data offers better information for identification and analysis.[7] This provides more separation and therefore better detection and characterization of different types of fluorescent compounds. Comparison of two – dimensional excitation and emission spectra with the three – dimensional EEMs show no variations in compound fluorescence.[8] As mentioned in the introduction first order and second order Rayleigh scattering can be seen in some compounds due to the overlapping of wavelengths scanned in the excitation and emission monochromators.[2,3]

Compound Name	λ_{ex} (nm) (range)	λ_{em} (nm) (range)
Acenaphthene	260-315	319-360
Anthracene	260-365	365-455
Benzo [a] pyrene	260-388	390-460
Fluoranthene	260-380	375-550
Fluorene	260-314	280-400
Naphthalene	260-300	300-380
1 – Naphthol	260-330	306-580
2 – Naphthol	260-350	330-430
Phenanthrene	260-300	330-450
9 – Phenanthrol	260-375	350-470
Pyrene	260-350	350-475
1 – Pyrenol	260-375	375-475

Table 14: Optimum EEM Parameters in a microwell plate.

Figure 101: Contour plot of acenaphthene in 75 % ethanol in a microwell plate.

Figure 102: Three – dimensional mesh plot of acenaphthene in 75 % ethanol in a microwell plate.

The EEM spectrum of acenaphthene in 75 % ethanol is shown in Figures 101 and 102. In the contour plot, the intensity of the fluorescence signal (CPS/mV) corresponds to the color shown in the legend. The most intense signal (1.29 x 10^6) can be seen at an excitation wavelength of 290 nm and an emission wavelength of 321 nm. The intensity of signal is slightly shifted in the plate when compared to the signal in the cuvette. The maximum intensity is seen at an excitation wavelength of 288 nm in the cuvette. The cause of this shift is the decrease of signal in the plate.

Figure 103: Contour plot of anthracene in 75 % ethanol in a microwell plate.

Figure 104: Three – dimensional mesh plot of anthracene in 75 % ethanol in a microwell plate.

The EEM spectrum of antrancene in 75 % ethanol is shown in Figures 103 and 104. In the contour plot, the intensity of the fluorescence signal (CPS/mV) corresponds to the color shown in the legend. The most intense signal (6.63×10^5) can be seen at an excitation wavelength of 377 nm and an emission wavelength of 424 nm. The most intense signal placement in the plate and the cuvette differ drastically from each other. The excitation wavelengths are 377 and 356 nm in the plate and the cuvette respectively, while the emission wavelengths are 424 and 399 nm in the plate and the cuvette respectively. The change is due to first order Rayleigh scattering present in the cuvette at an excitation wavelength of approximately 375 – 380 nm. The plate shows additional first order Rayleigh scattering in this same region, however, the peak at an emission of 424 overpowers the scattering signal.
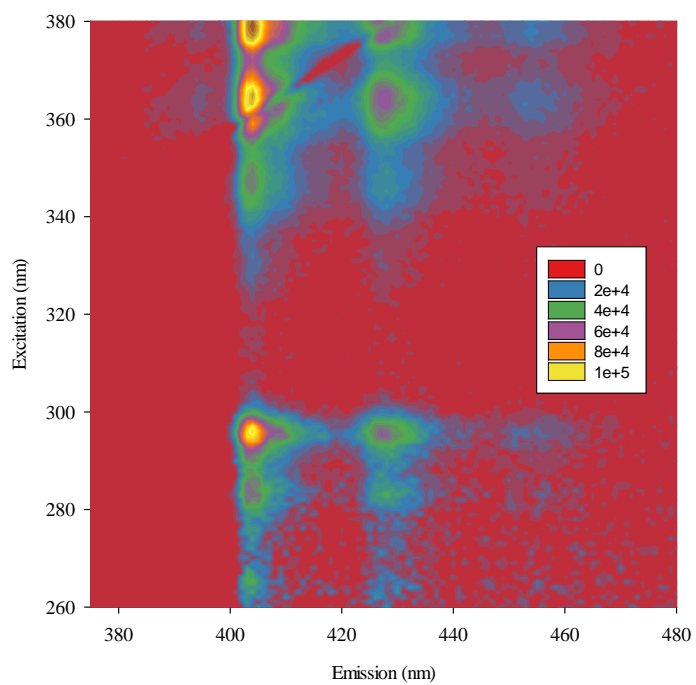
Figure 105: Contour plot of benzo [a] pyrene in 75 % ethanol in a microwell plate.
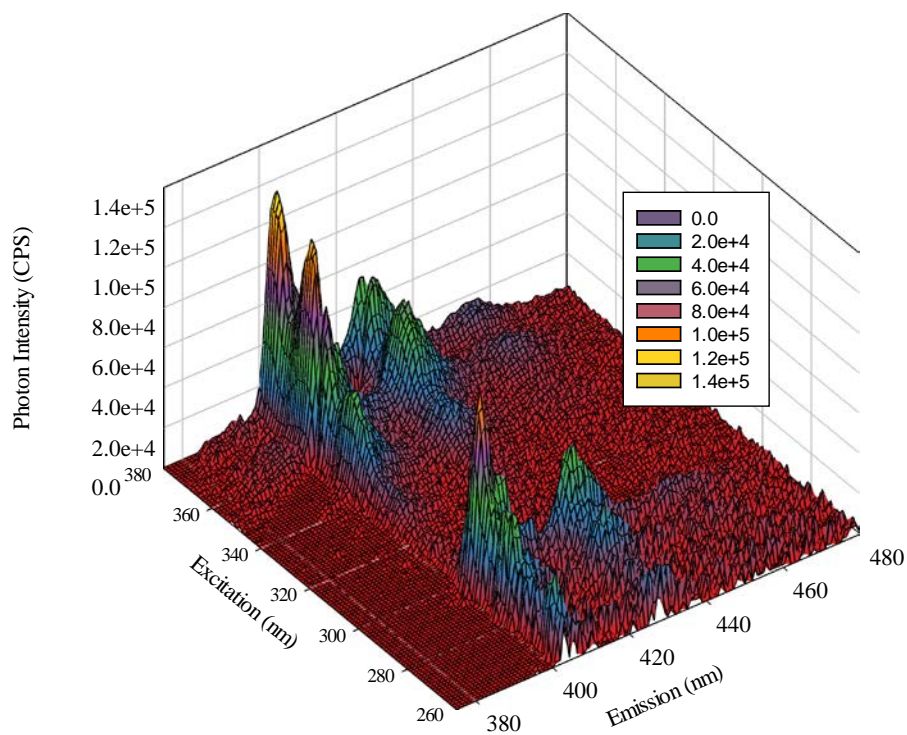
Figure 106: Three – dimensional mesh plot of benzo [a] pyrene in 75 % ethanol in a microwell plate.

The EEM spectrum of benzo [a] pyrene in 75 % ethanol is shown in Figures 105 and 106. In the contour plot, the intensity of the fluorescence signal (CPS/mV) corresponds to the color shown in the legend. The most intense signal (1.05×10^5) can be seen at an excitation wavelength of 367 nm and an emission wavelength of 404 nm. The most intense signal placement in the plate and the cuvette differ from each other. The excitation wavelengths are 367 and 296 nm in the plate and the cuvette respectively. The change is due to first order Rayleigh scattering present in the plate at the excitation wavelength of 367 nm adding to the fluorescence signal and therefore having a larger intensity then at the excitation wavelength of 296 nm.

Figure 107: Contour plot of fluoranthene in 75 % ethanol in a microwell plate.

Figure 108: Three – dimensional mesh plot of fluoranthene in 75 % ethanol in a microwell plate.

The EEM spectrum of fluoranthene in 75 % ethanol is shown in Figures 107 and 108. In the contour plot, the intensity of the fluorescence signal (CPS/mV) corresponds to the color shown in the legend. The most intense signal (1.26×10^5) can be seen at an excitation wavelength of 358 nm and an emission wavelength of 404 nm. The most intense signal placement in the plate and the cuvette differ from each other. The excitation wavelengths are 358 and 286 nm in the plate and the cuvette respectively. This change is due to the increase of excitation signal in the plate versus the cuvette which could be due to fluorescence of precipitate formation in the plate. Fluoranthene does not readily dissolve in 75 % ethanol, therefore there is an increase of dissolution. First order Rayleigh scattering can be seen in the plate at an emission of 355 nm – 450 nm. Second order Rayleigh scattering can be seen in the plate at an emission of 500 nm – 600 nm.

Figure 109: Contour plot of fluorene in 75 % ethanol in a microwell plate.

Figure 110: Three – dimensional mesh plot of fluorene in 75 % ethanol in a microwell plate.

The EEM spectrum of fluorene in 75 % ethanol is shown in Figures 109 and 110. In the contour plot, the intensity of the fluorescence signal (CPS/mV) corresponds to the color shown in the legend. The most intense signal (4.4 x 10^7) can be seen at an excitation wavelength of 297 nm and an emission wavelength of 399 nm. The most intense signal placement in the plate and the cuvette differ from each other. The excitation wavelengths are 297 and 261 nm in the plate and the cuvette respectively, while the emission wavelengths are 299 and 302 in the plate and the cuvette respectively. This only a minor difference when you take into consideration that the second most intense signal occurs at the same placement as in the cuvette and an excitation wavelength of 261 nm and an emission wavelength of 302 nm at an intensity of 1.55 x 10^7 CPS/mV.
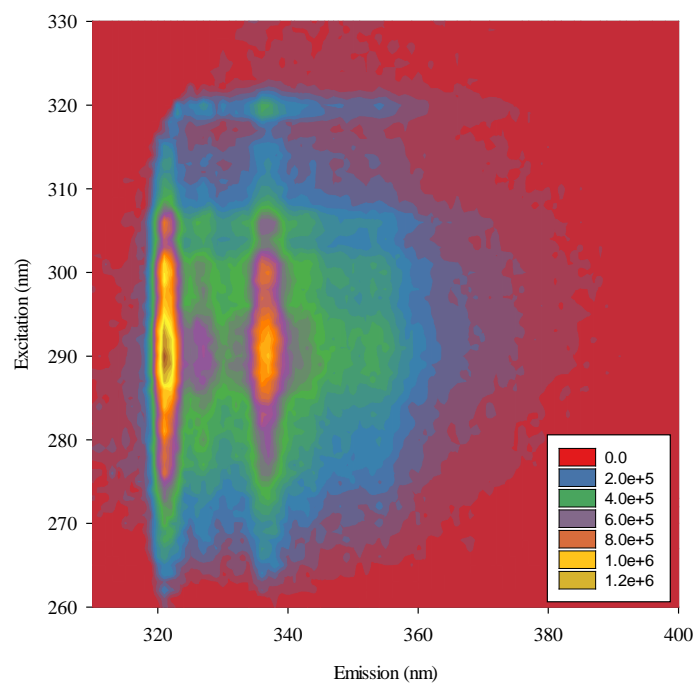
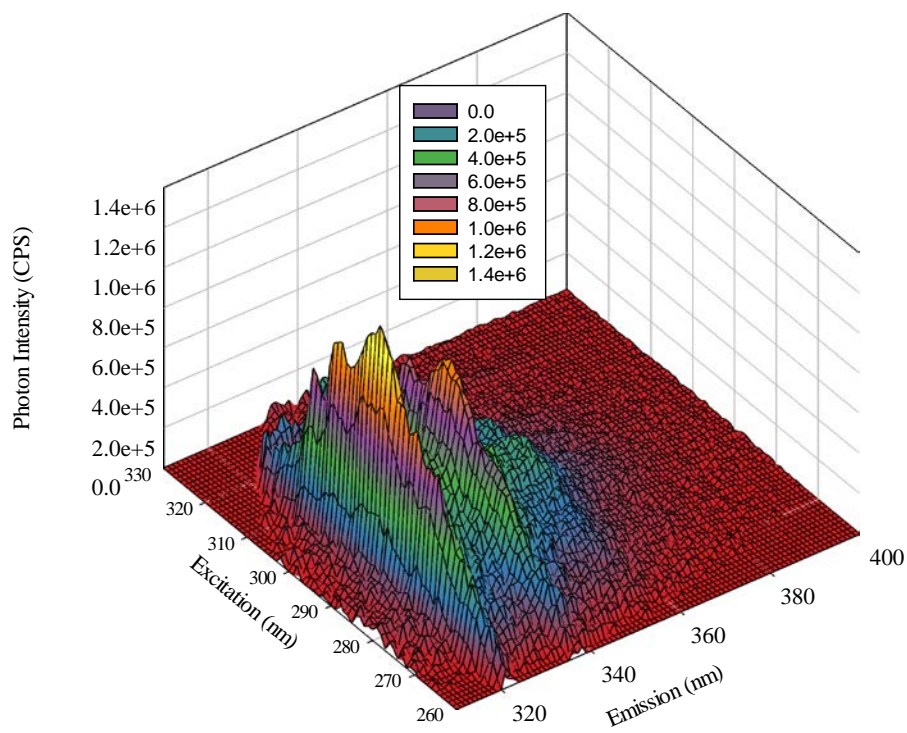Figure 111: Contour plot of naphthalene in 75 % ethanol in a microwell plate.

Figure 112: Three – dimensional mesh plot of naphthalene in 75 % ethanol in a microwell plate.

The EEM spectrum of naphthalene in 75 % ethanol is shown in Figures 111 and 112. In the contour plot, the intensity of the fluorescence signal (CPS/mV) corresponds to the color shown in the legend. The most intense signal (5.50 x 10^5) can be seen at an excitation wavelength of 275 nm and an emission wavelength of 322 nm. The intensity of signal is slightly shifted in the plate when compared to the signal in the cuvette. The maximum intensity is seen at an emission wavelength of 321 nm in the cuvette. The cause of this shift is the decrease of signal in the plate.
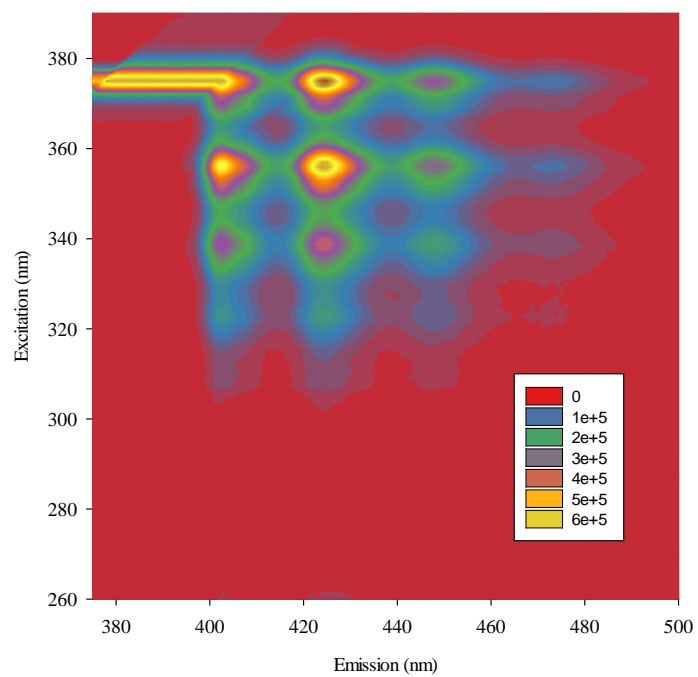
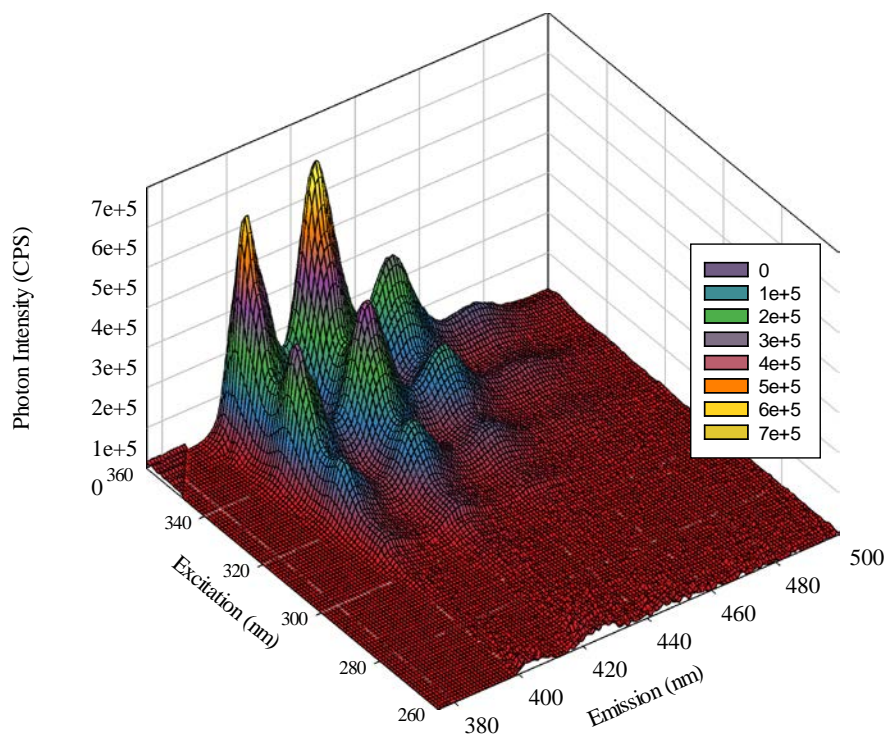Figure 113: Contour plot of 1 – naphthol in 75 % ethanol in a microwell plate.

Figure 114: Three – dimensional mesh plot of 1 – naphthol in 75 % ethanol in a microwell plate.

The EEM spectrum of 1 – naphthol in 75 % ethanol is shown in Figures 113 and 114. In the contour plot, the intensity of the fluorescence signal (CPS/mV) corresponds to the color shown in the legend. The most intense signal (4.22 x 10^6) can be seen at an excitation wavelength of 261 nm and an emission wavelength of 536 nm. The most intense signal placement in the plate and the cuvette differ drastically from each other. The excitation wavelengths are 261 and 295 nm in the plate and the cuvette respectively, while the emission wavelengths are 536 and 464 nm in the plate and the cuvette respectively. This change of maximum intensity is due to the decrease of signal intensity between the plate and the cuvette. Second order Rayleigh scattering can be seen in 1 – naphthol at an emission of 525 nm – 600 nm.

Figure 115: Contour plot of 2 – naphthol in 75 % ethanol in a microwell plate.
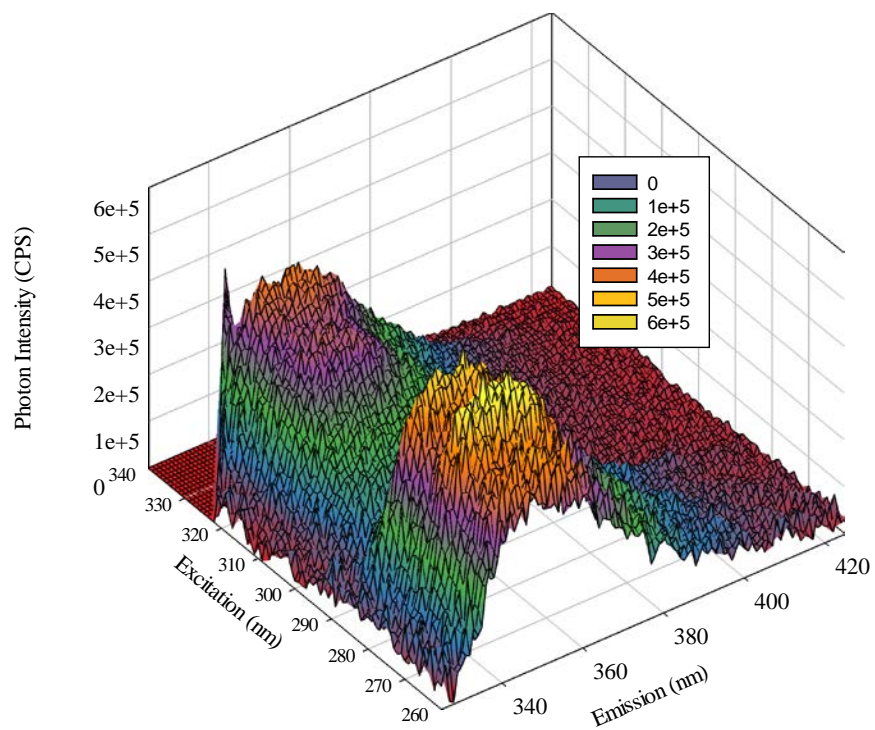
Figure 116: Three – dimensional mesh plot of 2 – naphthol in 75 % ethanol in a microwell plate.

The EEM spectrum of 2 – naphthol in 75 % ethanol is shown in Figures 115 and 116. In the contour plot, the intensity of the fluorescence signal (CPS/mV) corresponds to the color shown in the legend. The most intense signal (5.56×10^5) can be seen at an excitation wavelength of 274 nm and an emission wavelength of 348 nm. The most intense signal placement in the plate and the cuvette differ slightly from each other. The excitation wavelengths are 274 and 273 nm in the plate and the cuvette respectively, while the emission wavelengths are 348 and 355 nm in the plate and the cuvette respectively. This change of maximum intensity is due to the decrease of signal intensity between the plate and the cuvette. First order Rayleigh can be seen at an emission of 320 nm – 350 nm.
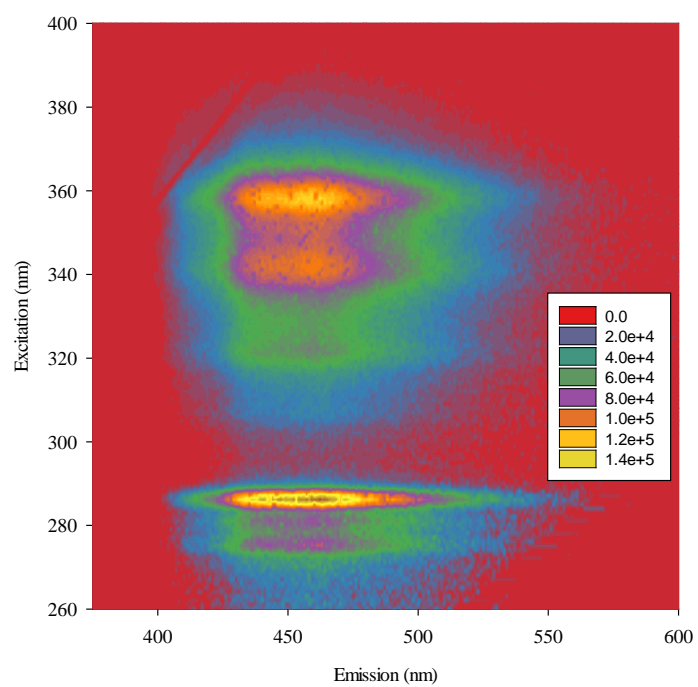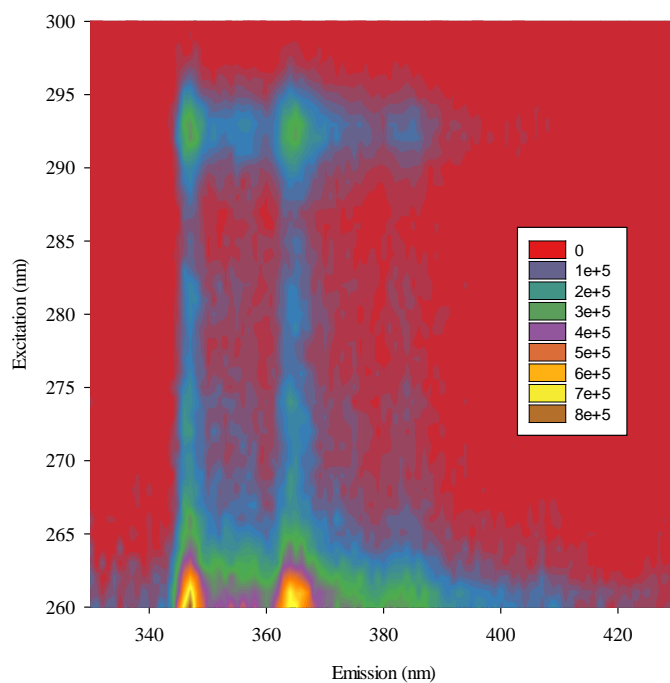
Figure 117: Contour plot of phenathrene in 75 % ethanol in a microwell plate.
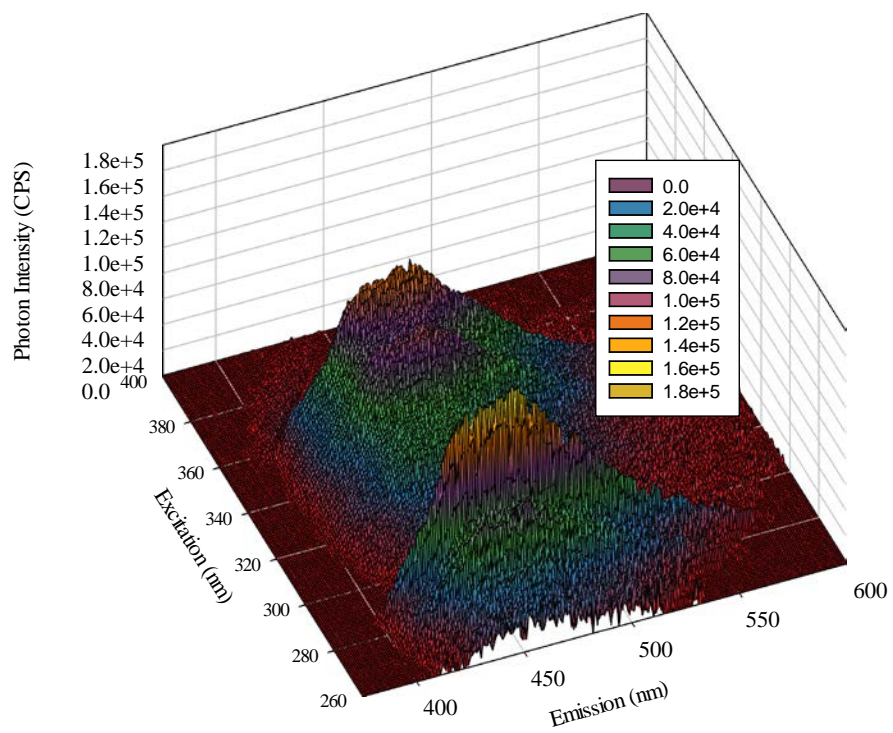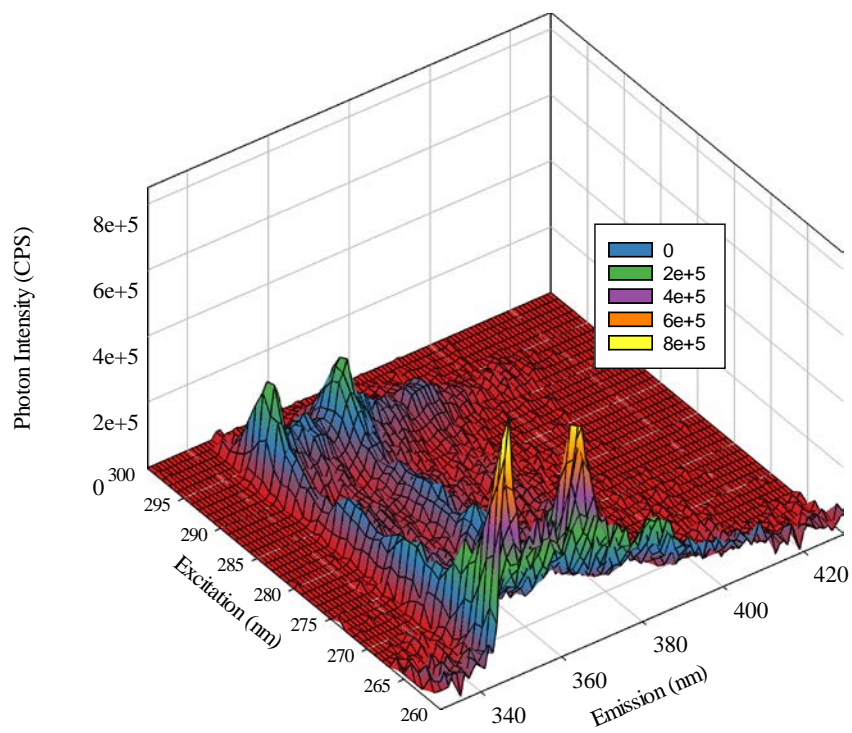

Figure 118: Three – dimensional mesh plot of phenanthrene in 75 % ethanol in a microwell plate.

The EEM spectrum of phenanthrene in 75 % ethanol is shown in Figures 117 and 118. In the contour plot, the intensity of the fluorescence signal (CPS/mV) corresponds to the color shown in the legend. The most intense signal (8.02×10^5) can be seen at an excitation wavelength of 260 nm and an emission wavelength of 347 nm. The most intense signal placement in the plate and the cuvette differ slightly from each other. The emission wavelengths are 347 and 346 nm in the plate and the cuvette respectively. This change of maximum intensity is due to the decrease of signal intensity between the plate and the cuvette.
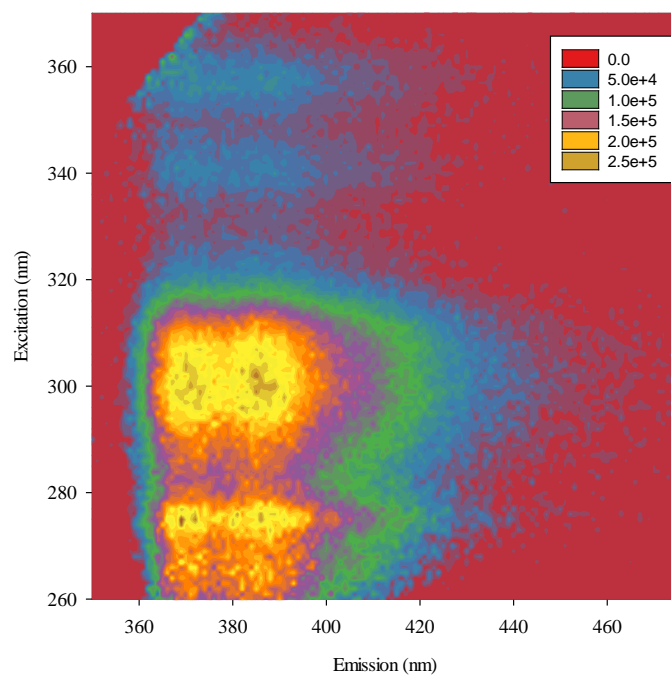
Figure 119: Contour plot of 9 – phenanthrol in 75 % ethanol in a microwell plate.
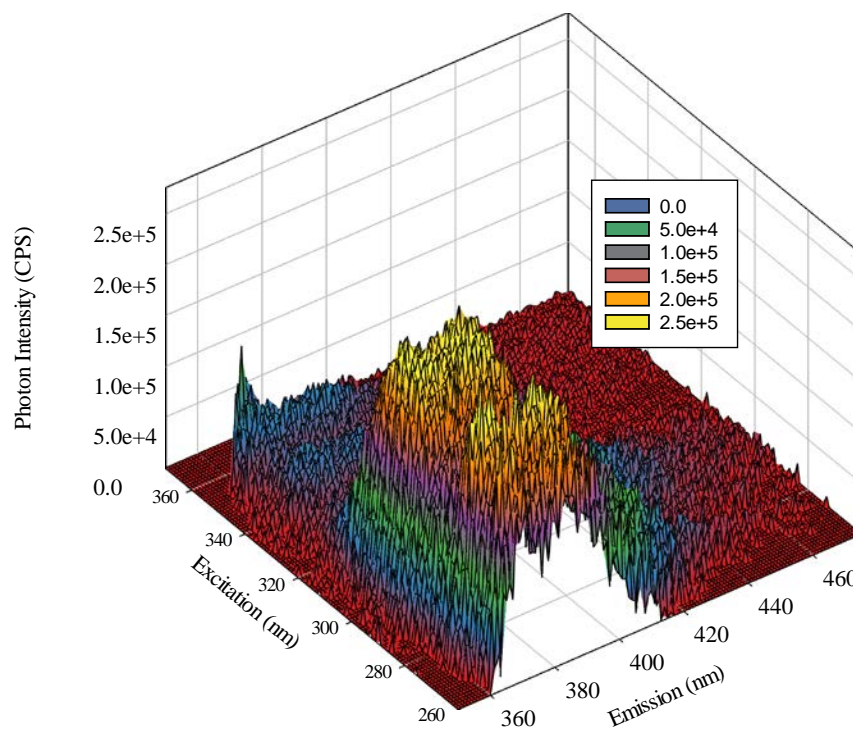
Figure 120: Three – dimensional mesh plot of 9 – phenanthrol in 75 % ethanol in a microwell plate.

The EEM spectrum of 9 – phenanthrol in 75 % ethanol is shown in Figures 119 and 120. In the contour plot, the intensity of the fluorescence signal (CPS/mV) corresponds to the color shown in the legend. The most intense signal (2.66×10^5) can be seen at an excitation wavelength of 275 nm and an emission wavelength of 369 nm. The most intense signal placement in the plate and the cuvette differ drastically from each other. The excitation wavelengths are 275 and 260 nm in the plate and the cuvette respectively, while the emission wavelengths are 369 and 387 nm in the plate and the cuvette respectively. This change of maximum intensity is due to the decrease of signal intensity between the plate and the cuvette. Rayleigh scattering lines can be observed at an emission of 350 nm – 380 nm.
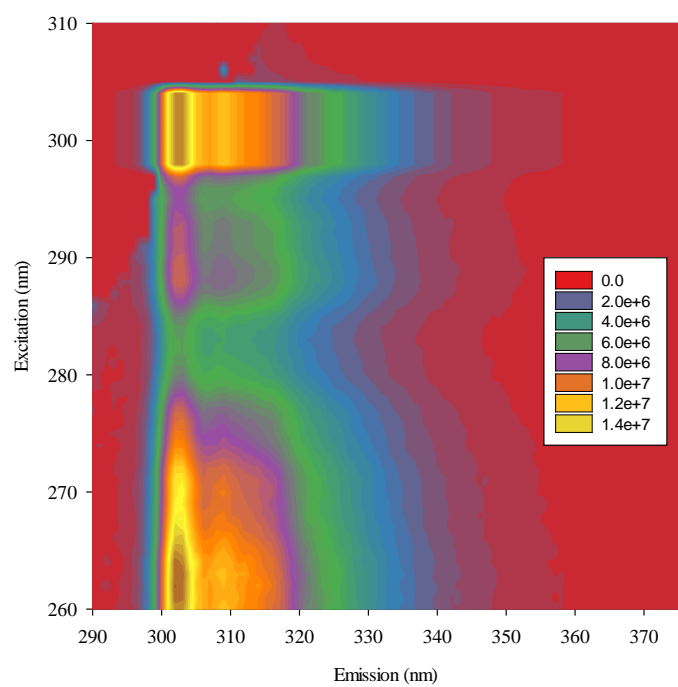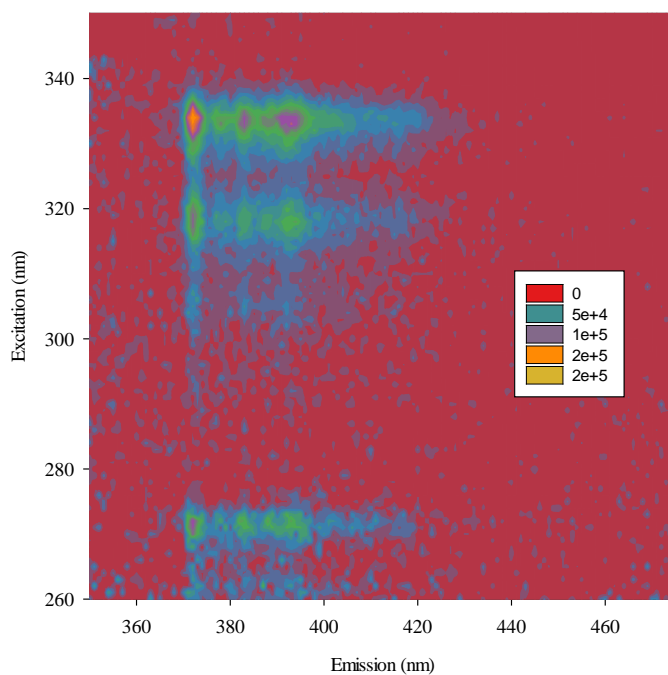
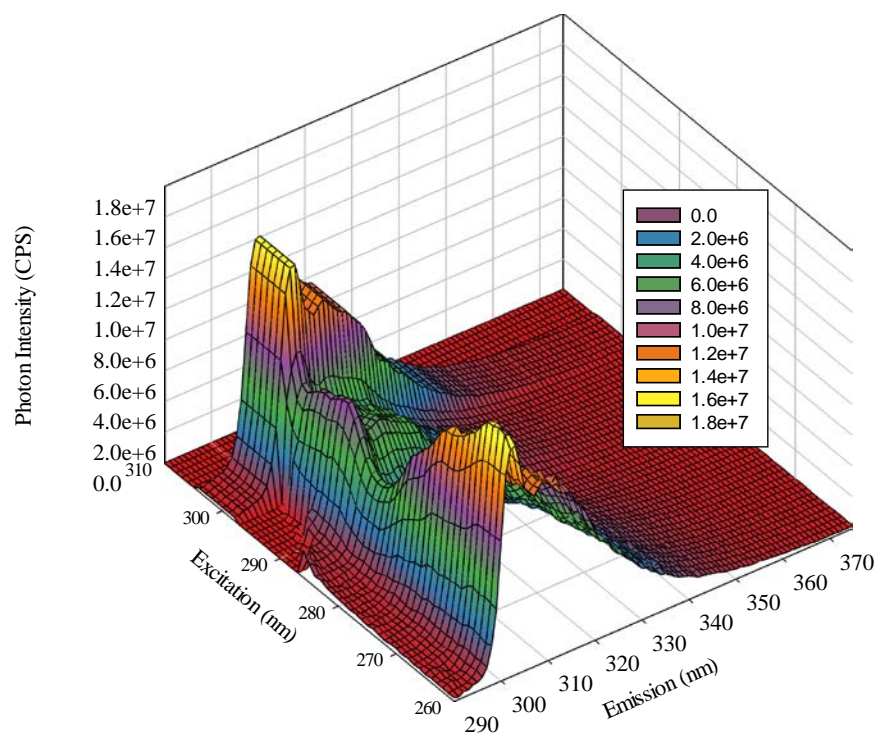Figure 121: Contour plot of pyrene in 75 % ethanol in a microwell plate.
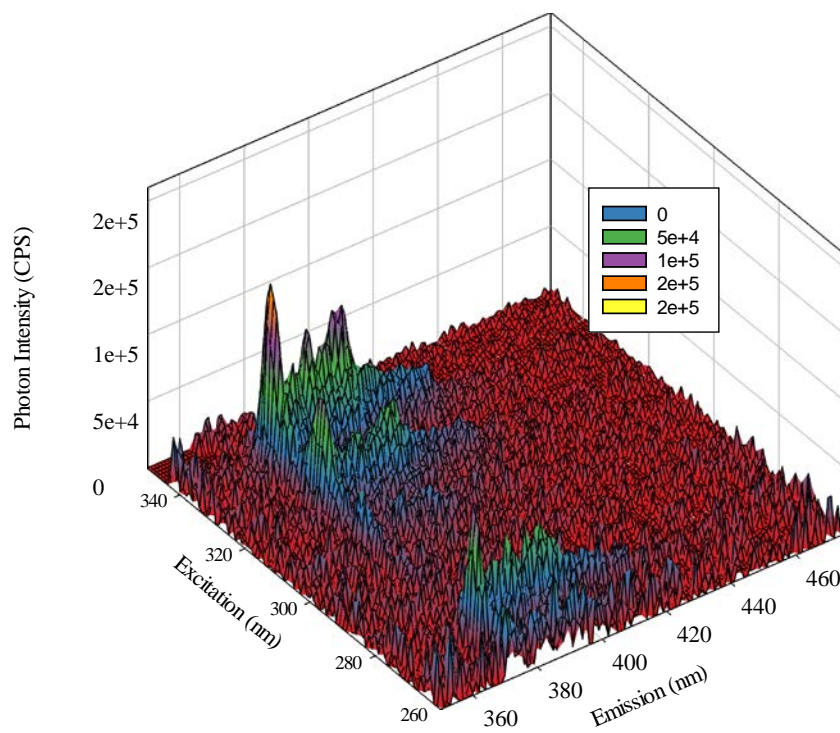
Figure 122: Three – dimensional mesh plot of pyrene in 75 % ethanol in a microwell plate.

The EEM spectrum of pyrene in 75 % ethanol is shown in Figures 121 and 122. In the contour plot, the intensity of the fluorescence signal (CPS/mV) corresponds to the color shown in the legend. The most intense signal (1.48×10^5) can be seen at an excitation wavelength of 334 nm and an emission wavelength of 372 nm. The most intense signal placement in the plate and the cuvette differ slightly from each other. The excitation wavelengths are 334 and 272 nm in the plate and the cuvette respectively. The change in the maximum peak intensity placement is not of much consideration when looking at the excitation spectrum observed in a plate, the maximum peak observed is at an excitation wavelength of 334 nm and the second intense peak appears at an excitation wavelength of 272 nm. This "flip" of intensities could be due to the fluorescence of precipitate formation on the walls and bottom of the well. Pyrene does not readily dissolve in 75 % ethanol, therefore the potential for precipitation is greater. The second maximum peak in the EEM spectrum in the plate has an intensity of 1.07×10^5 CPS/mV at an excitation wavelength of 272 nm and an emission wavelength of 372 nm.
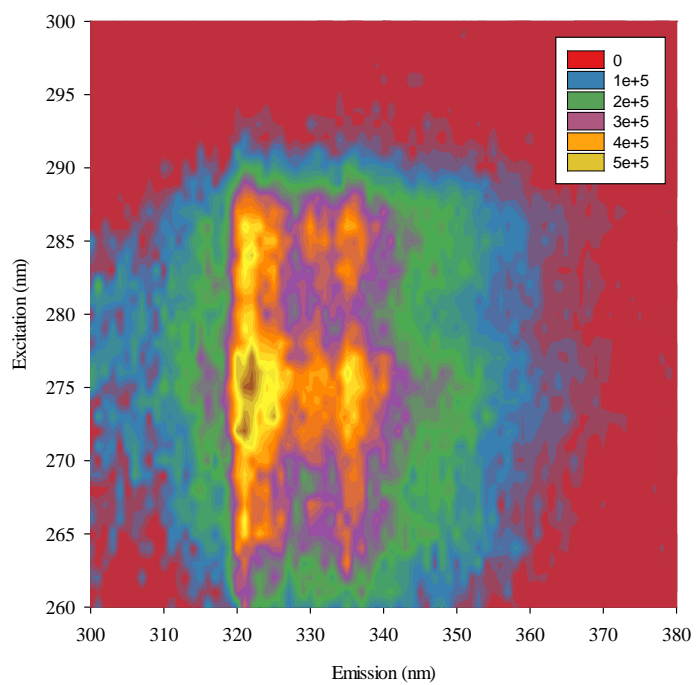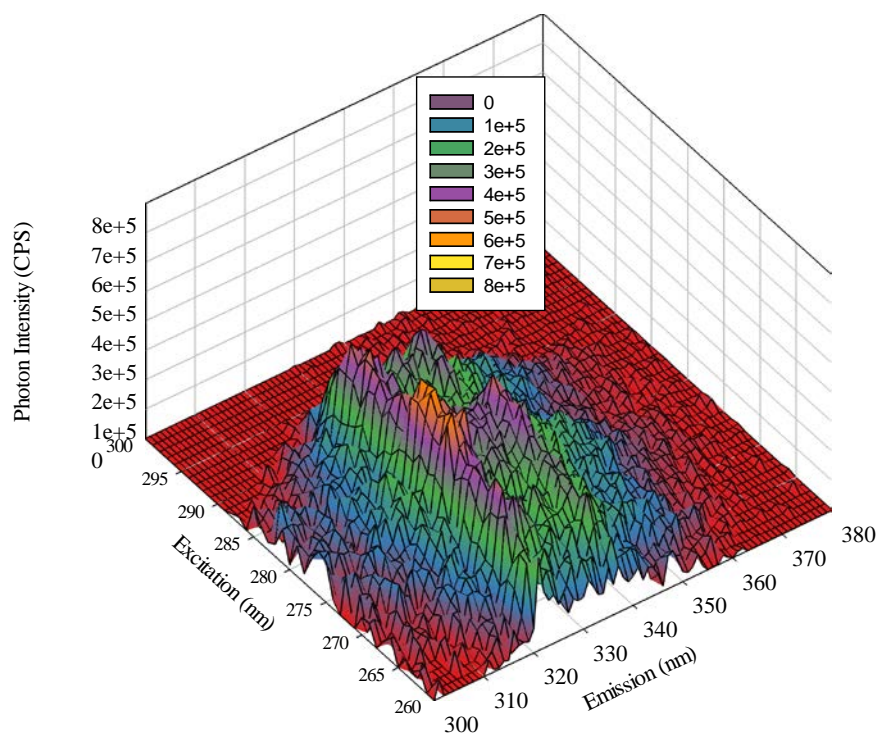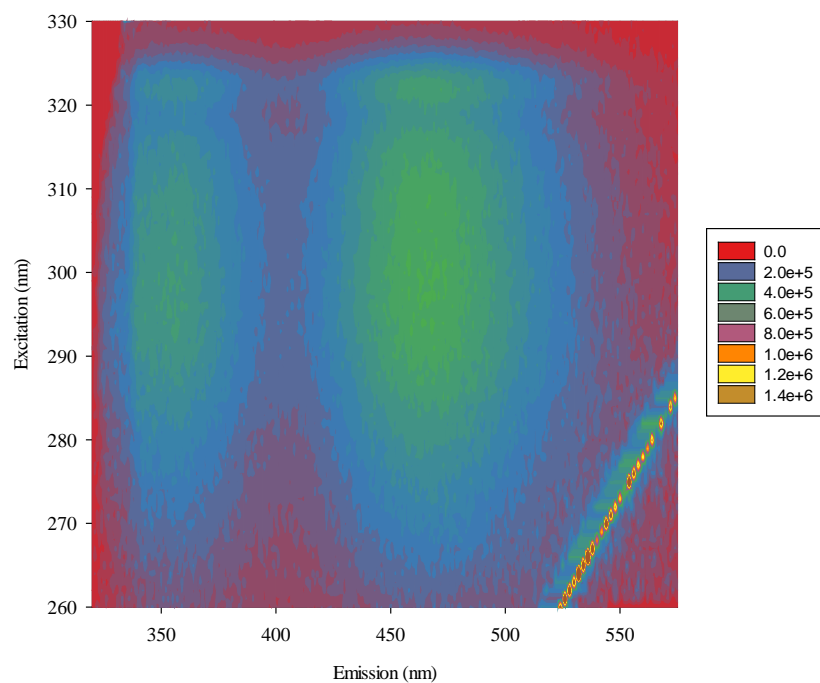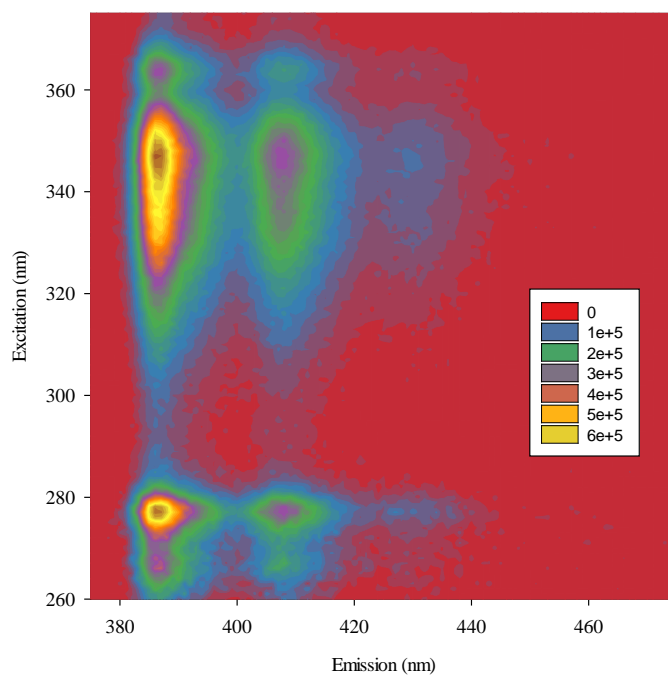
Figure 123: Contour plot of 1 – pyrenol in 75 % ethanol in a microwell plate.
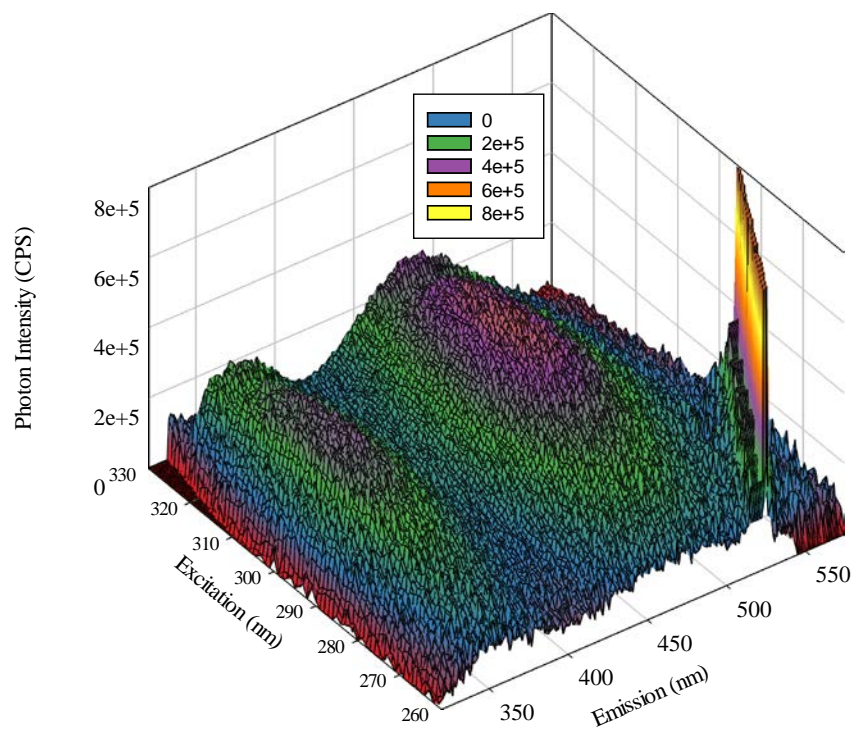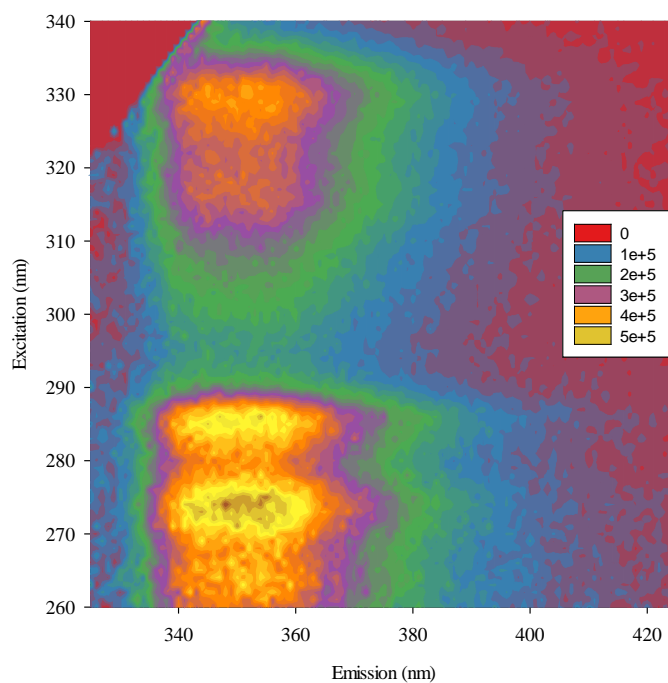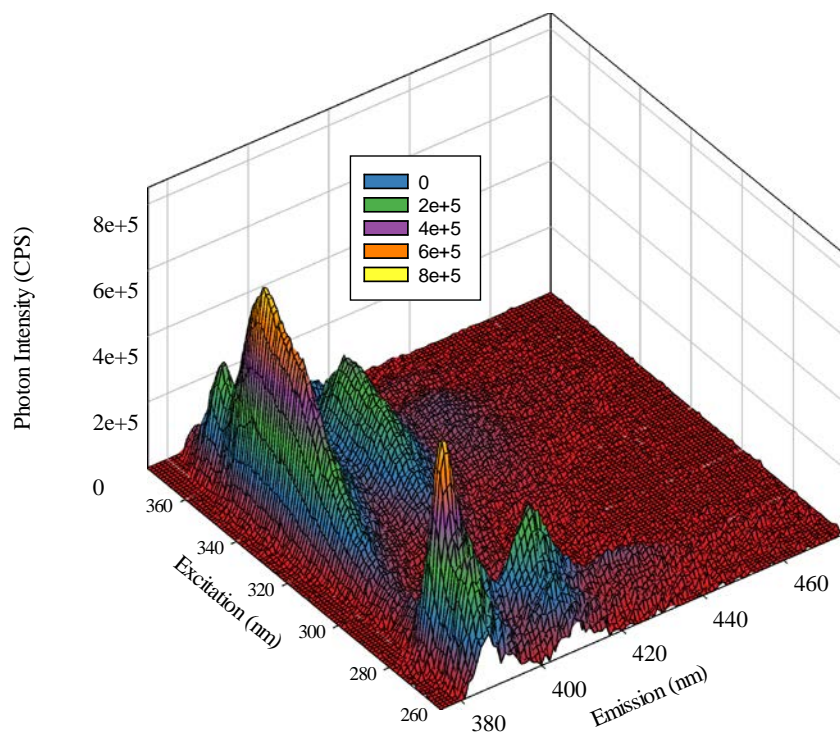

Figure 124: Three – dimensional mesh plot of 1 – pyrenol in 75 % ethanol in a microwell plate.

The EEM spectrum of 1 – pyrenol in 75 % ethanol is shown in Figures 123 and 124. In the contour plot, the intensity of the fluorescence signal (CPS/mV) corresponds to the color shown in the legend. The most intense signal (6.69 x 10^5) can be seen at an excitation wavelength of 347 nm and an emission wavelength of 386 nm. The most intense signal placement in the plate and the cuvette differ slightly from each other. The excitation wavelengths are 347 and 277 nm in the plate and the cuvette respectively. The change in the maximum peak intensity placement is not of much consideration when looking at the excitation spectrum observed in a plate, the maximum peak observed is at an excitation wavelength of 347 nm and the second intense peak appears at an excitation wavelength of 277 nm. This "flip" of intensities could be due to the fluorescence of precipitate formation on the walls and bottom of the well. Pyrene does not readily dissolve in 75 % ethanol, therefore the solubility of 1 – pyrenol is likely to be lower, increasing the potential for precipitation. The second maximum peak in the EEM spectrum in the plate has an intensity of 6.47 x 10^5 CPS/mV at an excitation wavelength of 277 nm and an emission wavelength of 386 nm.

vii.   Limits of Detection and Quantitation

Calibration plots for each compound were made with the concentrations adjusted because of the variation in quantum yields. Low quantum yield fluorophores produced higher concentrations for calibration than high quantum yield fluorophores. It is useful to think of the quantum yield as the equivalent of the extinction coefficient in absorption spectroscopy. The signal intensity of the highest peak from the emission spectra was used in the plot. Calibration plots for each compound were used to determine both the limit of detection (LoD) and the limit of quantitation (LoQ).[14]Calibration plots can be seen in odd numbered Figures 125 – 147. LoD and LoQ were determined by Equation 5 and 6. Limits of detection range from 7.7×10^{-6} and 8.2×10^{-3} mg/mL while limits of quantitation range from 2.6×10^{-5} and 2.7×10^{-2} mg/mL. The accuracy of the limits of detection and quantitation were also tested and can be seen in even numbered Figures 126 – 148. The method for calculating the LoD and LoQ for each compound is on the conservative side, underestimating a true concentration for detection and quantitation.

Compound	Slope	Intercept	R^2
Acenaphthene	3.87×10^6	1.69×10^3	0.998
Anthracene	2.05×10^6	1.76×10^3	0.997
Benzo [a] pyrene	5.33×10^7	2.09×10^3	0.992
Fluoranthene	9.81×10^5	1.57×10^2	0.998
Fluorene	4.55×10^6	2.20×10^4	0.991
Naphthalene	8.02×10^5	4.33×10^2	0.994
1 – Naphthol	1.28×10^5	1.29×10^3	0.981
2 – Naphthol	4.84×10^5	1.45×10^2	0.998
Phenanthrene	3.44×10^6	6.55×10^2	0.999
9 – Phenanthrol	2.43×10^6	3.99×10^2	0.993
Pyrene	1.35×10^7	5.39×10^1	0.989
1 – Pyrenol	8.37×10^6	2.97×10^1	0.999

Table 15: Calibration plot analysis of PAHs and metabolites in 75 % ethanol in a microwell plate.

Table 15 shows the regression analysis of the calibration plots including the slope, intercept, and r^2 value.[12] Correlation of the slope (r^2 value) for most of the compounds were 0.99. 1 – Naphthol was the only compound that showed a lower correlation of 0.981. This lower correlation can be explained by the quantum yield of 1 – naphthol. It has the lowest quantum yield of the compounds tested therefore it was the hardest to regulate the intensity of signal at low concentrations.

Compound	LoD (mg/mL)	LoQ (mg/mL)
Acenaphthene	3.8×10^{-4}	1.3×10^{-3}
Anthracene	3.8×10^{-4}	1.3×10^{-3}
Benzo[a]pyrene	7.7×10^{-6}	2.6×10^{-5}
Fluoranthene	3.5×10^{-4}	1.2×10^{-3}
Fluorene	8.8×10^{-4}	2.9×10^{-3}
Naphthalene	5.7×10^{-4}	1.9×10^{-3}
1 – Naphthol	8.2×10^{-3}	2.7×10^{-2}
2 – Naphthol	4.2×10^{-4}	1.4×10^{-3}
Phenanthrene	1.3×10^{-4}	4.2×10^{-4}
9 – Phenanthrol	5.5×10^{-4}	1.8×10^{-3}
Pyrene	1.3×10^{-4}	4.2×10^{-4}
1 – Pyrenol	4.2×10^{-5}	1.4×10^{-4}

Table 16: Limits of detection and quantitation values of PAHs and metabolites in 75 % ethanol in a microwell plate.

Table 16 shows the values of limit of detection and quantitation for all the compounds. When comparing the limits of detection found using a standard quartz fluorescence cuvette and a microwell plate, limits of detection of eight of the compounds of study were on the same order of magnitude (10^{-4}). Fluorene, 1 – naphthol , phenanthrene, and pyrene all had limits of detection that were an order of magnitude larger in the plate versus the cuvette. That means that for those four compounds, you were able to detect lower concentrations in the cuvette.
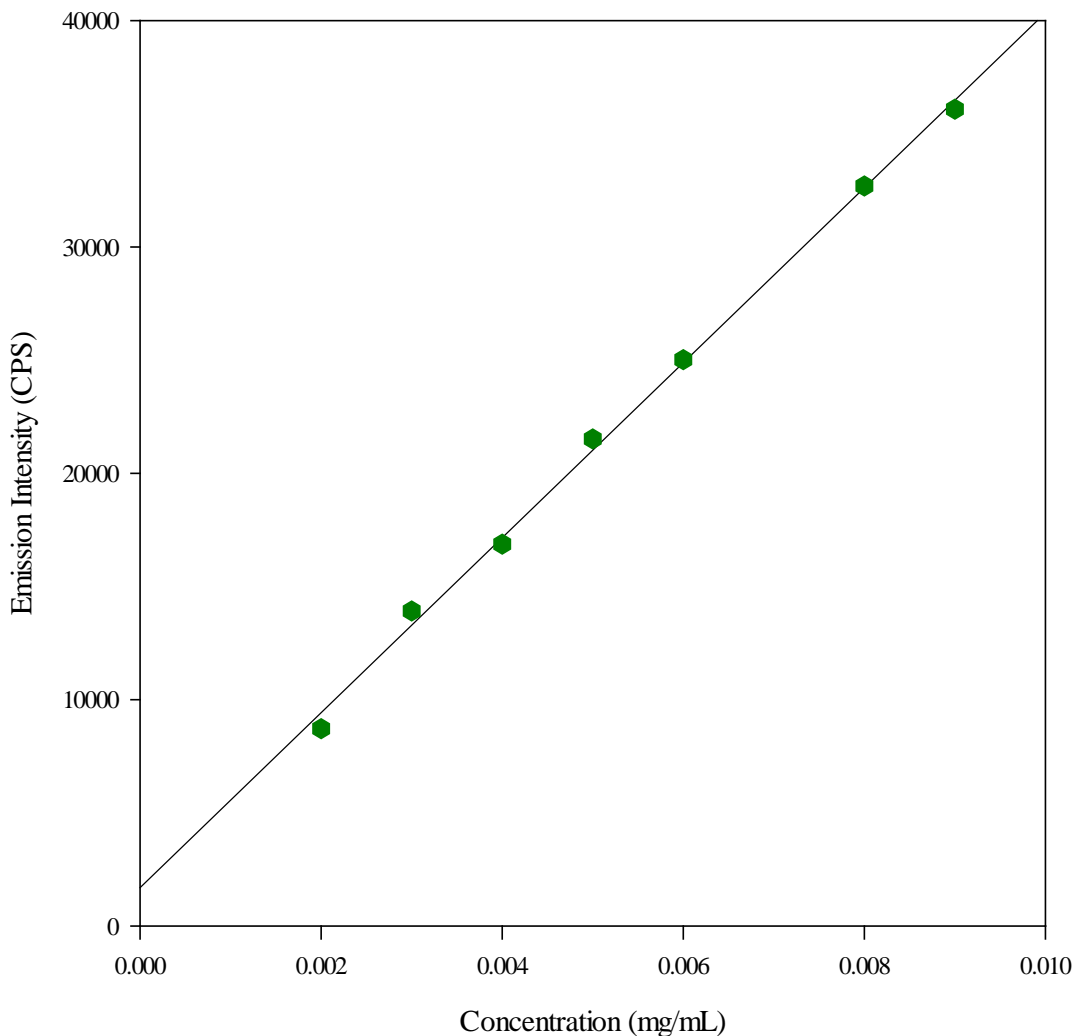
Figure

125: Calibration plot of acenaphthene in 75 % ethanol in a microwell plate.

The calibration plot of acenaphthene in 75 % ethanol can be seen in Figure 125. Seven points were used to construct the plot using an excitation wavelength of 290 nm and an emission wavelength of 338 nm. The concentration of the samples tested range from 0.002 mg/mL producing a fluorescence intensity of 8.7×10^3 CPS/mV to 0.009 mg/mL producing a fluorescence intensity of 3.6×10^4 CPS/mV. When compared to the calibration plot produced in the cuvette, both R^2 values are 0.998 although concentrations of the sample used are higher in the plate due to the loss of signal intensity when using the fiber optic cable.

Figure 126: Accuracy of calculations for limit of detection and quantitation of acenaphthene in 75 % ethanol in a microwell plate.

An emission spectrum was generated to test the accuracy of the calculations performed using the calibration plots LoD and LoQ of acenaphthene in 75 % ethanol and can be seen in Figure 126. The calculated LoD was 3.80×10^{-4} mg/mL and produced a fluorescence intensity of 3.2×10^{3} CPS/mV. The calculated LoQ was 1.27×10^{-3} mg/mL and produced a fluorescence intensity of 6.6×10^{3} CPS/mV. The emission spectrum in the plate shows some additional noise when compared to the spectrum generated in the cuvette, however the spectrum is intact and clearly visible.

177

Figure 127: Calibration plot of anthracene in 75 % ethanol in a microwell plate.

The calibration plot of anthracene in 75 % ethanol can be seen in Figure 127. Seven points were used to construct the plot using an excitation wavelength of 340 nm and an emission wavelength of 425 nm. The concentration of the samples tested range from 0.0008 mg/mL producing a fluorescence intensity of 3.5×10^3 CPS/mV to 0.009 mg/mL producing a fluorescence intensity of 2.0×10^4 CPS/mV. When compared to the calibration plot produced in the cuvette, the R^2 values are 0.999 in the cuvette and 0.997 in the plate. This is a minimal decrease in the precision of the calibration.

Figure 128: Accuracy of calculations for limit of detection and quantitation of anthracene in 75 % ethanol in a microwell plate.

An emission spectrum was generated to test the accuracy of the calculations performed using the calibration plots LoD and LoQ of anthracene in 75 % ethanol and can be seen in Figure 128. The calculated LoD was 3.82×10^{-4} mg/mL and produced a fluorescence intensity of 2.5×10^3 CPS/mV. The calculated LoQ was 1.27×10^{-3} mg/mL and produced a fluorescence intensity of 4.4×10^3 CPS/mV. The emission spectrum in the plate shows some additional noise when compared to the spectrum generated in the cuvette, as well as showing that the limit of detection produced is much closer to baseline signal in the plate versus the cuvette.

Figure 129: Calibration plot of benzo [a] pyrene in 75 % ethanol in a microwell plate.

The calibration plot of benzo [a] pyrene in 75 % ethanol can be seen in Figure 129. Seven points were used to construct the plot using an excitation wavelength of 382 nm and an emission wavelength of 404 nm. The concentration of the samples tested range from 0.00003 mg/mL producing a fluorescence intensity of 3.8×10^3 CPS/mV to 0.00009 mg/mL producing a fluorescence intensity of 6.8×10^3 CPS/mV. When compared to the calibration plot produced in the cuvette, the R^2 values are 0.994 in the cuvette and 0.992 in the plate. This is a minimal decrease in the precision of the calibration.

Figure 130: Accuracy of calculations for limit of detection and quantitation of benzo [a] pyrene in 75 % ethanol in a microwell plate.

An emission spectrum was generated to test the accuracy of the calculations performed using the calibration plots LoD and LoQ of benzo [a] pyrene in 75 % ethanol and can be seen in Figure 130. The calculated LoD was 7.74 x 10^{-6} mg/mL and produced a fluorescence intensity of 2.5 x 10^3 CPS/mV. The calculated LoQ was 2.58 x 10^{-5} mg/mL and produced a fluorescence intensity of 3.5 x 10^3 CPS/mV. The emission spectrum in the plate shows significant noise when compared to the spectrum generated in the cuvette. The emission spectrum also has lost most of its structure confirming correct calculations of LoD and LoQ.

Figure 131: Calibration plot of fluoranthene in 75 % ethanol in a microwell plate.

The calibration plot of fluoranthene in 75 % ethanol can be seen in Figure 131. Seven points were used to construct the plot using an excitation wavelength of 308 nm and an emission wavelength of 462 nm. The concentration of the samples tested range from 0.002 mg/mL producing a fluorescence intensity of 2.1×10^3 CPS/mV to 0.008 mg/mL producing a fluorescence intensity of 7.8×10^3 CPS/mV. When compared to the calibration plot produced in the cuvette, both R^2 values are 0.998 although concentrations of the sample used are higher in the plate due to the loss of signal intensity when using the fiber optic cable.
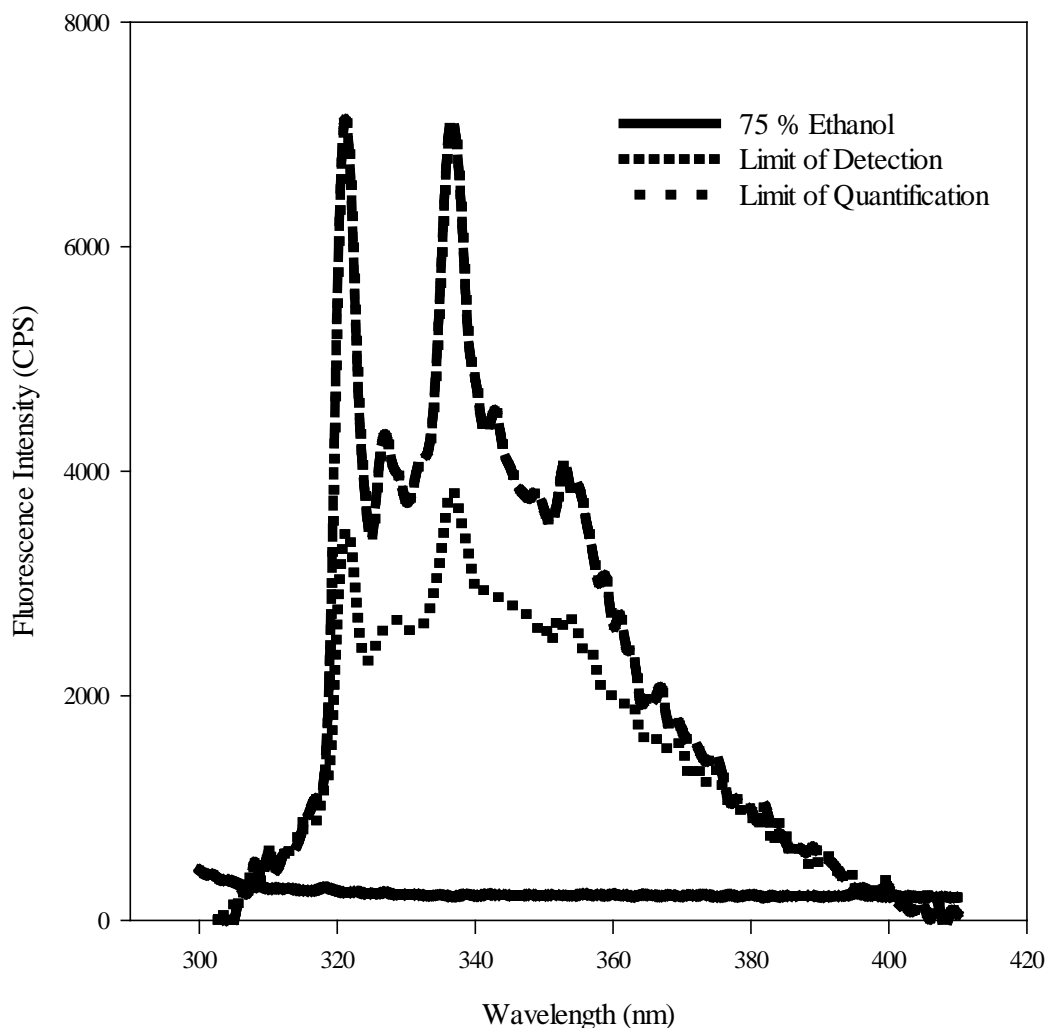
Figure 132: Accuracy of calculations for limit of detection and quantitation of fluoranthene in 75 % ethanol in a microwell plate.

An emission spectrum was generated to test the accuracy of the calculations performed using the calibration plots LoD and LoQ of fluoranthene in 75 % ethanol and can be seen in Figure 132. The calculated LoD was 3.50×10^{-4} mg/mL and produced a fluorescence intensity of 5.0×10^2 CPS/mV. The calculated LoQ was 1.17×10^{-3} mg/mL and produced a fluorescence intensity of 1.3×10^3 CPS/mV. The emission spectrum in the plate shows significant noise when compared to the spectrum generated in the cuvette. The emission spectrum also has lost most of its fine structure.
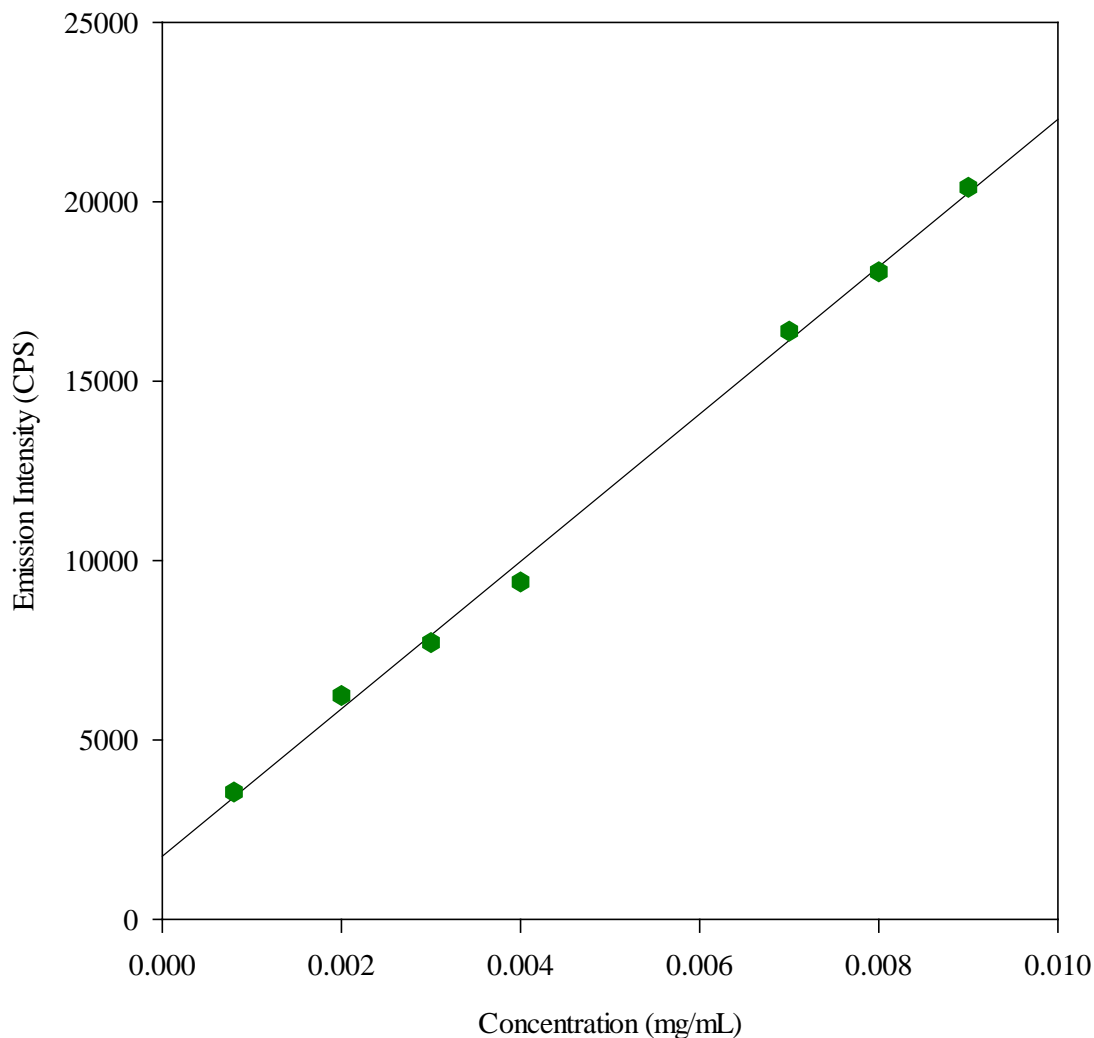
Figure 133: Calibration plot of fluorene in 75 % ethanol in a microwell plate.

The calibration plot of fluorene in 75 % ethanol can be seen in Figure 133. Seven points were used to construct the plot using an excitation wavelength of 262 nm and an emission wavelength of 303 nm. The concentration of the samples tested range from 0.005 mg/mL producing a fluorescence intensity of 4.5×10^4 CPS/mV to 0.009 mg/mL producing a fluorescence intensity of 6.2×10^4 CPS/mV. When compared to the calibration plot produced in the cuvette, the R^2 values are 0.998 in the cuvette and 0.991 in the plate. This is a minimal decrease in the precision of the calibration.
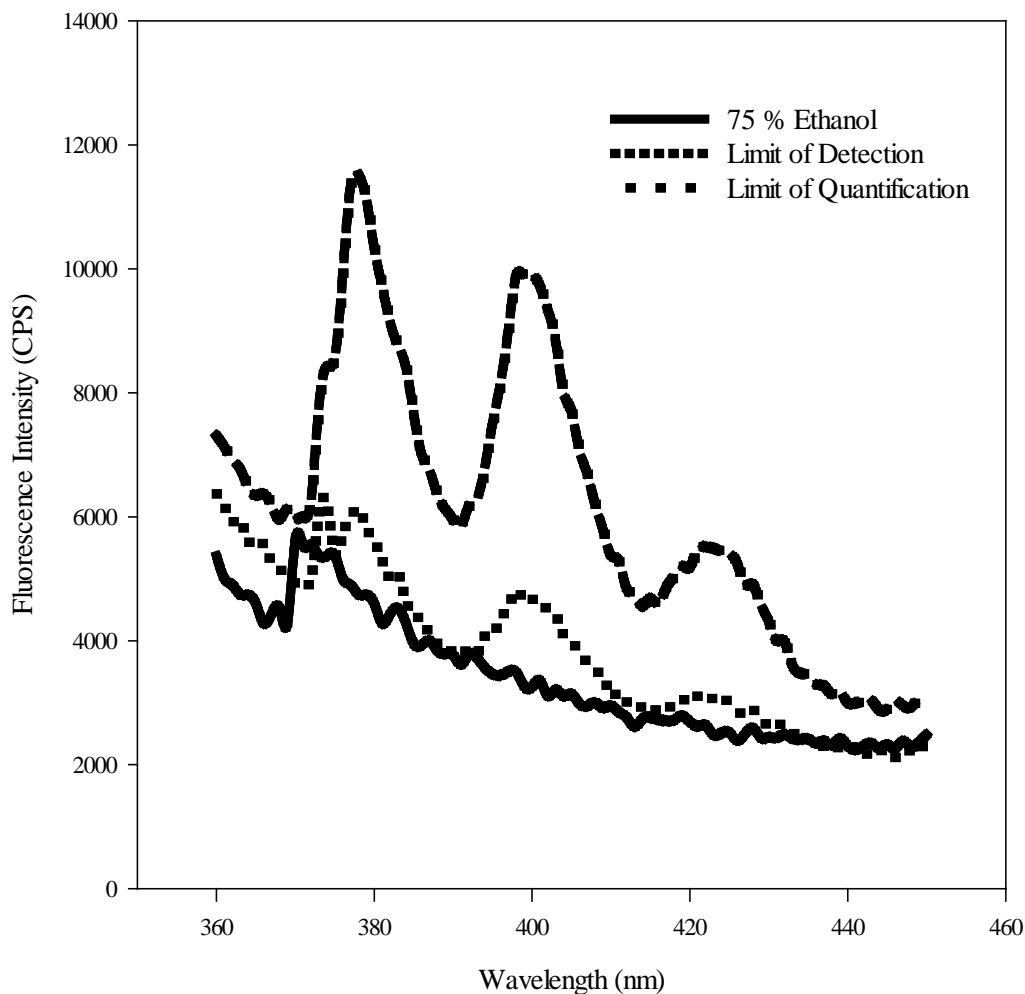
Figure 134: Accuracy of calculations for limit of detection and quantitation of fluorene in 75 % ethanol in a microwell plate.

An emission spectrum was generated to test the accuracy of the calculations performed using the calibration plots LoD and LoQ of fluorene in 75 % ethanol and can be seen in Figure 134. The calculated LoD was 8.77×10^{-4} mg/mL and produced a fluorescence intensity of 2.6×10^{4} CPS/mV. The calculated LoQ was 2.92×10^{-3} mg/mL and produced a fluorescence intensity of 3.5×10^{4} CPS/mV. The emission spectrum in the plate intact and clearly visible, therefore showing that the calculations performed for fluorene were conservative.
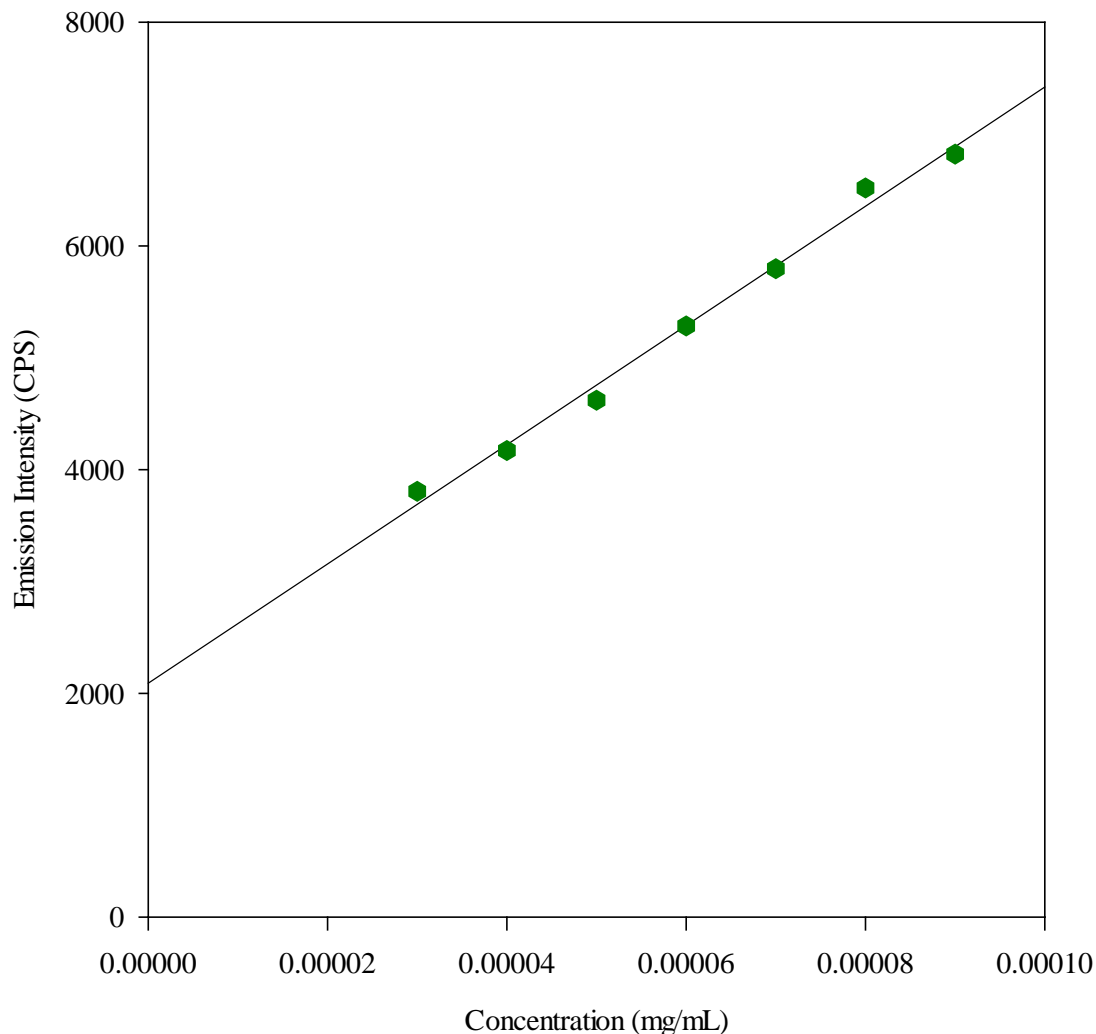
Figure 135: Calibration plot of naphthalene in 75 % ethanol in a microwell plate.

The calibration plot of naphthalene in 75 % ethanol can be seen in Figure 135. Seven points were used to construct the plot using an excitation wavelength of 286 nm and an emission wavelength of 337 nm. The concentration of the samples tested range from 0.002 mg/mL producing a fluorescence intensity of 2.2×10^3 CPS/mV to 0.008 mg/mL producing a fluorescence intensity of 6.8×10^3 CPS/mV. When compared to the calibration plot produced in the cuvette, the R^2 values are 0.998 in the cuvette and 0.994 in the plate. This is a minimal decrease in the precision of the calibration.
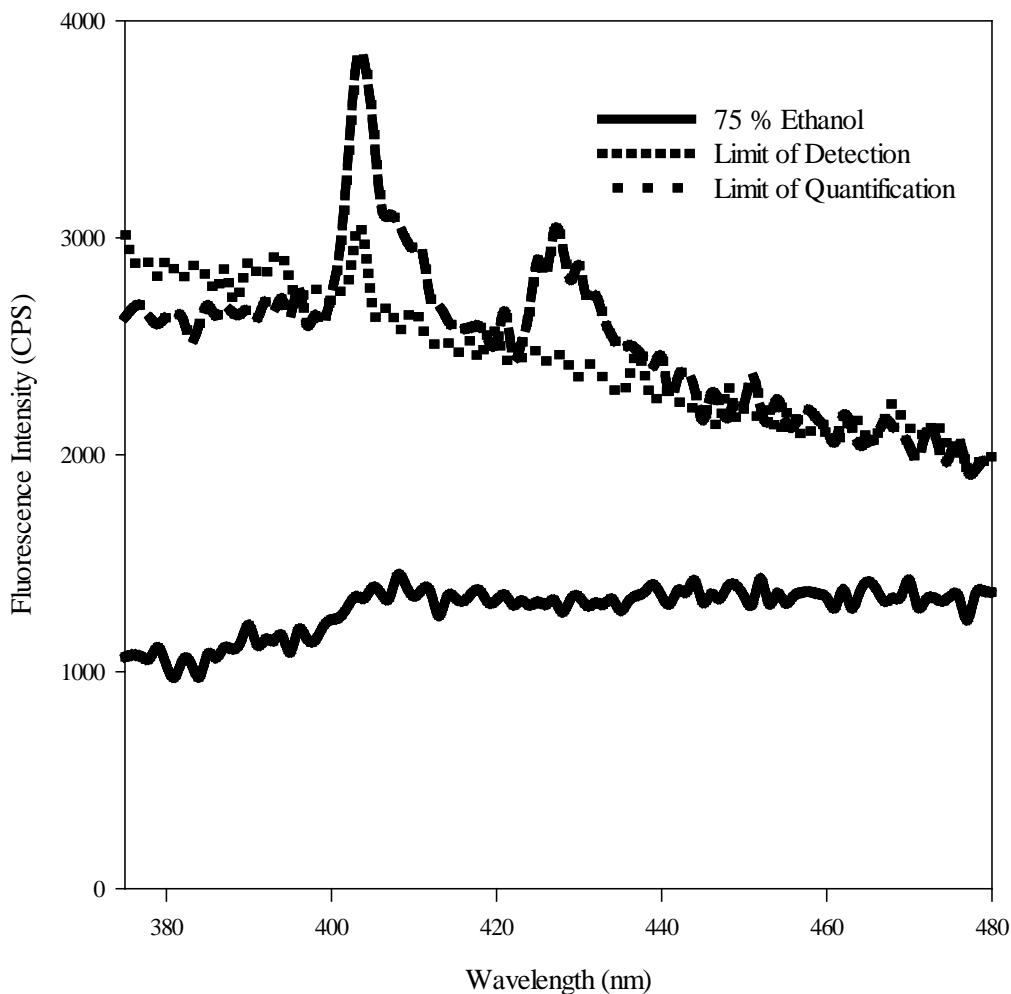
Figure 136: Accuracy of calculations for limit of detection and quantitation of naphthalene in 75 % ethanol in a microwell plate.

An emission spectrum was generated to test the accuracy of the calculations performed using the calibration plots LoD and LoQ of naphthalene in 75 % ethanol and can be seen in Figure 136. The calculated LoD was 5.71×10^{-4} mg/mL and produced a fluorescence intensity of 8.9×10^2 CPS/mV. The calculated LoQ was 1.90×10^{-3} mg/mL and produced a fluorescence intensity of 2.0×10^3 CPS/mV. The emission spectrum in the plate shows significant noise when compared to the spectrum generated in the cuvette. The emission spectrum also has lost most of its fine structure.
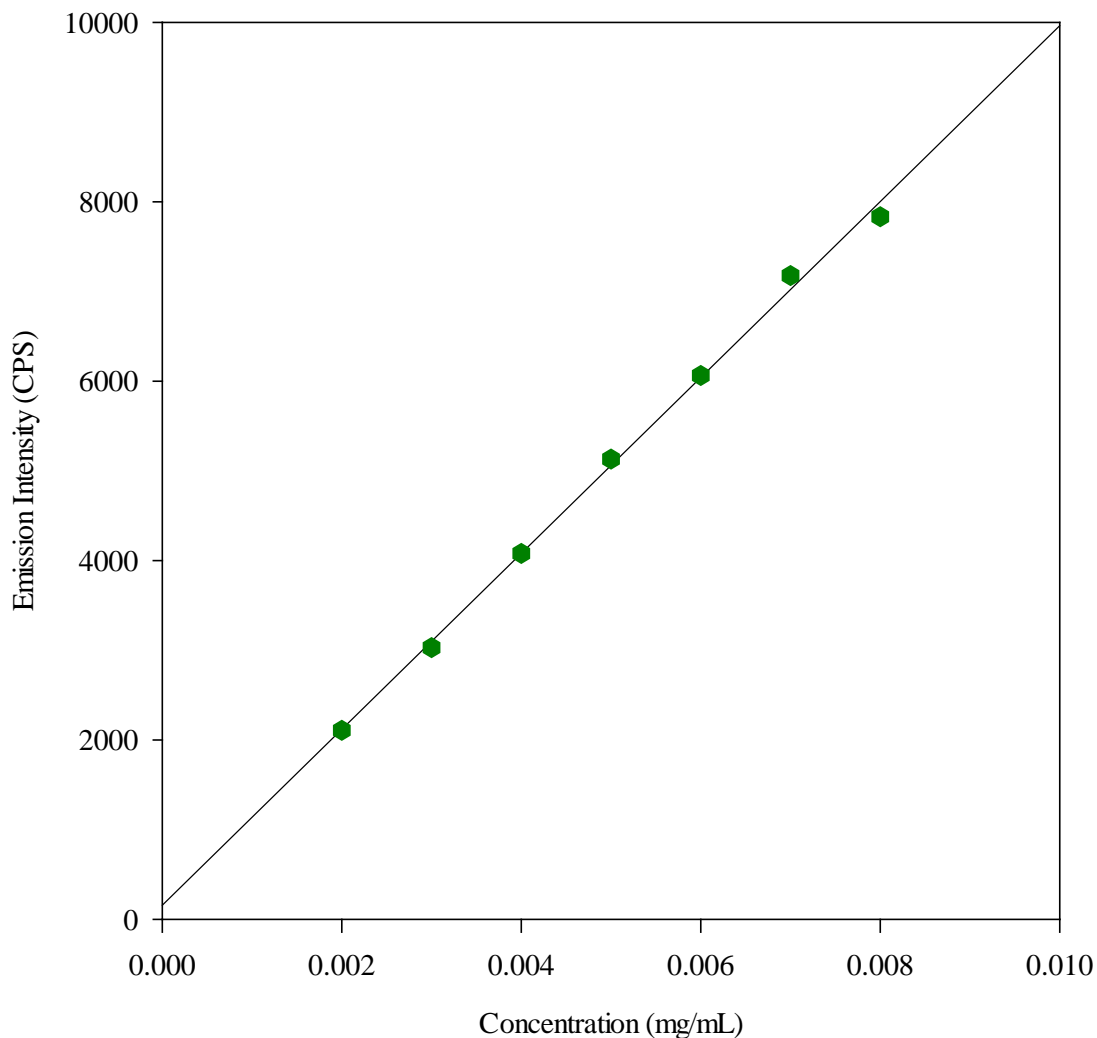
Figure 137: Calibration plot of 1 – naphthol in 75 % ethanol in a microwell plate.

The calibration plot of 1 – naphthol in 75 % ethanol can be seen in Figure 137. Seven points were used to construct the plot using an excitation wavelength of 296 nm and an emission wavelength of 368 nm. The concentration of the samples tested range from 0.01 mg/mL producing a fluorescence intensity of 2.6×10^3 CPS/mV to 0.07 mg/mL producing a fluorescence intensity of 1.1×10^4 CPS/mV. When compared to the calibration plot produced in the cuvette, the R^2 values are 0.985 in the cuvette and 0.981 in the plate. This is a minimal decrease in the precision of the calibration.
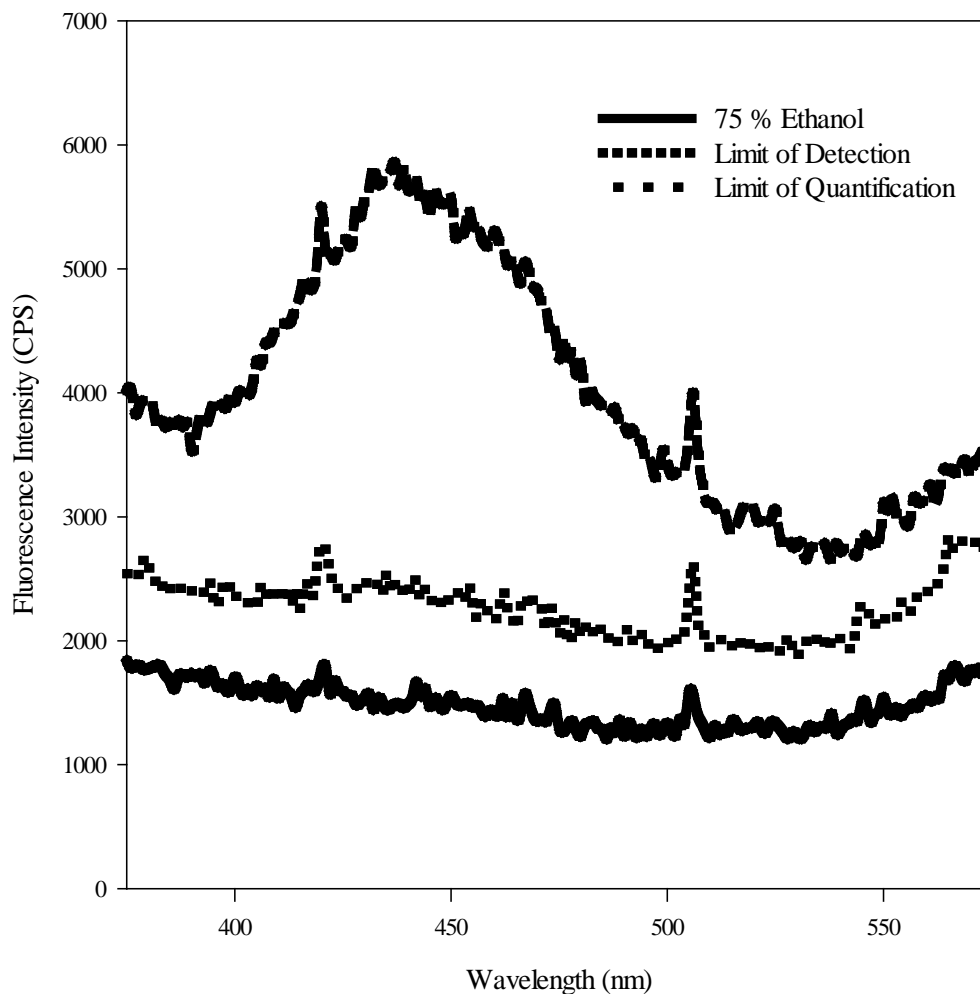
Figure 138: Accuracy of calculations for limit of detection and quantitation of 1 – naphthol in 75 % ethanol in a microwell plate.

An emission spectrum was generated to test the accuracy of the calculations performed using the calibration plots LoD and LoQ of 1 – naphthol in 75 % ethanol and can be seen in Figure 138. The calculated LoD was 8.24×10^{-3} mg/mL and produced a fluorescence intensity of 2.3×10^3 CPS/mV. The calculated LoQ was 2.75×10^{-2} mg/mL and produced a fluorescence intensity of 4.8×10^3 CPS/mV. The emission spectrum in the plate shows significant noise when compared to the spectrum generated in the cuvette. The emission spectrum also has lost most of its fine structure.
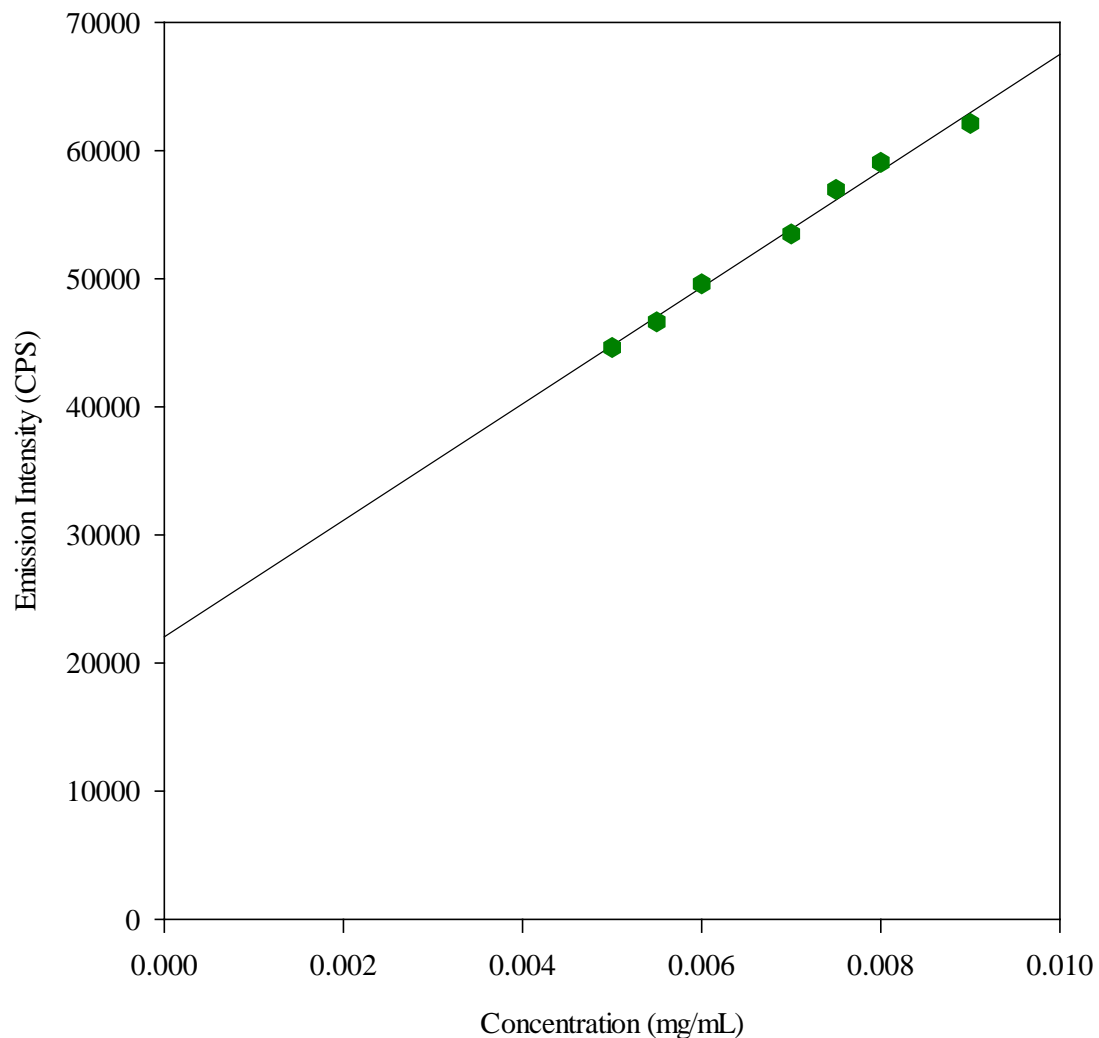
189

Calibration plot of 2 – naphthol in 75 % ethanol in a microwell plate.

The calibration plot of 2 – naphthol in 75 % ethanol can be seen in Figure 139. Seven points were used to construct the plot using an excitation wavelength of 264 nm and an emission wavelength of 358 nm. The concentration of the samples tested range from 0.003 mg/mL producing a fluorescence intensity of 1.6×10^3 CPS/mV to 0.009 mg/mL producing a fluorescence intensity of 4.6×10^3 CPS/mV. When compared to the calibration plot produced in the cuvette, the R^2 values are 0.999 in the cuvette and 0.998 in the plate. This is a minimal decrease in the precision of the calibration.
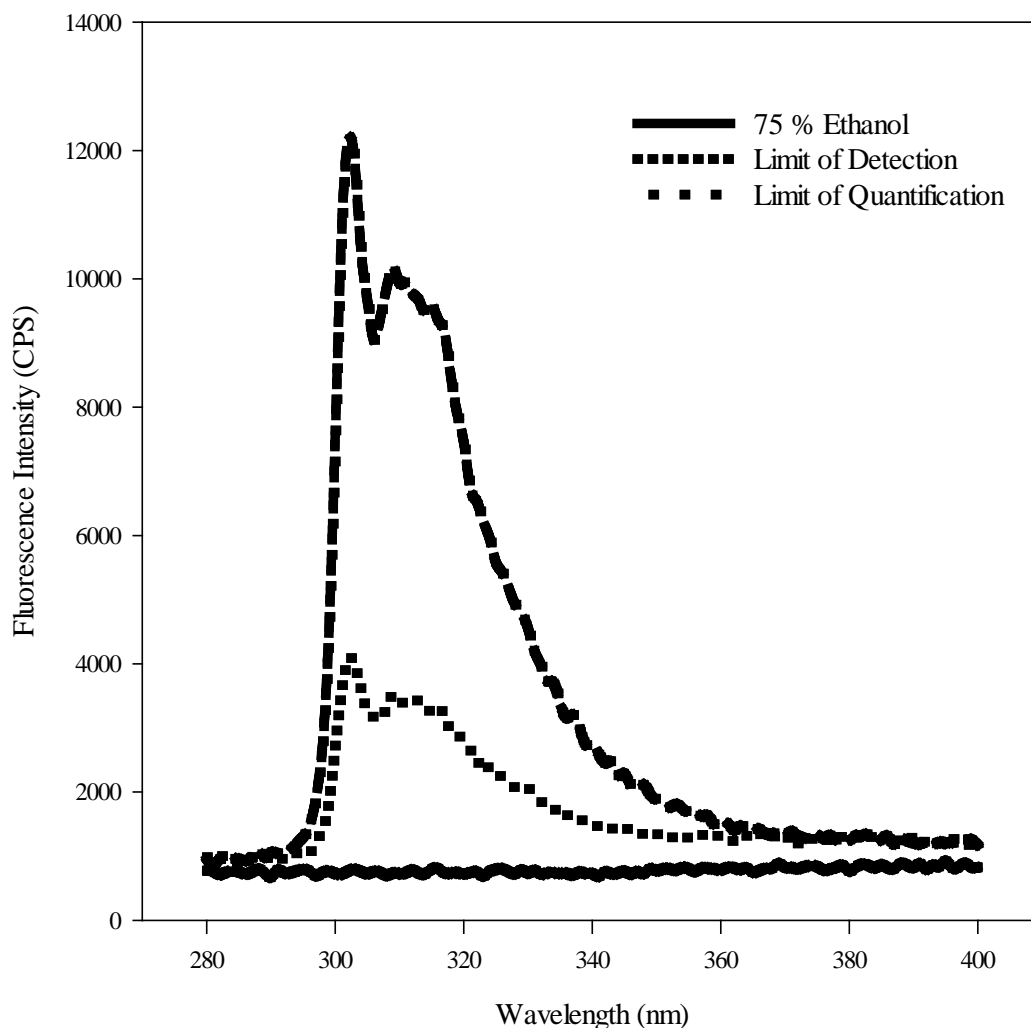
Figure 140: Accuracy of calculations for limit of detection and quantitation of 2 – naphthol in 75 % ethanol in a microwell plate.

An emission spectrum was generated to test the accuracy of the calculations performed using the calibration plots LoD and LoQ of 2 – naphthol in 75 % ethanol and can be seen in Figure 140. The calculated LoD was 4.20×10^{-4} mg/mL and produced a fluorescence intensity of 3.5×10^2 CPS/mV. The calculated LoQ was 1.40×10^{-3} mg/mL and produced a fluorescence intensity of 8.2×10^2 CPS/mV. The emission spectrum in the plate shows significant noise when compared to the spectrum generated in the cuvette. The emission spectrum also has lost all of its fine structure and is barely recognizable as the spectrum of 2 – naphthol at all.
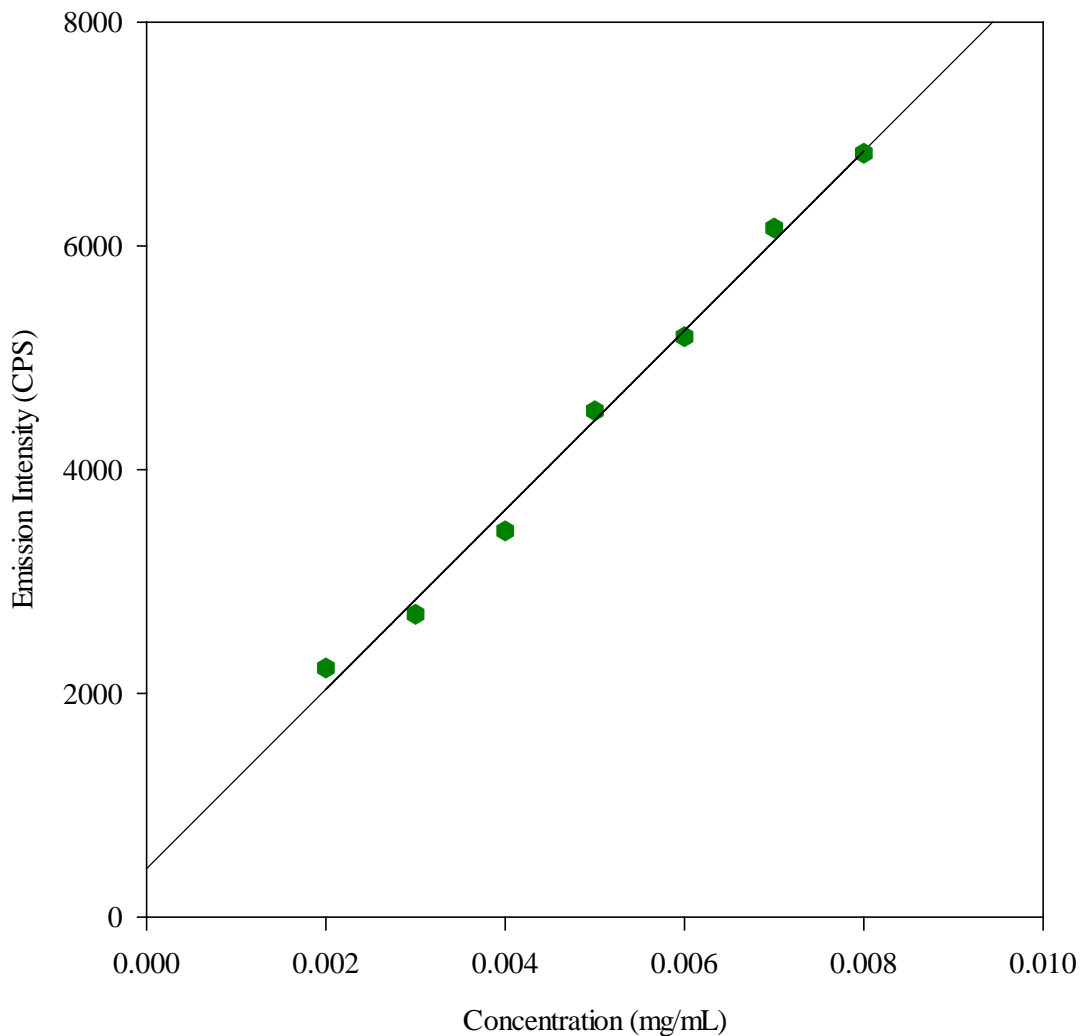
Figure 141: Calibration plot of phenanthrene in 75 % ethanol in a microwell plate.

The calibration plot of phenanthrene in 75 % ethanol can be seen in Figure 141. Seven points were used to construct the plot using an excitation wavelength of 294 nm and an emission wavelength of 366 nm. The concentration of the samples tested range from 0.001 mg/mL producing a fluorescence intensity of 4.1 x 10^3 CPS/mV to 0.004 mg/mL producing a fluorescence intensity of 1.4 x 10^4 CPS/mV. When compared to the calibration plot produced in the cuvette, both R^2 values are 0.999.
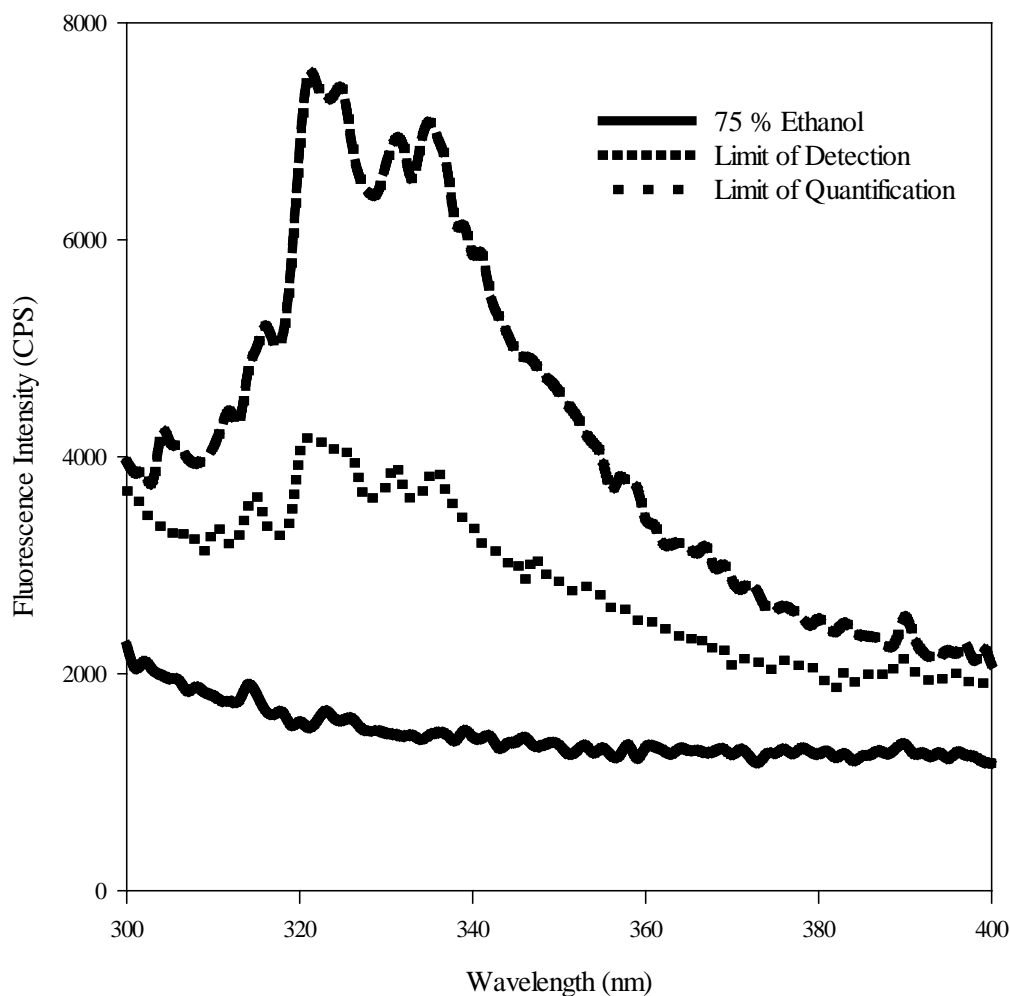
Figure 142: Accuracy of calculations for limit of detection and quantitation of phenanthrene in 75 % ethanol in a microwell plate.

An emission spectrum was generated to test the accuracy of the calculations performed using the calibration plots LoD and LoQ of phenanthrene in 75 % ethanol and can be seen in Figure 142. The calculated LoD was 1.25×10^{-4} mg/mL and produced a fluorescence intensity of 1.1×10^3 CPS/mV. The calculated LoQ was 4.17×10^{-4} mg/mL and produced a fluorescence intensity of 2.1×10^3 CPS/mV. The emission spectrum in the plate shows some additional noise when compared to the spectrum generated in the cuvette, however the spectrum is intact and clearly visible.
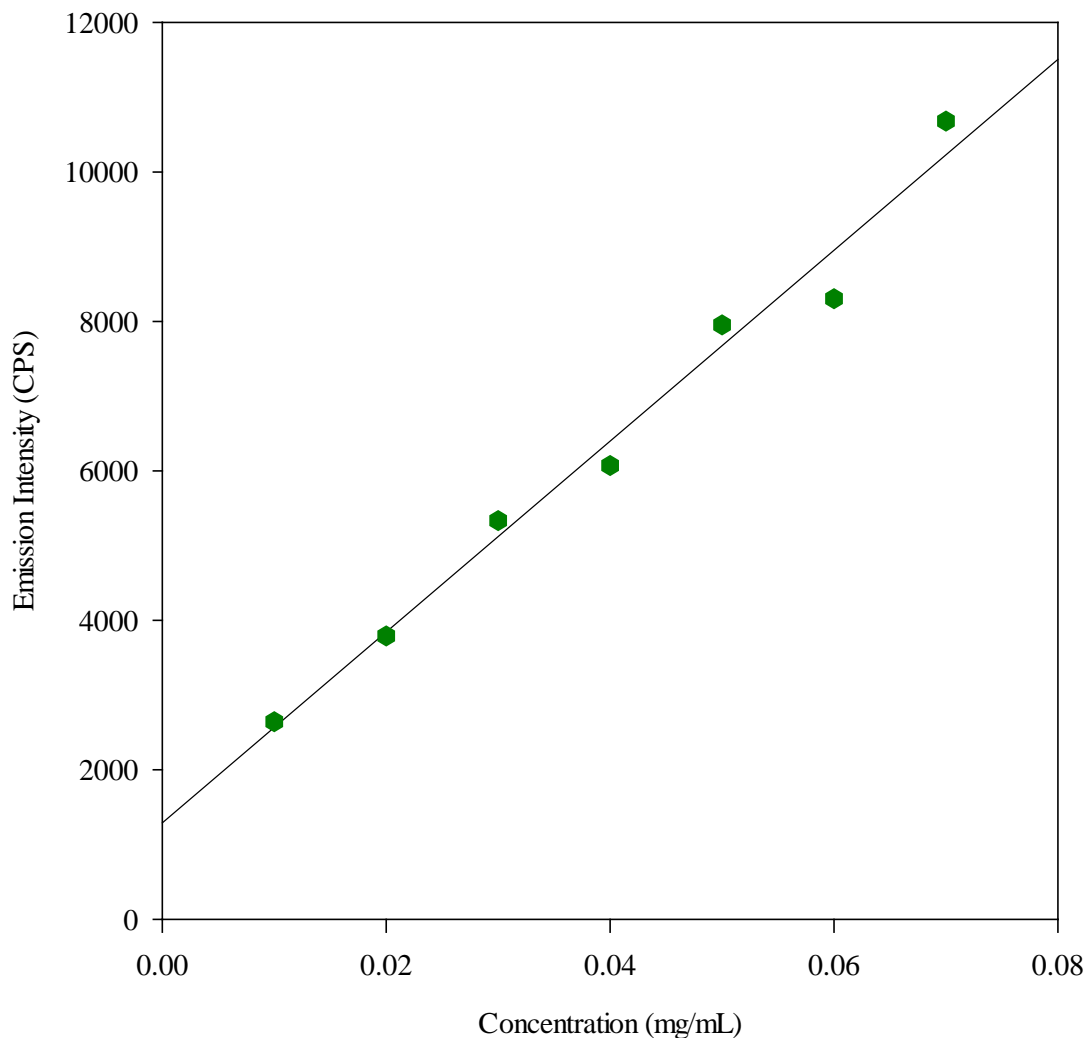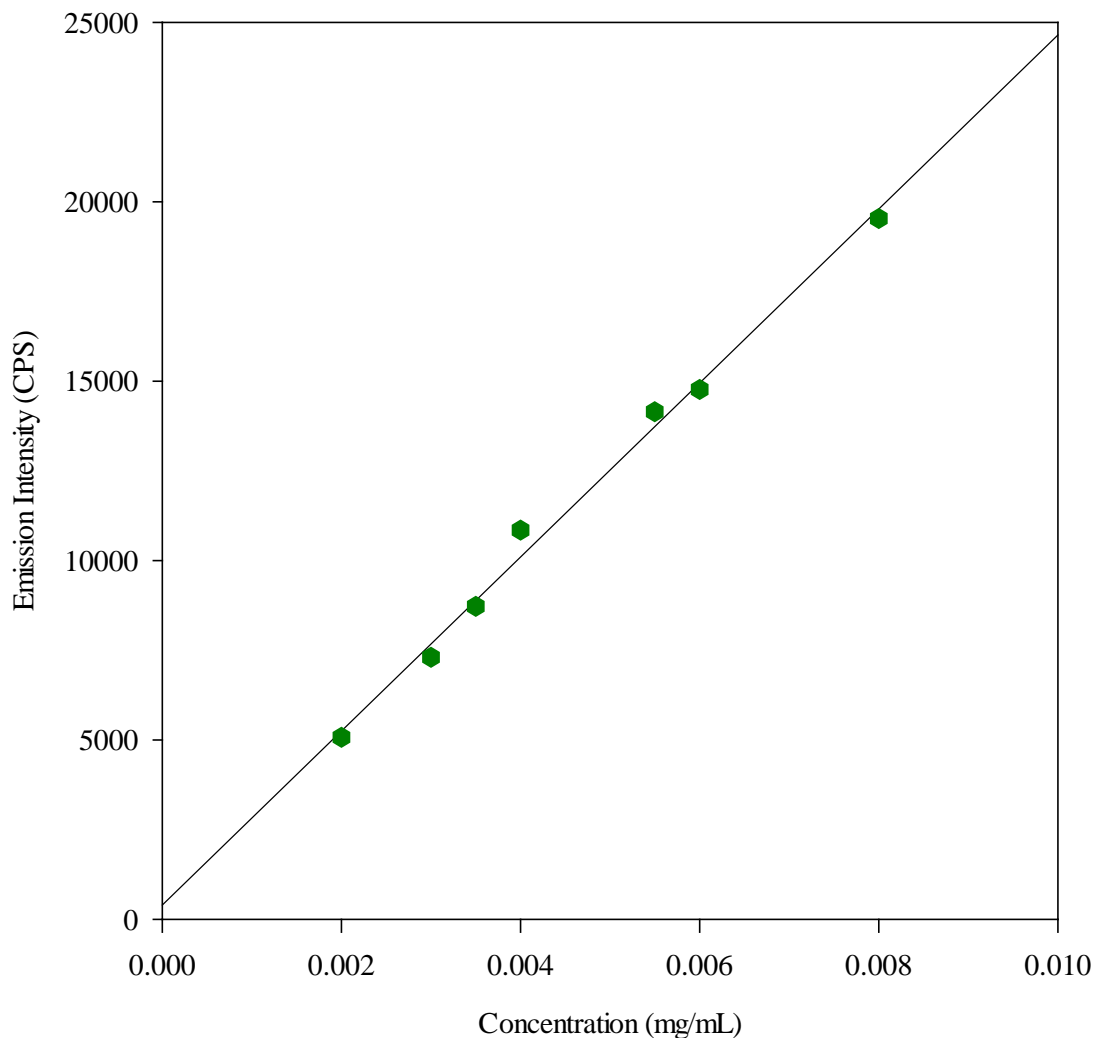
Figure 143: Calibration plot of 9 – phenanthrol in 75 % ethanol in a microwell plate.

The calibration plot of 9 – phenanthrol in 75 % ethanol can be seen in Figure 143. Seven points were used to construct the plot using an excitation wavelength of 304 nm and an emission wavelength of 389 nm. The concentration of the samples tested range from 0.002 mg/mL producing a fluorescence intensity of 5.1×10^3 CPS/mV to 0.008 mg/mL producing a fluorescence intensity of 2.0×10^4 CPS/mV. When compared to the calibration plot produced in the cuvette, the R^2 values are 0.999 in the cuvette and 0.993 in the plate. This is a minimal decrease in the precision of the calibration.
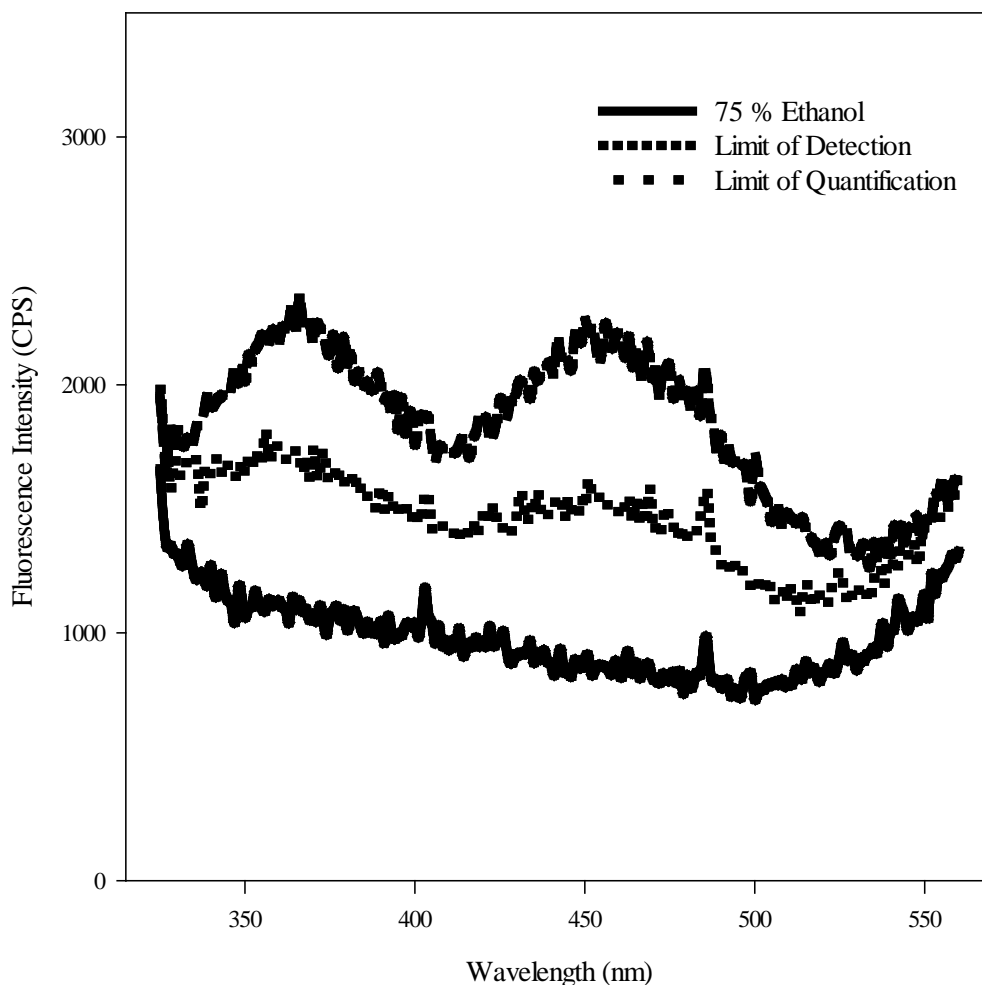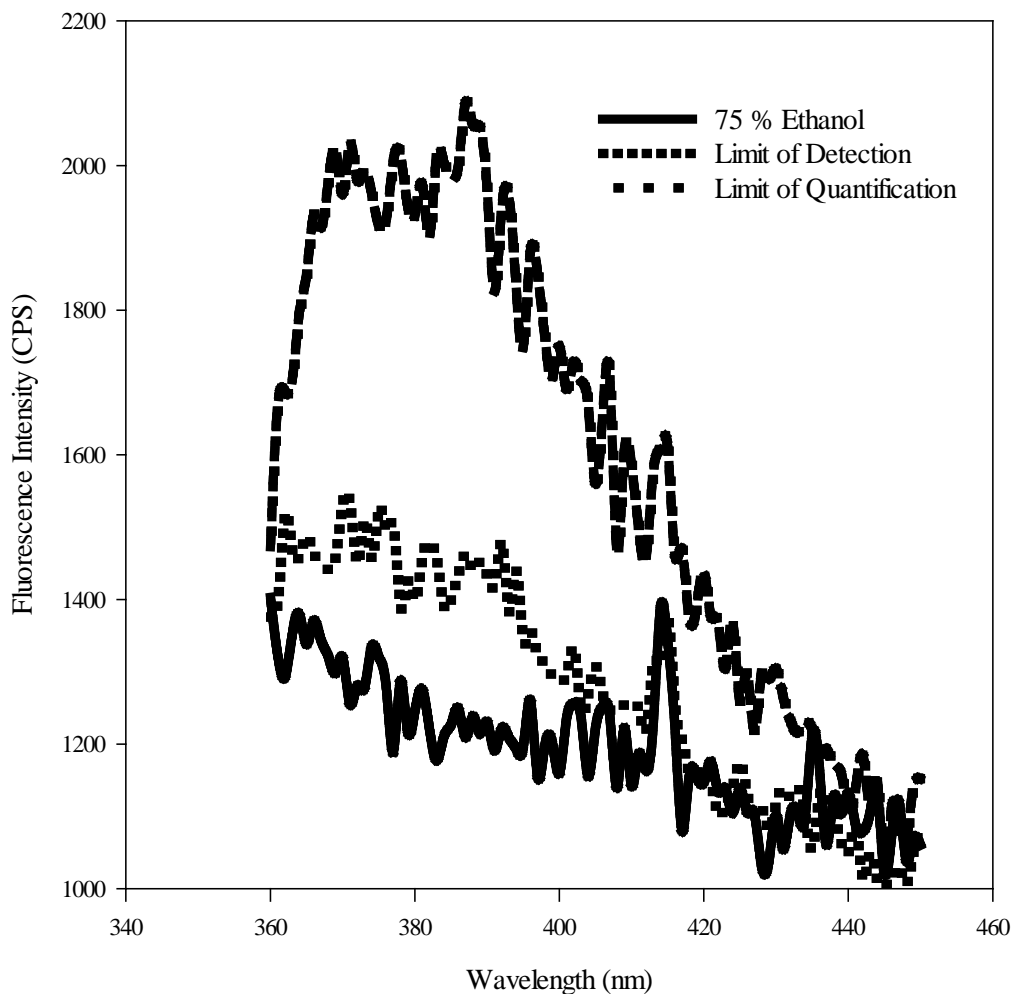
Figure 144: Accuracy of calculations for limit of detection and quantitation of 9 – phenanthrol in 75 % ethanol in a microwell plate.

An emission spectrum was generated to test the accuracy of the calculations performed using the calibration plots LoD and LoQ of 9 – phenanthrol in 75 % ethanol and can be seen in Figure 144. The calculated LoD was 5.53×10^{-4} mg/mL and produced a fluorescence intensity of 1.7×10^{3} CPS/mV. The calculated LoQ was 1.84×10^{-3} mg/mL and produced a fluorescence intensity of 4.9×10^{3} CPS/mV. The emission spectrum in the plate shows significant noise when compared to the spectrum generated in the cuvette. The emission spectrum also has lost all of its fine structure and is barely recognizable as the spectrum of 9 – phenanthrol at all.
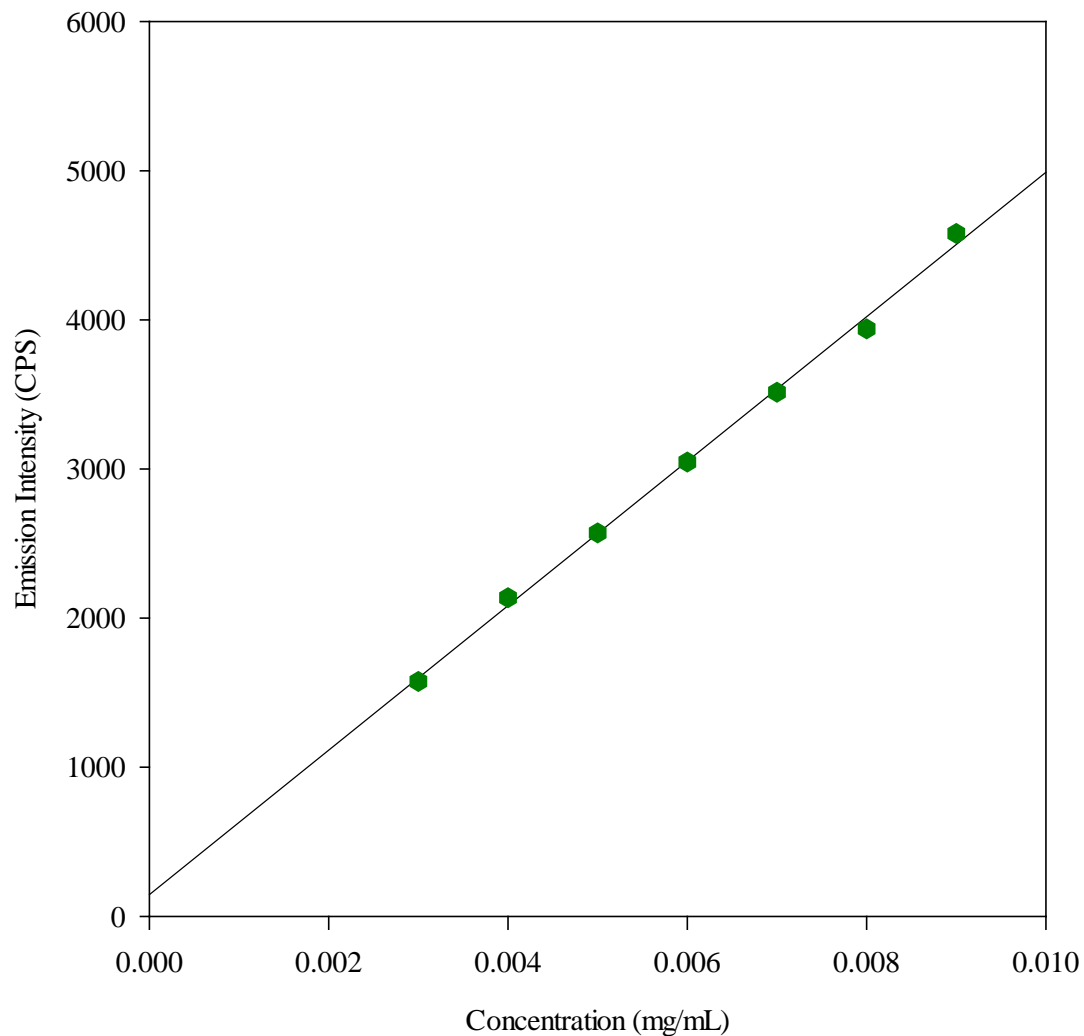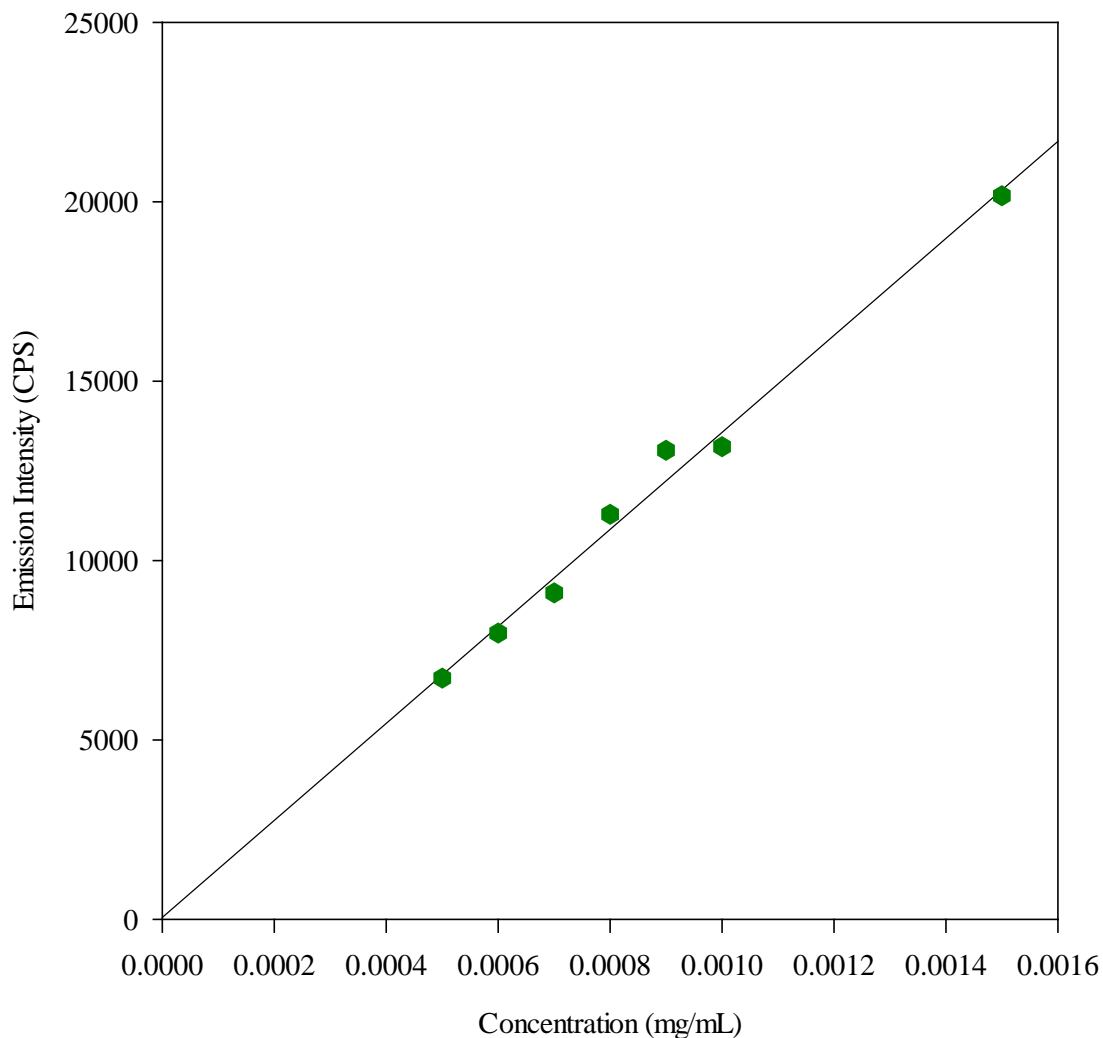
Figure 145: Calibration plot of pyrene in 75 % ethanol in a microwell plate.

The calibration plot of pyrene in 75 % ethanol can be seen in Figure 145. Seven points were used to construct the plot using an excitation wavelength of 334 nm and an emission wavelength of 372 nm. The concentration of the samples tested range from 0.0005 mg/mL producing a fluorescence intensity of 6.7 x 10^3 CPS/mV to 0.0015 mg/mL producing a fluorescence intensity of 2.0 x 10^4 CPS/mV. When compared to the calibration plot produced in the cuvette, the R^2 values are 0.991 in the cuvette and 0.990 in the plate. This is a minimal decrease in the precision of the calibration.
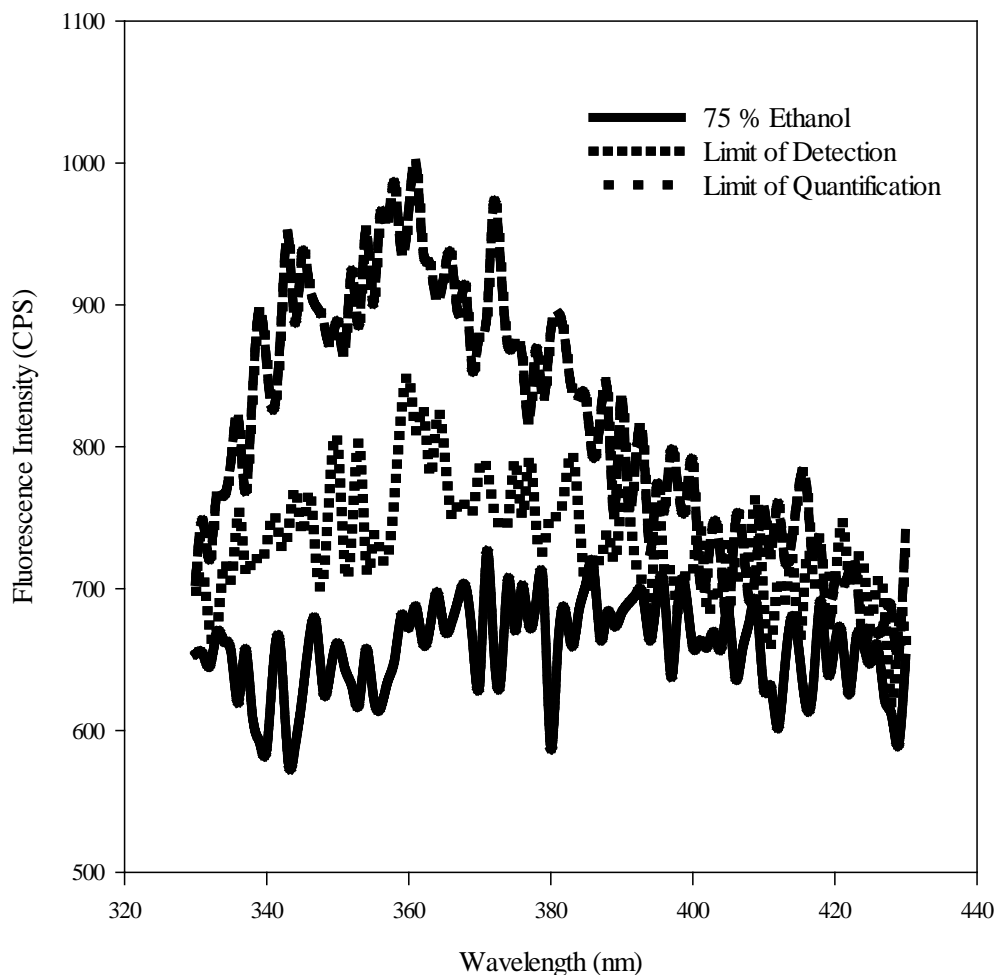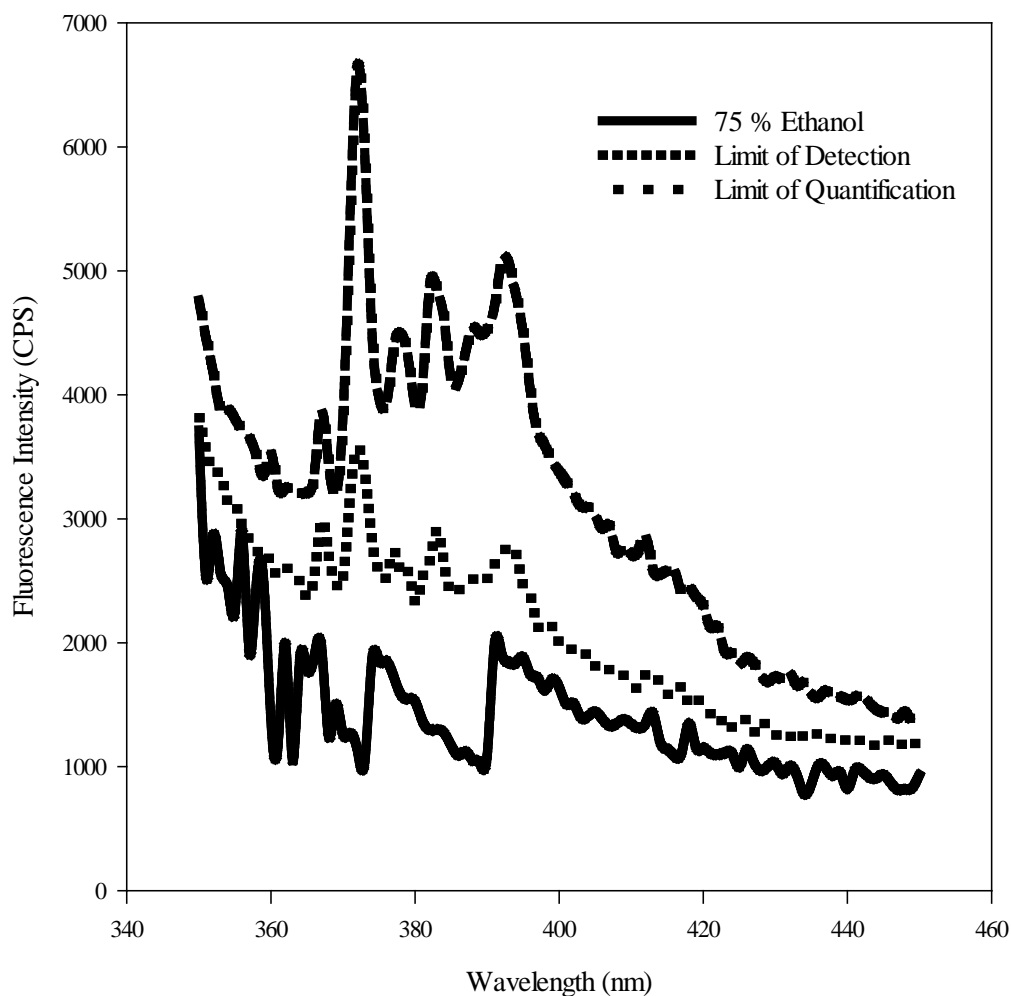
Figure 146: Accuracy of calculations for limit of detection and quantitation of pyrene in 75 % ethanol in a microwell plate.

An emission spectrum was generated to test the accuracy of the calculations performed using the calibration plots LoD and LoQ of pyrene in 75 % ethanol and can be seen in Figure 146. The calculated LoD was 1.27×10^{-4} mg/mL and produced a fluorescence intensity of 1.8×10^3 CPS/mV. The calculated LoQ was 4.25×10^{-4} mg/mL and produced a fluorescence intensity of 5.8×10^3 CPS/mV. The emission spectrum in the plate shows some additional noise when compared to the spectrum generated in the cuvette. The emission spectrum in the plate also lacks some of the fine structure as previously seen in the emission spectrum.
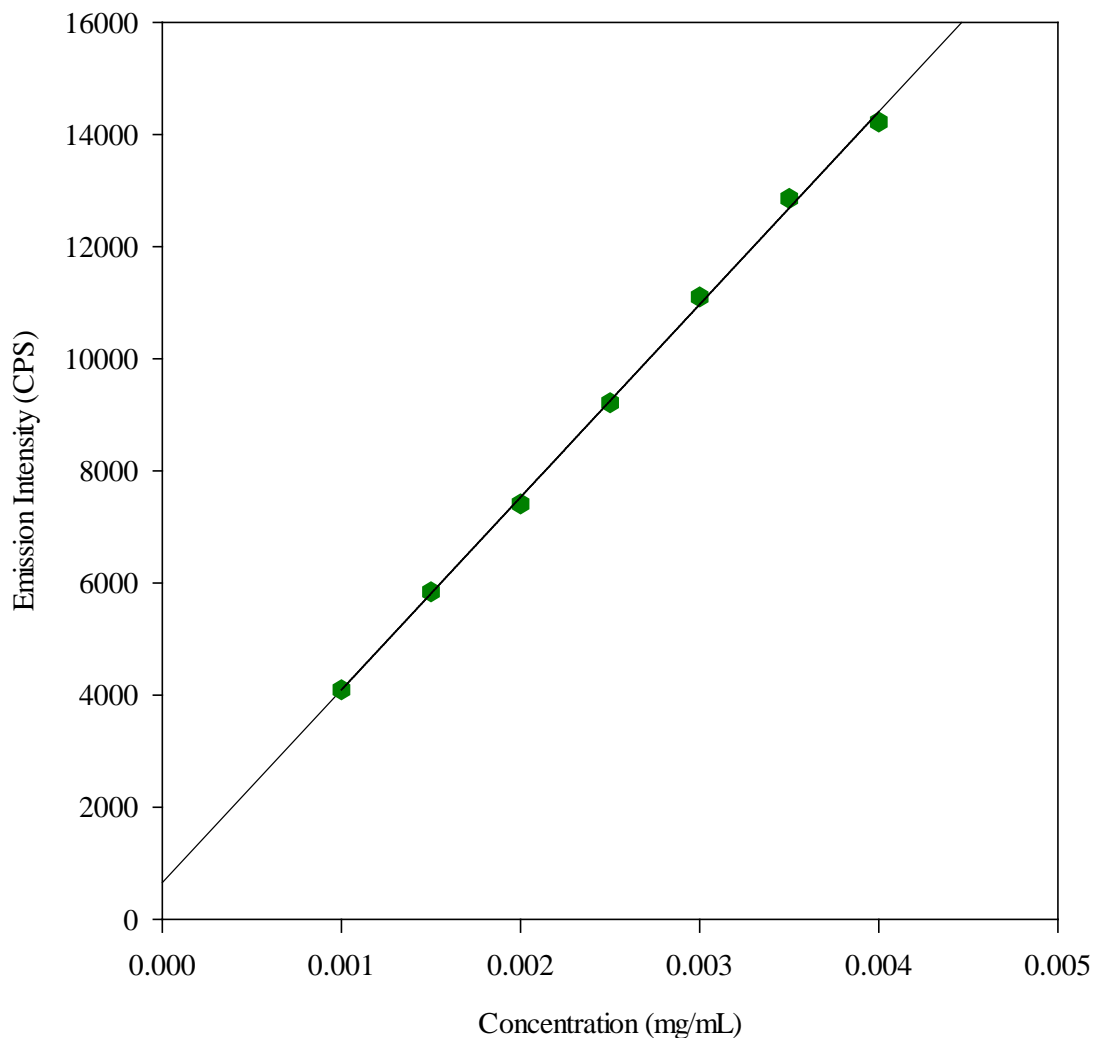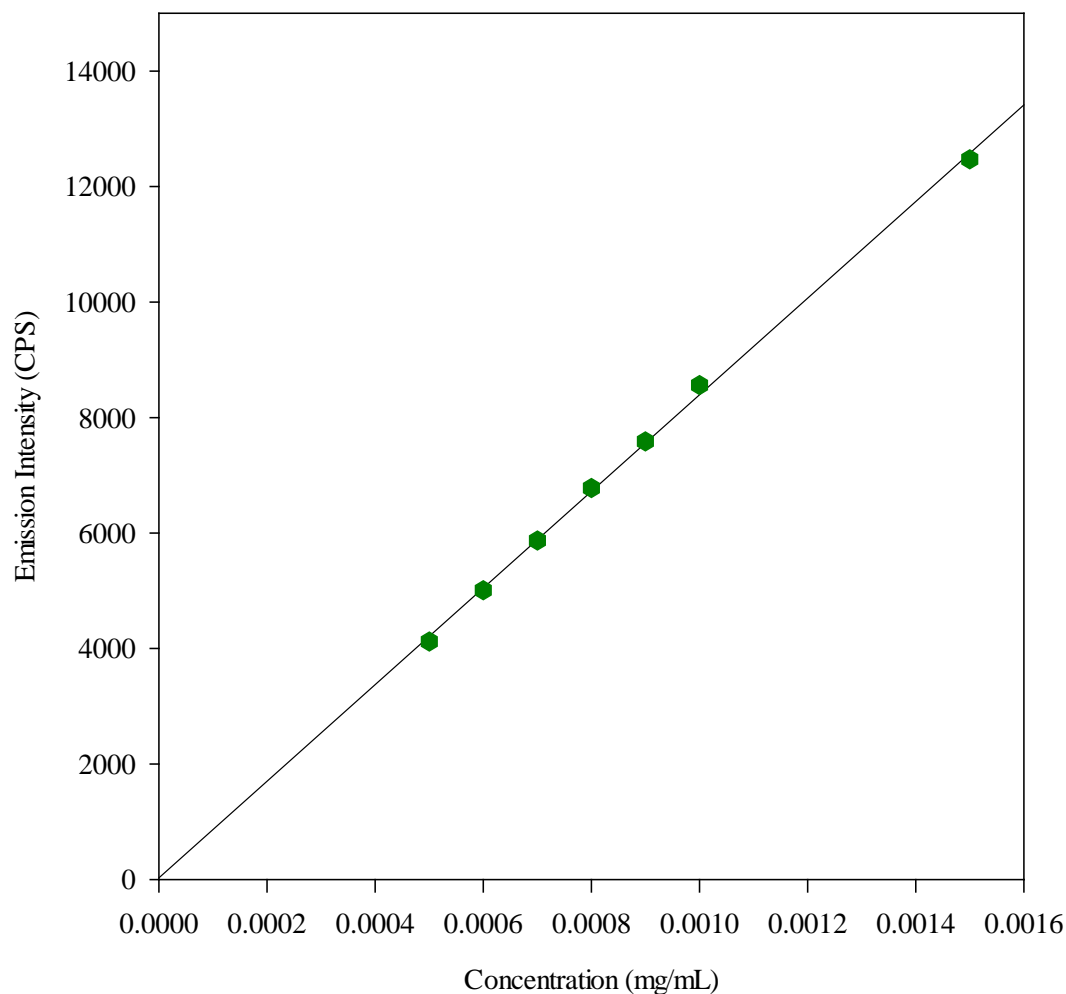
Figure 147: Calibration plot of 1 – pyrenol in 75 % ethanol in a microwell plate.

The calibration plot of 1 – pyrenol in 75 % ethanol can be seen in Figure 147. Seven points were used to construct the plot using an excitation wavelength of 268 nm and an emission wavelength of 409 nm. The concentration of the samples tested range from 0.0005 mg/mL producing a fluorescence intensity of 4.1×10^3 CPS/mV to 0.0015 mg/mL producing a fluorescence intensity of 1.2×10^4 CPS/mV. When compared to the calibration plot produced in the cuvette, the R^2 values are 0.997 in the cuvette and 0.999 in the plate. 1 – pyrenol was the only compound to show an increase in the correlation factor between the plate and the cuvette, which confirms the conclusion that the plate reader method is viable.
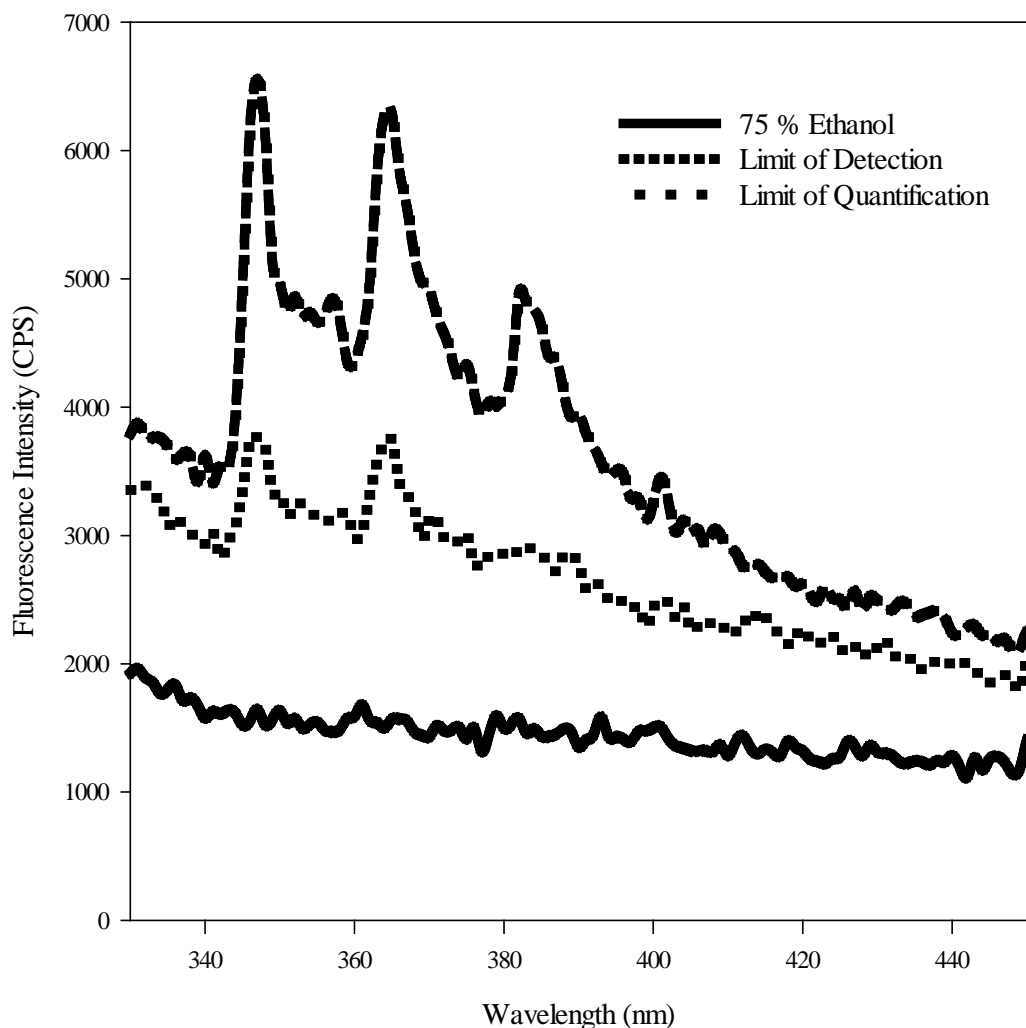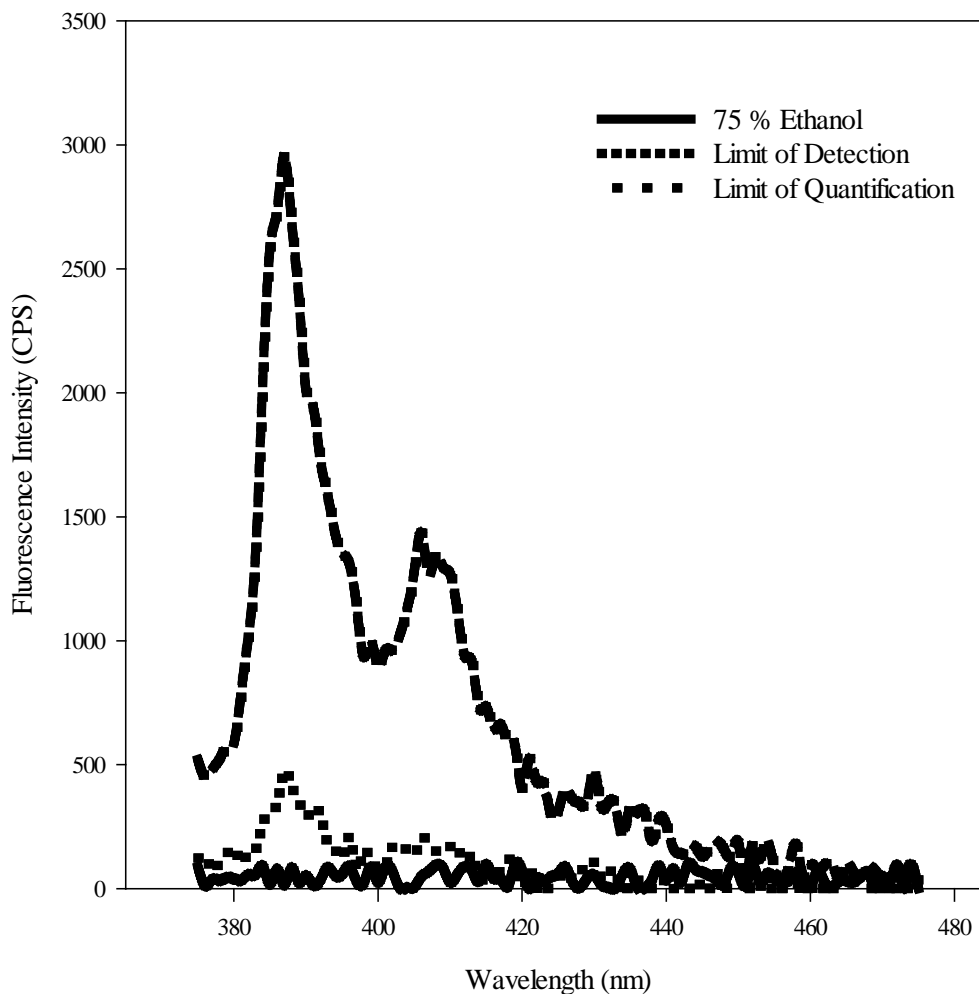
Figure 148: Accuracy of calculations for limit of detection and quantitation of 1 – pyrenol in 75 % ethanol in a microwell plate.

An emission spectrum was generated to test the accuracy of the calculations performed using the calibration plots LoD and LoQ of 1 – pyrenol in 75 % ethanol and can be seen in Figure 148. The calculated LoD was 4.18×10^{-5} mg/mL and produced a fluorescence intensity of 3.8×10^2 CPS/mV. The calculated LoQ was 1.39×10^{-4} mg/mL and produced a fluorescence intensity of 1.2×10^3 CPS/mV. The emission spectrum in the plate shows significant noise when compared to the spectrum generated in the cuvette. The emission spectrum also has lost all of its fine structure and is barely recognizable as the spectrum of 1 – pyrenol at all.

The calculated LoDs and LoQs in the plate are much closer to actual figures of merit. Since concentrations of samples used to generate calibration plots in both the cuvette and the plate did not differ greatly, the decrease in signal intensity is attributed to the loss of signal in the fiber optic assembly. This loss was expected before the method was developed, therefore there is no questions raised by the data collected.

References

1. Berlman, I. B. *Handbook of Fluorescence Spectra of Aromatic Molecules*, 1st ed.; Academic Press: New York, 1965.

2. Lakowicz, J. *Principles of Fluorescnece Spectroscopy*, 1st ed.; Plenum Press: New York, 1983.

3. Valeur, B.; Berberan-Santos, M. *Molecular Fluorescence: Principles and Applications*, 1st ed.; Wiley-VCH, 2013.

4. Kalyanasundaram, K. *Photochemistry in Microheterogeneous Systems*, 1st ed.; Academic Press: Orlando Florida, 1987.

5. Schulman, S. G.; Shangxian Chen; Bai, F.; Leiner, M. J. P.; Weis, L.; Wolfbeis, O. S. Dependence of the Fluorescence of Immobilized 1-Hydroxypyrene-3,6,8-Trisulfonate on Solution PH: Extension of the Range of Applicability of a PH Fluorosensor. *Analytica Chimica Acta* **1995**, *304* (2), 165–170.

6. K.K, H. P. Photomultiplier tube R928 http://www.hamamatsu.com/us/en/product/R928/index.html (accessed Dec 14, 2017).

7. Murphy, K. R.; Stedmon, C. A.; Graeber, D.; Bro, R. Fluorescence Spectroscopy and Multi-Way Techniques. PARAFAC. *Analytical Methods* **2013**, *5* (23), 6557–6566.

8. Horiba. Fluorescence Spectroscopy and Water Quality. Horiba Scientific 2009.

9. Birks, J. B. *Photophysics of Amromatic Molecules*, 1st ed.; Wiley-Interscience: New York, 1970.

10. Parker, C. A. *Phtoluminescence of Solutions*, 1st ed.; Elsevier: Amsterdam, The Netherlands, 1968.

11. Dawson, W. R.; Windsor, M. W. Fluorescence Yields of Aromatic Compounds. *J. Phys. Chem.* **1968**, *72* (9), 3251–3260.

12. Ivanec-Goranina, R.; Kulys, J. Kinetic Study of Peroxidase-Catalysed Oxidation of 1-Hydroxypyrene. Development of a Nanomolar Hydrogen Peroxide Detection System. *Cent. Eur. J. Biol.* **2008**, *3* (3), 224–232.

13. Parker, C. A.; Joyce, T. A. Determination of Triplet Formation Efficiencies by Measurement of Sensitized Delayed Fluorescnece. *Trans. Faraday Soc.* **1966**, *62* (0), 2785–2792.

14. Armbruster, D. A.; Pry, T. Limit of Blank, Limit of Detection and Limit of Quantitation. *Clin Biochem Rev* **2008**, *29* (Suppl 1), S49–S52.

15. Miller, J. N.; Miller, J. C. *Statistics and Chemometrics for Analytical Chemistry*, 4th ed.; Pearson Education, 2000.

16. Godax Laboratories. NOCHROMIX. *Laboratory Glass Cleaning Reagent*, 2017.

17. Horiba Scientific. Fluorolog-3 Spectrofluorometer Operation Manual. Horiba Instruments Inc. 2012.

18. SCIENCEWARE® Vakuwash® Cuvette Washer, Bel-art | VWR https://us.vwr.com/store/product/4830426/scienceware-vakuwash-cuvette-washer-bel-art (accessed Dec 14, 2017).

19. Nunc™ F96 MicroWell™ Black and White Polystyrene Plate https://www.thermofisher.com/order/catalog/product/136101 (accessed Dec 14, 2017).

20. Corning Life Sciences Catalog 3615 https://catalog2.corning.com/LifeSciences/en-US/Shopping/ProductDetails.aspx?productid=3615(Lifesciences)# (accessed Dec 14, 2017).

21. Corning Life Sciences Catalog 4580 https://catalog2.corning.com/LifeSciences/en-US/Shopping/ProductDetails.aspx?productid=4580(Lifesciences) (accessed Dec 14, 2017).

22. Gilson Inc. The Maximum Errors Tolerated by Norm ISO-8655 and Gilson Specifications. Gilson S.A.S. 2007.

23. MicroAmp Optical Adhesive Film Kit - Thermo Fisher Scientific https://www.thermofisher.com/order/catalog/product/4313663?SID=srch-srp-4313663 (accessed Dec 14, 2017).

24. VWR® Heat-Resistant Films for Real-Time qPCR, Ultra-Clear Polyester | VWR
https://us.vwr.com/store/product/4788795/vwr-heat-resistant-films-for-real-time-qpcr-
ultra-clear-polyester (accessed Dec 14, 2017).

Chapter 5

Conclusions

Results show that standard fluorescence cuvettes yield the lowest LoD and LoQs, however the microwell plate is only one order of magnitude less sensitive for most compounds studied. This is largely due to the optical losses in the fiber optic transmitting the excitation light to the sample, and returning the emission to the photomultiplier detector. Normal fluorescence measurements are optically configured as right angle (emission spectra is collected 90° from excitation wavelength) or front face detection (small angle). No intervening optics other than high quality front face mirrors are used to steer the light, and the path lengths are minimized. Microwells present an optically similar arrangement to front face detection, however, the excitation light must travel through an approximately 1 m fiber optic cable before striking the sample, then the emitted light must return to the detector through the same fiber optic. The losses in imperfect light transmission through the fiber optic cable is the primary reason for the loss of sensitivity. However, for the purposes of biomonitoring and screening, this loss is acceptable.

The advantages to using the microwell plates are still considerably high. A standard fluorescence quartz cuvette costs ca $200, while a microwell plate is $20 for 96 samples. Cleaning is also an issue while using a cuvette. Standard cleaning procedures call for the use of nitric acid and can take up to 8 hours of soaking time. This task is both time consuming and dangerous especially given the high number of individual samples needed for accurate biomonitoring. Once a microwell plate has been fully used it can easily be discarded as waste.

Another notable difference is that with a cuvette one must continuously change samples. While using the microwell plate the spectrofluorometer can be set to multiple spectroscopic protocols on as many as 96 samples without user intervention.

EEMs is an excellent way to measure PAHs for biomonitoring as it gives you a considerably larger amount of data to work with. This will play a significant role while looking at mixtures of compounds. Most real-life samples with have more than one compound or

metabolite present. Collection of data is made easier with the use of a microwell plate and gives more data at a faster rate as compared to a standard fluorescence cuvette.

The principle challenges in this work were the need to investigate compounds that were of limited analytical interest in the past, and to develop a new method of sample handling for EEMs. Hydroxylated PAH compounds have not been significant fluorescence analytical targets when not coupled to prior chromatographic steps,[1,2,3] particularly in the extraction matrix of 75% aqueous ethanol previously established by the colleagues investigating menhaden and killifish. It is critical to develop methods for biomonitoring such metabolites in the wild, as it has been found that these species are what is found in biological tissue.[4,5] Biomonitoring of human subjects, principally through urine samples, focuses on hydroxylated PAHs such as 3-hydroxybenzo[a]pyrene[6] and 1-hydroxypyrene.[7,3]

Multidimensional analysis necessitates the measurement of many samples, which in fluorescence is difficult using quartz cuvettes as it has been found that PAHs and hydroxylated PAHs are problematic materials to remove (vide supra). The microwell plate is an ideal sample holder for such measurements as each "cell" is used once, along with the ability afforded by the automation of spectral measurement. Mahmoud, et. al.[8] have shown the value of microwell plates in the analysis of omeprazole in quality control environments using single wavelength monitoring of a charge transfer sensitized reaction.

Most techniques reported used some sort of preconcentration step, such as absorption onto a nylon membrane,[4] solid phase extraction,[9] chemical derivatization[10] or adsorption onto a solid phase.[11] While such methods yield very low LoDs and LoQs, they are not often practical in a biomonitoring situation. Flow cell or sipper sampling methods suffer from the same issues as cuvettes, in that they will absorb PAH and PAHM compounds.

The current work reports LoDs and LoQs for one-way data (signal vs known concentration), but as multiway data analyses become ubiquitous, definitive methods of calculating similar figures of merit become more problematic.[12,13,] A review of the literature shows that modern fluorescence analyses seek to employ the second order advantage of EEMs

and deconvolution by computational methods such as PARAFAC.[14,15,16,17] The importance of multi-way techniques has even led to four-way analyses combining excitation and emission with time by following the Fenton degradation of large PAHs.[18]

In the present work, the focus was on direct analysis of lightly processed fish tissue extracts and developing the microwell plate as a sample holder for one-way and two-way data collection. Fewer manipulations of the sample minimize error. The microwell plate automates sample measurement. Further, microwell plate sampling eliminates fouling of the sample cell by analytes since it is only used once. The Environmental Protection Agency sets a maximum contaminant level (MCL) of 200 ng/L for benzo[a]pyrene (a marker for PAH contamination) of drinking water.[19] Generally, to achieve LoQ and LoQ sensitivities in this range, preconcentration and extraction techniques are required.[16]

The simple method presented here does not achieve those levels. For benzo[a]pyrene, the LoD and LoQ levels using cuvettes are 6.40×10^3 ng L^{-1} and 2.10×10^4 ng L^{-1}, respectively. In the microwell plate, the LoD and LoQ levels are 7.70×10^3 ng L^{-1} and 2.60×10^4 ng L^{-1}, respectively. Clearly these sensitivities are both conservative, and amenable to improvement. For example, preconcentration on a nylon membrane and multiway analysis can substantially improve sensitivities, and will be investigated in subsequent work.

References

1. Carmella, S. G.; Chen, M.; Han, S.; Briggs, A.; Jensen, J.; Hatsukami, D. K.; Hecht, S. S. Effects of Smoking Cessation on Eight Urinary Tobacco Carcinogen and Toxicant Biomarkers. *Chem. Res. Toxicol.* **2009**, *22* (4), 734–741.

2. Leroyer, A.; Jeandel, F.; Maitre, A.; Howsam, M.; Deplanque, D.; Mazzuca, M.; Nisse, C. 1-Hydroxypyrene and 3-Hydroxybenzo[a]Pyrene as Biomarkers of Exposure to PAH in Various Environmental Exposure Situations. *Science of The Total Environment* **2010**, *408* (5), 1166–1173.

3. Jongeneelen, F. J.; Anzion, R. B. M.; Henderson, P. T. Determination of Hydroxylated Metabolites of Polycyclic Aromatic Hydrocarbons in Urine. *Journal of Chromatography B: Biomedical Sciences and Applications* **1987**, *413*, 227–232.

4. Pena, E. A.; Ridley, L. M.; Murphy, W. R.; Sowa, J. R.; Bentivegna, C. S. Detection of Polycyclic Aromatic Hydrocarbons (PAHs) in Raw Menhaden Fish Oil Using Fluorescence Spectroscopy: Method Development. *Environmental Toxicology and Chemistry* **2015**, *34* (9), 1946–1958.

5. Zadlock, F. J., IV. *Transcriptome Approach for Identifying Potential Biomarkers for Endocrine Disruption Due to Crude Oil Exposure Using Killifish (Fundulus Heteroclitus)*; eRepository @ Seton Hall, 2017.

6. Hu, H.; Liu, B.; Yang, J.; Lin, Z.; Gan, W. Sensitive Determination of Trace Urinary 3-Hydroxybenzo[a]Pyrene Using Ionic Liquids-Based Dispersive Liquid–liquid Microextraction Followed by Chemical Derivatization and High Performance Liquid Chromatography–high Resolution Tandem Mass Spectrometry. *Journal of Chromatography B* **2016**, *1027*, 200–206.

7. Jongeneelen, F. J. Benchmark Guideline for Urinary 1-Hydroxypyrene as Biomarker of Occupational Exposure to Polycyclic Aromatic Hydrocarbons. *The Annals of Occupational Hygiene* **2001**, *45* (1), 3–13.

8. Mahmoud, A. M.; Ahmed, S. A. A Validated High-Throughput Fluorometric Method for Determination of Omeprazole in Quality Control Laboratory via Charge Transfer Sensitized Fluorescence. *Journal of Fluorescence* **2016**, *26* (2), 521–529.

9. García-Falcón, M. S.; Pérez-Lamela, M.; Simal-Gándara, J. Comparison of Strategies for Extraction of High Molecular Weight Polycyclic Aromatic Hydrocarbons from Drinking Waters. *J. Agric. Food Chem.* **2004**, *52* (23), 6897–6903.

10. Luo, K.; Gao, Q.; Hu, J. Derivatization Method for Sensitive Determination of 3-Hydroxybenzo[a]Pyrene in Human Urine by Liquid Chromatography–electrospray Tandem Mass Spectrometry. *Journal of Chromatography A* **2015**, *1379*, 51–55.

11. Tarpani, L.; Vocci, A.; Selvaggi, R.; Pellegrino, R.; Ruspolini, F.; Taglieri, L.; Latterini, L. Solid-Phase Analysis of Polycyclic Aromatic Hydrocarbons by Fluorimetric Methods. *Appl Spectrosc* **2011**, *65* (12), 1342–1347.

12. Olivieri Alejandro C.; Faber Nicolaas (Klaas) M. A Closed-form Expression for Computing the Sensitivity in Second-order Bilinear Calibration. *Journal of Chemometrics* **2006**, *19* (11-12), 583–592.

13. Olivieri Alejandro C.; Faber Nicolaas M.; Ferré Joan; Boqué Ricard; Kalivas John H.; Mark Howard. Uncertainty Estimation and Figures of Merit for Multivariate Calibration (IUPAC Technical Report). *pac* **2006**, *78* (3), 633.

14. Kumar, S.; Negi, S.; Maiti, P. Biological and Analytical Techniques Used for Detection of Polyaromatic Hydrocarbons. *Environmental Science and Pollution Research* **2017**, *24* (33), 25810–25827.

15. Yu, J.; Zhang, X.; Hou, D.; Chen, F.; Mao, T.; Huang, P.; Zhang, G. Detection of Water Contamination Events Using Fluorescence Spectroscopy and Alternating Trilinear Decomposition Algorithm https://www.hindawi.com/journals/jspec/2017/1485048/cta/ (accessed May 3, 2018).

16. (Bortolato, S. A.; Arancibia, J. A.; Escandar, G. M. Chemometrics-Assisted Excitation−Emission Fluorescence Spectroscopy on Nylon Membranes. Simultaneous

Determination of Benzo[a]Pyrene and Dibenz[a,h]Anthracene at Parts-Per-Trillion Levels in the Presence of the Remaining EPA PAH Priority Pollutants As Interferences. *Anal. Chem.* **2008**, *80* (21), 8276–8286.

17. (Vásquez, V.; Báez, M. E.; Bravo, M.; Fuentes, E. Determination of Heavy Polycyclic Aromatic Hydrocarbons of Concern in Edible Oils via Excitation–emission Fluorescence Spectroscopy on Nylon Membranes Coupled to Unfolded Partial Least-Squares/Residual Bilinearization. *Analytical and Bioanalytical Chemistry* **2013**, *405* (23), 7497–7507.

18. Carabajal, M. D.; Arancibia, J. A.; Escandar, G. M. Excitation-Emission Fluorescence-Kinetic Data Obtained by Fenton Degradation. Determination of Heavy-Polycyclic Aromatic Hydrocarbons by Four-Way Parallel Factor Analysis. *Talanta* **2017**, *165*, 52–63.

19. What are EPA's drinking water regulations for benzo(a)pyrene? http://safewater.zendesk.com/hc/en-us/articles/212077717-4-What-are-EPA-s-drinking-water-regulations-for-benzo-a-pyrene- (accessed May 4, 2018).